Electron and Scanning Probe Microscopies

2022 Principal Investigators' Meeting

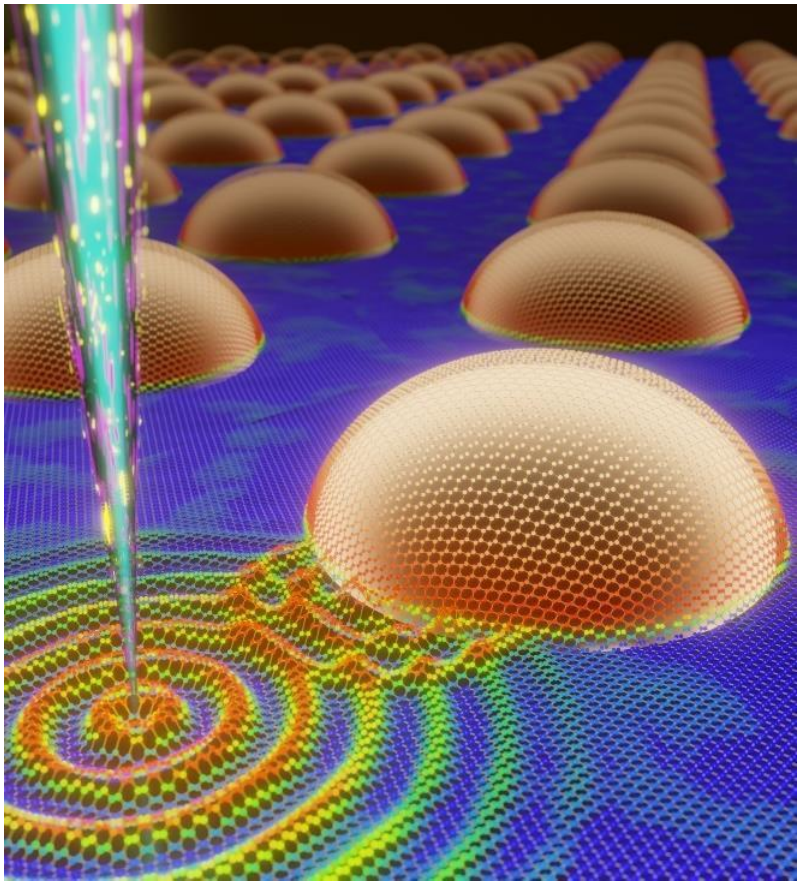

Virtual Meeting November 9-10, 2022

U.S. DEPARTMENT OF ENERGY | Office of Science

Office of Basic Energy Sciences Materials Sciences and Engineering Division

On the Cover

A beam of electrons generates vibrational waves in a crystal lattice that are then reflected by quantum dots. A nanoscale electron imaging method has been developed to reveal the dynamics of collective vibrations of atoms at the interface between two semiconducting materials, and their reflections dependent on the abruptness of interfaces. Work published in *Nature* **606**, 292 (2022).

***Courtesy**: Xiaoqing Pan, University of California, Irvine*

Foreword

This volume comprises the scientific content of the 2022 Electron and Scanning Probe Microscopies Principal Investigators' (PIs) Meeting sponsored by the Materials Sciences and Engineering Division (MSED) in the Office of Basic Energy Sciences (BES) of the U. S. Department of Energy (DOE). The meeting, held on November 9-10 virtually through Zoom and Gathertown, is the ninth biennial meeting in the Electron and Scanning Probe Microscopies (ESPM) area organized by BES. The purpose of the meeting is to bring together researchers funded in this core research area, to facilitate the exchange of new results and research highlights, to foster new ideas and collaborations among the participants, and to discuss how to advance electron and scanning probe microscopy, spectroscopy, and associated theoretical tools, in order to address forefront scientific challenges. The meeting also affords BES program managers an opportunity to assess the state of the entire program collectively on a periodic basis, to chart future directions and to identify new programmatic needs.

The Electron and Scanning Probe Microscopies Core Research Activity supports basic research in materials sciences using advanced electron and scanning probe microscopy and related spectroscopy techniques to understand the atomic, electronic, and magnetic structures and properties of materials. This activity also supports the development of new methods and techniques to advance basic science and materials characterizations for energy applications. The goal is to develop a fundamental understanding of materials, including quantum phenomena, through advanced microscopy, spectroscopy, and the associated theoretical tools. Topical areas highlighted in this year's meeting include cryogenic electron microscopy, two-dimensional and energy materials, quantum phenomena and microscopy, data science, and advanced microscopy and spectroscopy methods. This PI meeting features more poster sessions in virtual format using Gathertown in addition to oral presentations in live Zoom sessions, with the intent to provide enhanced PI interactions.

I would like to thank all the meeting attendees for their active participation and for sharing their ideas and new research results, which bring fresh insights for the continued development of this field and its value to DOE. Special thanks go to all session moderators. My sincere thanks also go to Teresa Crockett of BES and Tia Moua and her colleagues at the Oak Ridge Institute of Science and Education for their excellent work providing all the logistical support for the meeting.

Jane Zhu
Program Manager
Electron and Scanning Probe Microscopies
Materials Sciences and Engineering Division
Office of Basic Energy Sciences
U. S. Department of Energy

Table of Contents

Agenda

2022 Electron and Scanning Probe Microscopies
Virtual Principal Investigators' Meeting
November 9-10, 2022

All times are Eastern Time

Wednesday, November 9

10:45 – 11:00 AM Zoom *Log in*

11:00 - 11:15 Welcome and Introductory Remarks
Jane Zhu, Program Manager, *BES Electron and Scanning Probe Microscopies*

11:15 – 11:30 Materials Sciences and Engineering Division Update
Andy Schwartz, Division Director, *MSED, DOE-BES*

Oral Session 1 Cryogenic Electron Microscopy
Chair: **Shirley Meng**, University of California San Diego (University of Chicago)

11:30 – 11:45 **Amanda Petford-Long**, Argonne National Laboratory
BES Roundtable Report: Research Opportunities in the Physical Sciences Enabled by Cryogenic Electron Microscopy

11:45 – 12:00 **Yi Cui**, SLAC National Accelerator Laboratory
Developing Cryogenic Electron Microscopy for Electrochemical Energy Materials

12:00 – 12:15 **Nitash Balsara,** Lawrence Berkeley National Laboratory
Atomic- and Meso-Scale Electron Microscopy of Soft Matter

12:15 – 12:30 **Miaofang Chi,** Oak Ridge National Laboratory
Understanding Atomic and Mesoscopic Phenomena in Quantum Materials using Cryogenic STEM and Machine Learning Powered Data Analysis

12:30 – 12:55 **25-Minute Break**

12:55 – 1:00 **Poster Introduction**

1:00 – 2:20 **Poster Session 1**

2:20 – 2:30 **10-Minute Break**

Oral Session 2 2D Materials
Chair: **Abhay Pasupathy**, Brookhaven National Laboratory

2:30 – 2:45 **Ali Yazdani**, Princeton University
Probing Correlated Superconductors and Their Phase Transitions on the Nanometer Scale

2:45 – 3:00 **David Goldhaber-Gordon**, SLAC National Accelerator Laboratory
Beyond interlayer twist: Hidden control parameters for Van der Waals heterostructure

3:00 – 3:15 **Charudatta Phatak**, Argonne National Laboratory
Emergent Behavior in Nanoscale Functional Heterostructures

3:15 – 3:30 **Pinshane Huang**, University of Illinois at Urbana-Champaign
Deep learning studies for massive, atom-by-atom studies of atomic structure and rearrangements in two-dimensional materials

3:30 – 3:55 **25-Minute Break**

3:55 – 4:00 **Poster Introduction**

4:00 – 5:20 **Poster Session 2**

Thursday, November 10, 2022

10:45 – 11:00 a.m. Zoom *Log In*

11:00 - 11:05 **Welcome to Day 2**

Oral Session 3 Quantum Phenomena and Microscopy
Chair: **Amir Yacoby**, Harvard University

11:05 – 11:20 **Ben Lawrie**, Oak Ridge National Laboratory
Multiscale Quantum and Classical Microscopy for Superconducting Quantum Systems

11:20 – 11:35 **Weida Wu**, Rutgers University
Visualizing emergent phenomena in topological and quantum materials

11:35 – 11:50 **Ilija Zeljkovic**, Boston College
Visualizing the magnetic structure and domain formation using spin-polarized scanning tunneling microscopy and spectroscopy

11:50 – 12:05 **Keji Lai**, University of Texas at Austin
Multi-stimuli Nanoscale Conductivity Imaging of Strongly Correlated Materials

12:05 – 12:20 **Yimei Zhu,** Brookhaven National Laboratory
Unraveling Charge and Lattice Correlations and Exploring New Imaging Capabilities for Quantum Matter

12:20 – 12:45 **25-Minute Break**

12:45 – 12:50 **Poster Introduction**

12:50 – 2:10 **Poster Session 3**

2:10 – 2:20 **10-Minute Break**

Oral Session 4 Advance Microscopy and Energy Materials

Chair: Chair: **David Masiello**, University of Washington

2:20 – 2:35 **Xiaoqing Pan**, University of California, Irvine
Probing Exotic Vibrational States and Emergent Phonon Phenomena at Interfaces by Vibrational Electron Microscopy

2:35 – 2:50 **Pramod Reddy**, University of Michigan
Exploring Energy Conversion and Non-Equilibrium Carrier Distributions at the Nanoscale via Novel Scanning Probe Approaches

2:50 – 3:05 **Haimei Zheng**, Lawrence Berkeley National Laboratory
Liquid Cell Electron Microscopy: Heterogeneity and Fluctuations at Solid-Liquid Interfaces

3:05 – 3:20 **Chong-Yu Ruan**, Michigan State University
Quantum metastable materials and controls using pump-probe ultrafast electron microscopy

3:20 – 3:35 **David Ginger**, University of Washington
Probing Fast Local Photodynamics in Halide Perovskite Semiconductors: A Robust Regression Neural Network for Extracting Dynamics

3:35 – 4:00 **25-Minute Break**

4:00 – 4:05 **Poster Introduction**

4:05 – 5:25 **Poster Session 4**

Closing Session

5:25 – 5:40 **Closing Remarks - Jane Zhu, BES**

5:40 PM **Meeting Adjourns**

Poster session 1

Wednesday, November 9, 1:00 – 2:20 PM

1.1 **Abhay Pasupathy and Kazuhiro Fujita,** Brookhaven National Laboratory
Spectroscopic Visualization of Emergent Quantum Phenomena

1.2 **Amanda Petford-Long**, Argonne National Laboratory
Cryogenic Lorentz transmission electron microscopy of van der Waals materials

1.3 **Ben Lawrie, Eugene Dumitrescu, Gabor Halasz, Matt Brahlek, Chengyun Hua, Petro Maksymovych**, Oak Ridge National Laboratory
Multiscale Quantum and Classical Microscopy for Superconducting Quantum Systems

1.4 **David Masiello**, University of Washington
Optically Stimulated Electron Energy Gain/Loss Nanospectroscopy with Transverse Phase-Structured Electron Beams

1.5 **Greg Fuchs**, Cornell University
Magneto-thermal microscopy of complex topological spin textures

1.6 **Markus Raschke,** University of Colorado
Nano-optical imaging, spectroscopy, and control of quantum materials

1.7 **Matthew Yankowitz**, University of Washington
Atomic-scale characterization of strain-tunable moiré quantum materials

1.8 **Miaofang Chi, Andy Lupini, Christopher T Nelson, Joy Chao, Jordan Hatchel**, Oak Ridge National Laboratory
Understanding Atomic and Mesoscopic Phenomena in Quantum Materials using Cryogenic STEM and Machine Learning Powered Data Analysis

1.9 **Nitash Balsara, Xi Jiang, Andrew Minor, Brooks Abel, David Prendergast,** Lawrence Berkeley National Laboratory
Atomic- and Meso-Scale Electron Microscopy of Soft Matter

1.10 **Shirley Meng**, University of California San Diego (University of Chicago)
Probing solid-solid interfaces and phase changes with cryogenic and in situ analytical electron microscopy

1.11 **Yi Cui, Wah Chiu, Jennifer Dionne, Paul McIntyre, Michael Schmid, and Arunava Majumdar**, SLAC National Accelerator Laboratory
Developing Cryogenic Electron Microscopy for Electrochemical Energy Materials

Poster session 2

Wednesday, November 9, 4:00 – 5:20 PM

2.1 **Ali Yazdani**, Princeton University
Probing Correlated Superconductors and Their Phase Transitions on the Nanometer Scale

2.2 **Charudatta Phatak,** Argonne National Laboratory
Emergent Behavior in Nanoscale Functional Heterostructures

2.3 **David Goldhaber-Gordon, Marc Kastner, Hari Manoharan, Joseph Orenstein**, SLAC National Accelerator Laboratory
Beyond interlayer twist: Hidden control parameters for Van der Waals heterostructures

2.4 **Guangxin Ni,** Florida State University
Nano-polaritonics of graphene-based twisted heterostructures

2.5 **Huolin Xin**, University of California, Irvine
Machine Learning-Enabled Advanced Electron Microscopy for Resolving Chemical Inhomogeneity and Materials Dynamics

2.6 **Kai He**, University of California, Irvine
Cryogenic Electron Microscopy and Spectroscopy for Topological Spin Textures in Two-Dimensional van der Waals Magnetic Materials

2.7 **Lian Li**, West Virginia University
Tuning quantum paramagnetism and d-wave superconductivity in single layer Fe-chalcogenides by chemical pressure

2.8 **Peter Sutter and Eli Sutter**, University of Nebraska-Lincoln
Tunable Few-Layer van der Waals Crystals and Heterostructures as Emerging Energy and Quantum Materials

2.9 **Pinshane Huang and Bryan Clark**, University of Illinois at Urbana-Champaign
Deep learning studies for massive, atom-by-atom studies of atomic structure and rearrangements in two-dimensional materials

2.10 **Suzanne te Velthuis,** Argonne National Laboratory
Magneto-Optic Kerr Effect Microscopy of Magnetic Heterostructures

2.11 **Anshul Kogar**, University of California – Los Angeles
Ultrafast dynamics of correlated insulators

Poster session 3

Thursday, November 10, 12:50 – 2:10 PM

3.1 **Amir Yacoby and Jarillo-Herrero, Pablo**, Harvard University and MIT
Transport and Imaging of Mesoscopic Phenomena in Novel Low-Dimensional Materials

3.2 **Ilija Zeljkovic**, Boston College
Visualizing the magnetic structure and domain formation using spin-polarized scanning tunneling microscopy and spectroscopy

3.3 **Jay Gupta, Roland Kawakami and Michael Flatté**, Ohio State University and University of Iowa
Probing intrinsic and extrinsic exchange coupling in magnetic topological insulators

3.4 **John Miao**, University of California, Los Angeles
Three-Dimensional Structure Determination of Non-Crystalline Materials at the Single-Atom Level

3.5 **Keji Lai,** University of Texas at Austin
Multi-stimuli Nanoscale Conductivity Imaging of Strongly Correlated Materials

3.6 **Sokrates Pantelides,** Vanderbilt University
Combining microscopy and quantum calculations to unveil nanostructure properties

3.7 **Susanne Stemmer,** University of California, Santa Barbara
Probing Local Symmetry Breaking in Quantum Matter

3.8 **Weida Wu,** Rutgers University
Visualizing emergent phenomena in topological and quantum materials

3.9 **Yimei Zhu, Lijun Wu, Junjie Li, and Spencer Reisbick**, Brookhaven National Laboratory
Unraveling Charge and Lattice Correlations and Exploring New Imaging Capabilities for Quantum Matter

3.10 **Yuzhang Li**, University of California, Los Angeles
Cryo-EM imaging battery liquid-solid interfaces

3.11 **Stephen Jesse, O. Dyck, K. Kelley, C. Nelson, A. Lupini, M. Yoon, D. Englund, P. Narang**, Oak Ridge National Laboratory, MIT, UCLA
Atomic Manipulation Using Electron Microscopes to Build and Better Understand Material Systems for Quantum Information Science

Poster session 4

Thursday, November 10, 4:05 – 5:25 PM

4.1 **Sandra Biedron,** University of New Mexico
Data-Science Enabled, Robust and Rapid MeV Ultrafast Electron Diffraction Instrument System to Characterize Materials Including for Quantum and Energy Applications

4.2 **Ben Feldman,** Stanford University
Single-electron transistor microscopy of synthetic correlated quantum materials

4.3 **Chong-Yu Ruan,** Michigan State University
Nonthermal control of excited quantum materials

4.4 **David Ginger,** University of Washington
Data-Driven Multimodal Scanning Probe Microscopy for Understanding Energy Materials

4.5 **Haimei Zheng, Peter Ercius, Emory Chan, Lin-Wang Wang**, Lawrence Berkeley National Laboratory
Liquid Cell Electron Microscopy: Heterogeneity and Fluctuations at Solid-Liquid Interfaces

4.6 **Mark Oxley, A. R. Lupini, C. T. Nelson, S. V. Kalinin, M. Chi,** Oak Ridge National Laboratory
Applications of Machine Learning to Scanning Transmission Electron Microscopy

4.7 **Myung-Geun Han and Yimei Zhu**, Brookhaven National Laboratory
Direct Probing Charge and Spin Behaviors in Ferroic Materials

4.8 **Peter Crozier**, Arizona State University
Local Probing of Light Induced Excitations of Electronic and Photonic Modes in Oxide Nanoparticles

4.9 **Pramod Reddy and Edgar Meyhofer**, University of Michigan
Exploring Energy Conversion and Non-Equilibrium Carrier Distributions at the Nanoscale via Novel Scanning Probe Approaches

4.10 **Xiaoqing Pan**, University of California, Irvine
Probing Exotic Vibrational States and Emergent Phonon Phenomena at Interfaces by Vibrational Electron Microscopy

Laboratory
Abstracts

Atomic- and Meso-Scale Electron Microscopy of Soft Matter

Nitash Balsara[1,3], Xi Jiang[1], Andrew Minor[2,4], Brooks Abel[1,3], David Prendergast[2]

[1]Materials Sciences Division and [2]Molecular Foundry, Lawrence Berkeley National Laboratory, Berkeley, CA 94720; [3]College of Chemistry, and [4]Department of Materials Science and Engineering, University of California, Berkeley, CA 94720

Keywords: Electron microscopy, atomic-scale, soft materials, 3-D imaging

Research Scope

The purpose of this program is to push the boundaries of electron microscopy of radiation sensitive soft materials and thereby uncover the fundamental interactions and processes that govern structure formation in these systems from atomic to micrometer length scales. The main barrier of retrieving the atomic-scale structural information of soft materials is electron beam damage. Our mission is to combine atomic-scale and mesoscale theoretical models with atomic-scale cryogenic transmission electron microscopy (cryo-TEM) images and mesoscale four-dimensional scanning transmission electron microscopy (4D-STEM) data to elucidate the factors that govern the self-assembly of soft matter. Our cryo-TEM experiments were conducted on crystalline nanostructures formed by self-assembly of amphiphilic peptoid molecules and the ion-conducive diblock copolymers in thin films. We demonstrate the application of our techniques to capture the 3-D information of ordered molecules at the atomic level and reveal the roles of various interactions in the structure–property relationships in synthetic soft systems. Preliminary 4D-STEM data on the same systems are being collected and will be presented at the meeting.

Recent Progress

A fundamental challenge in materials science is to understand how different atomic-level interactions affect the structures of self-assembled synthetic polymers and other forms of soft matter. Here, we synthesized sequence-defined polypeptoids with tunable terminus and side chain properties. These polypeptoids form free-floating crystalline 2-D nanosheets and 3-D fibers. These atomic details are inaccessible by conventional scattering techniques. Using a combination of 2-D and 3-D atomic imaging and molecular dynamics simulations, we observed how these structures respond to various interactions at the atomic-length scale [1].

In Figure 1, we compare the crystal motifs in the nanosheets formed by two diblock polypeptoids [2]. The first polypeptoid consists of a hydrophilic poly-N-2-(2-(2-methoxyethoxy) ethylglycine) (Nte) block and a hydrophobic N-(2-phenylethyl)glycine (Npe) block. The second polypeptoid comprises the same Nte block but a hydrophobic poly-N-(2-phenylethyl)glycine (pNbrpe) block with bromine atoms at the para position phenylethyl side chains. They are referred as Nte_4-Npe_6 and Nte_4-$N4Brpe_6$, respectively. The morphologies and high-resolution images obtained by averaging the projections through the a-c plane of the two systems are shown in

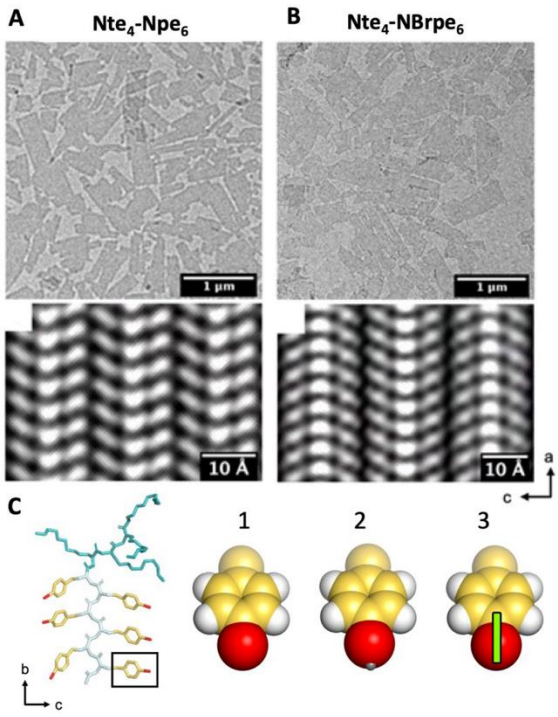

Figure 1. TEM images show the morphology of nanosheets (top) and the averaged experimental cryo-TEM images (bottom) of the nanosheets comprising A. Nte4-Npe6 and B. Nte4-N4Brpe6 C. An atomic model of Nte4-N4Brpe6. The phenyl sidechain (black square) is enlarged in panels 1-3. Panel 1: without the positively charged extra point. Panel 2: with the extra point in gray. Panel 3: same as 2 with a green line segment collinear with the C-Br bond.

Figures 1A and B. The geometry of the σ-hole and its relationship to the C-Br bond in N4Brpe6 is clarified in Figure 1C. The non-brominated polypeptoid exhibits the parallel configuration while the brominated polypeptoid exhibits the antiparallel configuration. The atomic-scale images enable direct evaluation of the importance of the halogen bond, which is obtained when the positive σ-hole of one halogen atom is near the electronegative equator of a neighboring.

Significant insight into the importance of σ-holes was obtained from MD simulations. Two simulations were run: one in which neighboring polypeptoids were initially arranged in a parallel configuration and a second in an antiparallel configuration. Then, the simulation was started, and the molecules were allowed to relax. In one set of simulations, we used standard interatomic potentials that only account for the electronegative nature of Br atoms. In these simulations, there was no change in the chain arrangements during either simulation, which were typically run for 80 ns – molecules in simulation boxes starting in the parallel configuration remained parallel, while molecules in simulation boxes starting in the perpendicular configuration remained perpendicular. In addition, the nonbonded internal energies (defined as the sum of electrostatic and van der Waals contributions) of the two relaxed systems were comparable. Entirely different results were obtained when a massless positive charge was attached to the Br atom to account for the σ-hole. The peptoid nanosheet disassembles when placed initially in the parallel configuration at 7 nanoseconds. In contrast, the polypeptoids that were initially placed in the antiparallel configuration with the σ-hole remains stable after 50 nanoseconds. By validating atomic-scale simulations with atomic-scale images, we can discern the presence or absence of weak interactions. We aim to leverage this combination of imaging and simulations to explore other intra and intermolecular interactions.

We explored the structure of fibrils formed by a block copolypeptoid with a poly-N-decylglycine (Ndc) block and a hydrophilic poly-N-2-(2-(2-methoxyethoxy)ethoxy) ethylglycine (Nte) block. It is referred as H-Ndc_{10}-Nte_{10}. Figure 2 shows the chemical structure of this polymer and the nanofibrils formed when 4M urea is added to the aqueous phase. The fibrils are also formed in the absence of urea, but they are less ordered. The structural details of H-Ndc10-Nte10 nanofibrils were resolved by using single particle analysis. The results are shown in Figure 2. It is noteworthy that this is the first time individual peptoid backbone is directly observed using TEM. The distance between the adjacent repeating unit along polymer backbone (*b* direction) is 5.6 Å, indicating the polymer adopt a universal extended *cis* configuration in the crystal lattice.[3] The combined information from top and side view images reveals the polymer adopt an all-*cis* extended board-like chain packing geometry.

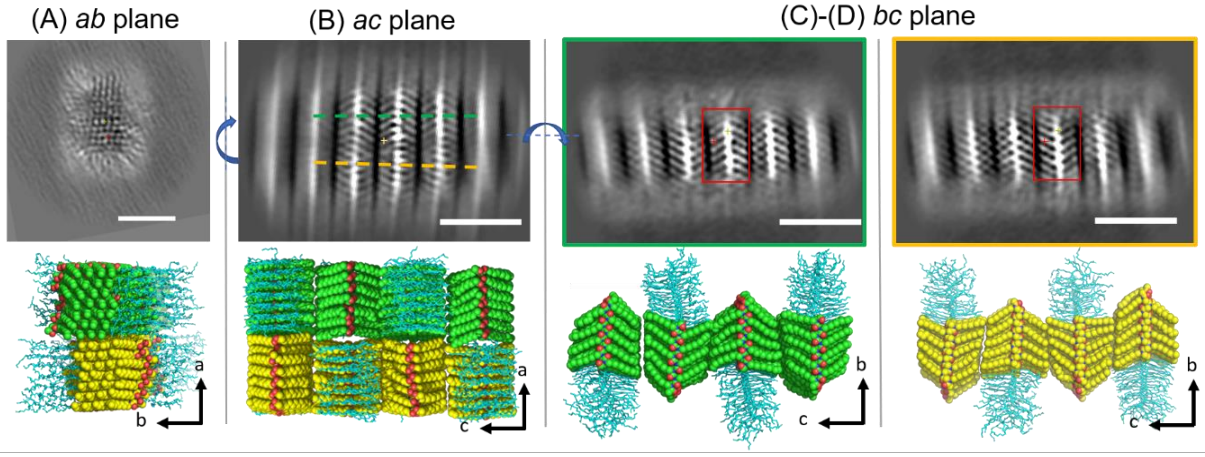

Figure 2. Slices from the cryo-TEM 3D reconstructions of the H-Ndc_{10}-Nte_{10} nanofibrils with 4M urea (top row) and the MD simulation results (bottom row) **A**. *ab* cross-section (end view), **B**. *ac* cross-section (top view), The top view shows the fiber is composed of two identical segments with inverted symmetry marked in yellow and green respectively. **C** and **D** are side view slices of these two segments projected from the positions marked with green and yellow dash lines in the top view slice in B. The scale bar is 5 nm. The thickness of each cross-section slice is 3.5 Å.

Four-dimensional scanning transmission electron microscopy (4D-STEM) is a flexible and powerful approach to the elucidate structure of a wide variety of materials [4]. Much of the 4D-STEM work in the literature is on samples that are stable under electron beam [5]. We have outlined key parameters necessary for applying 4DSTEM to beam sensitive soft materials. In this technique, at each X and Y probe position on the specimen, a 2D diffraction pattern is acquired with a pixelated camera. The two reciprocal space dimensions of the diffraction pattern together with the real space probe positions are the four dimensions referred to in the term "4D-STEM" (Figure 3A). It faces similar challenges to those found in cryo-TEM because the structures are easily damaged by the electron beam. Holding the sample at cryogenic temperatures minimizes diffusion of radicals and the resulting damage and disorder caused by the electron beam. Low-dose imaging modes for 4D-STEM can be explored empirically for soft materials by varying the experimental parameters that contribute to the total electron fluence as shown in Figures 3B to D. Through this program, we explored the optimized low-dose conditions for minimizing the beam damage of an important class of polymeric semiconductors where π-π stacking facilitates electron transport; results are reported in [5].

To summarize, we have applied and developed imaging methods based on both transmission and scanning transmission electron microscopy to study the intermolecular interactions in crystalline-driven self-assembled soft matter at unprecedented spatial resolution.

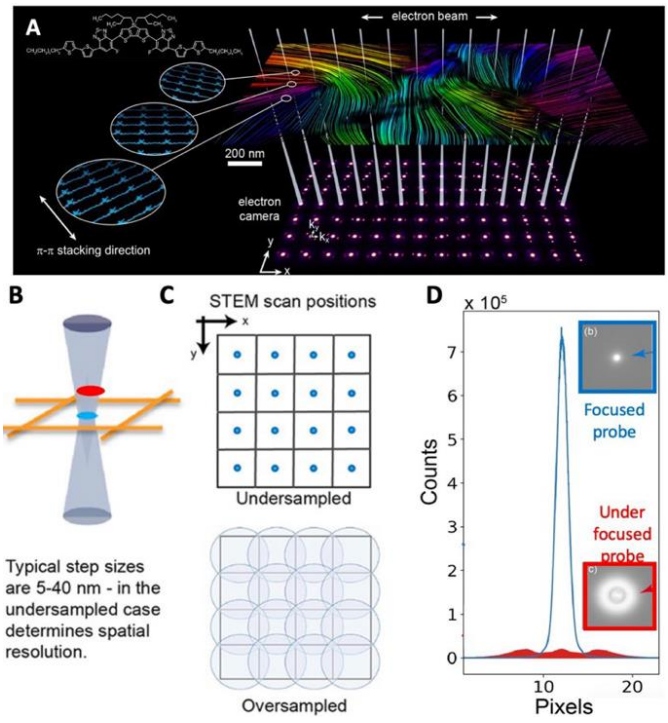

Figure 3. Low-dose 4D-STEM experiment. **A**. Schematic of focused beam stepping across organic small molecule shown in upper left. π–π stacking of the conjugated polymer backbones is represented by colored lines. **B**. Focus (blue) and defocused (red) states. **C**. Probe intersecting sample determines exposure area, typical step sizes of 5–40 nm can result in either undersampled or oversampled region of interest **D**. Line scan through focused (blue) and defocused (red) real space image of focused probe and defocused probe (insets).

Future Plans

We have demonstrated the atomic-scale 2-D imaging of halogenated polypeptoid crystalline membrane in previous study where the importance of side chain σ-holes on crystal motifs was revealed. Cryo-TEM and single particle analysis of nanofibrils enabled the 3-D reconstruction at near atomic-level. It thus illustrated the role that a bridging agent plays in the self-assembly process. In addition to the self-assembled amphiphilic diblock polypeptoids, we will build 3D crystals comprising homo polypeptoid with tunable capping groups and side chains. Micro electron diffraction (micro-ED) will be used to resolve the Angstrom-level structural changes in sample structure.

4D-STEM study will be extended to the ion-conductive diblock copolymers with semicrystalline blocks, such as polystyrene-*b*-poly(ethylene oxide) oxide (PS-*b*-PEO). The effect of salt on the crystalline structures in the PEO domain as functions of concentration, temperature and spatial distribution can be revealed using 4D-STEM in future study. In addition, we aim to push the resolution of soft matter imaging of conventional polymers. A benchmark of soft matter imaging will be established at atomic level by comparing the conventional TEM images with direct phase information and the 4DSTEM images with computed phase information. The ultrafast 4D camera developed in Molecular Foundry will be used to obtain the center-of-mass and ptychographic reconstructions using 4DSTEM data set obtained from for the PS-*b*-PEO single crystals. The ultra-short dwell time allows us to minimize beam damage even at room temperature with enhanced phase contrast of soft materials.

References

1. S. T. Xuan, X. Jiang, R. K. Spencer, N. K. Li, D. Prendergast, N. P. Balsara and R. N. Zuckermann, "Atomic-level engineering and imaging of polypeptoid crystal lattices", Proceedings of the National Academy of Sciences of the United States of America, 2019, 116 (45), 22491-22499

2. M. Seidler, N. K. Li, X. Luo, S.T. Xuan, R. N. Zuckermann, N. P. Balsara, D . Prendergast, and X Jiang "Importance of the Positively Charged σ-Hole in Crystal Engineering of Halogenated Polypeptoids" J. Phys. Chem. B 126, 2022 (22), 4152–4159

3. D.R. Greer, M.A. Stolberg, J. Kundu, R. K. Spencer, T. Pascal, D. Prendergast, N. P. Balsara, R. N. Zuckermann, Universal Relationship between Molecular Structure and Crystal Structure in Peptoid Polymers and Prevalence of the cis Backbone Conformation. Journal of the American Chemical Society 2018, 140 (2), 827-833.

4. C. Ophus, Four-Dimensional Scanning Transmission Electron Microscopy (4D-STEM): From Scanning Nanodiffraction to Ptychography and Beyond. Microsc Microanal 2019, 25 (3), 563-582

5. K. C. Bustillo. S. E. Zeltmann, M. Chen, J. Donohue, J. Ciston, C. Ophus, A. M. Minor, 4D-STEM of Beam-Sensitive Materials. Accounts Chem Res 2021, 54 (11), 2543-2551

Publications

1. X. Jiang, J. Sun, R. N. Zuckermann and N. P. Balsara, "Effect of hydration on morphology of thin phosphonate block copolymer electrolyte membranes studied by electron tomography", Polymer Engineering and Science 61 (4), 1104-1115 (2021).

2. X. Jiang, S. T. Xuan, R. N. Zuckermann, R. M. Glaeser, K. H. Downing and N. P. Balsara, "Minimizing Crinkling of Soft Specimens Using Holey Gold Films on Molybdenum Grids for Cryogenic Electron Microscopy", Microscopy and Microanalysis 27 (4), 767-775 (2021).

3. X. Jiang and N. P. Balsara, "High-Resolution Imaging of Unstained Polymer Materials", ACS Applied Polymer Materials 3 (6), 2849-2864 (2021).

4. K. C. Bustillo, S. E. Zeltmann, M. Chen, J. Donohue, J. Ciston, C. Ophus and A. M. Minor, "4DSTEM of Beam-Sensitive Materials", Accounts of Chemical Research 54 (11), 2543-2551 (2021).

5. S. T. Xuan, X. Jiang, N. P. Balsara and R. N. Zuckermann, "Crystallization and self-assembly of shape-complementary sequence-defined peptoids", Polymer Chemistry 12 (33), 4770-4777 (2021). 10.1039/d1py00426c

6. M. Seidler, N. K. Li, X. Luo, S.T. Xuan, R. N. Zuckermann, N. P. Balsara, D . Prendergast, and X Jiang "Importance of the Positively Charged σ-Hole in Crystal Engineering of Halogenated Polypeptoids" J. Phys. Chem. B 126, (22), 4152–4159, (2022)

Understanding Atomic and Mesoscopic Phenomena in Quantum Materials using Cryogenic STEM and Machine Learning Powered Data Analysis

Miaofang Chi, Andy R. Lupini, Christopher T. Nelson, Joy Chao, Jordan Hatchel

Center for Nanophase Materials Sciences, Oak Ridge National Laboratory, TN 37831

Keywords: Cryogenic, Scanning Transmission Electron Microscopy, Monochromated EELS, Quantum materials, Machine learning

Research Scope

Rich functionalities of strongly correlated quantum materials emerge from the interplay between the electronic, orbital, lattice, and spin degrees of freedom that often lead to complex structural and electronic phenomena spanning atomic to mesoscopic scales. In many cases, these phenomena are associated with symmetry breaking, local frozen disorder, or correlated structural or electronic transitions. However, the emergence of macroscopic quantum phenomena and the role of individual local disorders often remain unclear, partially due to limited real-space investigations of local features and their evolutions at a sufficient spatial resolution upon the emergence of interesting quantum phenomena. This project aims to unravel the underpinning static and dynamic structures, local functionalities, and collective phenomena in quantum materials by advancing and utilizing new STEM imaging and spectroscopy techniques. We focus on directly probing critical spatial variations in lattice, spin, charge, chemistry, and most critically, their correlations with each other, which are often challenging for peer characterization techniques such as neutron, X-ray, and scanning probing microscopy.

Recent progress

In the past two years, we have focused on two primary challenges in this project. Our efforts are aimed at (1) advancing cryogenic atomic-resolution imaging and vibrational electron energy loss spectroscopy (EELS) to study quantum phase transitions at relevant temperatures; and (2) harnessing the power of machine learning methods to extract the chemistry and physics of quantum materials embedded in large complex STEM datasets. The first effort is necessary because although atomic resolution STEM imaging and spectroscopy can now be routinely applied in S/TEM labs, there are experimental challenges in robustly probing atomic and electronic structural changes across transition temperatures, primarily due to the instability of commercial cryogenic stages. Techniques such as spectrum imaging, 4D-STEM and in situ imaging are even more challenging at cryogenic temperatures since they often require an extended acquisition time. We have been working with vendors to advance the stability of liquid nitrogen-cooled stages (as part of a collaboration with the ECA headed by Chi) and with data scientists in ORNL to develop algorithms for STEM acquisitions to compensate for “instability” challenges. The second effort is motivated by the complexity of structural and chemical information encoded in STEM datasets. Effectively revealing the physically meaningful information embedded in STEM image and spectroscopy datasets, especially multi-dimensional large datasets that involve correlated structural, chemical, and bonding features often obtained for quantum materials, has been a

challenge in microscopy. Notable progress has been made in both efforts. Initial applications of these methods in studying quantum materials and their phenomena have been performed.

Phase transitions in topological materials

The presence of unusual phases in many-layered transition-metal chalcogenides often introduce rich electronic characteristics and exotic physical properties, making them ideal systems to explore new controllable quantum phases. For example, the 1T' phase of $MoTe_2$ undergoes a phase transition into the orthorhombic T_d phase at about 250 K. Although these two phases share the same in-plane structure, The vertical stacking order in the T_d phase belongs to the non-centrosymmetric space group Pmn21. In contrast, the 1T' phase with distorted stacking belongs to the centrosymmetric space group P21/m. T_d was predicted to show type-II Weyl semimetal characteristics, whereas the centrosymmetric 1T' phase is topologically trivial. More interestingly, it was reported that topological phase transitions and unusual quantum transport emerge when a 1T' $MoTe_2$ crystal is thinned down to thin flakes. However, the exact thickness at which changes occur is still highly debated.

We aim to understand the thickness dependence of structural and physical property transitions in thin 1T' $MoTe_2$. Results of this work will reconcile the existing discrepancies in the field and provide insights into adapting topological behavior and plasmon modes via dimensional control. This work takes advantage of recently advanced atomic-scale cryogenic scanning transmission electron microscopy (STEM) imaging and monochromated electron energy loss spectroscopy (EELS) capabilities at ORNL. **Figure 1 a** show an atomic-resolution STEM-HAADF (high angle annular dark field) image of a 20 nm thin $MoTe_2$ flake taken at room temperature with a convergence angle of 28 mrad. It clearly exhibits the 1T' structure, matching well with the simulated STEM image along the [001] zone axis (**Fig. 1 c)**. The specimen was then cooled to 100 K, below the expected phase transition temperature (250 K). **Fig. 1 b** shows an image that is a sum of 10 fast-scan frames acquired consequentially to minimize the impact of stage drift and scanning

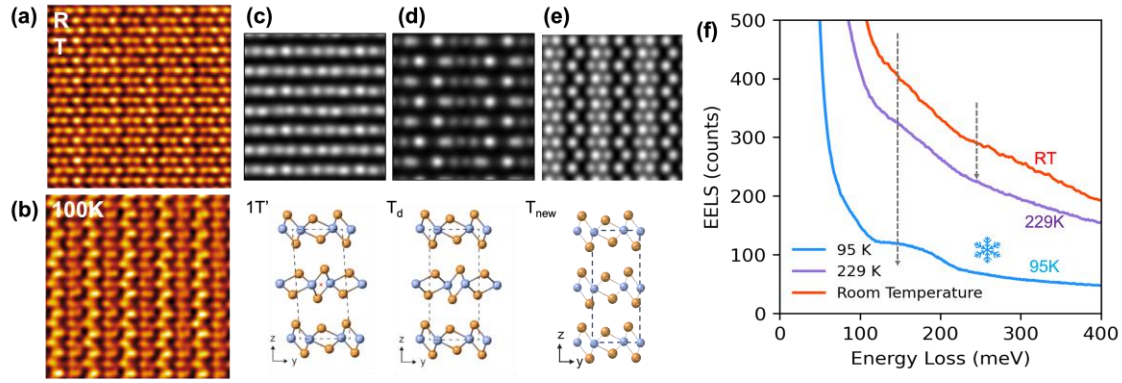

Figure 1. Phase transition and plasmon state evolution of thin-flake $MoTe_2$. Atomic resolution HAADF-STEM images along [001] at (a) RT and (b) 100 K reveal drastic lattice structural transformation. (c-e) HAADF Simulations showing that while thin $MoTe_2$ exhibits (c) 1T' structure at RT, the low T phase deviates from the (d) expected T_d phase. (e) A new low-T structure was proposed based on our experimental results. (f) Monochromated EELS reveals revolutions in plasmon excitations upon cooling.

noise. One observes apparent structural changes at the two temperatures, indicating a phase

transition at low temperature. The observed lattice structure at 100 K show obvious deviations from the simulated T_d phase (**Fig. 1 d)**, indicating that the structural evolution of a 20 nm flake does not behave the same as that of the bulk, which is a thickness many magnitudes larger. STEM simulations revealed that the low-T structural deviation most likely is due to an unpredicted layer shift (**Fig. 1 e**). These results indicate that the crystallographic transition in layered metal chalcogenides is thickness dependent. A direct correlation between physical properties and layer thickness is crucial in understanding the topological behavior of MoTe2 thin flakes.

The collective excitation of electrons due to their long-range Coulomb interaction, i.e., the plasmon, has attracted increasing attention in the field of topological materials recently. Due to their exotic electronic properties, various novel plasmons have been predicted in topological insulators and topological semimetals. Investigating plasmons can directly help to understand their Fermi surfaces. We have recently upgraded the monochromated aberration corrected Nion STEM at ORNL to enable LN2 cryogenic capabilities and installed an improved EELS spectrometer camera to allow the study of low temperature physics in 2D and layered systems. It allows us to detect plasmon and phonon excitations in materials with an energy resolution of 5 meV within a temperature range between 100 K to 1000 K. Plasma excitation transitions in a thin-flake MoTe2 as a function of temperature is shown in Fig. 1 f. Two distinctive plasmon peaks were observed at room temperature, at 170 meV (α) and ~ 280 meV (β) and respectively. Both become weaker as the specimen is cooled to 229 K. At 100 K, the plasma excitation α shows a much stronger signal with a slightly lower energy loss shift, while β nearly disappears. The excitation α is most likely dominated by the inter-band correlations between the topologically nontrivial bands and trivial bands in Td phase. It can be used as a signature feature to explore the thickness dependence of plasmon modes. Future studies will follow in this direction.

Low Latency Physical Parameterization by Neural Networks

Atomic-structure parameterization traditionally relies on either Fourier analysis methods or real-space atom finding and parametric fitting. Availability of this parameterization in near real-time would be advantageous for feedback at data collection in STEM experiments to identify features and reduce artifacts (e.g., mistilt). Further, low latency processing is a pre-requisite for scaling to automated STEM acquisition or to very large datasets. Neural networks have the potential for atom finding and local-neighborhood labeling. We have deployed a deep-convolutional neural network (DCNN) to perform the $Sm_xBi_{1-x}FeO_3$ parameterization of the above section. The DCNN can utilize the full image as the input with a sliding window for segmentation and the trained network has inference times of < 2s for an ~ 50,000 atom image, compared to ~ 31 min for the parametric fitting, which is far below the acquisition time of the image itself. The DCNN outputs are a good match as shown in the comparison of the P_{xy} polar-displacement parameter in **Fig. 2 a-b**.

High-local disorder typically maps onto a high-symmetry structure in geometrically frustrated systems. Physical interpretability of a NN recommends accounting for similar features in symmetry-allowed transformations, such as ferroelectric polarization or ferroelastic variants. We employed the use of a rotationally-invariant variational autoencoder (r-VAE) on the SmxBi1-xFeO3 dataset. An x = 0 dataset shown in Fig. 2 c-f illustrates the correct 90° spaced clusters output by the r-VAE corresponding to expected equivalent four-fold projections of the ferroelectric direction, as well as their equivalent spatial distributions (Fig. 2 d vs. 2 f). The latent space manifold (Fig. 2 g) contains only a single axis of the cation non-centrosymmetric distortion (offset of central cation) that characterizes this Pxy feature. This image analysis method can be applied to detect intrinsic lattice disorders and strains and measure their spatial distributions that are embedded in any STEM datasets.

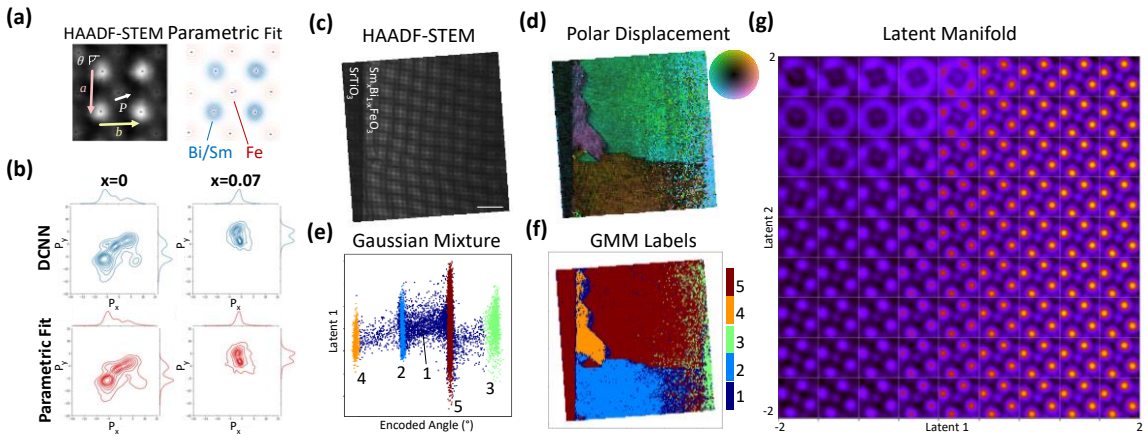

Figure 2. Parameterization from Parametric Fitting and Neural Networks (a) $Sm_xBi_{1-x}FeO_3$ example Gaussian fitting of HAADF-STEM and unit-cell neighborhood parameterization. (b) Comparative heat maps of Pxy distributions in x=0 and x=0.07 datasets for parametric fit and the DCNN output. (c-g) Rotationally invariant autoencoder. (c) Input x=0 HAADF-STEM dataset. (d) Pxy from parametric-fit parameterization. (e) Encoded angle output of r-VAE vs first latent variable shows expected 90° separation of Pxy directions. Colors correspond to gaussian mixture clustering with spatial distributions shown in (f). (g) The manifold for the 2-latent variable r-VAE for this dataset.

Future Work

Understand topological behavior and plasmon excitations of few-layer 2D transition-metal dichalcogenides

The intriguing properties of topological materials are tied to their non-trivial band-structure in momentum-space. In momentum-resolved monochromated EELS, we will utilize the simultaneous spatial, spectral, and momentum resolution to probe the band-structure of transition metal dichalcogenides, such as $MoTe_2$ in both the 1T' phase and the T_d phase. We will explore these properties on the same flakes to control for thickness effects. The ability to observe topological band structure in EELS is unprecedented, meaning that the reliable observation of the topological bands in monochromated EELS represents a significant breakthrough. Further, plasmon interactions between two dissimilar 2D materials often induce exotic physical phenomena. Given that the characteristic plasmon excitations in T_d and 1T' $MoTe_2$ are associated

with topological properties, we hypothesize that intriguing plasmonic interactions can be induced by layering $MoTe_2$ with 2D materials that have excitations at similar energies. We will start this exploration with heterostructures of h-BN and $MoTe_2$.

Explore the impact of strain and defects on exotic electronic states in quantum dots superlattice

Quantum dots, once epitaxially fused into superlattices, exhibit emergent electronic states that do not exist in individual quantum dots. These materials systems have been predicted to exhibit novel quantum transport properties, such as electronic minibands that facilitate high carrier mobility. However, although these materials are fundamentally limited by defects that occur between epitaxially fused QDs, the direct influence of defects on the local electronic structure is unknown. Heating is expected to release strain and reduce defects in the system. Therefore, we will probe electronic states in quantum dots superlattices, such as PbSe using monochromated EELS undergoing in-situ heating to understand the influence of strain and defects. Because these experiments provide correlated lattice and electronic structures, information about how different types of defects modify the local electronic structure can be expected. New electronic states are anticipated in the intermediate structures during annealing.

Physics-based latent 2D kernels

Currently existing spatial-order kernels are useful as proof-of-concept but simple in terms of physics-inspired latent constraints and input signals. Our goal is to extend towards higher dimensional and multimodal data with kernels closer to finite-element style energy functionals. Notably, systems known a-priori to exhibit non-trivial scalar and vector topologies are a prime target. A relevant example would be using a network to extract electric field and charge density information from high-convergence angle 4D-STEM data. This extraction can be achieved using constraints driving a latent variable to map to this parameter such that it will match the known physics. For example, an energy kernel implemented on the latent space might rely on the knowledge that it is non-trivial, exhibits high-divergence, minimal curl, and is expected to order in some manner to minimize electrostatic energy. Similar constructions can be made for magnetic fields (e.g., zero divergence), strain, chemical gradients, and other phenomena, opening new vistas for STEM imaging.

Publications (selected):

1. Y.M. Guo, S.V. Kalinin, H. Cai, K. Xiao, S. Krylyuk, A.V. Davydov, Q.Y. Guo, A.R. Lupini, Defect detection in atomic-resolution images via unsupervised learning with translational invariance, NPJ Computational Materials 7(1), 180 (2021). DOI: 10.1038/s41524-021-00642-1
2. S. M. P Valleti, R. Ignatans, S. V. Kalinin, and V. Tileli, Decoding the mechanisms of phase transitions from in situ microscopy observations, Small 18, 40 (2022), DOI: 10.1002/smll.202104318
3. M. Ziatdinov, N. Creange, X. Zhang, A. Morozovska, E. Eliseev, R. K. Vasudevan, I. Takeuchi, C. Nelson, and S. V. Kalinin, Predictability as a probe of manifest and latent physics: The case of atomic scale structural, chemical, and polarization behaviors in multiferroic Sm-doped BiFeO3, Appl. Phys. Rev. 8, 011403 (2021). DOI: 10.1063/5.0016792
4. M. P. Oxley, M. Ziatdinov, O. Dyck, A. R. Lupini, R. Vasudevan, and S. V. Kalinin, Probing atomic-scale symmetry breaking by rotationally invariant machine learning of multidimensional electron scattering, npj Comput. Mater. 7, 65 (2021). DOI: 10.1038/s41524-021-00527-3

5. K. M. Roccapriore, N. Creange, M. Ziatdinov, and S. V. Kalinin, Identification and correction of temporal and spatial distortions in scanning transmission electron microscopy, Ultramicroscopy 113337 (2021). DOI: 10.1016/j.ultramic.2021.113337
6. S. V. Kalinin, O. Dyck, S. Jesse, and M. Ziatdinov, Exploring order parameters and dynamic processes in disordered systems via variational autoencoders, Sci. Adv. 7, eabd5084 (2021). DOI: 10.1126/sciadv.abd5084
7. S. M. Prudhvi Valleti, Q. Zou, R. Xue, L. Vlcek, M. Ziatdinov, R. Vasudevan, M. Fu, J. Yan, D. Mandrus, Z. Gai, and S. V. Kalinin, Bayesian learning of Adatom interactions from atomically resolved imaging data, ACS Nano 15, 9649 (2021). DOI: 10.1021/acsnano.0c10851
8. S. V. Kalinin, A. R. Lupini, R. K. Vasudevan, and M. Ziatdinov, Gaussian process analysis of electron energy loss spectroscopy data: multivariate reconstruction and kernel control, npj Comput. Mater. 7, 154 (2021). DOI: 10.1038/s41524-021-00611-8
9. C. T. Nelson, A. Ghosh, M. Oxley, X. Zhang, M. Ziatdinov, I. Takeuchi, and S. V. Kalinin. Deep learning ferroelectric polarization distributions from STEM data via with and without atom finding. npj Comput. Mater. 7, 149 (2021). DOI: 10.1038/s41524-021-00613-6
10. S. V. Kalinin, M. Ziatdinov, J. Hinkle, S. Jesse, A. Ghosh, K. P. Kelley, A. R. Lupini, B. G. Sumpter, and R. K. Vasudevan, Automated and autonomous experiments in electron and scanning probe microscopy, ACS Nano 15, 8, 12604 (2021). DOI: 10.1021/acsnano.1c02104.

Developing Cryogenic Electron Microscopy for Electrochemical Energy Materials

Yi Cui [1,5], Wah Chiu [2,3,5], Jennifer Dionne [1], Paul McIntyre [1,7], Michael Schmid [5], and Arunava Majumdar [4]

[1]Department of Materials Science and Engineering, Stanford University, Stanford, CA 94305. [2]Department of Bioengineering, Stanford University, Stanford, CA 94305. [3]Department of Microbiology and Immunology, Stanford University School of Medicine, Stanford, CA 94305. [4]Department of Mechanical Engineering, Stanford University, Stanford, CA 94305. [5]Photon Science, SLAC National Accelerator Laboratory, Menlo Park, CA 94025. [6]Stanford Institute for Materials and Energy Sciences, SLAC National Accelerator Laboratory, CA 94025. [7]Stanford Synchrotron Radiation Laboratory, SLAC National Accelerator Laboratory, 2575 Sand Hill Road, Menlo Park, CA 94025.

Keywords: cryoEM, cryoET, dynamic electrochemical processes, electrochemical energy storage, battery

Research Scope

In the past decade, the development of cryo-EM technology by structural biologists have enabled near-atomic resolution imaging of sensitive biomolecules in their native state.[1,2] Cui and Chiu labs collaborated to adopt this technique for materials science and have demonstrated breakthrough results on first atomic resolution imaging of sensitive energy materials.[3–5] The focus of this research task under the FWP 100886 is to establish an integrated research program to explore the use of cryogenic electron microscopy (cryoEM) and tomography (cryoET) to characterize the spatial organization of atoms and molecules and the compositional and structural variations underlying dynamic chemical processes in an exciting family of electrochemical energy materials relevant to DOE missioned research. We develop cryogenic preservation techniques to freeze materials in operando under voltage bias to capture their authentic structural and chemical configuration and keep the samples frozen during the electron microscopy examination. We explore state of the art image processing methods to retrieve the 3D structure and chemical mapping of their constituents with high spatial and temporal resolution. We pursue advances and establishes cryoEM as a foundational technique for discovering and understanding fundamental aspects of electrochemical energy materials and devices.

Recent Progress

We leveraged the cryoEM methods to resolve several important yet unanswered scientific questions among the battery community. The rich information and fundamental findings of batteries at nanoscale in native states provide a better understanding of crucial failure mechanisms in batteries and introduce new discoveries in energy science.

Corrosion of lithium metal anodes during calendar aging and its microscopic origins

Rechargeable Li metal batteries must have long cycle life and calendar life (retention of capacity during storage at open circuit). Particular emphasis has been placed on prolonging the cycle life of Li metal anodes, but calendar aging is less understood. Here, we show that Li metal loses at least 2–3% of its capacity after only 24 hours of aging, regardless of the electrolyte chemistry. These losses of capacity during calendar aging also shorten the cycle life of Li metal batteries. CryoEM shows that chemical corrosion of Li and the continuous growth of the solid electrolyte interphase—a passivation film on Li—cause the loss of capacity. Fig. 1a shows a representative cryo-STEM image of Li with a conformal and thin 10 nm solid electrolyte interphase (SEI) after being freshly deposited in $LiPF_6$ (EC:DEC). The annular dark field (ADF) STEM image shows a low intensity core from the low atomic number of Li ($Z = 3$). The brighter intensity shell is attributed to the SEI and its C- and O-rich composition (Fig. 1a). This form of SEI is often called the compact SEI, as it exists as a thin film and is directly interfaced with Li. After Li anodes are aged in the electrolyte for 24 hours, the thickness of the compact SEI noticeably increases. A lower density layer grows above the initially formed SEI (Fig. 1b). By comparing electrolytes with different cyclability (Fig. 1e-g), we found that electrolytes with long cycle life do not necessarily form a solid electrolyte interphase with more resistance to chemical corrosion. So functional electrolytes must simultaneously minimize the rate of solid electrolyte interphase growth and the surface area of electrodeposited Li metal.

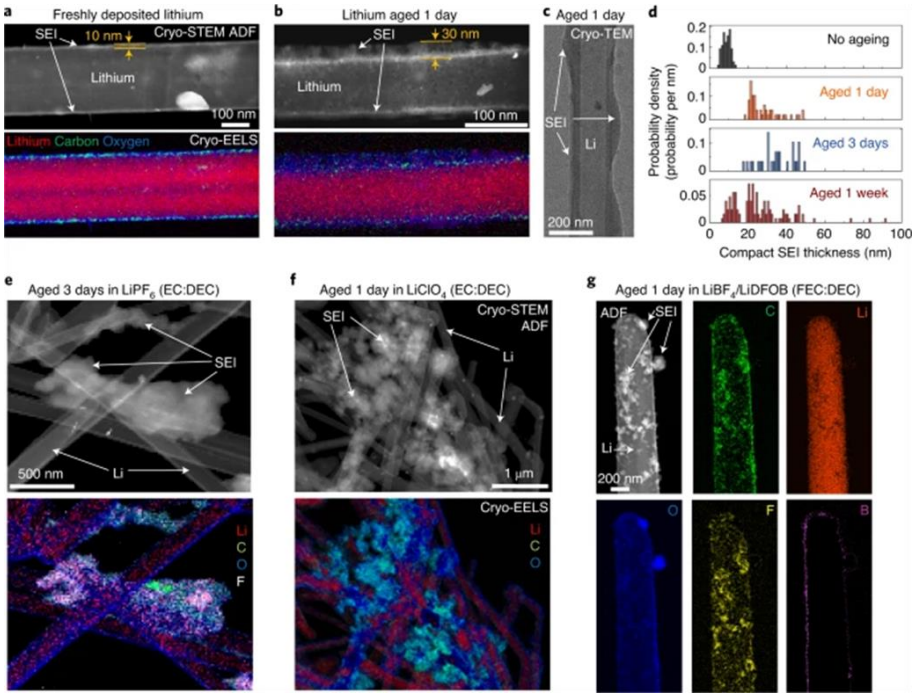

Figure 1: Cryo-(S)TEM mapping of SEI growth on Li metal during calendar ageing in both low- and high-performance electrolytes. a,b, Representative cryo-STEM ADF image and EELS map of freshly deposited Li (a) and Li aged for 24 hours in LiPF6 (EC:DEC) (b). c, Representative bright-field TEM image of a Li filament after calendar ageing in LiPF6 (EC:DEC). d, Histogram of the time-dependent thickness of the compact SEI. e–g, Cryo-STEM ADF images and EELS maps of a Li anode aged in LiPF6 (EC:DEC) (e), LiClO4 (EC:DEC) (f) and LiBF4/LiDFOB (FEC:DEC) (g) with representative examples of extended SEIs.

Swollen states of battery solid-electrolyte interphases (SEI) in native electrolyte environments

Although liquid-solid interfaces are foundational in broad areas of science, characterizing this delicate interface remains inherently difficult because of shortcomings in existing tools to access liquid and solid phases simultaneously at the nanoscale. This leads to substantial gaps in our understanding of the structure and chemistry of key interfaces in battery systems. In this work, we adapt a thin-film vitrification method to ensure the preservation of liquid electrolyte so that the samples taken for analysis using microscopy and spectroscopy better reflect the state of the battery during operation. A key finding is that the SEI is in a swollen state, in contrast to current belief that it only contained solid inorganic species and polymers. Such results are supported by nanoindentation experiments in liquid AFM from a mechanical perspective in electrolytes. The swelling behavior is dependent on electrolyte chemistry and is highly correlated to battery performance. Higher degrees of SEI swelling tend to exhibit poor electrochemical cycling.

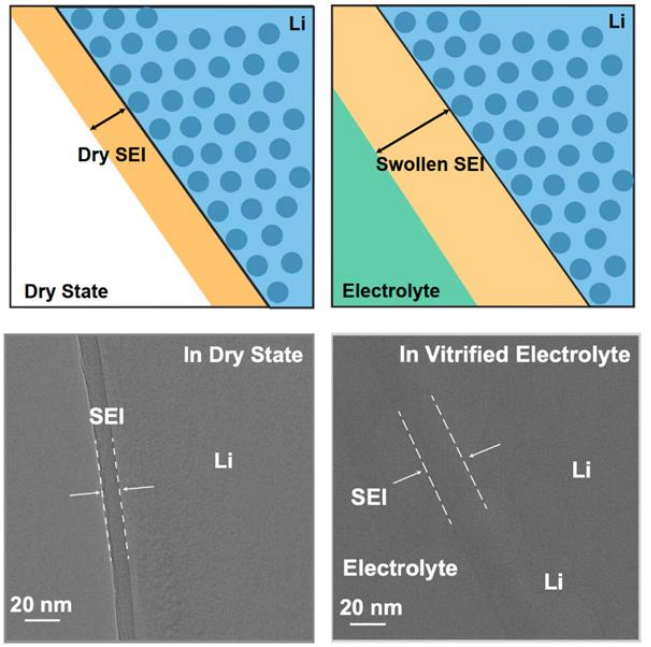

Figure 2. Schematic of SEI swelling in electrolyte (top). Cryo-EM images of SEI on lithium metal anodes in dry state and swollen state (bottom).

Future Plans

Many electrochemical reactions involve dynamic processes like adsorption, proton-coupled electron transfer, and capacitive double layer formation that are often short-lived. Therefore, capturing and studying such metastable intermediates has remained a grand challenge in electrochemistry. Some stable intermediate states in batteries (e.g. phase change, alloying) may exist within a time scale of minutes to hours (and beyond), which allows them to be characterized with the cryoEM methods we developed in previous studies. However, a number of important yet metastable intermediates (e.g. electrochemical double layer formation) exist on a much shorter time scale (<1 s) and will quickly relax back to their equilibrium state after battery operation and disassembly (~mins) prior to cryogenic freezing and imaging. To capture these metastable intermediates, we will develop cryoEM techniques to directly plunge-freeze the entire device during its operation without shutting off the applied current or voltage. Success in kinetically trapping metastable intermediates will largely be determined by the freezing rate, which can vary depending on several parameters (e.g., sample thickness, materials properties, cryogen, plunging speed, etc.). Various solid-liquid interfaces will be examined, including but not limited to electrode/electrolyte interfaces in batteries and catalyst/electrolyte interface in electrocatalysis. Combined with the operando freezing technique, we will further establish how electrochemical energy systems operate across multiple length scales, from individual particle to full device level.

References

1. W. Chiu and K.H. Downing. *Editorial Overview: Exciting Advances in CryoEM Herald a New Era in Structural Biology*, Curr Opin Struct Biol **46**, iv–viii (2017).

2. A. Merk, A. Bartesaghi, S. Banerjee, V. Falconieri, P. Rao, M. Davis, R. Pragani, M. Boxer, L.A. Earl, J. Milne and S. Subramaniam. *Breaking Cryo-EM Resolution Barriers to Facilitate Drug Discovery*, Cell **165**, 1698–1707 (2016).

3. Y. Li, Y. Li, A. Pei, K. Yan, Y. Sun, C. Wu, L. Joubert, R, Chin, A.L. Koh, Y. Yu, J. Perrino, B. Butz, S. Chu and Y. Cui. *Atomic structure of sensitive battery materials and interfaces revealed by cryo–electron microscopy*, Science **358**, 506–510 (2017).

4. Y. Li, W. Zhou, Y. Li, W. Huang, Z. Zhang, G. Chen, H. Wang, G. Wu, N. Rolston, R. Vila, W. Chiu and Y. Cui. *Unravelling Degradation Mechanisms and Atomic Structure of Organic-Inorganic Halide Perovskites by Cryo-EM*. Joule **3**, 2854–2866 (2019).

5. Y. Li, K. Wang, W. Zhou, Y. Li, R. Vila, W. Huang, H. Wang. G. Chen, G. Wu, Y. Tsao, H. Wang, R. Sinclair, W. Chiu and Y. Cui. *Cryo-EM Structures of Atomic Surfaces and Host-Guest Chemistry in Metal-Organic Frameworks*. Matter 1, 428–438 (2019).

Publications

1. Y. Li. Y. Li, W. Huang. W. Chiu, Y. Cui, *Opportunities for cryogenic electron microscopy in materials and nano science*, ACS Nano **14**, 9263–9276 (2020).

2. Z. Zhang, Y. Cui, R. Vila, Y. Li, W. Zhang, W. Zhou, W. Chiu, Y. Cui. *Cryogenic electron microscopy for energy materials*, Accounts of Chemical Research, **54.18**, 3505-3517 (2021).

3. D. T. Boyle, W. Huang, H. Wang, Y. Li, H. Chen, Z. Yu, Z. Bao, Y. Cui, *Corrosion of Lithium Metal Anodes During Storage and its Nanoscopic Origins*" Nature Energy **6**, 487–494 (2021).

4. K. Sytwu, M. Vadai, F. Hayee, D. Angell, A. Dai, J. Dixon, J. Dionne, *Driving energetically-unfavorable dehydrogenation dynamics with plasmonics*, Science **371**, 280–283 (2021).

5. D. Swearer, S. Fischer, D. Angell, C. Siefe, P. Alivisatos, S. Chu, J. Dionne. *Single Particle Cathodoluminescence Spectroscopy with Sub-20 Nm*, ACS Photonics, **8.6**, 1539-1547(2021).

6. Z. Zhang, Y. Li, R. Xu, W. Zhou, Y. Li, S. T. Oyakhire, Y. Wu, J. Xu, H. Wang, Z. Yu, D. T. Boyle, W. Huang, Y. Ye, H. Chen, J. Wan, Z. Bao, W. Chiu, Y. Cui. *Capturing the swelling of solid-electrolyte interphase in lithium metal batteries*, Science **375**, 66 (2022).

Beyond interlayer twist: Hidden control parameters for Van der Waals heterostructures

David Goldhaber-Gordon, PI. Marc Kastner, Co-PI. Hari Manoharan, Co-PI. Stanford Physics Department, and Stanford Institute for Materials and Energy Sciences, SLAC National Accelerator Laboratory. Joseph Orenstein, Co-PI. Lawrence Berkeley National Laboratory.

Keywords: Graphene, 2D Materials, Moiré, Magnetism, Topological bands.

Research Scope

In the early days of 2D Van der Waals (VdW) materials, mm-scale crystals and office tape were all that were needed to generate high-quality samples for cutting-edge transport studies. But we are in a new era, in which cleaner and more complex samples are sensitive to unanticipated, hidden tuning parameters such as additional interlayer twist, or uniaxial strain. We aim to address this need and opportunity by tightly coupling novel stack synthesis methods with multiscale structural characterization and measurements of electronic structure including many-body electronic phases.

Recent Progress

We have linked dramatic behaviors in a twisted bilayer graphene sample to (inadvertent) uniaxial heterostrain in that sample: stretching of one layer relative to the other [1]; Fig. 1. A new sample made the same way behaved similarly, suggesting that the strain was likely induced by

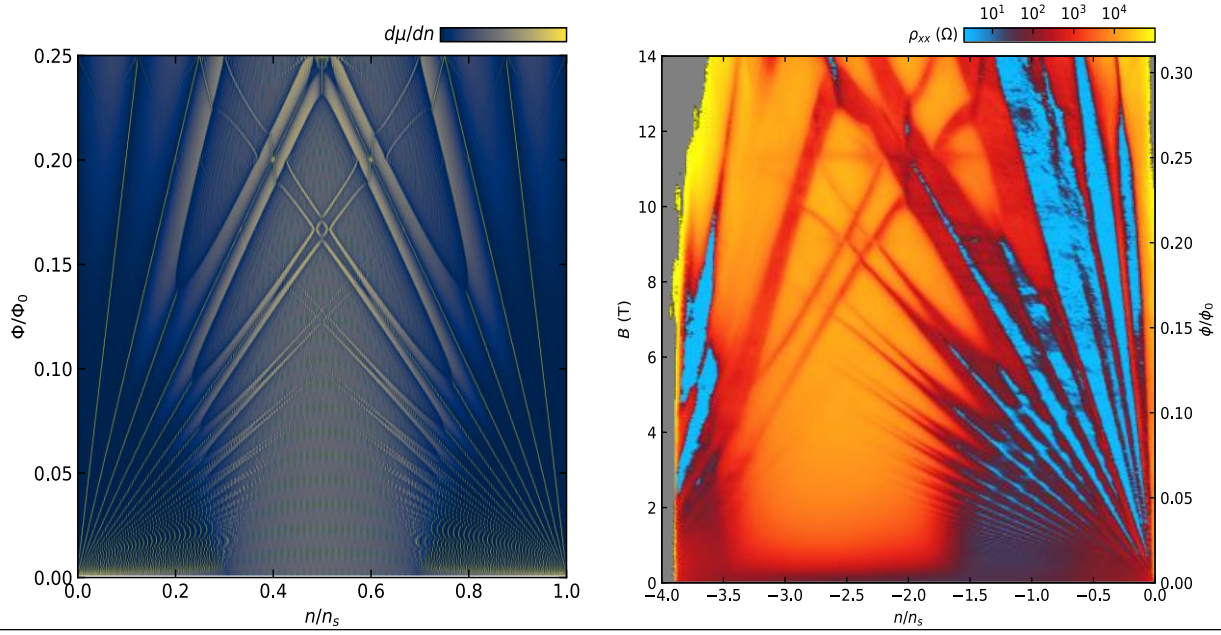

Fig. 1. Electrical resistance in twisted bilayer graphene as a function of electron density and magnetic field (right). A simple noninteracting model we developed that reproduces many of these newly-observed experimental features (left)

pulling on one layer during the fabrication process, and more broadly that strain and its spatial variations are hidden determinants of electronic structure in VdW moirés.

Several years ago we observed in twisted bilayer graphene (tBG) the first known example of orbital magnetism without applied magnetic field [2]. We identified an inadvertent alignment between the graphene layers and hexagonal boron nitride (hBN) cladding layers as a likely contributor. The group of Andrea Young at UCSB found a second tBG sample nearly aligned to hBN, and reproduced the orbital magnetism observed by our team, further proving that it was an analogue of quantum hall effect at zero magnetic field [3]. In the ensuring years, Young's team and ours have each elucidated this magnetism in our respective samples using a range of techniques – in our case, using tilted magnetic field to show that the magnetism is extremely anisotropic, with only the normal component of magnetic field being important to flipping the direction of magnetization [4]. But we and others around the world have tried and failed to obtain this behavior in further samples. Calculations by our collaborator Allan MacDonald suggest that here too there is a hidden control parameter: the twist angle between graphene and hexagonal boron nitride (hBN) not only must be small but must take a specific value precise to +/-0.05° to match the graphene/graphene moiré [5], Fig. 2.

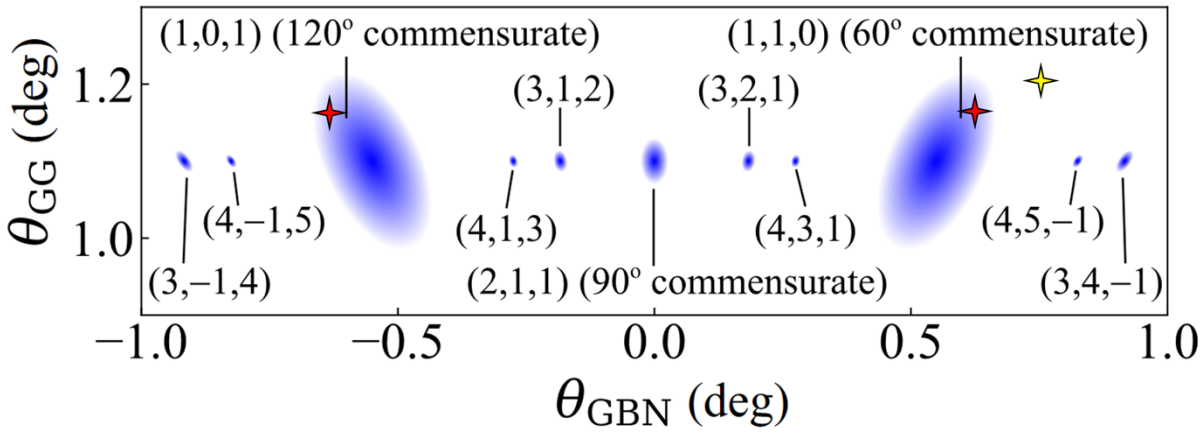

Fig. 2. Graphene-Graphene twist and Graphene-hBN twist for the two known tBG orbital magnet samples [2,3], compared with theoretical predictions of angles that should give rise to quantized Hall resistance. After [5]; we have added crosses to represent electrically measured twist angles in samples from [2] (yellow) and [3] (red).

Motivated by the near-ubiquitous observation of bubbles in VdW stacks, and the recognition that these bubbles cause inhomogneous strain and twist angle even if they are around the periphery of a stack, PI Goldhaber-Gordon partnered with Andy Mannix to launch a FY21-22 SLAC LDRD "Q-BALMS". Under that LDRD we have built a motorized system for stacking VdW layers in vacuum (Fig. 3), and are developing software which is already capable of simple, robust automation. Within the present program we have been using this system to produce stacks, and have characterized over a hundred samples to inform the operation of the system and optimize the quality of the resulting stacks (Fig. 3). This characterization has been based on optical microscopy (fast, but only sensitive to features far larger than the ~10 nm moiré periods of

interest), techniques based on commercial room-temperature AFMs to map features at the moiré scale, and complementary optical spectroscopies such as Raman.

We have also demonstrated that monolayer hBN can serve as an electronically-transparent protective layer for air-sensitive electronic surface states or 2D materials.

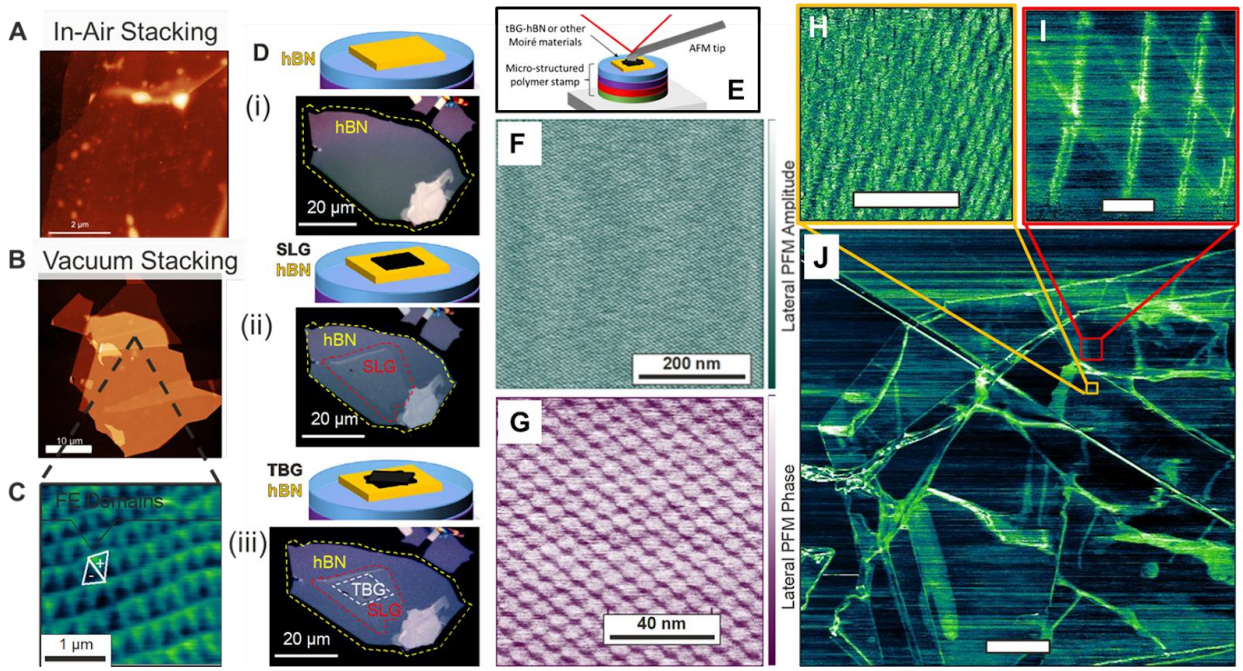

Figure 3. Automated van der Waals assembly and moiré metrology. (A, B) AFM topography images of twisted hBN stacks fabricated via (A) in-air and (B) in-vacuo stacking, highlighting improved morphology from the vacuum process. (C) Kelvin probe image of workfunction variation from region within (B), indicating presence of ferroelectric moiré in twisted hBN. [These ferroelectric moirés were established under a complementary, distinct DOE program on moiré excitons in QIS, under PI Jennifer Dionne; they are shown here to demonstrate the in-vacuo stacking and metrology capabilities, and because we may use them to impose a periodic potential on graphene or other VdW materials within the present program. (D) Schematics and optical micrographs of hBN/tBG sample which we imaged by Piezo Force Microscopy (PFM) after successive steps of stack construction. (E) Schematic showing PFM of hBN/tBG on micro-structured polymer stamp used for vacuum stacking. (F,G) Lateral PFM images of completed hBN/tBG stack: (F) large-area amplitude map and (G) zoom-in of phase signal. Subtle spatial variations in moiré period can be analyzed to reveal variations in twist angle or strain. (H,I,J) Lateral PFM amplitude of a disordered hBN/tBG heterostructure showing (H) small-period and (I) large-period moiré patterns acquired on the same structure, showing wrinkles spread over a large area (J). Scale bar is (H,I) 100nm and (J) 1μm.

Future Plans

We plan to add strain control to stack production, and will continue to develop and investigate the stamps and processes used in stacking, to avoid introducing unintended wrinkles into the delicate atomically-thin monolayers.

Transport and Microwave Spectroscopy: Microwave spectroscopy can powerfully complement near-DC transport for diagnosing electronic phases such as exotic magnets and superconductors by probing their excitations. We plan to expand its sensitivity by coupling microfabricated superconducting resonators (Fig. 4; inspired by developments for manipulating solid-state qubits) to VdW stacks, something just beginning to be explored worldwide to date.

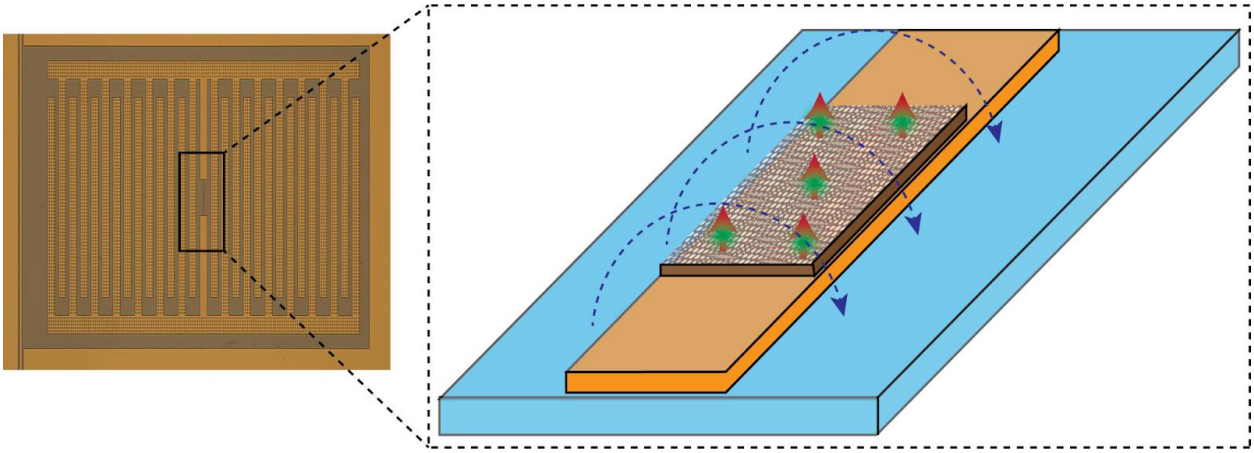

Fig. 4. **Microwave resonator can be designed to probe spin response**. This superconducting resonator design, which we have built and tested, drives current through a short, narrow wire, producing a strong local microwave magnetic field. Because the resonator Q is high (~10^6), its resonance can measurably broaden and/or split when coupled to spins at even the very low densities expected from a magnetically-polarized state in a VdW moiré. Such a resonator should also be able to probe the magnetic response of a superconductor even in the dilute monolayer limit relevant to VdW moirés.

References

1. J. Finney, A.L. Sharpe, E.J. Fox, C.L. Hsueh, D.E. Parker, M.Yankowitz, S. Chen, K. Watanabe, T. Taniguchi, C.R. Dean, A. Vishwanath, M.A. Kastner and D. Goldhaber-Gordon, *Unusual magnetotransport in twisted bilayer graphene*, Proceedings of the National Academy of Sciences **119**, e2118482119 (2022).
2. A.L. Sharpe, E.J. Fox, A.W. Barnard, J. Finney, K. Watanabe, T. Taniguchi, M.A. Kastner, D. Goldhaber-Gordon, *Emergent magnetism near three-quarters filling in twisted bilayer graphene aligned to hexagonal boron nitride*. Science **365**, 605-608 (2019).

3. M. Serlin, C. Tschirhart, H. Polshyn, Y. Zhang, J. Zhu T. Taniguchi, K. Watanabe, L. Balents, and A. F. Young, *Intrinsic quantized anomalous Hall effect in a moiré heterostructure*, *Science* **367**, 895-900 (2020).
4. A.L. Sharpe, E.J. Fox, A.W. Barnard, J. Finney, K. Watanabe, T. Taniguchi, M.A. Kastner, D. Goldhaber-Gordon, *Evidence of orbital ferromagnetism in twisted bilayer graphene aligned to hexagonal boron nitride*. Nano Letters **21**, 4299-4304 (2021).
5. J. Shi, J. Zhu, and A. H. MacDonald, *Moiré commensurability and the quantum anomalous Hall effect in twisted bilayer graphene on hexagonal boron nitride*, Phys. Rev. B **103**, 075122 (2021).

Publications

1. A.L. Sharpe, E.J. Fox, A.W. Barnard, J. Finney, K. Watanabe, T. Taniguchi, M.A. Kastner, D. Goldhaber-Gordon, *Evidence of orbital ferromagnetism in twisted bilayer graphene aligned to hexagonal boron nitride*. Nano Letters **21**, 4299-4304 (2021).
2. J. Finney, A.L. Sharpe, E.J. Fox, C.L. Hsueh, D.E. Parker, M.Yankowitz, S. Chen, K. Watanabe, T. Taniguchi, C.R. Dean, A. Vishwanath, M.A. Kastner and D. Goldhaber-Gordon, *Unusual magnetotransport in twisted bilayer graphene*, Proceedings of the National Academy of Sciences **119**, e2118482119 (2022).
3. C.Z. Zerger, L.K. Rodenbach, Y.-T. Chen, B. Safvati, M.Z. Brubaker, S. Tran, T.-A. Chen, M.-Y. Li, L.-J. Li, D. Goldhaber-Gordon, and H.C. Manoharan, *Nanoscale Electronic Transparency of Wafer-Scale Hexagonal Boron Nitride*, Nano Letters **22**, 4608-4615 (2022).
4. C. Lee, C.P. Vir, K. Manna, C. Shekhar, J. E. Moore, M. A. Kastner, C. Felser, and J.Orenstein, *Observation of a phase transition within the domain walls of ferromagnetic* $Co_3Sn_2S_2$, Nature Communications **13**, Article number: 3000 (2022).
5. L.K. Rodenbach, I.T. Rosen, E.J. Fox, P. Zhang, L. Pan, K.L. Wang, M.A. Kastner, D. Goldhaber-Gordon, *Bulk dissipation in the quantum anomalous Hall effect*, APL Materials **9**, 081116 (2021).
6. C. Parra, F.C. Niestemski, A.W. Contryman, P. Giraldo-Gallo, T.H. Geballe, I.R. Fisher, and H.C. Manoharan, *Signatures of Two-Dimensional Superconductivity Emerging within a Three-Dimensional Host Superconductor*, Proceedings of the National Academy of Sciences **118**, e2017810118 (2021).
7. E. Mikheev, I.T. Rosen, and D. Goldhaber-Gordon, *Quantized critical supercurrent in* $SrTiO_3$*-based quantum point contacts*, Science Advances **7**, eabi6520 (2021).
8. E. Mikheev, T. Zimmerling, A. Estry, P.J.W. Moll, and D. Goldhaber-Gordon, *Ionic Liquid Gating of* $SrTiO_3$ *Lamellas Fabricated with a Focused Ion Beam*, Nano Letters **22**, 10, 3872 (2022).
9. C.L. Hsueh, P. Sriram, T. Wang, C. Thomas, G. Gardner, M.A. Kastner, M.J. Manfra, and D. Goldhaber-Gordon, *Clean quantum point contacts in an InAs quantum well grown on a lattice-mismatched InP substrate*, Phys. Rev. B. **105**, 195303 (2022).
10. L. Bishop-Van Horn and K.A. Moler, *SuperScreen: An open-source package for simulating the magnetic response of two-dimensional superconducting devices*, Computer Physics Communications **280**, 108464 (2022).

Direct Probing Charge and Spin Behaviors in Ferroic Materials

Myung-Geun Han and Yimei Zhu

Department of Condensed Matter Physics & Materials Science, Brookhaven National Laboratory, Upton, NY 11973

Keywords: Multiferroics, Topological defects, Skyrmions, Cryogenic and *in situ* TEM, Domain switching dynamics

Research Scope

The focus of this research task under the FWP Number MA-015-MACA is to study charge or spin structures, especially in topologically nontrivial configurations, including domain walls, vortices, and skyrmions in ferroic materials and their dynamic behaviors under external stimuli to unveil the underlying physical principles and to harness functional properties for future applications. The research areas include 1) intriguing electronic or magnetic phenomena at domain walls and interfaces, and 2) understanding topological natures and switching pathways of charge and spin textures under external stimuli. We utilize *in situ* electron microscopy to study dynamics and functionalities of topological defects across phase transitions under external electric/magnetic fields under controlled cooling down to liquid helium temperatures. The research areas of ultrafast electron microscopy and instrumentation as well as electronic inhomogeneities are covered by a separate abstract.

Recent Progress

In the last two years, our research focus was mainly on the manipulation of domain walls and magnetic skyrmions in various ferroic systems using *in situ* TEM methods.

Controlled nucleation and stabilization of vertically oriented domain walls

Ferroelectric domain walls exhibit unique functional properties that are not observed in the bulk domains. Thus, the ferroelectric domain walls are considered an active element of devices that can be manipulated by external electric fields, promising for domain-wall-based programmable nanoelectronics. To this end, precise control of domain walls in terms of their orientation, location, and density is a prerequisite for realizing practical applications. In the last two years, we found three distinct mechanisms that lead to vertically oriented domain walls that are formed by external electric fields at predictable sites in the (110)-oriented $BiFeO_3$ thin films; at the nanoscale edges of the "crest and sag" pattern-like electrode, at the vertex of flux-closure domains, and at antiphase boundaries[1,2]. These results represent critical advancements in exploiting domain walls for next-generation ferroelectric devices.

Electric field control of magnetic skyrmions in magnetoelectric Cu_2OSeO_3

Electric field control of topologically nontrivial magnetic skyrmions provides a paradigm shift for future spintronics beyond current silicon-based technology. While significant progress has been made by X-ray and neutron scattering studies in the momentum space, direct real-space observation of such nanoscale spin structures in reduced dimensions and their dynamics driven by external electric fields remains a challenge to understand underlying mechanisms and harness functionalities for future applications. Using real-space Lorentz TEM (LTEM) imaging, we directly observed electric field effects on hexagonally packed SkLs in the (100)- and (110)-oriented thin slabs of Te-doped CSO crystals under an external magnetic field applied along the [100] and [110] directions, respectively, while the external electric fields were applied along the [010] and [001] directions, respectively. We found that the (110)-oriented thin films show a linear response of helix and skyrmion lattice (SkL) including the electric-field-induced skyrmion-helix phase transition. However, for the (001)-oriented thin films, we found a remarkable hysteretic response including SkL formation occupying the entire sample with a well-defined wave vector ***q*** that is controlled by the electric field direction. Based on our micromagnetic simulation, our results point to the strain effects induced by external electric fields on magnetocrystalline anisotropy and Dzalloshinski-Moriya interaction (DMI), which are identified as a driving force for hysteretic responses of skyrmions to the external electric fields. The collective skyrmion-lattice control with non-volatility and energy-efficient operation by electric fields demonstrated in this work[3] provides an important foundation for designing skyrmion-based qubits and memory devices. In addition, the experimental method developed in

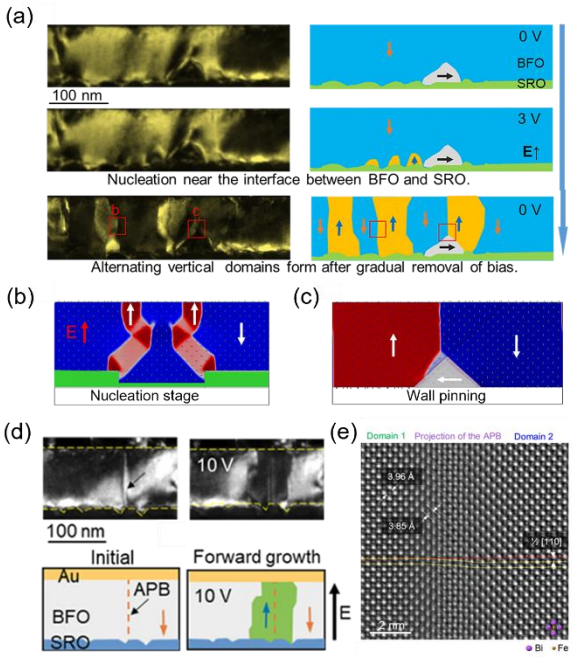

Fig. 1. Inducing vertically oriented domain walls in (110)-oriented $BiFeO_3$ thin films by pattern-like electrodes, domain wall pinning at the vertex point in the flux-closure domain, and antiphase-boundary (APB)-induced domain nucleation and growth. a) Dark-field TEM images showing ferroelectric domain switching to induce vertical domain walls and its schematics. b) Phase-field simulation showing domain wall orientation during domain switching. c) Phase-field simulation showing domain wall pinning at the vertex point in a flux-closure domain. d) Dark-field TEM images and schematics showing domain switching near the APB. e) Atomic resolution HAADF STEM image showing atomic structures of the APB. The APB is tilted with respect to the imaging direction. A half-unit-cell shift across the APB and a decrease in the unit cell parameter are indicated.

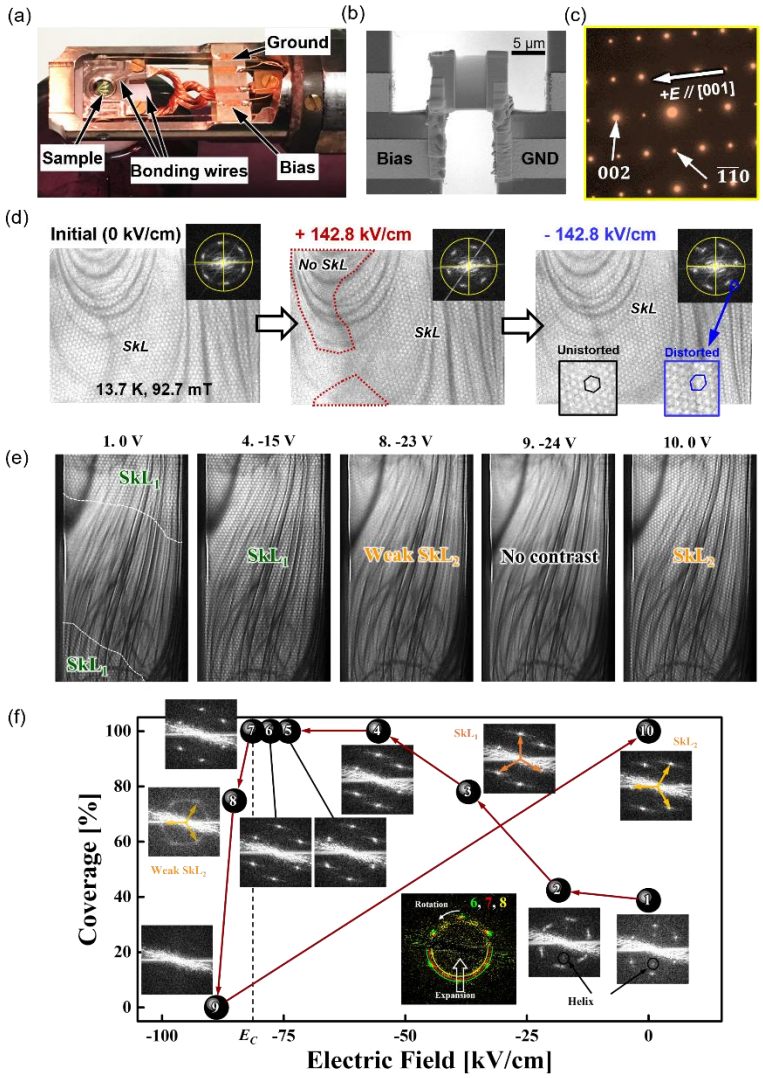

Fig. 2. Electric field control of magnetic skyrmions in magnetoelectric Cu_2OSeO_3 (a-b) Photograph and scanning electron micrograph showing a silicon nitride chip loaded and connected to the electrodes in the liquid helium cooling holder. (c) Electron diffraction patterns. (d) Lorentz images showing skyrmion evolution under external voltages at cryogenic temperature. (e) Hysteretic skyrmion behavior during the voltage cycle showing enhanced skyrmion lattices and their discrete wave vector rotation by 30°.

this work enables direct imaging of charge/spin states in quantum materials under external electric and magnetic fields at low temperatures to explore external-field-tunable novel quantum states for quantum information science.

Future Plans

We will study the dynamic behaviors of topological charge/spin textures and their emergent phenomena under magnetic and/or electric fields at low temperatures. We will also study how to control the chirality of spin textures by electric field or current.

Probing dynamics of skyrmion lattice under external electric fields

During the electric field control of skyrmion experiments, we found that the SkL ***q*** rotates under the external electric and magnetic fields. In addition, at the critical electric fields, the magnetic contrast completely disappears, necessitating a fast probe for dynamics study. We will explore the dynamics of SkL by combining resonant elastic x-ray scattering (REXS) with LTEM in collaboration with Claudio Mazzoli (NSLSII, BNL). LTEM imaging provides direct imaging of the static SkLs in the sample while REXS probes the dynamics of SkLs in the momentum space. These complimentary reciprocal/real space experiments on the same thin TEM samples under electric and magnetic fields will allow us to gain insights on electric field effects on the SkLs and their dynamics. In order to perform two separate experiments on the identical sample, we designed our silicon nitride chips with four electrodes. The customized chip has a 10 x 10 mm^2 observation window for LTEM imaging and REXS experiments in transmission mode. Two sets of orthogonally oriented electrodes allow two

perpendicular electric fields in the sample at the liquid helium temperatures. In our preliminary study, we were able to obtain LTEM images and REXS data, separately, on the identical TEM sample, as shown in Fig. 3. We will systematically explore various skyrmion dynamics as a function of magnetic/electric fields and sample temperatures.

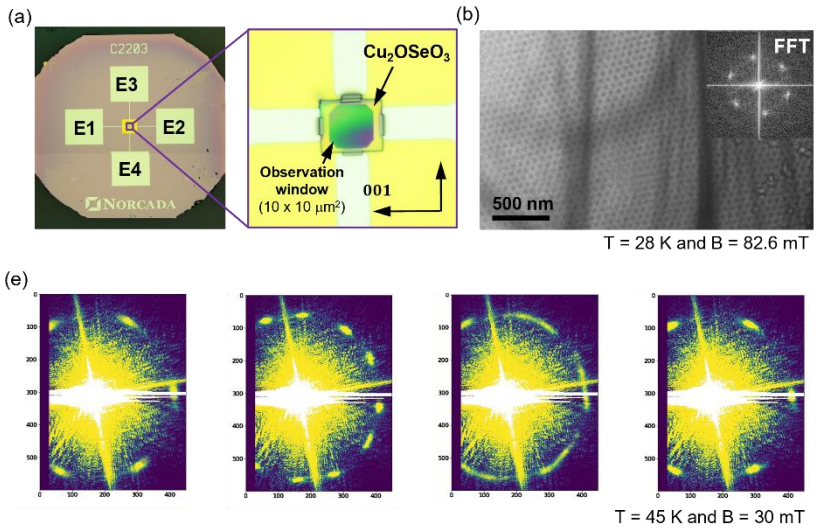

Fig. 3. Skyrmion rotation dynamics observed by x-ray scattering (a) Photograph showing TEM samples with two orthogonal sets of electrodes (E1-E4) prepared on the customized silicon nitride chip with 10 x 10 μm^2 observation window. (b) LTEM image obtained from the sample showing a skyrmion lattice. (c) Resonant elastic x-ray scattering data obtained from the same TEM sample shows accessible dynamics of the driven skyrmion lattice.

Controlling chirality in skyrmionic bubbles in 2D van der Waals magnets by electric field/current

In our previous study, we reported topologically nontrivial skyrmionic bubbles stabilized in the centrosymmetric two-dimensional (2D) van der Waals $Cr_2Ge_2Te_6$[4]. Due to the lack of symmetry-breaking DMI, the skyrmionic bubbles obtained after magnetic field cooling show random chiralities. We will explore the electric field/current effects on the skyrmionic lattices in 2D magnets and their heterostructures. For insulating 2D magnets ($Cr_2Ge_2Te_6$), the external electric fields can break the inversion symmetry by ionic and electronic polarization and thus induce nonzero DMI in centrosymmetric magnets. If the electric-field-induced DMI is not negligible compared to the dominating ferromagnetic exchange interaction, the chirality can be selectively tunable across the magnetic field cooling process. For metallic 2D magnets (Fe_3GeTe_2), it is shown that the spin transfer torque can select the chirality in helical spin states when the external magnetic field is parallel to the electric current[5]. In collaboration with Frances Ross (MIT), the heterostructures including 2D magnetic layers will be fabricated for *in situ* electric and magnetic biasing experiments at liquid helium temperatures. We will mainly seek an electric control of topologically nontrivial magnetic spin textures for future spintronics.

References

[1] Y. Zhang, Y. Tan, D. Sando, L.-Q. Chen, N. Valanoor, Y. Zhu, and M.-G. Han, *Controlled nucleation and stabilization of ferroelectric domain wall patterns in epitaxial (110) bismuth ferrite heterostructures*, Adv. Funct. Mater. 2003571, 1-8 (2020).

[2] Y. Zhang, M.-G. Han, D. Sando, L. Wu, V. Nagarajan, Y. Zhu, *Antiphase-boundary-engineered domain switching in a (110)-oriented $BiFeO_3$ film*, ACS Appl. Electron. Mater. 3 3226-3233 (2021).

[3] M.-G. Han, F. Camino, P.A. Vorobyev, J. Garlow, R. Rov, T. Söhnel, J. Seidel, M. Mostovoy, O.A. Tretiakov, and Y. Zhu, *Hysteretic responses of skyrmion lattices to electric fields in magnetoelectric Cu_2OSeO_3* (submitted).

[4] M.-G. Han, J. Garlow, Y. Liu, H. Zhang, D. DiMarzio, D. Jariwala, P. Cedomir, and Y. Zhu, *Topological magnetic spin textures in exfoliated two-dimensional van der Waals $Cr_2Ge_2Te_6$*, Nano Lett. **19**, 7859-7865 (2019).

[5] N. Jiang, Y. Nii, H. Arisawa, E. Saitoh, and Y. Onose, *Electric current control of spin helicity in an itinerant helimagnet*, Nat. Commun. **11**, 1601 (2020).

Publications

(10 most relevant, total journal articles from this research task: November. 2020 - October. 2022)

1. Zhang, Y.; Tan, Y.; Sando, D.; Chen, L.-Q.; Valanoor, N.; Zhu, Y.; and Han, M.-G., "Controlled nucleation and stabilization of ferroelectric domain wall patterns in epitaxial (110) bismuth ferrite heterostructures", Adv. Funct. Mater. 2003571, 1-8 (2020).
2. Zhang, Y.; Han, M.-G.; Sando, D.; Wu, L.; Nagarajan, V.; Zhu, Y., "Antiphase-boundary-engineered domain switching in a (110)-oriented BiFeO3 film", ACS Appl. Electron. Mater., 3 3226-3233 (2021).
3. Yao, X.; Yi, H.T.; Jain, D.; Han, M.-G.; Oh, S., "Spacer-layer-tunable magnetism and high-field topological Hall effects in topological insulator heterostructures", Nano Lett. 21 (14), 5914-5919 (2021).
4. Li, F., Zou, Y., Han, M.-G., Foyevtsova, K., Shin, H., Lee, S., Liu, C., Shin, K., Albright, S.D., Sutarto, R., He, F., Davidson, B.A., Walker, F.J., Ahn, C.H., Zhu, Y., Cheng, Z.G., Elfimov, I., Sawatzky, G.A., Zou, K., "Single-crystalline epitaxial TiO film: A metal and superconductor, similar to Ti metal", Sci. Adv., 7 : eabd4248 (2021).
5. Levin, I.; Han, M.-G.; Playford, H.Y.; Krayzman, V.; Zhu, Y.; Maier, R.A., "Nanoscale-correlated octahedral rotations in $BaZrO_3$", Phys. Rev. B 104(21), 214109 (2021).
6. Du, K.; Huang, F.-T.; Kim, J.W.; Lim, S.J.; Gamage, K.; Yang, J.; Mostovoy, M.; Garlow, J.; Han, M.-G.; Zhu, Y.; Cheong, S.-W., "Topological spin/structure couplings in layered chiral magnet $Cr_{1/3}TaS_2$: the discovery of spiral magnetic superstructure" PNAS, 118 (40), e2023337118 (2021).
7. Yao, X.; Mazza, A.R.; Han, M.-G.; Yi, H.T.; Jain, D.; Brahlek, M.; Oh, S., "Superconducting four-fold Fe(Te,Se) film on six-fold magnetic MnTe via hybrid symmetry epitaxy", Nano Lett. 22 (18), 7522-7526 (2022)
8. Telford, E.J.; Dismukes, A.H.; Dudley, R.L.; Wiscons, R.A.; Lee, K.; Chica, D.G.; Ziebel, M.E.; Han, M.-G.; Yu, J.; Shabani, S.; Scheie, A.; Watanabe, K.; Taniguchi, T.; Xiao, D.; Zhu, Y.; Pasupathy, A.N.; Nuckolls, C.; Zhu, X.; Dean, C.R.; Roy, X., "Coupling between magnetic order and charge transport in a two-dimensional magnetic semiconductor", Nat. Mater. 21, 754-760 (2022)
9. Liu, Y.; Han, M.-G.; Lee, Y.; Ogunbunmi, M.O.; Du, Q.; Nelson, C.; Hu, Z.; Stavitski, E.; Graf, D.; Attenkofer, K.; Bobev, S.; Ke, L.; Zhu, Y.; and Petrovic, C., "Polaronic Conductivity in $Cr_2Ge_2Te_6$ Single Crystals", Adv. Funct. Mater. 32, 2105111 (2022).
10. Han, M.-G.; Camino, F.; Vorobyev, P.A.; Garlow, J.; Rov, R.; Söhnel, T.; Seidel, J.; Mostovoy, M.; Tretiakov, O.A.; and Zhu, Y., "Hysteretic responses of skyrmion lattices to electric fields in magnetoelectric Cu_2OSeO_3" (submitted).

Probing intrinsic and extrinsic exchange coupling in magnetic topological insulators

Jay A. Gupta[1] , Roland Kawakami[1] and Michael E. Flatté[2]
[1]Department of Physics, Ohio State University, Columbus OH 43210, USA
[2]Department of Physics and Astronomy, University of Iowa, Iowa City, IA 52242, USA
Keywords: 2D magnets, spin polarized STM, spin transport theory, magnetic semiconductors, magnetic topological insulators

Research Scope

New paradigms for energy-efficient and high-performance computing are possible if quantum phenomena associated with topological states can be realized at elevated temperatures. For example, the quantum anomalous Hall effect has been demonstrated in magnetic topological insulators, which offers the potential for tunable transport through dissipationless states that are of interest for on-chip interconnects, new metrology standards, or efficient spintronics devices. However, QAHE is only realized at temperatures much lower than the ferromagnetic ordering temperature, which might be attributed to charge and/or magnetic disorder from native defects or dopants, or additional interfacial disorder. Our program addresses this central question with an integrated approach of materials epitaxy, atomic- and spin-resolved microscopy, and theoretical magnetotransport modeling with the following objectives:

Achieve and quantify controlled coupling of magnetic order to topological states – Here we address key questions raised in the efforts to integrate magnetism into TI hosts, either through introduction of magnetic dopants, or through proximity to magnetic thin films. Our starting point in this objective has been to integrate nonmagnetic TIs (Bi_2Se_3, Bi_2Te_3) with epitaxial films of the van der Waals ferromagnet, Fe_3GeTe_2 (FGT). We also deposit transition metal adatoms (Fe, Cr, V, Mn) onto the surface, with coverage spanning the regime between isolated moments and clusters. In both approaches, we can introduce a nonmagnetic insulating layer such as vdW $SnSe_2$ to control coupling between the topological surface states and the magnetic moments by tuning the thickness in the range ~ 1-3 monolayers. Spin-polarized STM imaging is used to spatially-resolve spin-dependent quasiparticle interference (QPI) near single magnetic impurities and magnetic domain structures. Spin-resolved tunneling spectroscopy in vector magnetic fields is compared with theoretical calculations of dc magneto-transport to quantify exchange coupling strengths, both to the underlying topological surface states and to neighboring moments as a function of distance and local environment.

Surface state engineering of intrinsic magnetic TIs – Antiferromagnetic TIs are predicted to alternate between quantum anomalous Hall and axion insulator states as a function of layer parity, and host chiral edge states with a quantized e^2/h conductance. Here we study aspects of the surfaces in a family of layered TIs based on the $Mn(Bi,Sb)_2(Se,Te)_4$ family that offers tunable anti/ferromagnetic inter/intra layer coupling, and tuning between trivial/non-trivial topologies via stoichiometry. Surface features such as edge/surface terminations, decoration by adsorbates, and height variation near screw dislocations are correlated with SP-STM imaging of the magnetic order (e.g., domains/spin textures, anisotropy) to better understand the connection between structure, topology and magnetism. This will include spin dynamics measurements by developing a new technique for ferromagnetic-resonance STM (FMR-STM), building on theoretical frameworks we have developed for transport in spin coherent systems.

Recent Progress

Kinetically-controlled van der Waals epitaxy of FGT on Ge(111)

Fe_3GeTe_2 (FGT) is one of the most well-studied vdW magnets due to its strong perpendicular magnetic anisotropy (PMA), relatively high Curie temperature (T_C) ranging from ~200 K to above room temperature, and the observation of novel phenomena such as spin-orbit torque switching and skyrmion spin textures. While many efforts have focused on small flakes exfoliated from bulk crystals, epitaxial growth of thin films and heterostructures by methods such as molecular beam epitaxy (MBE) enables scaling up to large areas for electronic and magnetic applications. To date, there have been several reports of epitaxial growth of FGT by MBE, but critical issues of the growth process such as the relative importance of thermodynamic equilibrium (energetics) and growth/reaction rates (kinetics) remain largely unexplored. Understanding these issues are important for improving the material quality, as it relates to important properties of thin films and heterostructures including interdiffusion and defect formation. We have recently demonstrated that kinetics play an important role in the epitaxial growth of FGT films by MBE (Figure 1) (*1*). For FGT grown on Ge(111), we find that growth rate is a critical parameter that determines whether FGT grows directly on Ge(111) with an atomically abrupt interface or whether a Te-deficient non-vdW Fe_3Ge_2 alloy forms at the interface. Contrary to expectations for reactive MBE growth, our studies show that the Fe_3Ge_2 alloy forms at lower growth rates while the abrupt FGT/Ge(111) interface is obtained for higher growth rates. This behavior suggests that energetic considerations favor the formation of non-vdW Fe-Ge alloys, while the growth kinetics can favor the stabilization of pure FGT.

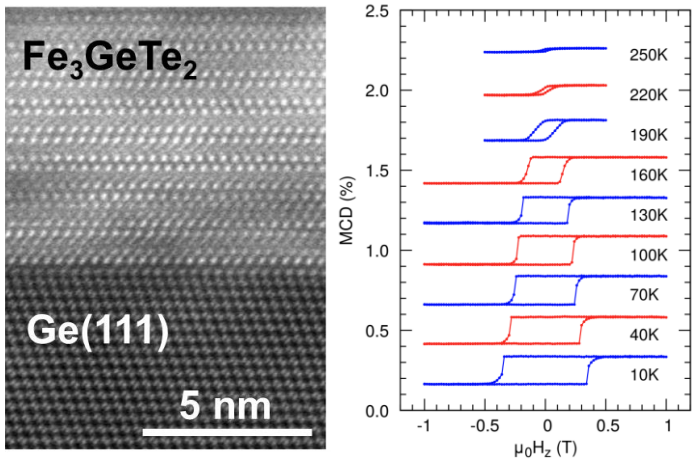

Figure 1. Atomically-abrupt interface in fast-grown FGT/Ge(111). (left) Cross-sectional STEM image (right) magneto-circular dichroism measurements indicating a ferromagnetic TC of ~ 250 K. Curves have been vertically offset. Data from (*1*)

Integration of monolayer FGT and Bi_2Te_3

We have recently developed high quality MBE growth of FGT/Bi_2Te_3 thin film heterostructures to probe the roles of defects and interface disorder on coupling between magnetic order and topological surface states. Initial samples consisted of ~ 1-2 ML FGT coverage, grown on 20 u.c. of Bi_2Te_3, grown on a *c*-sapphire substrate. In this low coverage regime, STM images reveal that most of the surface is covered with single quintuple layer (QL) FGT, but with patches of bare Bi_2Te_3. The atomic resolution STM image shown in Figure 2 indicates single-QL FGT growing outward from a Bi_2Te_3 step. The lattices of both regions produce spots in the corresponding FFT and are consistent with bulk values, indicating there is little strain associated with the interface. The two lattices are also aligned, evident from the FFT, as well as the moiré lattice resolved on the FGT, which has a spacing expected for zero rotation between FGT and the

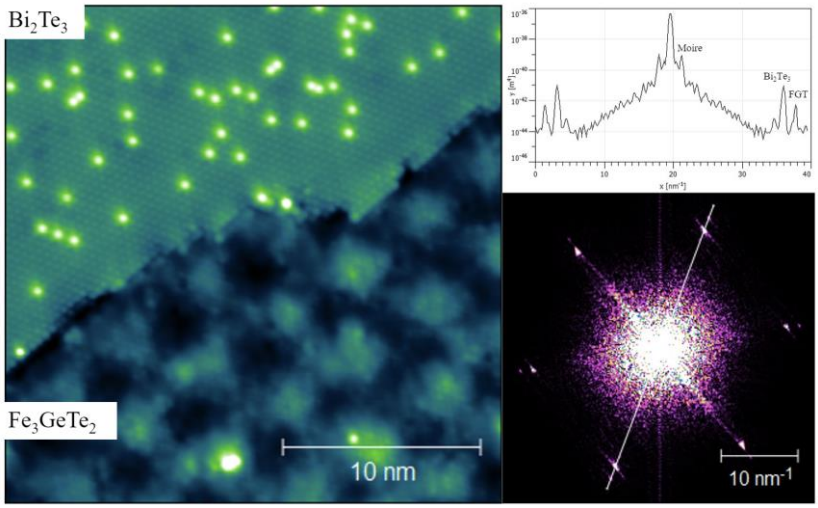

Figure 2. (left) Atomic-resolution STM imaging showing a Fe_3GeTe_2 QL growing outward from a Bi_2Te_3 step. (right panels) corresponding FFT and FFT linecut showing the two atomic lattices and the moire lattice observed on FGT.

underlying Bi_2Te_3. A similar moiré lattice and atomic spacing is also observed for free-standing FGT islands of Bi_2Te_3 terraces, suggesting that this aligned growth is preferred regardless of the FGT nucleation site. STM imaging in the low-coverage samples also indicates small patches of bilayer FGT, as well as regions with fractional QL thickness that we attribute to partial FGT terminations. The discrete range of apparent step heights is used to identify Fe- and FeGe-terminated regions. Similar moiré lattices are observed on all regions, consistent with the preservation of the FGT atomic lattice spacing.

Signatures of spin-coherent transport in SP-STM measurements of magnetic adatoms

We have developed a theoretical framework for modeling charge and spin transport through single spin defects in a variety of tunnel junction configurations with both magnetic and non-magnetic contacts (*2–4*). These theoretical studies emphasize the importance of exchange coupling between defects, spin- and charge-dependent tunneling rates to/from the defects, and the influence of microwave excitation. For example, Figure 3A shows our predictions for dc magnetotransport through exchange-coupled defects, as would be realized in an SP-STM experiment, or more generally in a nanoscale magnetic tunnel junction. We find that current flow is suppressed through spin defects at specific values of transverse magnetic fields, determined by the exchange coupling and tunneling rate onto the defect from the bulk.

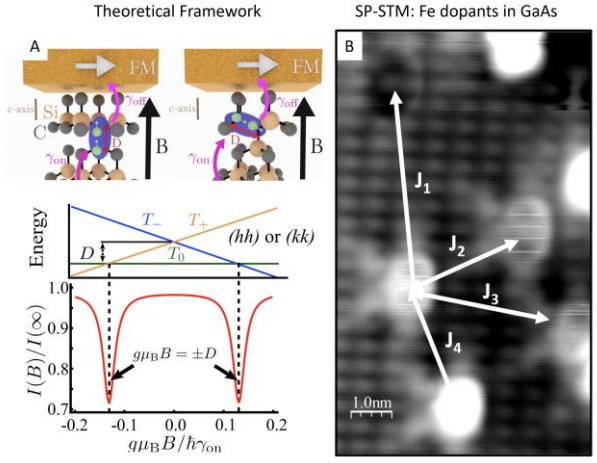

Figure 3. Spin transport through exchange coupled magnetic defects. A) Calculation for dc magnetotransport under transverse field. The SPSTM tip is positioned over a magnetic defect, which exhibits a zero-field splitting due to crystal anisotropy or exchange coupling to neighboring spins. Resonant dips in spin-polarized current flow occur at values related to applied field, coupling and tunneling rates. B) Preliminary SP-STM of Fe dopants in GaAs (110) with a Cr tip. Distinct contrast between otherwise identical Fe acceptors may reflect local exchange interactions and tunneling conditions.

Experimentally, we have started to probe this situation as shown in the SP-STM image of Fig. 3B, which shows 4 Fe acceptors that were substituted for Ga sites in a GaAs(110) surface. Data here were taken with a bulk Cr tip; and it is likely that the distinct contrast reflects the distinct magnetic properties of the Fe acceptors, as unpolarized measurements do not show this difference between Fe. This set of measurements requires additional investigation to identify the source of the different magnetic environment, which could be (1) the unique net exchange coupling summing over nearest neighbors, (2) the unique spin lifetime for an acceptor spin due to fluctuations of this exchange coupling (magnetic noise), or (3) differences in zero-field splitting of the spin-5/2 core state of iron due to local charge environments.

Future Plans

Our overarching plan for the next year is to continue applying experimental tools such as SPSTM and theoretical tools such as spin-dependent two-level transport modeling to the 2DM/TI heterostructures that are now being grown in high quality thin films. SP-STM tunneling spectroscopy measurements with bulk Cr tips on FGT/Ge(111) revealed magnetic hysteresis at a critical field consistent with MCD measurements (*1*). Initial SP-STM measurements on FGT/Bi_2Te_3 reveal prominent contrast associated with the different terminations, but further measurements are needed to identify contrast as a function of magnetic field. In the growth effort, we will continue refining our MBE methods for the FGT/Bi_2Te_3 system, with a focus on correlating magnetic properties with thickness in the few-QL regime. We will also continue to expand our portfolio of layered magnetic materials to include telluride-based $CrGeTe_2$ and $MnBi_2Te_4$. Theoretically, we will continue to build on our foundation of spin-coherent transport theory to include magnetic impurities on TI surfaces, as well as coupled to 2DM/TI heterostructures.

References

1. W. Zhou, A. J. Bishop, M. Zhu, I. Lyalin, R. Walko, J. A. Gupta, J. Hwang, R. K. Kawakami, Kinetically Controlled Epitaxial Growth of Fe3GeTe2 van der Waals Ferromagnetic Films. *ACS Appl. Electron. Mater.* **4**, 3190–3197 (2022).

2. S. M. Mueller, D. Kim, S. R. McMillan, S. J. Tjung, J. J. Repicky, S. Gant, E. Lang, F. Bergmann, K. Werner, E. Chowdhury, A. Asthagiri, M. E. Flatté, J. A. Gupta, Tunable tunnel barriers in a semiconductor via ionization of individual atoms. *J. Phys.: Condens. Matter*. **33**, 275002 (2021).

3. S. R. McMillan, N. J. Harmon, M. E. Flatté, Image of Dynamic Local Exchange Interactions in the dc Magnetoresistance of Spin-Polarized Current through a Dopant. *Phys. Rev. Lett.* **125**, 257203 (2020).

4. N. J. Harmon, M. E. Flatté, Theory of oblique-field magnetoresistance from spin centers in three-terminal spintronic devices. *Phys. Rev. B.* **103**, 035310 (2021).

Publications

1. Zhou W, Bishop AJ, Zhu M, Lyalin I, Walko R, Gupta JA, Hwang J, Kawakami RK (2022) Kinetically Controlled Epitaxial Growth of Fe3GeTe2 van der Waals Ferromagnetic Films. *Acs Applied Electronic Materials*, 4(7):3190–3197. https://doi.org/10.1021/acsaelm.2c00185

2. Walko RC, Zhu T, Bishop AJ, Kawakami RK, Gupta JA (2022) Scanning tunneling microscopy study of the antiferromagnetic topological insulator MnBi2Se4. *Physica E-Low-Dimensional Systems & Nanostructures*, 143:115391. https://doi.org/10.1016/j.physe.2022.115391

3. Cheng S, Wang B, Lyalin I, Bagues N, Bishop AJ, McComb DW, Kawakami RK (2022) Atomic layer epitaxy of kagome magnet Fe3Sn2 and Sn-modulated heterostructures. *Apl Materials*, 10(6):061112. https://doi.org/10.1063/5.0094257

4. Zhu T, Bishop AJ, Zhou T, Zhu M, O'Hara DJ, Baker AA, Cheng S, Walko RC, Repicky JJ, Liu T, Gupta JA, Jozwiak CM, Rotenberg E, Hwang J, Zutic I, Kawakami RK (2021) Synthesis, Magnetic Properties, and Electronic Structure of Magnetic Topological Insulator MnBi2Se4. *Nano Letters*, 21(12):5083–5090. https://doi.org/10.1021/acs.nanolett.1c00141

5. Sierra JF, Fabian J, Kawakami RK, Roche S, Valenzuela SO (2021) Van der Waals heterostructures for spintronics and opto-spintronics. *Nature Nanotechnology*, 16(8):856–868. https://doi.org/10.1038/s41565-021-00936-x

6. Repicky J, Wu P-K, Liu T, Corbett JP, Zhu T, Cheng S, Ahmed AS, Takeuchi N, Guerrero-Sanchez J, Randeria M, Kawakami RK, Gupta JA (2021) Atomic-scale visualization of topological spin textures in the chiral magnet MnGe. *Science*, 374(6574):1484–1487. https://doi.org/10.1126/science.abd9225

7. Mueller SM, Kim D, McMillan SR, Tjung SJ, Repicky JJ, Gant S, Lang E, Bergmann F, Werner K, Chowdhury E, Asthagiri A, Flatte ME, Gupta JA (2021) Tunable tunnel barriers in a semiconductor via ionization of individual atoms. *Journal of Physics-Condensed Matter*, 33(27):275002. https://doi.org/10.1088/1361-648X/abf9bd

8. McMillan SR, Flatté ME (2021) Theory of spin-polarized current flow through a localized spin triplet state. *arXiv:2112.14805 [cond-mat]*, http://arxiv.org/abs/2112.14805

9. Harmon NJ, Flatté ME (2021) Theory of oblique-field magnetoresistance from spin centers in three-terminal spintronic devices. *Physical Review B*, 103(3):035310. https://doi.org/10.1103/PhysRevB.103.035310

10. Zhu T, O'Hara DJ, Noesges BA, Zhu M, Repicky JJ, Brenner MR, Brillson LJ, Hwang J, Gupta JA, Kawakami RK (2020) Coherent growth and characterization of van der Waals 1T-VSe2 layers on GaAs(111)B using molecular beam epitaxy. *Physical Review Materials*, 4(8):084002. https://doi.org/10.1103/PhysRevMaterials.4.084002

11. Vedmedenko EY, Kawakami RK, Sheka DD, Gambardella P, Kirilyuk A, Hirohata A, Binek C, Chubykalo-Fesenko O, Sanvito S, Kirby BJ, Grollier J, Everschor-Sitte K, Kampfrath T, You C-Y, Berger A (2020) The 2020 magnetism roadmap. *Journal of Physics D: Applied Physics*, 53(45):453001. https://doi.org/10.1088/1361-6463/ab9d98

12. Noesges BA, Zhu T, Repicky JJ, Yu S, Yang F, Gupta JA, Kawakami RK, Brillson LJ (2020) Chemical migration and dipole formation at van der Waals interfaces between magnetic transition metal chalcogenides and topological insulators. *Physical Review Materials*, 4(5):054001. https://doi.org/10.1103/PhysRevMaterials.4.054001

13. McMillan SR, Harmon NJ, Flatte ME (2020) Image of Dynamic Local Exchange Interactions in the dc Magnetoresistance of Spin-Polarized Current through a Dopant. *Physical Review Letters*, 125(25):257203. https://doi.org/10.1103/PhysRevLett.125.257203

14. Krammel CM, Cruz AR da, Flatte ME, Roy M, Maksym PA, Zhang LY, Wang K, Li YY, Wang SM, Koenraad PM (2020) Probing the local electronic structure of isovalent Bi atoms in InP. *Physical Review B*, 101(2):024113. https://doi.org/10.1103/PhysRevB.101.024113

15. Corbett JP, Zhu T, Ahmed AS, Tjung SJ, Repicky JJ, Takeuchi T, Guerrero-Sanchez J, Takeuchi N, Kawakami RK, Gupta JA (2020) Determining Surface Terminations and Chirality of Noncentrosymmetric FeGe Thin Films via Scanning Tunneling Microscopy. *Acs Applied Materials & Interfaces*, 12(8):9896–9901. https://doi.org/10.1021/acsami.9b19724

16. Lee D, Gupta JA (2019) Perspectives on deterministic control of quantum point defects by scanned probes. *Nanophotonics*, 8(11):2033–2040. https://doi.org/10.1515/nanoph-2019-0212

Atomic Manipulation Using Electron Microscopes to Build and Better Understand Material Systems for Quantum Information Science

Stephen Jesse[1], Ondrej Dyck[1], Kyle Kelley[1], Christopher T. Nelson[1], Andy Lupini[1], Mina Yoon[2], Dirk Englund[3], Prineha Narang[4]

[1]Center for Nanophase Materials Sciences and Materials Science and Technology Division[2], Oak Ridge National Laboratory; [3]Massachusetts Institute of Technology; [4]University of California, Los Angeles

Keywords: atomic-scale manipulation and fabrication, in situ synthesis, quantum emitters, scanning transmission electron microscope

Research Scope

Delivering on the promise of quantum information science requires the ability to tailor and control minute interactions in coupled quantum states of a system, protect them from perturbations, and establish connections to the macroscopic world. Despite advances in precision synthesis that offer a new level of insight into the control and functional properties of defects in quantum materials, understanding quantum entanglement has proven to be difficult due to the interplay between defects and the host lattice environment, and intertwined interactions (e.g., electronic, phononic, and photonic) of the quantum state. To address this knowledge gap, it is essential to identify the underlying coherence and decoherence mechanisms and extract their modes of interaction. We seek to accomplish this through the application of atomically precise manipulation and characterization. Hence, our overarching goal is to understand the formation, behavior, and enhancement of entangled quantum states in solid state quantum emitters through atomic-level control over dopant and vacancy positions and material geometry enabled by electron beam-based atomic manipulation. We aim to develop new ways to create predefined defect-dopant complexes controllably and reliably at specific locations and in arrays that are electrically and optically accessible. We use and further develop advanced (ideally *in situ*) characterization methods to enable direct correlation of atomic structure to function. This information, in combination with theory and modelling developments, will be used to predict and better understand material dynamics during fabrication and emergent properties of the engineered structures.

Recent Progress

To examine the interplay between atomic-scale morphological artifacts, the host lattice, and longer-range structures such as Moire patterns and larger sculpted features, we need a detailed study of the beam-sample interactions that underpin predictable transformations. Understanding these atomic-scale processes and establishing the causal flow between governing *in situ* environmental parameters and the desired material modification outcomes is the key to atomic fabrication. Our research efforts have been aimed at revealing these fundamental atomic processes, identifying and reconciling the idealized and simplified theoretical understanding with the experimental observations, and the iterated implementation of experimental protocols to refine control over these material alterations, ultimately converging on atomic precision.

One fundamental unit of material modification is the introduction of a single vacancy. To replace a single lattice atom with that of another elemental species requires the removal of an atom from the host lattice. This step also forms the fundamental unit of any milling or sculpting process where structural reshaping of the base material relies upon the removal of atoms. For these reasons we have performed detailed investigations into the atomic ejection process that forms the foundation for atomic-scale construction.

Specifically, we examined the interplay between vacancies, extended reconstructed defects, dopants, and nanoparticle dynamics on single- and multilayer suspended graphene as a function of thermal excitation. Here, the sample temperature coupled with spatially modulated e-beam exposure form our governing *in situ* environmental parameters. To gain control over the system, we want to find repeatable inputs that result in repeatable (predictable) outputs. This process is facilitated by using a custom-built data acquisition and control platform that steers the microscope scan coils to direct the e-beam exposure, collects detector output signals, ensures temporal registration of the signals (i.e. keeps track of events through time), and performs real-time analysis to drive a decision/control workflow. This schema, depicted in Figure 1(a), enables the automation of repeated experiments ensuring uniform starting conditions and prespecified outcomes. This automated experimentation is critical as the number of structurally possible outcomes expands dramatically with the number of possible modifications, such that the statistical analysis of experimental observations is the only tractable way forward.

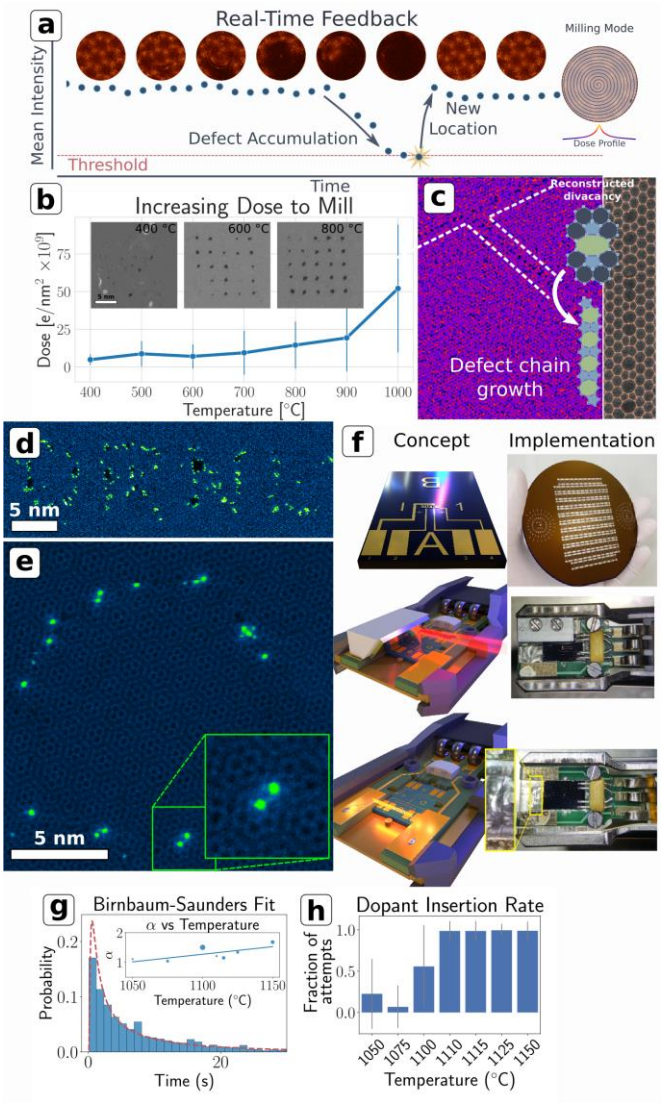

Figure 1 E-beam atomic fabrication. (a) Automated feedback-based experiment. (b) Aggregate hole milling data vs temperature. (c) Atomistic understanding of vacancy diffusion and defect chain growth. (d) First atom patterning demonstration. (e) Refinement of atom patterning. (f) Atomized material delivery concepts and implementations. (g) Statistical distribution of dopant insertion. (h) Dopant insertion rate vs temperature.

Thousands of observations of the creation of holes in suspended graphene at various temperatures were compiled and showed surprising results when analyzed statistically, Figure 1(b). At elevated temperatures, graphene becomes apparently very robust against beam damage and rupture. The current theoretical description of the effect of phonon excitation on ejection cross-sections predicts a slight enhancement of ejection probability with increasing temperature. However, our experimental observations show a strong trend in the opposite direction. These observations can be understood by accounting for vacancy-lattice and vacancy-vacancy dynamics at elevated temperatures. Extensive measurements and detailed modelling were used in combination to explain the temperature dependent nature of this behavior. Specifically, we identified spontaneous high-temperature vacancy diffusion and lattice restructuring which results in the formation of extended chains of restructured divacancies, Figure 1(c). The rapid diffusion of vacancies away from the irradiated region is responsible for the apparent robustness of the graphene. The discovery of the spontaneous formation of divacancy chains indicates a possible pathway towards creating embedded 1D functional structures in graphene.

With this enhanced foundational understanding of the simple creation of a hole, revised experiments were performed using bilayer graphene as a means to suppress vacancy mobility and fix vacancies close to their point of generation. Because one of the envisioned

purposes of vacancy generation in graphene is the directed attachment of dopant atoms, we simultaneously supplied adatoms (Cu) to promote the rapid attachment of these atoms to the generated vacancy sites. With this approach we were able to pattern Cu atoms into the twisted bilayer graphene, Figure 1(d) and (e).

This success has prompted the generation of a variety of strategies to supply atomized material in situ to e-beam generated defect sites. Concept renderings of on-chip, laser, and off-chip design strategies are shown in Figure 1(f) next to photographs of their realized implementation. The automated approach to dopant insertion has afforded the collection of a database of outcomes. The distribution of outcomes is shown in Figure 1(g) and the success rate as a function of temperature is shown in (h). A full structural analysis of this rich dataset is ongoing.

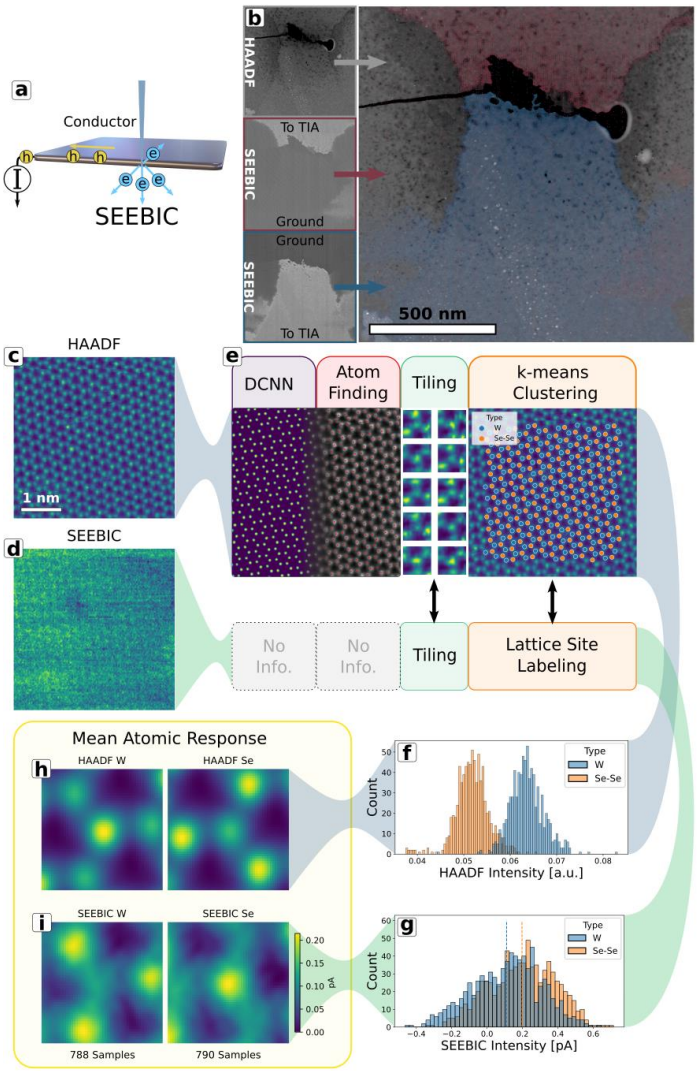

Figure 2 SEEBIC imaging. (a) Schematic diagram of SEEBIC imaging mode. (b) Example HAADF/SEEBIC composite image where color corresponds to electrically conductive and connected regions. (c) and (d) simultaneously acquired HAADF and SEEBIC images. (e) image analysis workflow. (f) and (g) extracted HAADF and SEEBIC atomic intensities. (h) and (i) mean HAADF and SEEBIC atomic response for the W and Se-Se lattice sites.

Secondary-electron e-beam imaging in STEM. This year saw substantial advances in the sensitivity and spatial resolution of measuring and imaging the current generated by the electron beam in STEM in 2D material systems. This approach can be used to visualize electron/hole transport with high resolution and was used to map electrical conductivity and connectivity in prototype 2D devices. A simplified schematic of the beam-induced emission and detection via an amplifier is shown in Figure 2(a). Contrast is generated by the total secondary electron emission yield measured directly by an amplifier connected to the sample, thus the name secondary-electron e-beam induced current (SEEBIC). In this imaging mode, conductive regions that are electrically connected to the amplifier appear bright and insulating or electrically disconnected regions of the sample appear dark. Parallel acquisition with other detector channels affords the opportunity to assemble composite images that map electrically conductive regions on top of standard HAADF (high angle annular dark field) images. Figure 2(b) shows an example mapping of a single layer of graphene supported on a SiN membrane. Notably, the graphene in the HAADF imaging mode is completely invisible due to the much larger signal from the SiN substrate. Imaging using the SEEBIC channel enables visualization of the device conductivity and electrical connectivity.

Because this imaging mode relies upon interactions with sample electrons, instead of nuclear scattering like HAADF imaging, the

contrast generation mechanism is fundamentally different. Notably, at the atomic scale (everything else being equal) the contrast is proportional to the projected electron orbital cross section. In Figure 2(c) and (d) we show the first images of this kind where atomically resolved HAADF and SEEBIC images were acquired on a 2D heterostructure device stack. The contrast in the HAADF signal corresponds to an encapsulated WSe_2 layer. The contrast in the SEEBIC signal is much more difficult to interpret directly because of the presence of the other layers. To extract the signal from just the encapsulated WSe_2 layer we leverage the dual information stream afforded by parallel acquisition modes. A deep covolutional neural network was used to identify atomic positions in the HAADF image on a pixel-by-pixel level, with this information registered, tiling followed by k-means clustering was performed on the HAADF image tiles to unambiguously identify the two lattice sites (W and Se-Se). Using this identification procedure, both the HAADF and SEEBIC image tiles could be registered to the WSe_2 lattice and build up a mean atomic response from the WSe_2 (all other signals being smeared out into a constant background). The mean atomic responses are shown in Figure 2(h) and (i). This result suggests that SEEBIC imaging could provide direct insight into the electron valance distribution and bonding interactions between atoms.

SEM-CL/PL as a platform to modify and measure single photon emission. Substantial effort this year was placed on making cathodoluminescence measurements an important component of the workflow to allow us to measure the response of engineered single photon emitters. In keeping with the overall spirit of this project, we have also demonstrated that the SEM can be used to controllably etch and drill diamond in situ (by introducing water into the chamber) while performing CL and photoluminescence measurements. We are able to controllably change the geometry of diamond microstructures that host NV and other optical centers while tracking the optical properties of the microstructures in real-time. We aim to use this approach to form and modify optical resonators while simultaneously measuring their influence on individual single photon emitter optical output.

Future Plans

A lot of the effort within this project is devoted to building new capabilities to use as we move forwards. Current examples include the UHV-compatible laser probe, the microchip platform capable of electrical and thermal control of the sample, and the custom scan-control unit for fast, patterned and variable scans. Each of these capabilities represents an individual advance but taken together they provide a unique opportunity to work towards the overarching goals of the project.

Laser driven evaporation and deposition of atomic species in situ. In a collaborative effort between ORNL, Waviks Inc, and Nion Co, we have designed and built a system that integrates a laser delivery system into the STEM column and focuses the light onto the sample for illuminating, heating, cleaning, and ablating of the sample or nearby targets. This is a first of its kind implementation on a Nion microscope and will enable many new paths to achieve in situ processing, atomic-scale manipulation, and enable photoexcited EELS measurements. Using the custom laser system and understanding developed this period we plan to extend the capabilities for in situ fabrication by implementing laser-driven evaporation and deposition of atomic species. We plan to vary the sample temperature and use independent control of the laser excitation to optimize dopant delivery, control, and insertion conditions.

Direct measurement of strain/distortion of defects under e-fields. In nanoscales structures, even a few volts of potential difference can create an enormous local field strength. Initial results suggest that this has a differential effect on the atomic motion at single defect sites. Using the microchip sample platform we developed, we plan to investigate the role of strain and distortions under locally applied electric fields.

Advanced characterization of manufactured nanostructures. Novel EELS measurements of patterned 2D materials will be used to capture changes in phonon and plasmon resonances. Using the controllable

patterned drilling, we plan to deterministically create patterned arrays of defects in 2D materials and experimentally investigate the changes in the phonon and plasmon resonance. Our hypothesis is that the theoretical components of this project will be able to indicate promising structures to create and signatures of novel quantum modes to search for. A key component of testing this hypothesis will be to map out the dispersion relationships for the quantum structures as a function of temperature. Cathodoluminescence in a CL/PL-SEM will be used to measure the created defects and to correlate their structures with observed properties. A cross-cutting feature of this program is the combination of techniques spanning different length scales and modalities. The sample holder that was developed for the STEM can also be used in the STM bringing a new way to explore the engineered structures.

FY22 Publications

Publications intellectually led by this FWP:

1. O. Dyck, J. L. Swett, C. Evangeli, A. R. Lupini, J. Mol, and S. Jesse, Mapping conductance and switching behavior of graphene devices in situ, *Small Methods* **6** (2022). DOI: 10.1002/smtd.202101245
2. O. Dyck, J. L. Swett, C. Evangeli, A. R. Lupini, J. Mol, and S. Jesse, Contrast mechanisms in secondary electron E-beam-induced current (SEEBIC) imaging, *Microsc. Microanal.* **28**, 1567 (2022). DOI: 10.1017/S1431927622000824
3. S. V. Kalinin, S. Jesse, and A. R. Lupini, A quantum lab in a beam, *Phys. Today* **75**, 30 (2022). DOI: 10.1063/PT.3.5018.
4. O. Dyck, S. Yeom, S. Dillender, A. R. Lupini, M. Yoon, and S. Jesse, The role of temperature on defect diffusion and nanoscale patterning in graphene, *Carbon* **201**, 212 (2023). DOI: 10.1016/j.carbon.2022.09.006

Other collaborative papers

5. N. Creange, O. Dyck, R.K. Vasudevan, M. Ziatdinov, S. V. Kalinin, Towards automating structural discovery in scanning transmission electron microscopy, *Mach. Learn.: Sci. Technol.* (2021). DOI: 10.1088/2632-2153/ac3844
6. J. Lapano, Y.-Y. Pai, A. R. Mazza, J. Zhang, T. Issacs-Smith, P. Gemperline, L. Zhang, H. Li, H. N. Lee, G. Eres, M. Yoon, R. Comes, T. Z. Ward, B. J. Lawrie, M. A. McGuire, R. G. Moore, C. T. Nelson, A. F. May, M. Brahlek, Self-regulated growth of candidate topological superconducting parkerite by molecular beam epitaxy, *APL Mater*. **9**, 101110 (2021). DOI: 10.1063/5.0064746
7. X. Kong, W. Luo, L. Li, M. Yoon, T. Berlijn, and L. Liang, Floquet band engineering and topological phase transition in two-dimensional transition metal dichalcogenides, *2D Mater.* **9**, 025005 (2022). DOI: 10.1088/2053-1583/ac4957
8. K. M. Roccapriore, O. Dyck, M. P. Oxley, M. Ziatdinov, and S. V. Kalinin, Automated experiment in 4D-STEM: Exploring emergent physics and structural behaviors, *ACS Nano* **16**, 7605 (2022). DOI: 10.1021/acsnano.1c11118
9. A. Ghosh, M. Ziatdinov, O. Dyck, B. G. Sumpter, and S. V. Kalinin, Bridging microscopy with molecular dynamics and quantum simulations: an atomAI based pipeline, *npj Comput. Mater*. **8**, 1 (2022). DOI: 10.1038/s41524-022-00733-7
10. K. M. Roccapriore, S.-H. Cho, A. R. Lupini, D. J. Milliron, and S. V. Kalinin, Sculpting the plasmonic responses of nanoparticles by directed electron beam irradiation, *Small* **18**, 2105099 (2022). DOI: 10.1002/smll.202105099
11. C. Park and M. Yoon, Topography inversion in scanning tunneling microscopy of single-atom-thick materials from penetrating substrate states, *Sci Rep* **12**, 7321 (2022). DOI: 10.1038/s41598-022-10870-0
12. A. Okmi, X. Xiao, Y. Zhang, R. He, O. Olunloyo, S. B. Harris, T. Jabegu, N. Li, D. Maraba, Y. Sherif, O. Dyck, I. Vlassiouk,; K. Xiao, P. Dong, B. Xu, and S. Lei, Discovery of graphene-water membrane

structure: Toward high-quality graphene process, *Adv. Sci.* 2201336 (2022). DOI: 10.1002/advs.202201336

13. Dyck, O.; Bao, F.; Ziatdinov, M.; Nobakht, A. Y.; Law, K.; Maksov, A.; Sumpter, B. G.; Archibald, R.; Jesse, S.; Kalinin, S. V.; Lingerfelt, D. B. Strain-Induced Asymmetry and on-Site Dynamics of Silicon Defects in Graphene. *Carbon Trends* **2022**, *9*, 100189. https://doi.org/10.1016/j.cartre.2022.100189.

Multiscale Quantum and Classical Microscopy for Superconducting Quantum Systems

Ben Lawrie, Eugene Dumitrescu, Gabor Halasz, Matt Brahlek, Chengyun Hua, Petro Maksymovych

Oak Ridge National Laboratory

Keywords: Quantum sensing, Vortex motion, Superconducting nanowire single photon detectors, topological quantum information

Research Scope

A fundamental understanding of superconducting and topological order is important for the advancement of new quantum sensors and qubits. Furthermore, microscopic control of vortex motion in disordered topological superconductors could enable coherent control of quantum information encoded in topological quantum states. Likewise, photon-induced vortex motion in disordered superconducting nanowire single photon detectors drives the device functionality needed for long-range quantum networking and sensing applications. In each case, limited microscopic understanding of vortex interactions in disordered superconductors constrains the development and advancement of the next generation of quantum technologies. Thus, *the overarching goal of this project is to understand and control disorder-induced changes in superconducting and topological states across atomic to mesoscopic length scales with quantum microscopies that will guide the development of emerging superconducting quantum devices.* In pursuit of this goal, we are addressing two research aims: (1) Understand the emergence of superconducting and topological order in the presence of disorder, and (2) Manipulate vortex motion in superconducting quantum devices with *in situ* and *ex situ* control of disorder and topology. We are addressing these aims with a unique combination of ultralow temperature quantum optical microscopies, nanoscale tunable Josephson junction spectroscopies, and operando characterization of superconducting quantum devices with close integration of materials synthesis and predictive approaches. The enhanced measurement sensitivity offered by our quantum microscopies will result in an unprecedented understanding of superconducting and topological quantum phenomena needed for the next generation of quantum sensing and fault tolerant quantum computation.

Recent Progress

Over the past two years, we have developed new understanding of the effects of atomic- to meso-scale disorder on the properties of quantum materials and devices, and we have developed squeezed light sources, color centers in two-dimensional materials, and tunable superconducting tunnel junctions as probes capable of providing classically inaccessible sensitivity in the study of superconducting and topological materials and devices. Furthermore, in collaboration with other BES-MSE projects at ORNL, we have advanced mK quantum transport capabilities for probing superconducting and topological phase transitions at the device scale. In collaboration with ASCR-funded QIS projects at ORNL, we have contributed to the development of a quantum network that allows for flexible distribution of optical and quantum optical resources to mK environments for entanglement distribution and quantum microscopies. Here, we provide a few representative accomplishments, including control of vortex dynamics in SNSPDs and disordered TSCs,

suppression of quantum noise in squeezed optical microscopies, control of hBN defect photophysics as a path toward integrated 2D quantum sensing, and understanding of the effect of atomic defects on unconventional superconductors at the nanoscale.

Control of vortex dynamics in SNSPDs

As shown in Fig. 1, we have measured and controlled vortex dynamics in silicide SNSPDs with field-, temperature-, bias-current-, and photon-position-dependent measurements at the device scale[1]. This work fills a critical gap in the literature by describing vortex crossing rates in SNSPDs in large magnetic fields. The dark-count scaling with temperature and magnetic field also allows for a single SNSPD to be used as a highly sensitive magnetometer and thermometer simply by tuning the bias current to an appropriate regime. The dark counts exhibit an asymmetry with magnetic field that results from symmetry constraints associated with the nanowire geometry and the vector field orientation[1]. We have also measured vortex dynamics more directly with temperature, bias-current, and magnetic field dependent rf reflection spectroscopy of large area superconducting microwire single photon detectors. These multidimensional spectroscopies provide detailed maps of microwave resonances that we can use to probe vortex dynamics and understand fundamental single photon detection mechanisms.

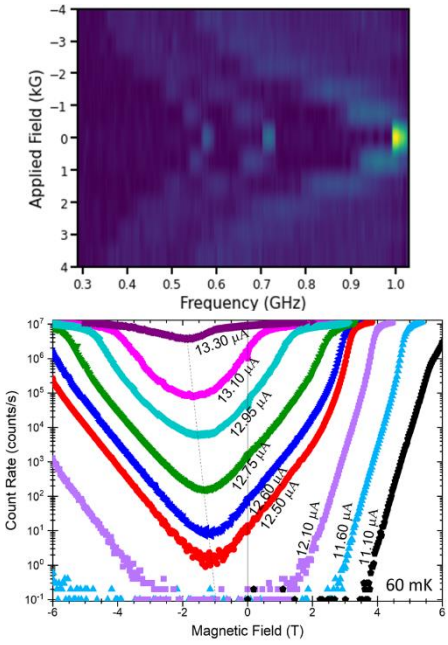

Fig. 1: (top) Vortex motion in Mo_xSi_{1-x} microwire detectors induced by variable out-of-plane magnetic fields and moderate bias currents induces changes in rf resonances at T=100 mK. (Bottom, adapted from ref. 1) Symmetry constraints in SNSPDs induce an asymmetric detector response to magnetic field that we've used for magnetometry and thermometry.

Control of vortex dynamics in disordered TSCs

We have recently found evidence of a new kind of Little-Parks oscillation in the candidate TSC $Pd_3Bi_2Se_2$ that corresponds to fractional magnetic-flux quantization. Such fractional Little-Parks oscillations reveal the spin-triplet nature of the underlying superconductor and the presence of exotic half-quantum vortices harboring Majorana zero modes (MZMs). Fast vortex manipulation in TSCs is crucial to the plausibility of quantum computation with vortex-bound MZMs. To that end, we proposed a scheme for the use of local heating based on scanning optical microscopy to manipulate Majorana bound states emergent in TSC vortex cores[2]. Specifically, we derived the conditions required for transporting a single vortex between two stationary defects by trapping it with a "hot spot" generated by local heating. Using these critical conditions for the vortex motion, we then established the ideal material properties for the implementation of our manipulation scheme. Guided by this theory, we have recently established preliminary evidence of vortex manipulation in FeSe with a STM. Together, these efforts provide an initial framework for the scalable manipulation of vortices and, ultimately, for MZM braiding.

Suppression of quantum noise in squeezed optical microscopies

We have recently described the fundamental limits of squeezed magneto-optical microscopies with classical and squeezed readout fields[3]. Because the shot noise limit is defined by the total number of photons at the detector, we can take advantage of a high-power local oscillator and a low power squeezed state to optimize the sensitivity at the SNL without introducing unwanted optical heating or backaction effects in low temperature environments. Moreover, for phase-based measurements, both channels of a two-mode squeezed state can be used to transduce the measurement signal. Phase-sum squeezing allows us to add the phase modulation on each channel while suppressing the quantum noise below the SNL. The ability to suppress quantum noise while introducing orders of magnitude less optical heating than conventional measurements allows us to perform high-throughput quantum enhanced microscopies that can be used to probe small fluctuations at mK temperatures.

Understanding and control of defects in hBN as integrated spin-based quantum sensors

We have recently used correlative cathodoluminescence and photoluminescence microscopies to characterize nanoscale strain enhancement of boron vacancy defect luminescence in hBN and demonstrate the potential for strain control of spin defects[4]. The ability to probe magnetic and topological excitations with spin defects in layered van der Waals systems will allow us to use a quantum sensor to encapsulate materials of interest, thus minimizing risks due to environmental sensitivity when vacuum transfer is not an option.

Understanding nanoscale disorder in superconducting materials

We have leveraged metric learning and compressive sensing techniques to image defects in unconventional superconductors like FeSe with greater statistical accuracy and fewer measurements than conventional raster-scanned images. Compressive sensing alone can enhance the imaging rate by at least 5-fold. Machine learning techniques allow us to abstract measured signals into low-dimensional representations and a probabilistic model for the measured data. Disparate measurements can then be rigorously compared on equal footing, enabling representative sampling of materials and their defects. We can then begin to close the nano-mesoscale gap, bringing the promise of multi scale imaging closer to reality.

Moreover, as shown in Fig. 2, we have also measured Josephson currents by tunneling microscopy with a superconducting tip. Because of thermal broadening, robust distinction between Josephson, Andreev and quasiparticle currents in such junctions presents an experimental challenge. To this end, we introduced two new approaches to consistently interpret the specific transport mechanism[5]. One utilizes the fundamental physics of Cooper pair tunneling across nanoscale gaps, while the other one relies on purely statistical arguments in the presence of disorder. The complementarity and consistency of the two mechanisms allows us to pursue more rigorous analysis of Josephson tunneling for unconventional and candidate topological superconductors.

Future Plans

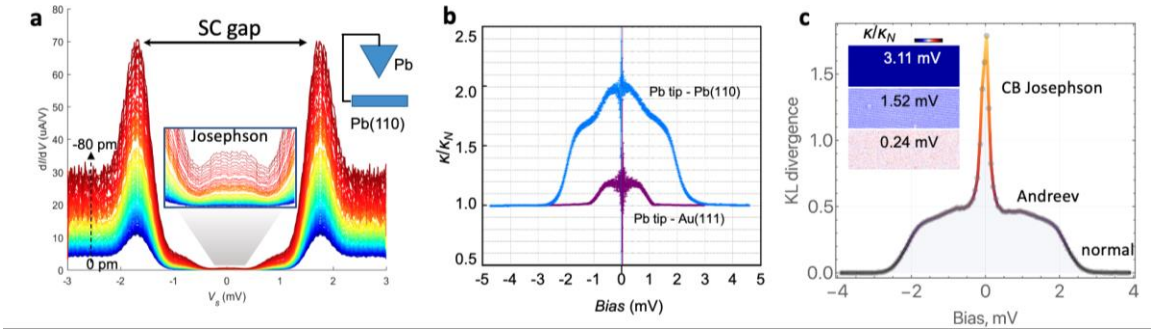

Fig. 2: (adapted from Ref. 5) (a) Josephson tunneling in STM at ~3K. (b) Renormalized tunneling decay rate (higher decay rate corresponds to faster current suppression with increased junction width), revealing three distinct regimes from 1.0 to 2.0, with intermediate plateau around 1.7. The value of 2.0 is characteristic of sequential Cooper pair tunneling due to a Coulomb blockade. (c) A statistical approach to differentiate tunneling mechanisms, utilizing energy-resolved effects of disorder (upper left corner). The approaches based on physical mechanism (b) and statistical analysis (c) exhibit excellent agreement with respect to the energy window for quasiparticle, Andreev and Josephson currents.

Over the next two years, we will build on our recent progress and develop new understanding and control of disorder-induced changes in superconducting and topological states across atomic to mesoscopic length scales. Our research plans combine quantum cryo-optical microscopies and Josephson scanning tunneling microscopy (JSTM) with complementary low temperature microscopies, materials synthesis and patterning, and multiscale modeling based on Ginzburg-Landau theory, the Bogoliubov-de Gennes formalism, and analytical descriptions of squeezed-light interactions with matter. By bootstrapping today's quantum sensors to provide a classically inaccessible understanding of nano to mesoscale heterogeneities in superconducting and topological order parameters, we will provide a fundamental contribution to the next generation of quantum technologies.

References

1. B. J. Lawrie, C. E. Marvinney, Y.Y. Pai, M. A. Feldman, J. Zhang, A. J. Miller, C. Hua, E. Dumitrescu, and G. B. Halász, Multifunctional Superconducting Nanowire Quantum Sensors. *Phys. Rev. Appl.* **16**, 064059 (2021).

2. C. Hua, G.B. Halász, E. Dumitrescu, M. Brahlek, and B. Lawrie, Optical vortex manipulation for topological quantum computation. *Phys. Rev. B* **104**, 104501 (2021).

3. Y.Y. Pai, C.E. Marvinney, C. Hua, R.C. Pooser, and B.J. Lawrie, Magneto-Optical Sensing Beyond the Shot Noise Limit. *Adv. Quantum Technol.* **5**, 2100107 (2021).

4. D. Curie, J. T. Krogel, L. Cavar, A. Solanki, P. Upadhyaya, T. Li, Y.-Y. Pai, M. Chilcote, V. R. Iyer, A. Puretzky, I. Ivanov, M.-H. Du, F. Reboredo, and B. Lawrie, Correlative Nanoscale Imaging of Strained hBN Spin Defects. *ACS Appl. Mater. Interfaces* **14**, 41361–41368 (2022).

5. W. Ko, E.F. Dumitrescu, and P. Maksymovych, Statistical detection of Josephson, Andreev, and single quasiparticle currents in scanning tunneling microscopy. *Phys. Rev. Res.* **3**, 033248 (2021).

Publications (10 most relevant)

1. D. Curie, J. T. Krogel, L. Cavar, A. Solanki, P. Upadhyaya, T. Li, Y.-Y. Pai, M. Chilcote, V. R. Iyer, A. Puretzky, I. Ivanov, M.-H. Du, F. Reboredo, and B. Lawrie, Correlative nanoscale imaging of strained hBN spin defects, ACS App. Mater. Int. **14**, 41361 (2022).
2. W. Ko, J.L. Lado, P. Maksymovych, Noncontact Andreev Reflection as a Direct Probe of Superconductivity on the Atomic Scale, Nano Letters, **22**, 4042 (2022).
3. Y.Y. Pai, C.E. Marvinney, L. Liang, J. Xing, A. Scheie, A.A. Puretzky, G.B. Halász, X. Li, R. Juneja, A.S. Sefat, D. Parker, L. Lindsay, and B.J. Lawrie "Mesoscale interplay between phonons and crystal electric field excitations in quantum spin liquid candidate CsYbSe2" J. Mat Chem. C, **10**, 4148 (2022).
4. Y.Y. Pai, C.E. Marvinney, C. Hua, Raphael C. Pooser, and Benjamin J. Lawrie, "Magneto-Optical Sensing Beyond the Shot Noise Limit", Advanced Quantum Technologies, **5**, 2100107 (2022).
5. B. J. Lawrie, C.E. Marvinney, Y.Y. Pai, M.A. Feldman, J. Zhang, A.J. Miller, C. Hua, E. Dumitrescu, and G.B. Halász, Multifunctional Superconducting Nanowire Quantum Sensors, Phys Rev. Applied, **16**, 064059 (2021).
6. M. Alshowkan, B. P. Williams, P. G. Evans, N. S.V. Rao, E. M. Simmerman, H.H. Lu, N. B. Lingaraju, A. M. Weiner, C. E. Marvinney, Y.Y. Pai, B. J. Lawrie, N. A. Peters, and J. M. Lukens, Reconfigurable Quantum Local Area Network Over Deployed Fiber, PRX Quantum, **2**, 040304 (2021).
7. J. Lapano, Y.Y. Pai, A. Mazza, J. Zhang, T. Isaacs-Smith, P. Gemperline, L. Zhang, H. Li, H.N. Lee, H. Miao, G. Eres, M. Yoon, R. Comes, T. Z. Ward, B. J. Lawrie, M. McGuire, R. G. Moore, C. T. Nelson, D. May, M. Brahlek, Self-regulated growth of candidate topological superconducting parkerite by molecular beam epitaxy, APL Materials **9**, 101110 (2021).
8. A. Dinerstein, C. Gorham, and E. Dumitrescu, "The hybrid topological longitudinal transmon qubit." *Materials for Quantum Technology*. **1**, 021001 (2021).
9. C. Hua, G. B. Halász, E. Dumitrescu, M. Brahlek, and B. Lawrie, Optical vortex manipulation for topological quantum computation, Phys. Rev. B **104**, 104501 (2021).
10. H. Li, T. T. Zhang, T. Yilmaz, Y.Y. Pai, C. Marvinney, A. Said, Q. Yin, C. Gong, Z. Tu, E. Vescovo, C. S. Nelson, R. G. Moore, S. Murakami, H. C. Lei, H. N. Lee, B. J. Lawrie, and H. Miao, Observation of unconventional charge density wave without acoustic phonon anomaly in kagome superconductors AV3Sb5 (A=Rb, Cs), Phys. Rev. X **11**, 031050 (2021).

Applications of Machine Learning to Scanning Transmission Electron Microscopy

Principle Investigators: Mark P. Oxley, Andy R. Lupini, Christopher T. Nelson, Sergei V. Kalinin, Miaofang Chi.

Center for Nanophase Materials Sciences, Oak Ridge National Laboratory, TN 37831

Keywords: STEM, 4D-STEM, EELS, Autoencoders

Research Scope

Machine learning (ML) is a rapidly advancing field with broad application to many areas of research. While many ML methods are well established, it is only recently that have become broadly applied to scanning transmission electron microscopy (STEM)[1]. The STEM offers a rich environment for data analysis. Signals such as annular dark field (ADF), electron energy loss spectroscopy (EELS) and scanning nano diffraction (4D-STEM) all offer insights into material functionality. Recent advances in monochromator construction have expanded the application of EELS to the phonon range, previously inaccessible to most electron microscopes. Machine learning provides a powerful tool to maximize the information that can be obtained from these datasets. Most current methods of analysis of 4D-STEM data are limited to thin crystals where the phase object approximation is at least partially valid. While appropriate to monolayer materials, this approximation fails rapidly for the majority of practical specimens. This offers an opportunity for ML to advance analysis beyond such simplistic approaches. ADF has long been the mainstay of STEM imaging and advances in machine stability and specialized facilities to minimize external vibrations has led to the ability to rapidly scan large fields of view. ML can be applied to these datasets to provide information about subtle changes in structure such as polarization and reordering at interfaces and routinely provide accurate atomic column locations. EELS can offer a wealth of information about local bonding within specimens but, because of low cross sections, the signal to noise ratio often makes analysis difficult. Autoencoders offer a method of "cleaning" these data sets without washing out local variations in structure. Perhaps the most exciting application of ML is not simple after the fact data analysis, but the possibility of facilitating automated experiments, allowing the experiment to focus explicitly on areas of interest and minimizing specimen damage.

Recent Progress

Aberration correction has allowed the routine acquisition of high-quality atomic resolution ADF images over large fields of view. ADF provides a signal proportional to the atomic number of the atoms in a column, allowing it to differentiate, for example, between the A and B sites of perovskite structures. Perhaps the simplest application of ML to these images if atom location and segmentation. This often provides the first step in further analysis. We have applied ML to characterize the distribution of ferroelectric polarization in $BiFeO_3$ with and without atom location[2]. An alternative approach is so called "Bayesian Crystallography"[3]. In this approach atom location is used as the first step. We then generate a data set by forming a stack subimages about each atom location using a suitable window size. The best window size depends on a number of factors, including the size of the features we want to characterize. For example, a window size

commensurate with the size of perovskite unit cell will easily differentiate between the A and B sites. These stacks are then used to train a rotationally invariant variational auto encoder (rVAE)[3]. Shown in figure 1 is the rotational variation in an ADF image of $(La_xSr_{1-x})MnO_{3-}$with NiO inclusions. The checkerboard pattern is characteristic of the alternating A and B sites in the perovskite. The NiO inclusions are clearly differentiated. In addition, horizontal stripes due to scan distortions a are clearly seen. This analysis can be expanded by examining the latent spaces obtained during the training of the data set. Using these latent spaces, a Gaussian mixture model can be applied to further differentiate between the different regions within the crystal structure. For example, the A and B sites in the perovskite are clearly defined, while the NiO structure is also clearly different. The boundary between the perovskite and the NiO inclusions is also identified as a different feature due to distortions at the interface. Local distortions in the perovskite structure are also highlighted in this manner.

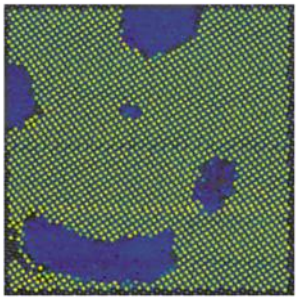

Figure 1. The rotational variation obtained using rVAE $(La_xSr_{1-x})MnO_3$ with NiO inclusions.

4D-STEM, or scanning nano-diffraction, where a diffraction pattern is recorded at each probe position also offers a wealth of information, but this is often complicated by channeling of the probe electrons in many circumstances. There are two common approaches to the ML analysis of convergent beam electron diffraction (GBED) patterns. The first involves the simulation of CBED patterns covering a range of possibilities which may occur in experiment. These are then used to train a model which can be used to characterize experimental results. We have, for example, used simulated CBEDs to train a model to differentiate between diffusion across an interface and the possibility of a hidden step[4]. Such an approach requires a detailed understanding of the experimental conditions in order to provide a training set that matches closely with reality. Factors such as temporal and spatial incoherence become an essential part of the simulations.

An alternative approach is the application of the rVAE directly to CBED patterns. Since many CBED patterns are similar up to a rotation, depending on the probe position with respect to the atomic columns, this offers a method of analysis without the need for extensive calculations[5]. In figure 2 we show the rVAE analysis of experimental 4D-STEM results for graphene with a 3-fold Si impurity and vacancy. Shown on the left is the simultaneously obtained ADF image. The standard center of mass (COM) deflection is shown in the second column. While the defect is clearly mapped out, the Si impurity is more difficult to discern. The results of the rVAE analysis is shown in the last three columns, with the rotation shown in the central column and the two latent spaces in the last two columns. There is little obvious variation in the rotation maps for both cases. While the defect is seen in bothe latent spaces, only the second latent space clearly picks out the impurity. This approach will be tested on newer data where the signal to noise ratio is significantly better.

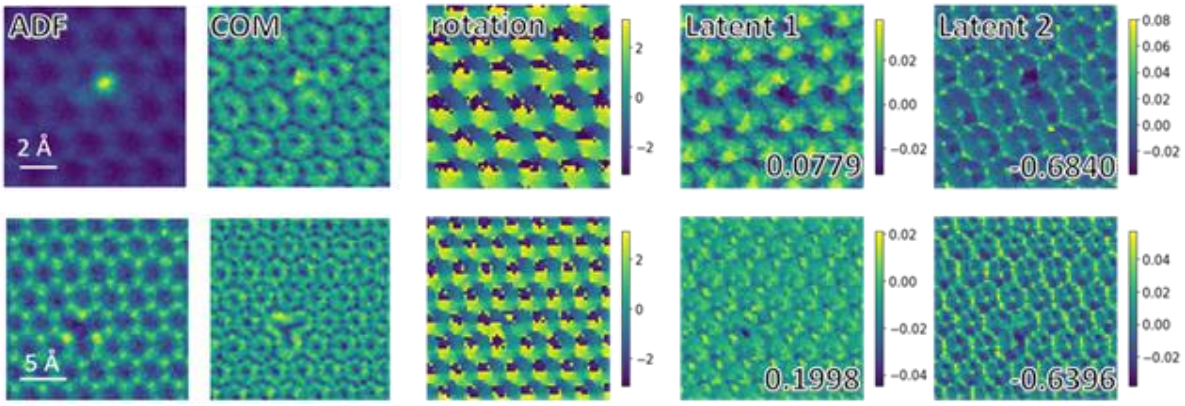

Figure 2: Top row: Graphene with a 3-fold Si impurity and 1 nm field of view. Bottom row: Graphene with a defect and 1.5 nm field of view.

Future Plans

We have applied autoencoders to the problem of denoising core-loss STEM EELS. This work is currently under review but offers the possibility of denoising other EELS signals without the loss of features commonly seen using principal component analysis. The use of models to match EELS near edge structure and the shape of phonon features will allow a robust way of denoising spectra for detailed analysis.

The availability of NERSCs new Perlmutter system greatly enhances the possibility of doing large scale simulations as an input to ML training sets. This will remove a bottleneck in current workflows since simulations have so far been limited by lack of GPU memory and threads.

New cameras on ORNLs Nion microscopes provide the opportunity for better quality datasets to analyze using new variations of the rVAE algorithms. In addition, new cryo stages and Lorentz microscopy capabilities offer fertile ground for additional application of ML.

References

1. S. V. Kalinin, C. Ophus, P. M. Voyles, R. Erni, D. Kepaptsoglou, V. Grillo, A. R. Lupini, M. P. Oxley, E. Schwenker, M. K. Y. Chan, J. Etheridge, X. Li, G. G. D. Han, M. Ziatdinov, N. Shibata and S. J. Pennycook, *Machine learning in scanning transmission electron microscopy.* Nature Reviews Methods Primers **2**, 11 (2022).

2. C. T. Nelson, A. Ghosh, M. P. Oxley, X. Zhang, M. Ziatdinov, I. Takeuchi and S. V. Kalinin, *Deep learning ferroelectric polarization distributions from STEM data via with and without atom finding*. npj Computational Materials **7**:149 (2021).

3. S. V. Kalinin, M. P. Oxley, M. Valleti, J. Zhang, R. P. Hermann, H. Zheng, W. Zhang, G. Eres, R. K. Vasudevan and M. Ziatdinov, *Deep Bayesian local crystallography.* npj Computational Materials **7**:181 (2021).

4. M P Oxley, J Yin, N Borodinov, S Somnath, M Ziatdinov, A R Lupini, S Jesse, R K Vasudevan and S V Kalinin, *Deep learning of interface structures from simulated 4D STEM data: cation intermixing vs. roughening.* Mach. Learn.: Sci. Technol. **1** 04LT01 (2020).

5. M. P. Oxley, M. Ziatdinov, O. Dyck, A. R. Lupinin, R. Vasudevan and S. V. Kalinin, *Probing atomic-scale symmetry breaking by rotationally invariant machine learning of multidimensional electron scattering*. npj Comput Mater **7**, 65 (2021).

Publications

1. S. V. Kalinin, C. Ophus, P. M. Voyles, R. Erni, D. Kepaptsoglou, V. Grillo, A. R. Lupini, M. P. Oxley, E. Schwenker, M. K. Y. Chan, J. Etheridge, X. Li, G. G. D. Han, M. Ziatdinov, N. Shibata and S. J. Pennycook, *Machine learning in scanning transmission electron microscopy.* Nature Reviews Methods Primers **2**, 11 (2022).

2. K. M. Roccapriore, N. Huang, M. P. Oxley, V. Sharma, T. Taylor, S. Acharya, D. Pashov, M. I. Katsnelson, D. Mandrus, J. L. Musfeldt, and S. V. Kalinin, *Electron-Beam Induced Emergence of Mesoscopic Ordering in Layered $MnPS_3$.* Accepted ACS Nano, (2022). DOI: 10.1021/acsnano.2c06253

3. K. M. Roccapriore, O. Dyck, M. P. Oxley, M. Ziatdinov, and S. V. Kalinin, *Automated Experiment in 4D-STEM: Exploring Emergent Physics and Structural Behaviors.* ACS Nano **16** (5), 7605-7614 (2022)

4. R. K. Vasudevan, M. Ziatdinov, V. Sharma, M. P. Oxley, L. Vlcek, A. N. Morozovska, E. A. Eliseev, S.-Z. Yang, Y. Gong, P. Ajayan, W. Zhou, M. F. Chisholm, and S. V. Kalinin, *Investigating phase transitions from local crystallographic analysis based on statistical learning of atomic environments in 2D MoS_2-ReS_2,* Applied Physics Reviews **8**, 011409 (2021)

5. M. P. Oxley, M. Ziatdinov, O. Dyck, A. R. Lupinin, R. Vasudevan and S. V. Kalinin, *Probing atomic-scale symmetry breaking by rotationally invariant machine learning of multidimensional electron scattering*. npj Comput Mater **7**, 65 (2021).

6. C. T. Nelson, A. Ghosh, M. P. Oxley, X. Zhang, M. Ziatdinov, I. Takeuchi and S. V. Kalinin, *Deep learning ferroelectric polarization distributions from STEM data via with and without atom finding*. npj Computational Materials **7**:149 (2021).

7. M. F. Chisholm, D. Shin, G. Duscher, M. P Oxley, L. F. Allard, J. D. Poplawsky and A. Shyam, *Atomic structures of interfacial solute gateways to θ′ precipitates in Al-Cu alloys.* Acta Materialia **212**, 116891 (2021).

8. S. V. Kalinin, M. P. Oxley, M. Valleti, J. Zhang, R. P. Hermann, H. Zheng, W. Zhang, G. Eres, R. K. Vasudevan and M. Ziatdinov, *Deep Bayesian local crystallography.* npj Computational Materials **7**:181 (2021).

9. M P Oxley, J Yin, N Borodinov, S Somnath, M Ziatdinov, A R Lupini, S Jesse, R K Vasudevan and S V Kalinin, *Deep learning of interface structures from simulated 4D STEM data: cation intermixing vs. roughening.* Mach. Learn.: Sci. Technol. **1** 04LT01 (2020).

Spectroscopic Visualization of Emergent Quantum Phenomena

Abhay Pasupathy and Kazuhiro Fujita
Condensed Matter Physics and Materials Science Division, Brookhaven National Laboratory

Keywords: Quantum Materials, Scanning Tunneling Microscopy, Superconductivity, 2D Materials, Thin films

Research Scope

The Scan Probe Microscopy FWP in the CMPMS division at Brookhaven National Laboratory is dedicated to the use of advanced spectroscopic tools to study the emergent quantum electronic properties of novel materials at cryogenic temperatures. This includes the study of unconventional superconductors grown in the division via molecular beam epitaxy and single crystal synthesis using scanning tunneling microscopy (STM) and Angle-Resolved Photoemission Spectroscopy (ARPES), the study of topological phenomena in solids using artificial heterostructures and the search for new quantum phases of matter in two dimensional materials.

Recent Progress

Recent progress in the area of unconventional superconductors includes (1) the discovery of smectic pair density wave order in $EuRbFe_4As_4$ (2) atomic scale visualization of electron-phonon coupling in BSCCO (3) Study of the disappearance of superconductivity in the overdoped cuprates (in collaboration with the neutron scattering group at CMPMS) (4) doping dependent machine learning assisted studies of superconductivity in cuprate films. In the area of two-dimensional materials, the group is studying the properties of heavily doped graphene synthesized by MBE-based metal doping. In the area of topological materials, the group is performing a search for topological superconductors in films of bismuth grown on BSCCO substrates. Finally, the group is also developing its instrumentation capabilities for the future. Details of this progress is briefly outlined below.

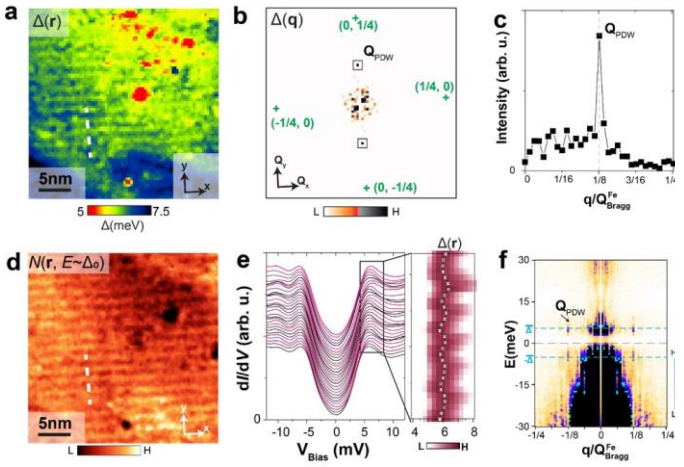

Figure. 1 PDW in Eu-1144 a, Superconducting gap map ($|\Delta(\mathbf{r})|$) showing unidirectional modulations. **b**, Fourier transform $|\Delta(\mathbf{q})|$ of a, showing a peak at $\mathbf{Q}_{\mathrm{PDW}}$. **c** Linecut of the Fourier transform in **b** through the $\mathbf{Q}_{\mathrm{PDW}}$ peak, showing a single pixel width. **d**, $N(\mathbf{r}, E \sim \Delta_0)$ map near the average superconducting gap energy, Δ_0 **e**, $N(\mathbf{r}, E)$ spectra along the white dashed line in **d**. The inset is the intensity map around the coherence peak energy, clearly showing the modulation of the coherence peaks in energy. **f**, Map of line cuts of the Fourier transform of $N(\mathbf{r}, E)$ through $\mathbf{Q}_{\mathrm{PDW}}$ as a function of energy.

1. Smectic Pair Density Wave Order in $EuRbFe_4As_4$

The pair density wave (PDW) is a novel superconducting state in which Cooper pairs carry center-of-mass momentum in equilibrium, leading to the breaking of translational symmetry. Experimental evidence for such a state exists in high magnetic field and in some materials that feature density wave orders that explicitly break translational symmetry. However, evidence for a zero-field PDW state that exists independent of other spatially ordered states has so far been elusive. In our work, we show that such a state exists in the iron pnictide superconductor $EuRbFe_4As_4$ (Eu-1144), a material that features coexisting superconductivity (T_c ~ 37 K) and magnetism (T_m ~ 15 K). We show from Spectroscopic Imaging Scanning Tunneling Microscopy (SI-STM) measurements that the superconducting gap at low temperature has long-range, unidirectional spatial modulations with an incommensurate period of ~8 unit cells (Figure 1). Upon raising the temperature above T_m, the modulated superconductor disappears, but a uniform superconducting gap survives to T_c. When an external magnetic field is applied, gap modulations disappear inside the vortex halo. The SI-STM and bulk measurements show the absence of other density wave orders, showing that the PDW state is a primary, zero-field superconducting state in this compound. Both four-fold rotational symmetry and translation symmetry are recovered above T_m, indicating that the PDW is a smectic order.

2. Visualization of electronic heterogeneity in doped graphene

We used OASIS-MBE to synthesize quasi-free-standing mononalyer graphene on SiC and achieved significant electron doping by intercalation of Yb, such that the $\pi*$ VHS is significantly shifted towards E_F. Angle-resolved photoemission spectroscopy (ARPES) confirms that the van Hove singularity has evolved from pointlike into an extended structure, as expected when the VHS approaches E_F (Figure 2). The spatial extent of Yb doping is explored via Spectroscopic Imagining Scanning Tunneling Microscopy (SI-STM) which reveals two striking features. First, the Yb dopants are randomly distributed along the carbon buffer layer in direct contrast with results involving Erbium dopants (Figure 2(c)). More strikingly, the position and amplitude of the VHS peak (Figure 2(d)) as well as Dirac point (Figure 2(e)) shows considerable spatial variation, and these variations appear to be directly linked to the positions of the ytterbium dopant atoms (Figure 2(f)).

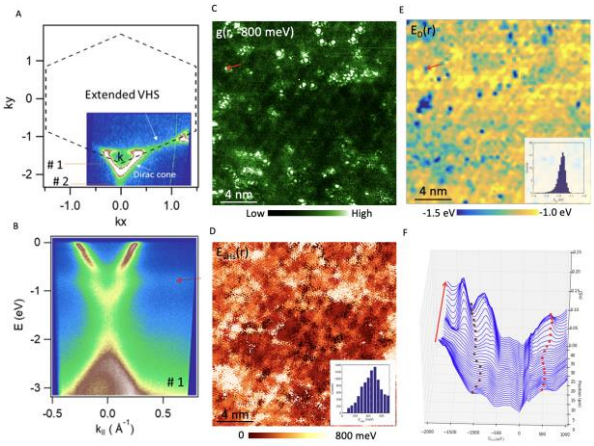

Figure 2 Doped graphene (a) Fermi surface of the doped Graphene measured by ARPES. (b) A(k,ω) along the line #1. (b) g(r,-800mV) in which local Yb states are observed. (d) $E_{vHS}(r)$ map showing electronic heterogeneity. Inset shows a distribution of the $E_{vHS}(r)$. (e) $E_D(r)$ map. Inset shows a distribution of the $E_D(r)$. (f) g(r,E) spectra extracted along the arrow in (c).

3. Periodic Atomic Displacements and Visualization of the Electron-Lattice Interaction in the Cuprate Superconductor

Traditionally, X-ray scattering techniques have been used to detect the breaking of the structural symmetry of the lattice, which accompanies a periodic displacement of the atoms associated with charge density wave (CDW) formation in the cuprate pseudogap states. Similarly, the Spectroscopic Imaging Scanning Tunneling Microscopy (SI-STM) has visualized the short-range CDW. However, local coupling of electrons to the lattice in the form of a short-range CDW has been a challenge to visualize, thus a link between these measurements has been missing. In this work, we introduce a novel STM-based technique to visualize the local bond length variations obtained from topographic imaging with picometer precision. Application of this technique to the high-T_c cuprate superconductor $Bi_2Sr_2CaCu_2O_{8+\delta}$ revealed a high-fidelity local lattice distortion of the BiO lattice as large as 2%. In addition, analysis of local breaking of rotational symmetry associated with the bond lengths reveals modulations around four-unit-cell periodicity in both B1 and E representations in the C4v group of the lattice(Figure 3(b, d)), which coincides with the uni-directional d-symmetry CDW (dCDW) previously identified within the CuO_2 planes (Figure3(a, c, d)), thus providing direct evidence of electron-lattice coupling in the pseudogap state and a link between the X-ray scattering and STM measurements. Overall, our results suggest that the periodic lattice displacements in E representations correspond to a locally-frozen version of the soft phonons identified by the X-ray scattering measurements, and a fluctuation of the bond length is reflected by the fluctuation of the dCDW formation near the quantum critical point.

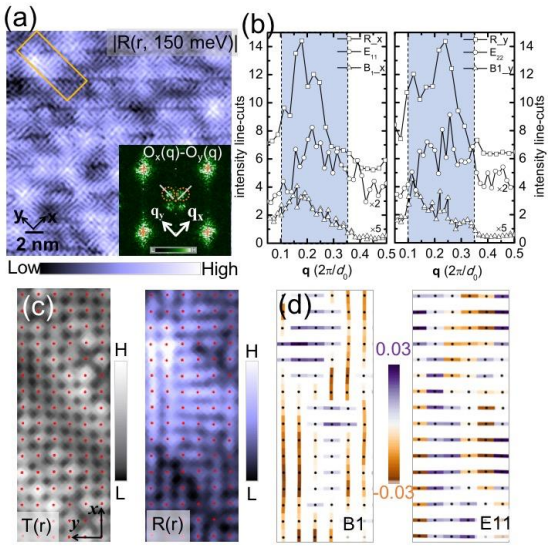

Figure 3, Visualizing atomic-scale electron-phonon coupling (a), Electronic modulations in the pseudogap states visualized in R(r,150mV) exhibiting the d-symmetry CDW (b), Line profiles extracted from the inset in A along grey lines, and line profiles along the same line trajectories in $B_1(r)$, $E_{11}(r)$ and $E_{22}((r)$ for both x (left) and y (right) Cu-O-Cu bond directions. (c), Topography, T(r) and R(r,150mV) extracted from a region in the solid orange rectangle in a, where a canonical d-symmetry CDW is observed. (d), B_1 and E_{11} maps from (c).

4. Overdoped $La_{2-x}Sr_xCuO_4$: Evidence for Josephson-coupled grains of strongly-correlated superconductor (collaboration with neutron spectroscopy and Advanced Energy materials groups at BNL).

How superconductivity disappears in cuprates at large hole doping has been controversial. To address this issue, we studied single-crystals and thin films of $La_{2-x}Sr_xCuO_4$ (LSCO)with $x \geq 0.25$. In particular, measurements of bulk susceptibility on LSCO crystals with x = 0.25 indicate an onset of diamagnetism at T_{c1} = 38.5 K, with a second transition to a phase with full bulk shielding at T_{c2} = 18 K, independent of field direction. In contrast, the in-plane resistivity only goes to zero at T_{c2}. Inelastic neutron scattering on x = 0.25 crystals confirms the presence of low-energy incommensurate magnetic excitations with reduced strength compared to lower dopings. The ratio of the spin gap to T_{c1} is anomalously large. These results are consistent with a picture in

which superconductivity initially develops within disconnected self-organized grains characterized by a reduced hole concentration. Bulk superconductivity occurs only after superconductivity is induced in the surrounding medium of higher hole concentration. Beyond the superconducting-to-metal transition, our local differential conductance measurements on an LSCO thin film suggest that regions with pairing correlations survive, but are too dilute to support superconducting order. Altogether, our results are consistent with a theoretical prediction by Spivak, Oreto, and Kivelson.

5. Doping dependent and machine learning studies of the $La_{2-x}Sr_xCuO_4$ thin films

LSCO thin films are synthesized in a sequence of different Sr compositions, equivalently controlling a hole density of the films spanning from the optimally to extremely overdoped regime where superconductivity is gone. We have observed superconducting spectra that show the particle-hole symmetry coherence peaks below 25mV virtually across all the doping levels even on the non-superconducting films in the overdoped regime. A systematic study of the spectral shape evaluating the superconducting gap Δ_0 and the zero bias conductance revealed that Δ_0 does not close but is rather 'filled' with increasing doping. Δ_0 decreases monotonically up to p~0.32 and then shows no doping dependence, while a reduction of the zero bias conductance continuously drops. These results suggest that the cuprate superconductivity in the overdoped regime is highly unconventional as opposed to a conventional BCS description.

We have developed a new algorithm using the unsupervised machine learning technique to classify domains that have different numbers of stacking layers of the MBE synthesized LSCO thin film (figure 4). These domains can be characterized by a local average and difference of the heights in the adjacent pixels and are classified by the k-means clustering, which is an unsupervised machine learning algorithm often used for a classification problem.

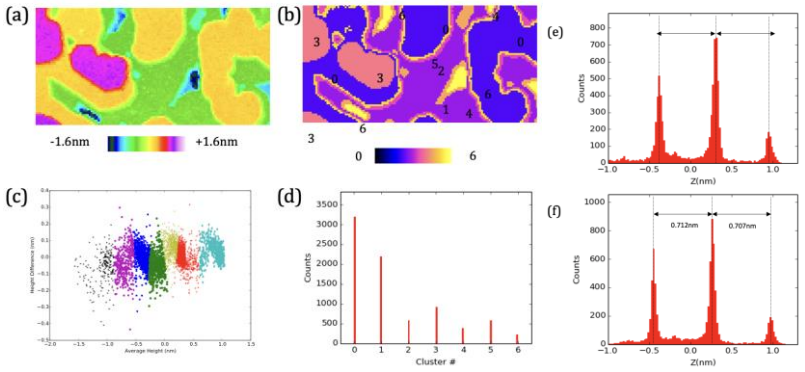

Figure 4 Machine-learning classifaction of STM spectra (a) Topograph in 500nm x 250 nm FOV. (b) Domain map. (c) Scatter plot for the height difference and average height that are divided into groups (domains) by the k-means clustering. (d) Number of counts(pixels) for each cluster (domain). (e, f) Distributions of the height before and after the domain-by-domain background subtraction.

It is expected that a height difference between domains is supposed to be integer multiples of the unit-cell length along c-axis. However, as shown in Figure 4, a distribution of the height shows peaks with inequivalent distances between them. This is because that the STM piezo scanner shows a non-linear response upon scanning over the large FOV, resulting in the inequivalent height difference (or background) between domains. As an application of our algorithm using the domain map in Figure 4(b), one can determine a local background in each domain and perform a

background subtraction domain by domain in order to mitigate an effect of the non-linear response of the piezo scanner. Figure 4(f) is a height distribution of the domain-by-domain background subtracted topograph, which now shows virtually equal distances between peaks. This technique can also be applied to identify a domain structure of the multi-layer-stacked graphenes and whatever other materials that show domain structures.

6. Study of the topological states on Bi(110) islands

We have synthesized Bi(110) islands on top of the cuprate superconductor $Bi_2Sr_2CaCu_2O_{8+d}$ by using MBE and studied higher order topological edge states as well as the topological nature of the Dirac fermions on the surface. Topography of the Bi (110) thin film shows islands that are extended along high symmetry directions of the material. Local density of state maps show enhanced intensities along the edges of the Bi (110) islands. In our experiments, we observe that the enhancement of the local density of states occurs at particular edges, but not all the way around, suggesting higher order topological edge states in this compound. Further, Dirac fermions are visualized by the quasiparticle interference imaging in these samples, giving us direct insights into the reciprocal space electronic structure of the films.

7. Development of the new SI-STM system

A new SI-STM system with the vector superconducting magnet and 3He fridge is under development. Figure 5(a) is a 3D assembly of the new SI-STM system that consists of the load-lock, room temperature UHV chamber, UHV sample storage, 3He insert, cryostat with the magnet and vibration isolation table. Recently, we have finished installing the vibration isolation table in the acoustic shielded room. Designing, procurement and installation of individual components are in progress.

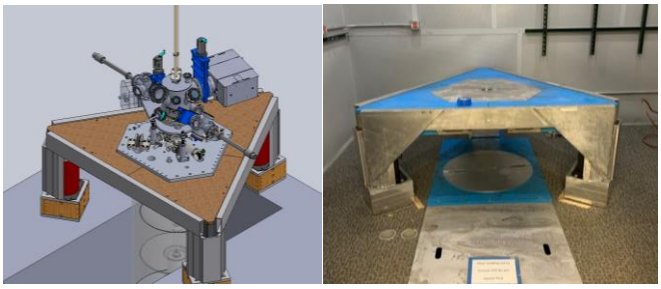

Figure 5 (a) 3D assembly of the new SI-STM system. (b) Vibration isolation table recently installed in the acoustic shielded room.

We are also developing high frequency circuitry, in which a shot noise that is generated at the tunneling junction when electrons are tunneling through can be measured. This circuit separates the tunneling current at low frequencies (DC – ~1kHz) from those at high frequencies (1GHz > f > 1kHz) through the bias tee. Since the 1/f and structural resonances are dominant at low frequencies, the high frequency signal is a good measure of the shot noise as the Johnson noise is small enough at low temperature. Such a high frequency signal is amplified by a cryogenic amplifier such that the shot noise signal is above the background noise level enabling us to perform a precise measurement of the shot noise. This circuitry will be installed to the existing SI-STM setup and/or new system.

Emergent Behavior in Nanoscale Functional Heterostructures

Charudatta Phatak, Saidur Bakaul, Amanda K. Petford-Long, Suzanne G. E. te Velthuis
Materials Science Division, Argonne National Laboratory, 9700 S Cass Avenue, Argonne, IL 60439

Keywords: Magnetic nanostructures, van der Waals materials, topological structures, microscopy

Research Scope

Our vision is to develop a framework to enable us to design, explore and control emergent behavior in functional nanoscale heterostructures that show ferromagnetic (FM), and ferroelectric (FE) properties. We seek to achieve this by gaining a deeper understanding of the local energy landscape that governs the novel behavior. Our research approach will make use of 2D and 3D aberration corrected Lorentz transmission electron microscopy (LTEM), advanced scanning probe microscopy and magneto-optic Kerr effect (MOKE) microscopy combined with theory and simulation to determine the quantitative parameters that control the spin textures and transport behavior in the heterostructures. We aim to design the emergent behavior by controlling the ferroic interactions using geometric parameters such as patterned shapes, curvature, interfaces, and the microstructural parameters such as defects, strain and coupling between adjacent nanostructures. Specific scientific challenges that we are addressing include elucidating the effects of geometric confinement and curvature on spin textures in ferromagnetic nanostructures, understanding the energy terms that control spin and charge transport in a heterogeneous energy landscape, and emergence of novel domain behavior in ferroelectric thin films.

Recent Progress

<u>Ferromagnetic van der Waals (vdW) materials:</u>

Two-dimensional (2D) magnetic vdW materials are an exciting material platform to explore novel spin interactions due to their strong in-plane spin coupling and weak out-of-plane coupling. We used in situ cryo LTEM to explore ferromagnetic domains in exfoliated flakes (thickness 40–150 nm) of Fe_3GeTe_2 (FGT) as a function of temperature and external magnetic field. FGT is an itinerant ferromagnet with a strong perpendicular anisotropy and T_C of 220 K. Quantitative reconstruction of magnetic induction maps showed the formation of Néel-type stripe domains under zero-field-cooling and skyrmion lattice under field-cooling (Fig 1(a)). Using a machine-learning approach we analyzed the behavior of skyrmion lattices and showed a thermally-induced hysteretic lattice ordering (Fig. 1(b)). We developed an analytical model to understand the skyrmion energy landscape, and by combining the model and experimental results, we could fully explain the effect of temperature

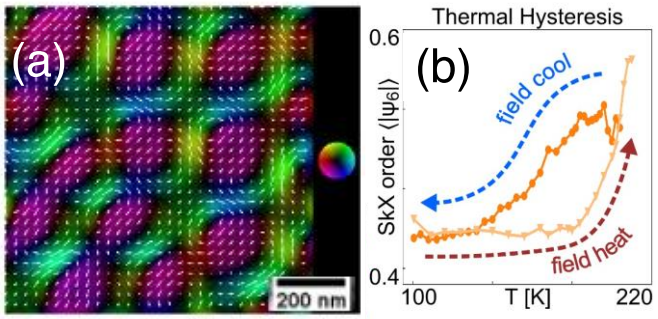

Figure 1. (a) Reconstructed magnetic induction map showing the formation of skyrmion lattice in Fe3GeTe2 at T = 100 K; (b) Thermal hysteresis of the skyrmion lattice order during field cooling and heating.

and applied field on skyrmion size and size distribution which results in the large-scale hysteresis and changes in order in the skyrmion liquid phase. Our fundamental understanding of how to control skyrmion size and order in the skyrmion lattices provides insights towards potential low-power skyrmionic computing devices.

Curved magnetic nanostructures:

Curvilinear magnetic structures exhibit unique magnetic behavior due to the curvilinear boundary conditions as well as the curvature induced anisotropy such as Dzyaloshinskii–Moriya-like interaction. We explored the magnetization reversal behavior of 3D cylindrical nanowires fabricated from Permalloy. Coupled with simulations, we were able to show the existence of a metastable double-helix spin texture in these nanowires with diameter larger than 100 nm (Fig 2(a) and (b)). We determined that this state is stabilized due to a fine balance between the magnetostatic energy modified due to cylindrical shape, and exchange energy in the nanostructure. This state was repeatedly achievable during the magnetization reversal. Our work provides insights into effect of curvature on stabilizing emergent magnetic spin textures in cylindrical nanowires that are of importance from a fundamental perspective as well as for technological applications.

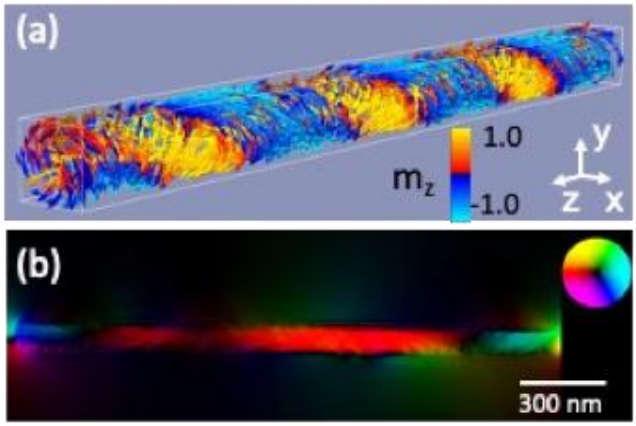

Figure 2. (a)3D vector map of the magnetization showing the double-helix state obtained using MuMax, (b) Reconstructed magnetic induction map showing the domain structure in cylindrical NiFe nanowire.

Coupled magnetic islands:

The coexistence of geometric frustration and antiferromagnetic coupling has been identified to lead to rich magnetic phases. We have explored this collective behavior in dimerized artificial spin ice lattices. We fabricated coupled Permalloy nanomagnets or dimers on a Kagome lattice with varied inter-island spacing as small as 20 nm. Using LTEM, we directly visualized the magnetic state of individual nanomagnets and the inter-island coupling as shown in Fig 3, showing a geometry-dependent antiferromagnetic phase in the lattices. Using micromagnetic modeling, and Monte Carlo simulations, we were able to quantitatively understand the competing local interactions that govern the emergence of a short-range ordered antiferromagnetic state wherein the vertex magnetic charge is uniform across the lattice. These results provide insights into the physics of magnetic frustration in antiferromagnets and low-dimensional spin systems.

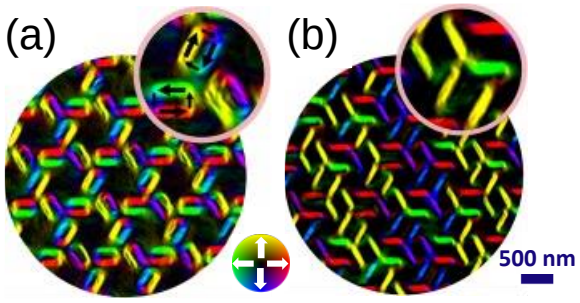

Figure 3. Reconstructed magnetic induction maps showing the magnetic state of each nanomagnet and its stray field in two lattices with different inter-island spacing of (a) 130 nm and (b) 250 nm.

We also investigated T and I-shaped permalloy islands deposited on a Nb superconducting layer with MOKE microscopy to characterize the magnetic domains and field dependence of the magnetization of these devices. The shape anisotropy of the devices results in differences in the saturation field, remanent magnetization, and domain configuration between T and I-shaped devices, and for different field strengths and directions. These results are important for understanding the Abrikosov vortex dynamics observed in the Nb superconductor covered by arrays of these devices.

Ferroelectric bubbles:

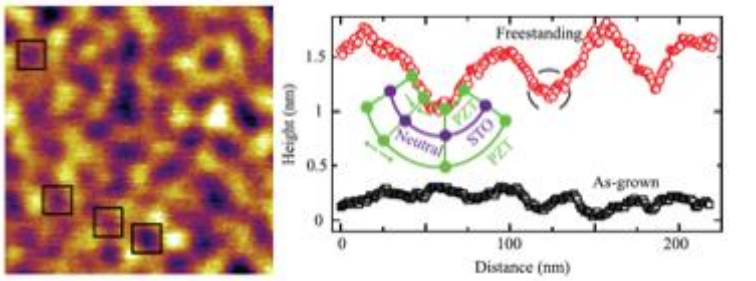

Figure 4. LH: PFM image of heterostructure. Squares indicate bubble domains. The image size is 200 nm. RH: Topology map across freestanding and as-grown films. Circle indicates flat region where bubbles are most abundant.

The competing correlations among elastic, electrostatic, and gradient energies in ferroelectric–dielectric–ferroelectric heterostructures can create topological objects with complex polar order. We used a new scanning probe method based on Fourier coefficients and piezoresponse correlation function analysis to explore ferroelectric bubble domains in a freestanding $PbZr_{0.2}Ti_{0.8}O_3$ (3nm)/$SrTiO_3$(2 nm)/$PbZr_{0.2}Ti_{0.8}O_3$ (3 nm) heterostructure. The bubble domain size is larger in the freestanding state than in the as-grown state, which results from the lack of epitaxial strain in the freestanding film. Our results also show that in most cases, the larger structural ripples in the freestanding films serve as long-wavelength modulation envelopes for the bubble domains, with bubbles clustered along the peaks and valleys of the ripples. This work demonstrates that films containing polar topological structures can be integrated with arbitrary substrates and potentially utilized for novel electronic applications.

AI-enabled magnetic imaging:

In order to obtain quantitative information on magnetic and electrostatic potentials of the sample, it is essential to retrieve the phase shift of electron wave after it interacts with the sample in LTEM. We have developed a machine learning method based on automatic differentiation (AD) that enables phase retrieval with higher spatial resolution and higher phase sensitivity. Our method vastly outperforms TIE and other iterative methods in terms of accuracy for both simulated and experimental datasets, under the same electron dose condition and experimental setup. Moreover, we can retrieve the experimental electron-optical parameters of the microscope that are typically not well known. Our method can be broadly applied across various TEM imaging modalities.

Future Plans

Topological Excitations in Ferromagnetic van der Waals materials

We are exploring ways to create novel topological excitations such as skyrmions or spin textures with higher winding numbers in van der Waals ferromagnets. We will continue exploration of differently doped compounds of Fe-Ge-Te and Cr-Ge-Te family. We seek to create heterostructures using such van der Waals materials that enable control of interfacial interactions

such as leading to interfacial Dzyaloshinkii-Moriya interaction or strain or other anisotropic interactions. We will use in-situ Lorentz TEM coupled with micromagnetic modeling that will enable us to correlate the domain behavior and determine the energy terms that govern the resulting behavior. We will also explore the transport behavior of such topological excitations using various effects such as spin transfer torque or spin obit torques.

Disordered Artificial spin ices

We are extending our studies of ASIs to systematically explore the role of lattice disorder on the magnetic frustration and magnetic ordering in the lattice. In particular, we are exploring lattices generated using various combinations of rhombus tiling that exhibit long range translational and orientational order to quasi periodic order and finally random order. We seek to understand the emergence of ground state behavior of these lattices. We will also explore the in-situ magnetization reversal to determine the role of certain motifs that control the reversal behavior thereby leading to emergence of frustrated sites in the lattices. We will explore transport of magnetic solitons across connected ASI lattices to understand the effect of their chirality and winding number on the magnetoresistance of the lattices. The resulting magnetoresistance will be correlated with the experimental magnetic configuration of the lattice which can enable us to understand the emergence of memristive behavior.

Synthetic antiferromagnets

We are exploring ways to control emergent spin textures in synthetic antiferromagnets.[1] Synthetic antiferromagnets consist of multiple magnetic thin films that are coupled through various interfacial interactions such as the RKKY interaction mediated through spacer layer that enables the individual thin films to be coupled antiferromagnetically. We have demonstrated previously that by controlling the thickness of the spacer layer and the shape of the magnetic structures, we can stabilize meron spin textures in Permalloy discs. We will continue to explore the energy landscape of such magnetic heterostructures by varying thicknesses, materials and shape to create compensated or uncompensated antiferromagnets. Some of the emergent phenomena that we will focus on are cross-over behavior from Bloch to Néel type domain walls which can give rise to novel magnetic singularities such as Bloch points, as well as interesting magnetic transport behavior due to dissipationless transport.

References

1. W. Legrand, D. Maccariello, F. Ajejas, S. Collin, A. Vecchiola, K. Bouzehouane, N. Reyren, V. Cros, and A. Fert, "Room-Temperature Stabilization of Antiferromagnetic Skyrmions in Synthetic Antiferromagnets", *Nat. Mater*. **19**, 34 (2020).

Publications

[1] A. R. C. McCray, T. Cote, Y. Li, A. K. Petford-Long, and C. Phatak, "Understanding Complex Magnetic Spin Textures with Simulation-Assisted Lorentz Transmission Electron Microscopy," *Phys. Rev. Appl.*, **15**, 044025 (2021).

[2] V. Brajuskovic and C. Phatak, "Understanding curvature effects on the magnetization reversal of patterned permalloy Archimedean spirals," *Appl. Phys. Lett.*, **118**, 152409 (2021).

[3] F. Barrows, H. Arava, C. Zhou, P. Nealey, T. Segal-Peretz, Y. Liu, S. Bakaul, C. Phatak, and A. Petford-Long, “Mesoscale Confinement Effects and Emergent Quantum Interference in Titania Antidot Thin Films”, *ACS Nano*, **15**, 12935 (2021).

[4] T. Zhou, M. Cherukara, and C. Phatak, “Differential programming enabled functional imaging with Lorentz transmission electron microscopy,” *npj Comput. Mater.*, **7**, 141 (2021).

[5] V. Brajuskovic, T. E. Gage, H. H. Liu, I. Arslan, A. K. Petford-Long, and C. Phatak, “Behavior of thermally quenched topological defects in quasicrystal artificial spin ices,” *Phys. Rev. B*, **104**, 144427 (2021).

[6] S. R. Bakaul, S. Prokhorenko, Q. Zhang, Y. Nahas, Y. Hu, A. Petford-Long, L. Bellaiche, and N. Valanoor, “Freestanding Ferroelectric Bubble Domains”, *Adv. Mater*. **33**, 2105432 (2021).

[7] Y. Li, R. Basnet, K. Pandey, J. Hu, W. Wang, X. Ma, A. R. C. McCray, A. K. Petford-Long, and C. Phatak, “Field-Dependent Magnetic Domain Behavior in van Der Waals Fe3GeTe2”, *Jom* **74**, 2310 (2022).

[8] Y. Li, F. Barrows, A. R. C. McCray, T. Cote, D. Friedman, R. N. S. Divan, A. K. Petford-Long, and C. Phatak, “Geometric Control of Emergent Antiferromagnetic Order in Coupled Artificial Spin Ices”, *Cell Reports Physical Science* **3**, 100846 (2022).

[9] V. Brajuskovic, A. McCray, Y. Zhang, and C. Phatak, “In situ observation of the magnetization configuration and reversal in cylindrical nanowires,” *APL Mater.*, **10**, 081109 (2022).

[10] A. R. C. McCray, Y. Li, R. Basnet, K. Pandey, J. Hu, D. P. Phelan, X. Ma, A. K. Petford-Long, and C. Phatak, “Thermal Hysteresis and Ordering Behavior of Magnetic Skyrmion Lattices”, *Nano Lett.*, https://doi.org/10.1021/acs.nanolett.2c02275 (2022).

Liquid Cell Electron Microscopy: Heterogeneity and Fluctuations at Solid-Liquid Interfaces

Principal Investigators: Haimei Zheng[1], Peter Ercius[2], Emory Chan[2], Lin-Wang Wang[1]

[1]Materials Sciences Division, Lawrence Berkeley National Laboratory, Berkeley, CA 94720

[2]The Molecular Foundry, Lawrence Berkeley National Laboratory, Berkeley, CA 94720

Keywords: Liquid cell electron microscopy, *in situ* transmission electron microscopy, nanoscale materials transformations, solid-liquid interfaces

Research Scope

The overarching goal of this program is to develop and utilize the advanced in situ liquid cell transmission electron microscopy (TEM) to elucidate how atomic level heterogeneity and fluctuations at solid-liquid interfaces determine the physical and chemical properties or processes of materials, with a focus on nucleation and precipitation/dissolution in liquids or at solid-liquid interfaces. Liquid cell TEM allows to gain critical insights into the underlying mechanisms on nucleation, growth, and other nanoscale transformations critical to novel materials discovery and their applications in functional devices. The development of advanced instrumentation for atomic imaging and chemical identification through liquids provides transformative opportunities unveil the mechanisms of nanoscale materials transformations, and dynamic phenomena at solid-liquid interfaces, especially those involving non-equilibrium processes.

Recent Progress

1. Atomic pathways of nanoscale materials transformations

We have made progress towards our program goals in the past two years. Following the previous success on development of high resolution liquid cells with thin membranes (e.g., amorphous carbon film, graphene, MoS_2, etc.), we have a series of discoveries on the atomic pathways of nanoscale materials transformations. We highlight a few publications achieved in the past two years as follows.

1.1 Defect-mediated ripening of core-shell nanostructures

Ripening of nanostructures frequently occurs in the growth of nanocrystals, nanoporous structure for mation, heterogeneous catalysis, and other nanoscale materials processes. To date, many ripening processes are described as thermodynamically driven through minimization of the surface energy, however the dynamical pathways of ripening remain elusive. At the nanoscale, heterogeneity and fluctuations often dominate, and defects may play a significant role in many physical and chemical transport processes underlying coarsening. Unfortunately, how defects impact the atomic pathways of ripening, especially in solution processes, has rarely been reported. This is largely due to the challenges in observing nanomaterial dynamics at atomic resolution. With cadmium-cadmium chloride core-shell nanostructures (Cd-$CdCl_2$) as a model system, we studied the ripening of core-shell nanostructures with a focus on the role of defects. Our

investigation reveals the atomic reconstruction of the whole nanoparticle during ripening, which has not been achieved previously.

The atomic structure evolution of two Cd-$CdCl_2$ core-shell nanoparticles during ripening is shown in **Fig. 1**. Throughout the ripening, nanoparticle 1 (P1) grows at the expense of nanoparticle 2 (P2) until one larger nanocrystal with almost perfect core-shell structure was achieved (**Fig. 1A, B**). The evolution of the two cores is shown by contour maps of the projected shapes (**Fig. 1C**). To better understand how mass transfers between the cores and shells, we tracked the evolution of each nanoparticle separately. We found that although the two particles were in contact with each other, the mass does not transmit directly through the shared surface. Instead, the core of P2 is first dissolved into the solution through defects in the shell, and the growth of the core of P1 is mediated through crack defects. Interestingly, the growth of P1 follows a nontraditional path: the core grows directionally along certain facets increasing the perimeter of the shell, but the shell thickness is maintained. Our experimental observation shows that mass transfer between particles does not depend on the size of the particles but instead on the existence of nanoscale crack defects, which mediate dissolution and growth. The shell structure fluctuates between crystalline and disordered states, which leads to the generation and annihilation of crack defects (**Fig. 1D**). This is distinctly different from any reported ripening processes, such as Ostwald ripening, digestive ripening, intra-particle ripening, and merging of core-shell particles.

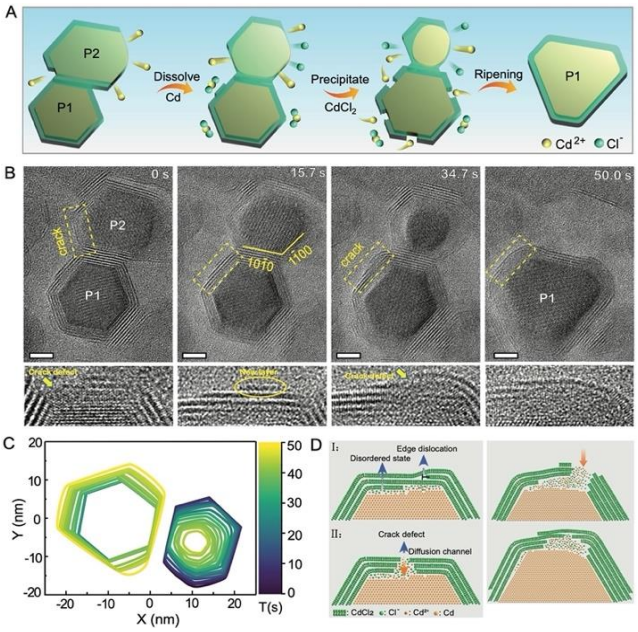

Fig. 1. The defect-mediated ripening process of Cd-$CdCl_2$ core-shell nanoparticles. A. Schematic illustration of the evolution pathway of Cd-$CdCl_2$ core-shell nanostructures undergoing the defects-mediated ripening. **B.** Sequential images from a movie show the ripening process. Scale bar, 5 nm. The enlarged images corresponding to the yellow boxes highlight defects in the shell, a new $CdCl_2$ layer, a crack defect, and healing of the shell. **C.** The contours indicate the shape evolution of the cores. **D.** Illustrations based on the experimental observation show the structural features of the two stages. In stage I, there is a disordered state layer located at the Cd-$CdCl_2$ interface and an edge dislocation among the $CdCl_2$ shell. In stage II, a crack defect is formed in the shell, which allows Cd ions to go through the shell.

To evaluate the generality of the crack-mediated ripening mechanism, we also developed a lattice model. With this highly simplified model, the basic kinetic processes observed within the liquid cell TEM have been recapitulated, which suggests that this defect-mediated ripening mechanism is applicable to other core-shell nanoparticle systems.

1.2 Ligand-controlled etching of nanoparticles

The adsorption of ligand molecules on nanocrystal surfaces strongly influences the nanocrystal behavior in a variety of applications, including catalysis, self-assembly, synthesis, and etching. Oxidative etching has emerged as a feasible approach to manipulate the shape of nanocrystals. During etching reactions, organic molecules or ions can be adsorbed on specific facets, which leads to facet-dependent etching and formation of nanocrystals with various morphologies. However, ma ny specifics, such as the binding location of ligands and their effect on nanocrystal shape transformations, still warrant experimental observation.

We investigated the etching of ~20 nm Pd nanocrystals in an aqueous solution of $FeCl_3$ and Fe (III) acetylacetonate ($Fe(acac)_3$). $Fe(acac)_3$ was used as the inhibitor molecule to control

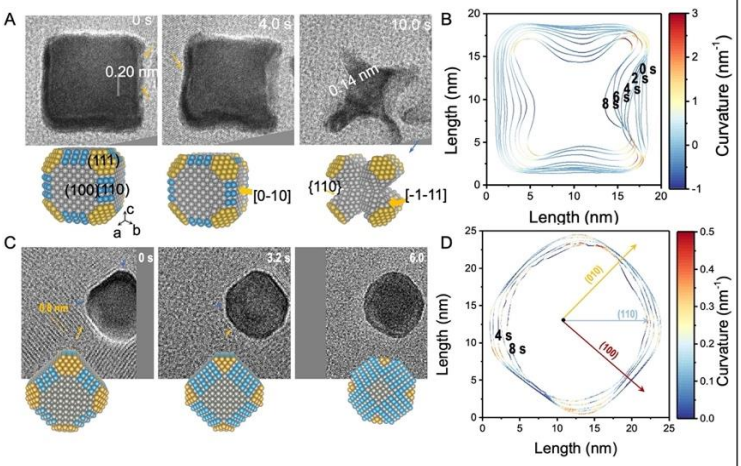

Fig. 2. Etching of Pd nanocrystals in an aqueous solution with different Fe^{3+} concentration. (**A**) Sequential images from a movie showing morphology evolution of a Pd nanocrystal during etching in a low concentration solution: 0.1 mM $Fe(acac)_3$. (**B**) Time-domain contour plots of the Pd nanocrystal in (A). (**C**) Shape evolution a Pd nanocrystal during etching with a high concentration solution: 1.0 mM $Fe(acac)_3$. (**D**) Time-domain contour plots of the Pd nanocrystal in (C)

the etching of Pd nanocrystals. Using liquid cell TEM, we directly observed the etching of Pd nanocrystals by tracking facet evolution. Our observations revealed that the etching was dominated by the interplay between Pd facets and ligands and that the etching exhibited different pathways at different concentrations of ligands. At a low concentration of $Fe(acac)_3$ (0.1 mM), rapid etching, primarily at {100} facets, led to a concave structure (**Fig. 2A,B**). At a high concentration (1.0 mM), the etch rate was decreased owing to a protective film of $Fe(acac)_3$ on the {100} facets producing a round nanoparticle (**Fig. 2C,D**). $Fe(acac)_3$ can transform into free Fe^{3+} and acetylacetonate (acac) molecules and vice versa in an aqueous solution. Our UV-vis spectroscopy experiments show that $Fe(acac)_3$ remains as a coordination complex at 1.0 mM. However, $Fe(acac)_3$ dissociates into acac molecules at the concentration of 0.1 mM. This is consistent with the poor solubility of $Fe(acac)_3$ in water. Ab initio calculations demonstrated the differences i n adsorption energy of inhibitor molecules on Pd facets were responsible for the etching behavior.

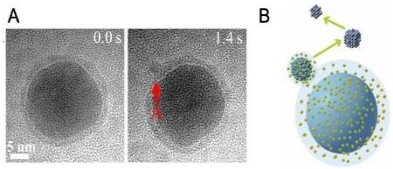

Fig. 3. Dynamic behavior of the quasi-liquid phase on Sn nanoparticles in an aqueous solution. (**A**) Sequential TEM images show In nanoclusters in the quasi-liquid phase. (**B**) Schematic illustration of the formation and transport of an In nanocluster where the quasi-liquid phase serves a medium between the Sn and solution.

2. Dynamic phenomena at solid-liquid interfaces

An understanding of solid–liquid interfaces is of great importance to fundamental research as well as industrial applications. Challenges remain in the direct imaging of solid–liquid interfaces with high resolution. We discovered a quasi-liquid phase between metal (In, Sn) nanoparticle surfaces and an aqueous solution using high resolution liquid cell TEM (**Fig. 3**). Our real-time high resolution imaging revealed a thin layer of liquid-like materials at the interfaces. Such a quasi-liquid phase serves as the intermediate for mass transport between the metal nanoparticles and the surrounding liquid. DFT-MD simulations demonstrated that the positive charges of metal ions greatly contributed to the stabilization of the quasi-liquid phase on the metal nanoparticle surfaces.

Solid–liquid–gas reactions are ubiquitous both in nature and industrial processes. A comprehensive description of gas transport in liquids and following reactions at the solid–liquid–gas interfaces remain unavailable. We reported a real-time imaging of the accelerated etching of gold nanorods at the presence of oxygen nanobubbles in an aqueous hydrobromic acid (**Fig. 4**). Our observation revealed that when an oxygen nanobubble is close to a nanorod below a critical distance (~1 nm), the local etching rate is significantly enhanced by over one order of magnitude. MD simulation results showed that the strong attractive van der Waals interaction between the gold nanorod and oxygen molecules facilitates the transport of oxygen through a thin liquid layer to the gold surface, and thus accelerating the etching. These results shed light on rational design principles for accelerating many wet chemical reactions.

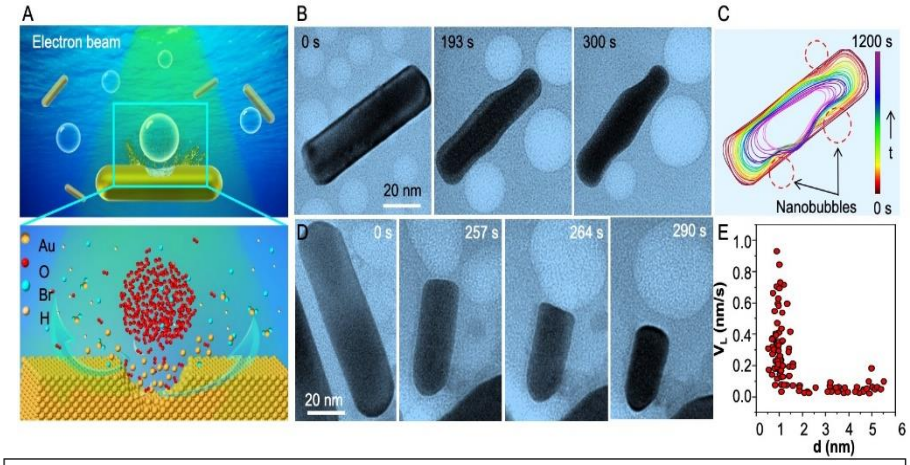

Fig. 4. Real-time observation and measurement of solid-liquid-gas reactions in a liquid cell. (**A**) Schematic illustration of the etching of gold nanorods in a HBr solution with O_2 nanobubbles in the near distance. (**B**) Sequential TEM images show etching of a Au nanorod in the presence of O_2 gas nanobubbles. (**C**) The corresponding contour map highlights the indents are developed near the nanobubbles. (**D**) Sequential TEM images show etching of a Au nanorod with a O_2 gas nanobubble at an end of the nanorod. (**E**) A statistic plot showing the longitudinal etching rate as a function of the distance between the nanobubble and nanorod surface.

Future Plans

We plan to develop novel liquid cells that will enable in situ high resolution imaging of electrochemical processes with various temperature control. We will use the development to study model systems, e.g., nanocatalysts, or alkali metals for controlled electrochemical reactions. Effort will also be made on the understanding and controlling of electron beam effects. With the novel liquid cells, advanced imaging and theoretical calculation, we will be able to achieve the understanding, and further develop strategies for controlling of the nanoscale materials transformations and dynamic phenomena at solid-liquid interfaces.

References

1. Q. Zhang, X. Peng,Y. Nie, Q. Zheng, J. Shangguan, C. Zhu, K. C. Bustillo, P. Ercius, L. Wang, D. T. Limmer, H. Zheng, "*Defect-mediated ripening of core-shell nanostructures*", Nature Communications **13**, 2211 (2022). https://doi.org/10.1038/s41467-022-29847-8

2. Q. Zheng, J. Y. Shangguan, X. L. Li, Q. B. Zhang, K. C. Bustillo, L. W. Wang, J. Y. Jiang, H. Zheng, *"Observation of Surface Ligands-Controlled Etching of Palladium Nanocrystals"*, Nano Letters **21** (15), 6640-6647 (2021). https://doi.org/10.1021/acs.nanolett.1c02104

3. X. Peng, F. Zhu, Y. Jiang, J. Sun, L. Xiao, S. Zhou, K. C. Bustillo, L. Lin, J. Cheng, J. Li, H. Liao, S. Sun. H. Zheng, "*Identification of a quasi-liquid phase at solid-liquid interface.*" Nature Communications **13**, 3601 (2022). https://doi.org/10.1038/s41467-022-31075-z

4. W. Wang, Tao Xu, J. Chen, J. Shangguan, H. Dong, H. Ma, Q. Zhang, J. Yang, T. Bai, Z. Guo, H. Fang, H. Zheng, L. Sun, "*Solid-liquid-gas reaction accelerated by gas molecule tunneling-like effect.*" Nature Materials **21**, 859–863 (2022). https://doi.org/10.1038/s41563-022-01261-x

Publications from Program

1. X. Peng, F. Zhu, Y. Jiang, J. Sun, L. Xiao, S. Zhou, K. C. Bustillo, L. Lin, J. Cheng, J. Li, H. Liao, S. Sun. H. Zheng, "*Identification of a quasi-liquid phase at solid-liquid interface.*" Nature Communications **13**, 3601 (2022). https://doi.org/10.1038/s41467-022-31075-z

2. S. B. Alam, G. Soligno, J. Yang, K. C. Bustillo, P. Ercius, H. Zheng, S. Whitelam, E. M. Chan, "*Dynamics of polymer nanocapsule buckling and collapse revealed by in situ liquid-phase TEM.*" Langmuir **38**, 7168-7178 (2022). https://doi.org/10.1021/acs.langmuir.2c00432

3. W. Wang, Tao Xu, J. Chen, J. Shangguan, H. Dong, H. Ma, Q. Zhang, J. Yang, T. Bai, Z. Guo, H. Fang, H. Zheng, L. Sun, "*Solid-liquid-gas reaction accelerated by gas molecule tunneling-like effect.*" Nature Materials **21**, 859–863 (2022). https://doi.org/10.1038/s41563-022-01261-x

4. Q. Zhang, X. Peng,Y. Nie, Q. Zheng, J. Shangguan, C. Zhu, K. C. Bustillo, P. Ercius, L. Wang, D. T. Limmer, H. Zheng, "*Defect-mediated ripening of core-shell nanostructures.*" Nature Communications 13, 2211 (2022). *https://doi.org/10.1038/s41467-022-29847-8*

5. Q. Zhang, J. Wan, J. Shangguan, S. Betzler, H. Zheng, "*Influence of sub-zero temperature on nucleation and growth of copper nanoparticles in electrochemical reactions.*" iScience **24**, 103289 (2021). https://doi.org/10.1016/j.isci.2021.103289

6. Q. Zheng, J. Jiang, X. Li, K. C. Bustillo, H. Zheng, *"In situ TEM observation of calcium silicate hydrate nanostructure at high temperatures.*" Cement and Concrete Research **149**, 106579 (2021). https://doi.org/10.1016/j.cemconres.2021.106579

7. H. Zheng, *"Imaging, understanding, and control of nanoscale materials transformations"*, MRS Bulletin **46** (5), 443-450 (2021). https://doi.org/10.1557/s43577-021-00113-4

8. Q. Zheng, J. Y. Shangguan, X. L. Li, Q. B. Zhang, K. C. Bustillo, L. W. Wang, J. Y. Jiang, H. Zheng, *"Observation of Surface Ligands-Controlled Etching of Palladium Nanocrystals."* Nano Letters **21** (15), 6640-6647 (2021). https://doi.org/10.1021/acs.nanolett.1c02104

9. P. Ercius, J. A. Hachtel, R. F. Klie, *"Chemical and bonding analysis of liquids using liquid cell electron microscopy."* MRS Bulletin **45** (9), 761-768 (2020). https://doi.org/10.1557/mrs.2020.230

10. U. Mirsaidov, J. P. Patterson, H. Zheng, *"Liquid phase transmission electron microscopy for imaging of nanoscale processes in solution."* MRS Bulletin **45** (9), 704-712 (2020). https://doi.org/10.1557/mrs.2020.222

Unraveling Charge and Lattice Correlations and Exploring New Imaging Capabilities for Quantum Matter

Yimei Zhu, Lijun Wu, Junjie Li, and Spencer Reisbick
Department of Condensed Matter Physics and Materials Science, Brookhaven National Laboratory, Upton, NY 11973

Keywords: Electron microscopy instrumentation, Electron-spin-lattice correlation, Electronic heterogeneities, Ultrafast and non-equilibrium, and Quantum materials

Research Scope

The goal of this FWP (MA-015-MACA) is to study property-sensitive nanoscale structure, defects, and interfaces of technologically important materials, such as high-temperature superconductors, transition-metal oxides, ferroelectric, spintronic and photovoltaic films, and other energy materials. We implement and develop advanced electron microscopy methods and instrumentation at the required spatiotemporal resolutions to reveal atomic disorder, electronic inhomogeneity, transient dynamics, and intertwined behaviors of these materials. We focus on three research themes: (1) Heterogeneities, (2) non-equilibrium dynamics, and (3) Advanced tools to facilitate the research theme (1) and (2). The study of ferroelectric and ferromagnetic materials and charge and spin ordering/switching in (1) is also covered by a separate abstract.

Recent Progress

In the past two years we have made great strides on materials research, unraveling several long-standing puzzles regarding charge-lattice and spin-lattice correlations, topological phenomena and interfaces in quantum materials as well as charge transfer and ionic-transport in energy materials. We've also made significant progress in advancing the frontier of electron microscopy instrumentation and methods, notably the development of the laser-free electron pulser for microwave stroboscopic ultrafast electron microscopy. We refer our research outcomes to the publications listed at the end of this abstract.

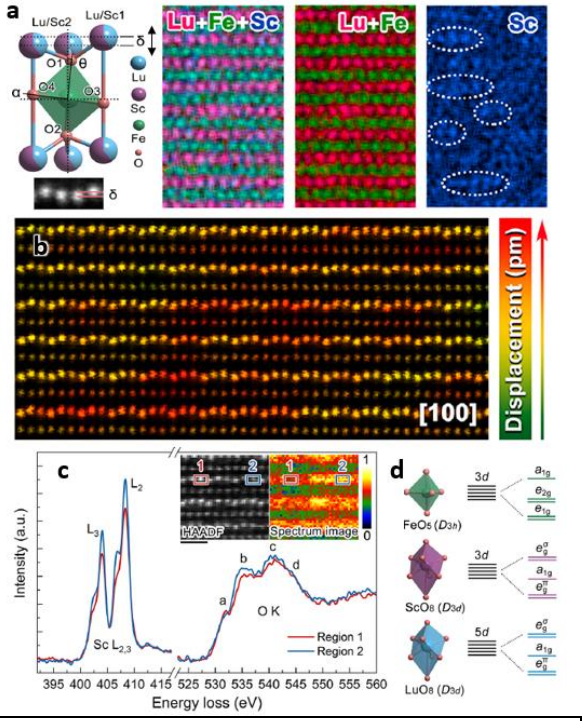

Fig.1. Role of substitution on polar displacement in Sc-doped multiferroic $LuFeO_3$. (a) Schematic of FeO_5 trimerization along with elemental maps with localized Sc enrichment circled. (b) Atomic image showing local variation of displacement and Sc concentration. (c) EELS spectra from two local regions. (d) Crystal field splitting for FeO_5, ScO_8, and LuO_8, consistent with DFT. Local FeO_5 trimerization and Lu/Sc−O hybridization are strengthened by Sc, clarifying the origin of the strong dependence of improper ferroelectricity on Sc content [2].

Heterogeneities

Our research in this area is focused on understanding the role of inhomogeneity and disorder, such as topological defects and interfaces, that control intriguing ferroic orders. [1,2]. For instance, through the study of critical roles of substitutions and disorder in multiferroic $Lu_{1-x}Sc_xFeO_3$ on local polarization (Fig.1) we show how individual dopants or substitutional atoms interact with host lattices, enabling us to manipulate, control, and improve the functionality of materials due to the intimate coupling among various degrees of freedom in multiferroics. Atomic variations in polar displacement of intriguing topological vortex domains stabilized by Sc substitution are directly correlated with Sc atom-mediated local chemical and electronic fluctuations and verified by DFT calculations. This study could pave the way for correlating dopant-regulated local structures with global properties to engineer emergent functionalities of numerous chemically doped functional materials.

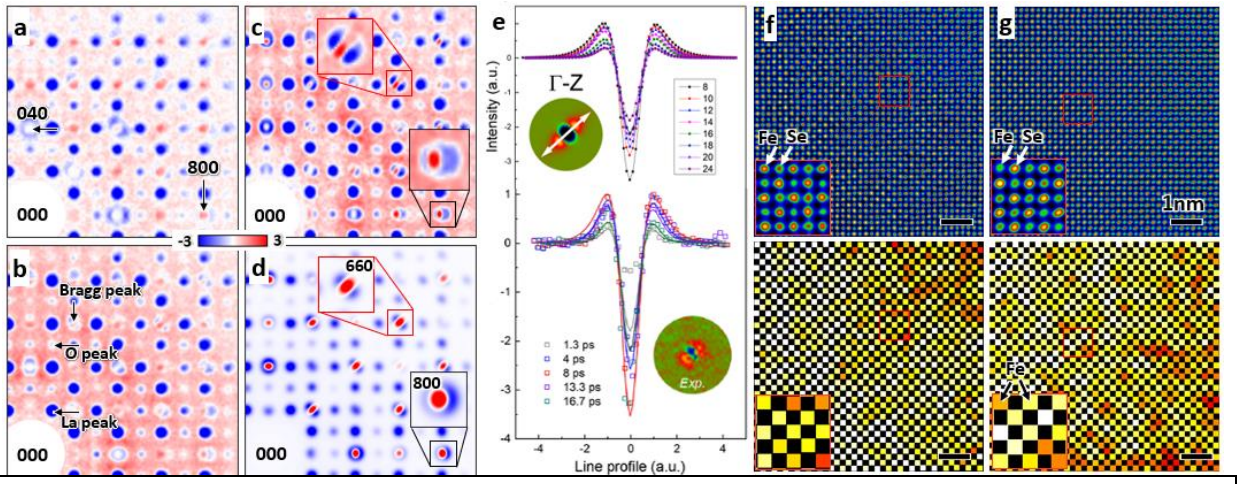

Fig.2. Static and dynamic behavior of defects and disorder. (a–d) Experimental UED difference maps of Bragg intensities I(t)-I(t_0) of $LaMnO_3$ at t=0.2ps (a), t=1ps (b), t=10ps (c); and (d) simulated difference map of (c), showing the evolution of Johan Teller distortion and twin-related orthorhombicity after femtosecond laser excitations [4]. (e) Line profiles of the (020)- diffraction intensity change along the Γ–Z direction in the Brillouin zone as a function of time showing photoinduced anisotropic lattice dynamics and transient domain formation in thermoelectric SnSe. Top: simulations, bottom: experiment [5]. (f-g) [001] STEM images of $FeSe_xS_{1-x}$ showing local Fe vacancy disorder due to the change of stoichiometry (only x=0.31 (f), and x=0.82 (g) are shown). Bottom panels are the peak intensity map of Fe columns refined from the corresponding images above. Each square represents a Fe column. The insets are the magnified images from the area marked by the red squares [9].

Non-equilibrium and ultrafast phenomena

We focus on exploring and manipulating charge-lattice interactions and transient phenomena using MeV ultrafast electron diffraction (UED). In the topological insulator $ZrTe_5$[3] we show how a chiral Dirac semimetal state can be induced by a femtosecond laser pulse and in the photoinduced transient state the bandgap is closed in the presence of strong spin-orbit coupling. In free-standing $LaMnO_3$ films [4] we reveal photoinduced evolution of Jahn-Teller distortion and lattice orthorhombicity based on the change of Bragg intensities and their diffuse scattering (Fig.2(a-d)) and reveal unexpected boost of ferromagnetism. In thermoelectric SnSe, we study the photoinduced transient domain state and its evolution to understand the soft, anharmonic lattice response related to the low thermal conductivity of the material (Fig.2(e)) [5]. In VO_2, we directly detect V-V atom dimerization and rotation dynamic pathways upon ultrafast photoexcitation as

well as nonlinear atomic motion trajectories during the early stage of the insulator-metal transition [6]. The knowledge we gain through these studies enables us towards using ultrafast external stimuli to engineer novel emergent states and properties modulated by the interplay of electronic and lattice degrees of freedoms.

Advanced characterization tools

The development and deployment of advanced imaging capabilities supported by this FWP is at the forefront of the field, especially in the area of ultrafast electron microscopy instrumentation. In the past two years, bedsides our efforts on MeV UEM development supported by BNL LDRD and DOE SBIR grants, we also continued the development of the Laser-Free Electron Pulser which allows us to directly observe materials' response under GHz excitation. We have successfully implemented a pulse picker, which covers the pump excitation at low frequencies from a few Hz to hundreds of MHz [7]. We also developed two-color near-field UEM (Fig. 3) to photo-induce the insulator-to-metal transition in a single VO_2 nanowire and probe the ensuing electronic dynamics with combined nanometer-femtosecond resolution (10^{-21}m· s). We take advantage of a femtosecond temporal gating of the electron pulse mediated by an infrared laser pulse and exploit the sensitivity of inelastic electron-light scattering to changes in the material dielectric function. Due to the high versatility and sensitivity of the electron probe, our approach demonstrates the reality in capturing the electronic dynamics of a wide range of nanoscale materials with ultimate spatiotemporal resolution.

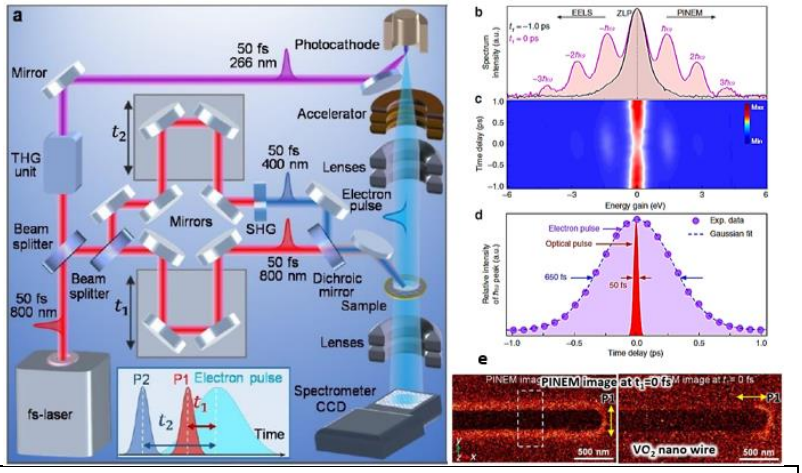

Fig.3. A new method based on two-color scheme using photo-induced near-field electron microscopy (PINEM), one for temporal gating, the other for pumping to achieve nm-fs spatiotemporal resolution. (a) Experimental set-up for two-color PINEM. (b-c) PINEM spectra and spectrogram using a VO_2 nanowire showing photon–electron coupling. (d) Cross-correlation temporal profile showing the original temporal profile of the electron pulse being ~650fs. After the optical gating, the temporal duration of the electron pulse (P1) is reduced to 50 fs. (e) Energy filtered PINEM images of the VO_2 nanowire with parallel and perpendicular polarizations [8].

Future Plans

We will continue to focus on our three research themes: Heterogeneities, Non-equilibrium/ ultrafast-phenomena and Advanced characterization tools, to understand electron-spin-lattice correlations in quantum and energy materials. Below are some proposed activities.

Probing the evolution of defects and disorder via time-resolved diffuse scattering analysis
We propose to study the role of topological defects in nonequilibrium phase transitions. Transient

defects and disorder are known to generate a variety of hidden orders not accessible in equilibrium (see e.g., Fig.2(f-g)). We plan to employ an intense laser pulse to create topological defects in a 2D charge density wave such as $TiSe_2$ and track their morphology and dynamics with ultrafast electron diffraction. Leveraging its high temporal resolution and sensitivity in detecting weak diffuse signals shown in Fig.2(a-e), we hope to reveal the length and time scale of the disordering process and its relationship with the nonthermal population of longitudinal/translational and optical/acoustic phonons. The results will provide crucial insights into ultrafast engineering of topological defects based on selective excitation of collective modes, opening avenues for dynamical control of nonequilibrium phases in correlated materials.

Mapping chiral spin texture in topological materials using 4D-STEM is an area we would like to explore. Currently 4D-STEM analysis relies on the center-of-mass of the diffraction patterns in electromagnetic field mapping, which often results in artifacts due to the non-uniform intensity distribution within the disks. We plan to develop a new approach via a robust refinement procedure through iteration of the spin-sensitive disk position in the circular Hough transform filtered Lorentz 4D-STEM images and explore when the rigid-body-shift model breaks down. Through quantitative analysis and comparison between experiment and simulation high quality induction maps can be obtained.

Probing dynamic response under GHz electrical excitations will be the focus of our ultrafast research. We propose to study lattice responses in CDW materials and spin wave dynamics in lithographically patterned devices using the Laser-Free Electron Pulser we developed (Fig.4(a,b)). We intend to explore various imaging modalities (Fig.4(c)) and optimize the instrument performance for different applications. Our objective is to expand new imaging capabilities across multiple spatial, temporal and energy scales to understand quantum materials and their behavior.

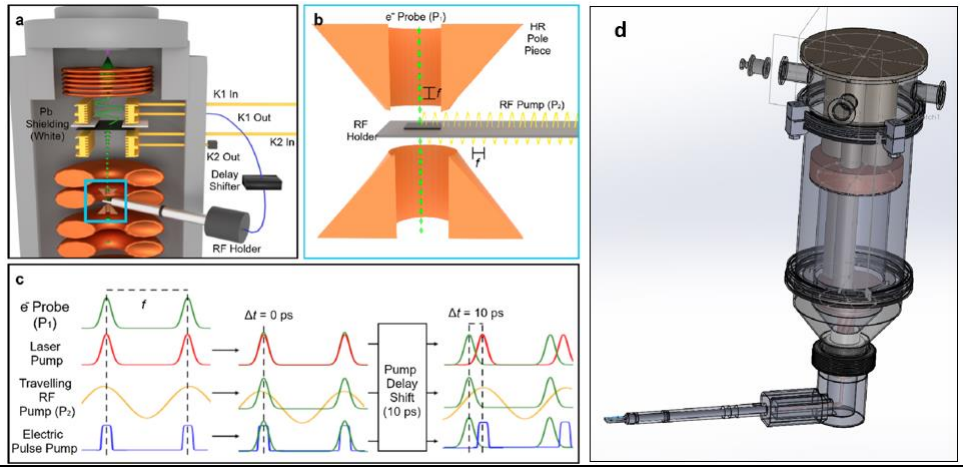

Fig.4. (a-b) Schematic of the Laser-Free Electron Pulser assembly develop at BNL showing the use of a travelling RF wave (blue box) for UEM. The probe and pump have been designated as P1 and P2. (c) Different pump-probe timing schemes and the mechanistic differences between each excitation style with respect to the image acquisition of the electron beam. (d) Rendering of the closed-cycle cryocooler sample holder currently under construction at BNL. It allows cryogenic experiments down to near liquid-He temperature with temperature stability and control below 1mK. No refilling of liquid-He is needed.

Development of a closed-cycle cryogenic liquid-He sample holder Cryogenic electron microscopy has been identified by the recent DOE Roundtable as one of the priority research directions. However, accurate control of temperature in TEM has been a long-standing issue and

liquid-He becomes increasingly less accessible. To address the challenges, we will construct based on our unique design a cryogenic TEM side entry sample holder which incorporates a closed-cycle cryocooler, a temperature stabilizer and a vibration damping system. The sample expects to reach a temperature close to liquid-He, and the temperature control accuracy and stability can be achieved down to 1mK. The holder has a temperature holding time up to a month. The closed cycle system has virtually zero helium consumption and requires no refilling for more than eight years with proper use. Combining the microwave excitation our cryo-holder development will someday enable us to probe Q-bit devices using cryogenic electron microscopy under their working environment for quantum computing and quantum information science.

Publications (I) cited in the abstract and supported by this FWP (Oct. 2020 - Sept. 2022).

1. Deng, S.Q.; Li, J; Smabraten, Didrik R.; Shen, S.D.; Wang, W.B.; Zhao, J.; Tao, J.; Aschauer, U.; Chen, J.; Zhu, Y.; Zhu, J., "Critical Role of Sc Substitution in Modulating Ferroelectricity in Multiferroic $LuFeO_3$", Nano Letters 21, 6648 (2021)
2. Lu, Q.; Cheng, Y.; Wu, L.; Guo, H.; Qi, F.; Zhang, H.; Yu, J.; Liu, Q.; Wang, Q.; Liang, G.; Chen, G.; Lu, Y.; Zhang, J.; Xiang, D.; Zhao, J.; Zhu, Y.; and Zhai, X., "Photoinduced evolution of lattice orthorhombicity and conceivably enhanced ferromagnetism in $LaMnO_3$ membranes", npj Quantum Materials 7:47 (2022).
3. Wang, W., Wu, L., Li, J., Aryal, N., Jin, X., Liu, Y., Fedurin, M., Babzien, M., Kupfer, R., Palmer, M., Petrovic, C., Yin, W., Dean, M.P.M., Robinson, I.K., Tao, J., and Zhu, Y., "Photoinduced anisotropic lattice dynamic response and domain formation in thermoelectric SnSe", npj Quantum Materials 6:97 (2021).
4. Fu, X.; Barantani, F.; Gargiulo, S.; Madan, I.; Berruto, G.; Lagrange, T.; Jin, L.; Wu, J.; Vanacore, G.M.; Carbone, F.; and Zhu, Y.; "Nanoscale-femtosecond dielectric response of Mott insulators captured by two-color near-field ultrafast electron microscopy", Nat. Comm., 11:5770 (Nov. 2020).
5. Reisbick, S.A.; Han, M.-G.; Liu, C.; Zhao, Y.; Montgomery, E.; Jing, C.; Gokhale, V.J.; Gorman, J.J.; Lau, J.W.; Zhu, Y., "Stroboscopic ultrafast imaging using RF strip-lines in a commercial transmission electron microscope", Ultramicroscopy 235 113497(2022).

Publications (II) additional 10 most relevant and supported by this FWP (Oct. 2020 - Sept. 2022).
For full list of publications (total 92), see https://www.bnl.gov/cmpmsd/tem/publications/

1. Cheng, S.; Lee, M.-H.; Tran, R.; Shi, Y.; Li, X.; Navarro, H.; Adda, C.; Meng, Q.; Chen, L.Q.; Dynes, R.C.; Ong, S.-P.; Schuller, I.K.; Zhu, Y.; "Inherent stochasticity during insulator-metal-transition in VO_2", PNAS, 118 e2105895118 (2021)
2. Cheng, S., Li, X., Xu, C., Liu, Y., Beleggia, M., Wu, L., Wang, W., Petrovic, C., Bellaiche, L., Tao, J., and Zhu, Y., "Coexistence and Coupling of Multiple Charge Orderings and Spin States in Hexagonal Ferrite", Nano Lett., 21 5782−5787 (2021).
3. Fu, X.; Liu, S.Y.; Chen, B.; Tang, J.; and Zhu, Y., "Observation and Control of Unidirectional Ballistic Dynamics of Nanoparticles at a Liquid-Gas Interface by 4D Electron Microscopy", ACS Nano, 15, 6801−6810 (2021).
4. Konstantinova, T.; Wu, L.; Yin, W.-G.; Tao, T.; Gu, G. D.; Wang, X.J.; Zaliznyak, I. A.; and Zhu, Y. "Photoinduced chiral Dirac semimetal in $ZrTe_5$", npj Quantum Materials, 5:80, 1-8 (Nov. 2020).
5. Li, J.; Wu, L.; Yang, S.; Jin, X.; Wang, W.; Tao, J.; Boatner, L.; Babzien, M.; Fedurin, M.; Palmer, M.; Yin, W.; Delaire, O.; and Zhu, Y., "Direct detection of V-V atom dimerization and rotation dynamic pathways upon ultrafast photoexcitation in VO_2", Phys. Rev. X 12, 021032 (2022).
6. Pollard, S.D., Garlow, J.A., Kim, K.-W., Cheng, S., Cai, K., Zhu, Y., and Yang, H., "Bloch Chirality Induced by an Interlayer Dzyaloshinskii-Moriya Interaction in Ferromagnetic Multilayers", Phys. Rev. Lett. 125, 227203 (Nov. 2020).
7. Telford, E.J.; Dismukes, A.H.; Dudley, R.L.; Wiscons, R.A.; Lee, K.; Chica, D.G.; Ziebel, M.E.; Han, M.-G.; Yu, J.; Shabani, S.; Scheie, A.; Watanabe, K.; Taniguchi, T.; Xiao, D.; Zhu, Y.; Pasupathy, A.N.; Nuckolls, C.; Zhu, X.; Dean, C.R.; Roy, X., "Coupling between magnetic order and charge transport in a two-dimensional magnetic semiconductor", Nature Materials 21, 754-760 (2022).

8. Zhang, H.T.; Park, T.J.; Islam, A.N.M.N.; Tran, D.S.J.; Manna, S.; Wang, Q.; Mondal, S.; Yu, H.; Banik, S.; Cheng, S.; Zhou, H.; Gamage, S.; Mahapatra, S.; Zhu, Y.; Abate, Y.; Jiang, N.; Sankaranarayanan, S.K.R.S.; Sengupta, A.; Teuscher, C.; Ramanathan, S., "Reconfigurable perovskite nickelate electronics for artificial intelligence", Science 375, 533–539 (2022).
9. Zhu, Y., "Cryogenic Electron Microscopy on Strongly Correlated Quantum Materials", Invited review article, special issue on Cryogenic Electron Microscopy. Guest editors: Y. Cui and L. Kourkoutis, Accounts of Chemical Research, 54, 3518−3528 (2021).
10. **US patent** No. US 11,410,829 B1, inventors: C. Jing, S. Ross, R. Kostin and Y. Zhu; "TEM sample holder with cryogenic cooling and broadbabd RF irradiation", issued date: Aug. 9, 2022.

University
Abstracts

Data-Science Enabled, Robust and Rapid MeV Ultrafast Electron Diffraction Instrument System to Characterize Materials Including for Quantum and Energy Applications

Sandra Biedron, The University of New Mexico (Principal Investigator)

Keywords: MeV ultrafast electron diffraction (MUED), pump photoexcitation, transfer learning, accelerator controls, machine learning, autoencoders, surrogate model

Research Scope: MeV ultrafast electron diffraction (MUED) is a powerful structural measurement technique recently demonstrated to provide several complementary capabilities for novel characterization of material samples. MUED takes advantage of the strong interaction between electrons and matter and minimizes space charge problems seen in other low-energy electron diffraction systems. An MUED instrument can resolve much finer structural details enabling us to see how atoms in molecules move and can make molecular movies of ultrafast chemical reactions by utilizing a pump-probe technique. While a few facilities have been constructed to provide these advanced capabilities to a growing user community, as a relatively young technology, progress is ongoing and much remains to be learned by improving these facilities, especially in maximizing throughput and ease of operation that results in a wider stream of new science. One class of advancement that can be immediately investigated at MUED facilities is the demonstration of real-time or near real-time data processing enabled by data science/machine learning/artificial intelligence mechanisms in conjunctions with high-performance computing (HPC) to bring automated operation, data acquisition and processing to the facility control and experiment analysis, thereby enabling faster measurement throughout. Or research efforts concern the MUED instrument being developed at Brookhaven National Laboratory [1].

The application of Machine Learning has been demonstrated in support of X-ray diffraction and other experiments, therefore there is high confidence that similar significant gains can be achieved at a system like MUED. For example, into the processing of MUED diffraction patterns. By fully automating the facility from machine operation to material property characterization, the user base will be expanded, as experimenters from a wide range of disciplines would no longer need to learn complex machine optimization procedures or rely on other facility experts to do measurements.

In recent years, machine learning (ML) approaches to materials and characterization techniques have provided a new path towards unlocking new physics by improving existing probes and increasing the user's ability to interpret data. With proper preprocessing, ML methods can be employed to control characterization probes in near-real time, acting as virtual diagnostics, or ML can be deployed to extract features and effectively denoise data. We have identified the application of ML for MUED data de-noising, where convolutional neural network architectures, such as auto encoder models, are an attractive and more powerful alternative to conventional denoising techniques. The autoencoder models provide a method of unsupervised learning of latent space representation of data that can help reduce the noise in the data [2]. By supplying a paired training dataset of "noisy" and "clean" data, these ML models can denoise measurements quite effectively. This method relies on the existence of an ideal dataset with no noise, which can be obtained by simulation or by averaging existing noisy datasets. Our autoencoder model can accurately reconstruct typical data sets, but in the case of anomalies, it produces a large reconstruction error or different feature vector values. Different strategies to detect anomalies were also tested.

Anomaly detection efforts are ongoing, and multiple approaches are being considered. The large datasets expected from the MUED system are well suited for data analysis on a high-performance computing system, such as at the Argonne Leadership Computing Facility.

We also have started the integration between two DOE user facilities, the MUED instrument at BNL and the HPC resources at the Argonne Leadership Computing Facility (ALCF) [3]. The idea is to exploit the data processing infrastructure of ALCF during online operation of MUED, this is achieved for example with a Globus connection or similar. This type of fast data transfer connecting points between multiple laboratories are already available for other scientific applications like High Energy Physics and here we try to adapt these resources for instrument control.

Computer simulations are generally used to understand the dynamics of a system, whether on the developing phase or when trying new system configurations. Simulations can provide accurate results, but often, the computing time required to produce a solution is not suitable for real-time operations. We are creating an end-to-end simulation of MUED that accurately replicates the experimental observations [4][5]. This simulation can then be used to calculate the expected output beam phase space given a set of input parameters. By running the simulation for thousands different sets of input parameters, we can produce data to train a surrogate model of the MUED instrument, effectively capturing the accuracy of the computer simulation into a ML model capable of producing an output fast enough that it can be used for real-time control [6]. We are basing our simulation on the nominal values of the instrument and will introduce random variations in the simulation input parameter space. A surrogate model can also be used to help diagnose the system by acting as virtual diagnostics where instrumentation is not physically available, or when the impact to operations is not acceptable, e.g., when using destructive diagnostics.

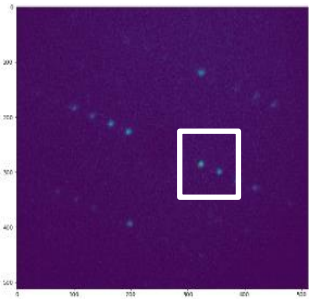

Original diffraction pattern.

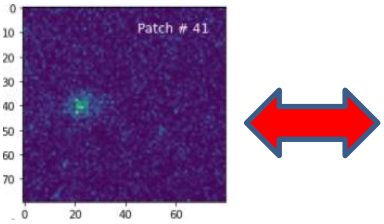

Original tile data. Reconstruction.

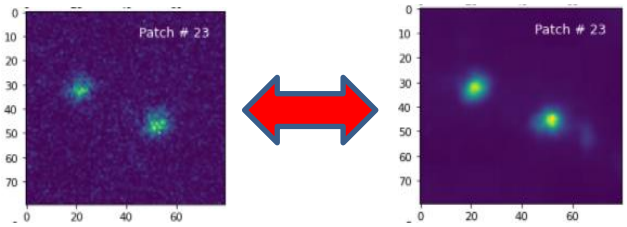

We are currently preparing two peer-review publications that showcase the technical efforts of this project. The first on is on the development of a surrogate model for MUED based on computer simulations, and the second one is on the autoencoder model for de-noising diffraction data. We are scheduled for dedicated beam-time at MUED and have also implemented remote tasks between UNM and MUED.

Collaborator(s): David Martins, Michael Papka, Thomas Uram (Argonne National Laboratory); Marcus Babzien, Mikhail Fedurin, Mark Palmer, Junjie Li, Kevin Brown (Brookhaven National Laboratory); Alan Hurd, John Sarrao, Christine Sweeney, Julian Chen (Los Alamos National Laboratory).

References and Papers

[1] X. J. Wang, X. Qiu and I. Ben-Zvi, "Experimental observation of high-brightness microbunching in a photocathode rf electron gun," in Phys. Rev. E 54.R3121, 1996.

[2] T.B. Bolin, S. Sosa Guitron, M. Martínez-Ramón, S.G. Biedron, "Data Analysis and Control of an MeV Ultrafast Electron Diffraction System Using Machine Learning," presented at LINAC'22, Liverpool, England, UK, Aug-Sep 2022, paper WE2AA04.

[3] T.B. Bolin, S.G Biedron, M. Martinez-Ramon, S.I. Sosa, M. Babzien, K. Brown, M. Fedurin, J. Li, M. Palmer, D.E. Martin, M.E. Papka, et al., "Updates in Efforts to Data Science Enabled MeV Ultrafast Electron Diffraction System," in Proc. IPAC'22, Bangkok, Thailand, Jun 2022, pp. 397-399, doi:10.18429/JACoW-IPAC2022-MOPOPT057.

[4] S.I. Sosa Guitron, T. B. Bolin, and S. Biedron, "Design of a Surrogate Model for MUED at BNL Using VSim, Elegant and HPC," presented at NAPAC'22, Albuquerque, NM, USA, Aug 2022, paper MOPA13" presented at NAPAC'22, Albuquerque, NM, USA, Aug 2022, paper MOPA11.

[5] D. Monk, S.G. Biedron, M. Martínez-Ramón, M.A. Fazio, S.I. Sosa, T. Talbott, M. Babzien, K. Brown, M. Palmer, J. Tao, D.E. Martin, M.E. Papka, "Surrogate Modeling for MUED with Neural Networks," in Proceedings of the 2021 International Particle Accelerator Conference, virtual conference, Campinas, Brazil, 2021, paper MOPAB314, 970-971, https://doi.org/10.18429/JACoW-IPAC2021-MOPAB314.3.

[6] M.A. Fazio, S.G. Biedron, M. Martínez-Ramón, D. Monk, S.I. Sosa, T. Talbott, M. Babzien, K. Brown, M. Fedurin, J. Li, M. Palmer, J. Tao, J. Chen, A. J. Hurd, N. Moody, R. Prasankumar, C. Sweeney, D.E. Martin, M.E. Papka, "Towards a Data Science Enabled MeV Ultrafast Electron Diffraction System," in Proceedings of the 2021 International Particle Accelerator Conference, virtual conference, Campinas, Brazil, 2021, paper MOPAB286, 906-908, https://doi.org/10.18429/JACoW-IPAC2021-MOPAB286.

Journal Articles in Preparation

S. Sosa, T. Bolin, S. G. Biedron, "End-to-end simulation of the MeV Ultrafast Electron Diffraction instrument at BNL towards a surrogate model", in Nuclear Instruments and Methods in Physics Research A, in preparation.

M. Fazio, S.G. Biedron, M. M. Martínez-Ramón, S.I. Sosa, "Unsupervised anomaly detection in MeV ultrafast electron diffraction," Physical Review B, in preparation.

Local Probing of Light Induced Excitations of Electronic and Photonic Modes in Oxide Nanoparticles

PI: Peter A. Crozier, Arizona State University, Tempe, AZ 85287-6106

Keywords: Photocatalysis, charge transfer, photonic modes, *in situ* TEM, oxides

Research Scope

Photon interactions with materials can give rise to a rich variety of phenomena leading to transient perturbation of electrons to long term materials phase transformation. For example, interactions associated with photon in energy regions where the imaginary part of the dielectric function is non-zero, can lead to absorption resulting in electron and phonon excitation, and possible creation of quasiparticles such as polaritons, plasmons etc. Interactions associated with photons in energy regions where the imaginary part of the dielectric function is small (or zero) can lead to non-absorbing processes such as excitation of photonic modes (e.g., waveguide modes, cavity modes, etc.). Energy conversion technologies including photovoltaics, photocatalysis and energy transport as well as sensing applications can exploit these different processes. We are investigating these fundamental processes taking place in oxides associated with both forms of interactions. Irradiation of oxides with photons above the bandgap can lead to electron-hole pair generation with potential applications to photocatalytic water splitting. Challenges include creation of stable composite systems, which absorb in the visible, and separation of the charge carriers to avoid recombination. Irradiation of certain oxide nanoparticles with photons below the bandgap can lead to creation of photonic modes in the systems. The characteristics of these modes depends on nanoparticle size, shape and the effective refractive index. The modes may have potential in energy transfer and sensing applications.

Recent Progress

For photocatalytic water splitting, there is a desire to develop stable oxides that can harvest light in the visible part of the spectrum to enhance solar-to-hydrogen efficiency [1]. Doping has proven to be quite successful in creating materials where the bandgap and band alignment are optimized for water splitting [2]. We have been investigating the effects of rhodium (Rh) doping in strontium titanate (STO) with emphasis on visible light absorption properties and charge separation.

Figure 1a plots the UV-Vis diffuse reflectance spectroscopy data showing the red shift of the bandgap onset upon Rh doping. There's a peak appearing at ~580 nm corresponding to Rh^{4+}. Inset shows the as synthetized pure STO and Rh-doped STO powders. We have chosen to load a Ni/NiO core-shell co-catalyst onto the Rh doped STO (**figure 1b**). Photocatalytic water splitting

under visible light with the Ni/NiO co-catalyst showed H_2 evolution suggesting a successful doping of STO with Rh to tune the catalyst for visible light absorption.

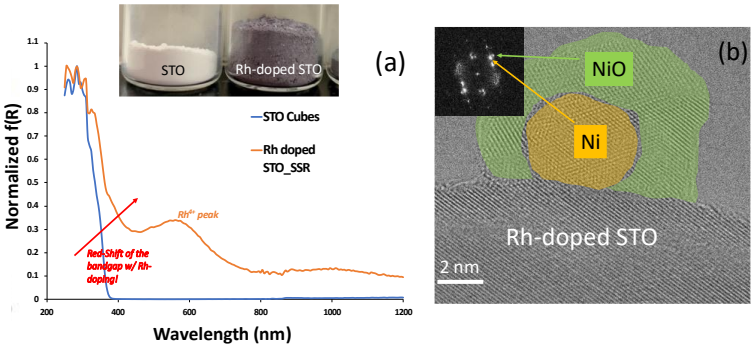

Figure 1: (a) UV-Vis spectra showing the shift of bandgap onset and the presence of Rh^{4+} peaks. (Inset shows as synthetized pure STO and Rh-doped STO, the change in color is evidently visible due to doping). (b) Ni-NiO core-shell is loaded onto Rh-doped STO support.

To study the charge transport across semiconductor-metal interfaces, *in situ* electron holography coupled with visible light illumination (405 nm) inside and FEI Titan environmental transmission electron microscope (TEM) has been used. The *in situ* visible light illumination system for the microscope was designed in the PI's lab [3]. During illumination, charge transport from the Rh-doped STO to the Ni metal nanoparticle may occur resulting in a change in the number of electrons in the metal. This change in charge density will lead to changes in the mean inner potential which may be detectable with electron holography since it will give rise to a phase shift in the fast electron wavefunction.

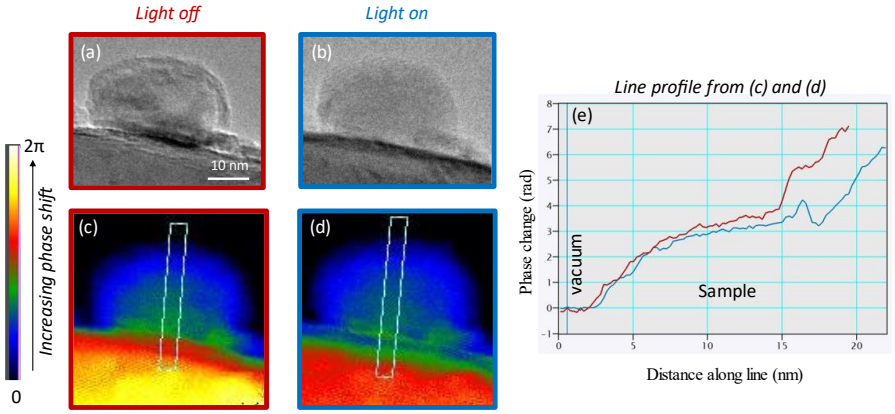

Figure 2: (a-b) TEM images of light off and light on of the co-catalyst/semiconductor assembly respectively (Ni/NiO core-shell particle loaded on Rh-doped STO) showing more diffuse contrast from the light on condition. (c-d) Reconstructed phase maps of the fast electron-material interaction, showing less intensity in the metal co-catalyst respectively from light off and light on conditions. Colorbar represents the phase shift values in radian. (e) Line profile from (c) and (d) showing the decrease in phase shift of the fast electron in light on condition as compared to light off.

Figure 2a and **b** shows an image of Ni-NiO co-catalyst loaded onto Rh-doped STO with and without photon illumination. In the "light off" condition, the contrast at the interface between the Ni core and oxide shell is visible but upon illumination the contrast becomes poor, possibly due to dynamics arising from the photon illuminations. **Figure 2c** and **d** represent the reconstructed phase maps from electron holography under "light off" and "light on" conditions respectively. Upon illumination, the phase shift decreases at the Rh-doped STO (substrate) and the Ni core (co-catalyst) possibly resulting from an increase in the number of electrons [4]. With favorable band alignment between Ni and the Rh-doped STO, photoelectrons would travel across the interface thus increasing the number of electrons in Ni's Fermi level. The resultant effect is visible in the phase shift of the fast electron when compared to the "light off" case as seen in the line profile of **figure 2e**.

Photonic Modes in Oxides

Photonic modes are standing waves in optical structures, e.g., nanocubes. Besides optical methods, e.g., Raman or infrared spectroscopy, we can also generate and probe such modes with fast electrons. In other words, with electron energy-loss spectroscopy (EELS) in a scanning transmission electron microscope (STEM), we can detect these modes with ~10 meV energy and nanoscale resolution, surpassing the spatial resolution of the usual optical methods which is ~1 micron [5]. We are interested in exploring coupling between modes for energy transfer and sensing applications. Initial investigation of the modes was performed on a well-defined 200 nm ceria (CeO_2) nanocube (**figure 3a**) in the aloof spectral geometry, i.e., the electron beam was placed 5 nm outside the sample surface. When the beam was placed at different locations, e.g., edge sites (blue) and face sites (red), four peaks were observed before the band gap edge, which corresponds to different modes (**figure 3b**). Notice that the intensity of the four modes at two locations are very different. This is due to the geometrical preference of the mode excitation. **Figure 3c** shows intensity maps of each of the four modes. The mapping shows the spatial variation in the excitation probability of the modes: for edge modes (peak I and IV) the probability is highest at the edge of the cube, while for the face modes (peak II and III), the probability is highest at the face of the cube.

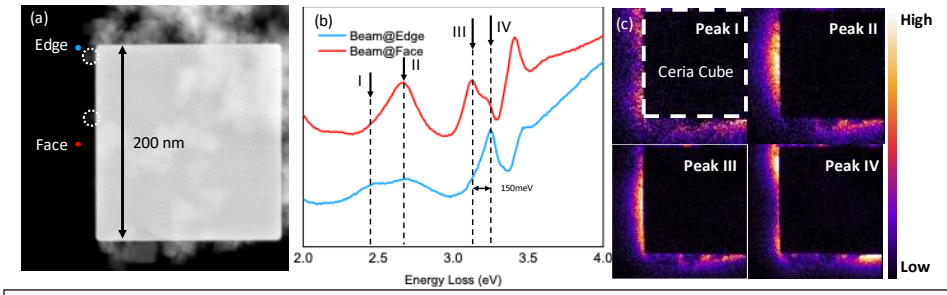

Figure 3: (a) STEM image of a ~200 nm well-defined shape CeO_2 cube. (b) Energy-loss spectra taken at two different geometries, i.e., edge (blue point) and face (red point). The two spectra show four different peaks before the band gap edge of ceria. (c) Intensity map of different peaks shows the different excitation of spatial distribution of different modes.

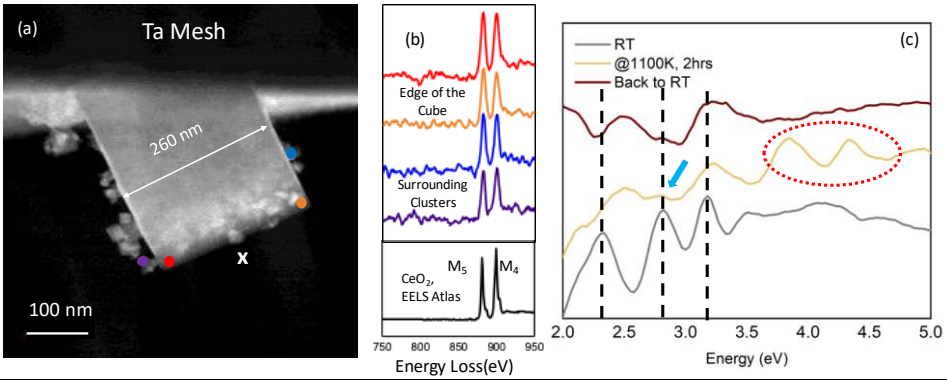

Figure 4: (a) STEM image of a 260 nm ceria cube, the dark bar above is the Ta grid. (b) Core-loss EELS at high temperature from different points to show that cerium's valence has changed due to the heating process. The red and orange spectra were taken at the edge of the cube, the blue and purple spectra were taken on the surrounding small cubes. The black spectrum is the standard spectrum for Ce^{4+}. (c) low-loss EELS taken at the white X mark in **figure 4(a)** at different temperatures. Black dash lines indicate the position of the peak before band gap edge at RT. The red dotted ellipse shows the disappearing peak after cooling down.

The character of the photonic modes will be sensitive to changes in the refractive index of the materials. To investigate this effect, *in situ* experiments were performed on CeO_2 nanocubes subject to reduction via heating. Due to the high oxygen ion mobility, heating will lead to reduction of ceria, thus changing the optical properties. **Figure 4** shows the change in behavior of 260 nm

ceria cube during heating to 1100K and subsequent cooling to room temperature. The Ce oxidation state is observed to change, as confirmed by core-loss EELS, by comparing the ratio between Ce M_4 and M_5 edge (**figure 4b**). As **figure 4c** shows, comparing the low-loss spectrum before and during heating show an obvious change of the photonic modes (e.g., room temperature modes largely suppressed, indicated by the blue arrow), while new peaks emerged, especially peaks beyond the valence band edge of CeO_2. After cooling to room temperature, the new peaks below the band gap edge are preserved, while peaks above 3.2 eV vanished (red dotted ellipse). This also confirmed that the change of the peaks was not related to temperature. Such results demonstrate our ability to engineer and characterize photonic modes simultaneously.

Future Plans

We will continue to explore the coupling behavior of photonic modes in oxide nanoparticles systems. The possible application to sensing and energy transfer will be the primary focus. For photo-generated electron-hole pairs, we will further refine our *in situ* holography approach to quantify charge transport across semiconductor-metal interfaces on systems of relevance to photocatalysis and photovoltaics.

References

[1] D. H. K. Murthy et al., "Revealing the role of the Rh valence state, La doping level and Ru cocatalyst in determining the H_2 evolution efficiency in doped $SrTiO_3$ photocatalysts," Sustain. Energy Fuels, vol. 3, no. 1, pp. 208–218, 2019, doi: 10.1039/C8SE00487K.

[2] S. Kawasaki et al., "Elucidation of Rh-Induced In-Gap States of Rh:$SrTiO_3$ Visible-Light-Driven Photocatalyst by Soft X-ray Spectroscopy and First-Principles Calculations," J. Phys. Chem. C, vol. 116, no. 46, pp. 24445–24448, Nov. 2012, doi: 10.1021/jp3082529.

[3] Q. Liu, B. D. A. Levin, D. M. Haiber, J. L. Vincent, and P. A. Crozier, "An *In Situ* Light Illumination System for an Aberration-Corrected Environmental Transmission Electron Microscope." arXiv, May 18, 2021. Accessed: Jul. 28, 2022. [Online]. Available: http://arxiv.org/abs/2104.02006

[4] L. Reimer, Transmission Electron Microscopy, vol. 36. Berlin, Heidelberg: Springer, 1997. doi: 10.1007/978-3-662-14824-2.

[5] R. L. McCreery, "Raman Spectroscopy for Chemical Analysis," Meas. Sci. Technol., vol. 12, no. 5, pp. 653–654, Apr. 2001, doi: 10.1088/0957-0233/12/5/704.

Publications

1. S. Kadkhodazadeh, F. C. Cavalca, B. J. Miller, L. Zhang, J. B. Wagner, P. A. Crozier, et al. *In Situ TEM under Optical Excitation for Catalysis Research,* Topics in Current Chemistry Vol. **380(6)** 52 (2022).

2. B. D. A. Levin, D. Haiber, Q. Liu and P. A. Crozier, *An Open-Cell Environmental Transmission Electron Microscopy Technique for In Situ Characterization of Samples in Aqueous Liquid Solutions* Microscopy and Microanalysis. **26**(1) Pages 134-138 (2020).

3. D. M. Haiber, B. D. A. Levin, M. M. J. Treacy and P. A. Crozier, *In-Plane Structural Fluctuations in Differently Condensed Graphitic Carbon Nitrides*, Chemistry of Materials. **33**(1) Pages 195-204 (2021).

4. K.Han, D. M. Haiber, J. Knöppel, C. Lievens, S. Cherevko, P. Crozier, et al., *CrOx-Mediated Performance Enhancement of Ni/NiO-Mg:SrTiO3 in Photocatalytic Water Splitting*, ACS Catalysis 2021 **11**(17) Pages 11049-11058 (2021).

5. Q. Liu, B. D. Levin, D. M. Haiber, J. L. Vincent and P. A. Crozier, *An In Situ Light Illumination System for an Aberration-Corrected Environmental Transmission Electron Microscope*, arXiv preprint arXiv:2104.02006 (2021)

6. P. Haluai, T. M. Boland, E. L. Lawrence, P. A. Crozier, Atomic Level Strain Induced by Static and Dynamic Oxygen Vacancies on Reducible Oxide Surfaces, arXiv preprint arXiv:2210.01764 (2022).

7.Y Wang, P Haluai, PA Crozier *In Situ Engineering and Characterization of Photonic Modes in Dielectric Nanocubes*, Microscopy and Microanalysis 28(S1), 1972-1974 (2022).
8. Y Wang, S Yang, PA Crozier, *Revealing Photonic Properties with High Spatial Resolution: An EELS Study on Ceria Nanocubes*, Microscopy and Microanalysis **28(S1)**, 1986-1988 (2022)
9. P Haluai, PA Crozier, *Rhodium Doping of Strontium Titanate for Enhanced Visible Light Absorption*, Microscopy and Microanalysis **28(S1),** 1880-1882 (2022).
10. P Haluai, MR McCartney, PA Crozier, *Detection of Adsorbates Induced Changes on Pt/CeO_2 Catalyst using In situ Electron Holography,* Microscopy and Microanalysis **28(S1)**, 1906-1907 (2022).

Single-electron transistor microscopy of synthetic correlated quantum materials

Ben Feldman

Department of Physics, Stanford University and SLAC National Accelerator Laboratory

Keywords: single-electron transistor, electronic compressibility, moiré superlattice, electronic interactions, two-dimensional materials

Research Scope

The main objective of this project is to integrate single-electron transistors (SETs) into nanoscale scanned probes to image emergent quantum phases in two-dimensional (2D) materials. The SET (Fig. 1a) is a distinctive sensor which can image electrostatic potential, charge, and electronic compressibility (*i.e.*, many-body density of states) of 2D systems with exquisite sensitivity[1]. One major research thrust will be to apply SET microscopy to measure electronic compressibility and visualize electronic states in novel moiré materials systems. We will focus especially on twisted transition metal dichalcogenides (TMDs) and 2D perovskite layers.

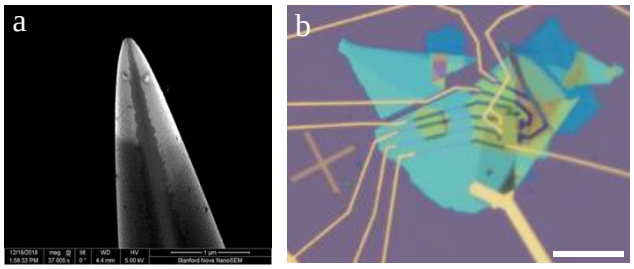

Figure 1. a) Scanning electron micrograph of a single-electron transistor tip. b) Optical image of a fabricated twisted bilayer WSe_2 device. Scale bar: 10 μm.

Building on this effort, we also aim to develop a hybrid sensor in which adjacent SET and Hall probes enable dual magnetic and electronic sensing. We seek to apply this probe to study the interplay between electronic and magnetic effects in quantum materials, such as coupled phase transitions and multiferroic tendencies. Targets of interest include magnetic topological insulators and moiré lattices, with many additional opportunities enabled by such a dual sensor.

Recent Progress

In the first two months of this project, we have successfully fabricated twisted bilayer WSe_2 ($tWSe_2$) devices (Fig. 1b) and have started to conduct electronic compressibility measurements with the scanning SET. Preliminary measurements indeed reveal evidence of correlation-driven gapped phases which we are in the process of characterizing in more detail.

Future Plans

Stacking van der Waals crystals with a small interlayer twist has been shown to produce flat electronic bands susceptible to the effects of Coulomb interactions in multiple materials, with a remarkable variety of possible exotic ground states[2]. In the immediate future, we seek to study the correlated phases in $tWSe_2$ with particular attention to their dependence on spatial position (including local twist angle), magnetic field, and electric displacement field. Both Chern insulating

and magnetic phases have been predicted in certain regimes[3]. Combined imaging and electronic compressibility measurements will enable us to identify which of the anticipated phases are present and the degree to which they can be externally tuned.

We next aim to extend these measurements of a triangular moiré superlattice to new materials systems which provide access to more exotic geometries. For example, honeycomb and kagome lattices are predicted in TMD systems whose low-energy bands lie at the Gamma point[4], accessible in twisted multilayers. Furthermore, recent advances now make it possible to stabilize and manipulate 2D perovskites using similar techniques as for van der Waals systems[5]. This opens a new and highly flexible class of materials with square lattices for investigation in the 2D limit and in heterostructures. Through study of these other twisted TMDs and/or perovskite layers, we hope to reveal novel ground and excited state properties associated with new effective Hubbard model geometries. Adjusting relative twist angle will provide a unique opportunity to modify effective parameters for quantum simulation of interacting electrons.

Finally, we will engage in efforts to develop a hybrid magnetic-electronic sensor with the ultimate goal of correlating both signatures locally in a single sample. Our initial approach will be to lithographically define adjacent SET and Hall probe at the corner of a GaAs wafer to be scanned above samples of interest. Early efforts will focus on developing a reliable fabrication process and characterizing the performance of each respective sensor, followed by investigation of coupled electromagnetic signatures in quantum materials. Individually, both magnetic and ferroelectric behavior has been observed in moiré superlattices. However, there has been no study to date of whether these orders are intertwined, and the hybrid probe will be an ideal tool to address this question. Similarly, combined magnetic and electronic topological phase transitions occur simultaneously in the layered antiferromagnet $MnBiTe_4$.

References

1. Yoo, M. J., Fulton, T. A., Hess, H. F., Willett, R. L., Dunkleberger, L. N., Chichester, R. J., Pfeiffer, L. N. & West, K. W. Scanning single-electron transistor microscopy: Imaging individual charges. *Science* **276,** 579–582 (1997).

2. Andrei, E. Y., Efetov, D. K., Jarillo-Herrero, P., MacDonald, A. H., Mak, K. F., Senthil, T., Tutuc, E., Yazdani, A. & Young, A. F. The marvels of moiré materials. *Nature Reviews Materials* **6,** 201–206 (2021).

3. Devakul, T., Crépel, V., Zhang, Y. & Fu, L. Magic in twisted transition metal dichalcogenide bilayers. *Nature Communications* **12,** 6730 (2021).

4. Angeli, M. & MacDonald, A. H. Γ valley transition metal dichalcogenide moiré bands. *Proceedings of the National Academy of Sciences* **118,** e2021826118 (2021).

5. Leng, K., Fu, W., Liu, Y., Chhowalla, M. & Loh, K. P. From bulk to molecularly thin hybrid perovskites. *Nature Reviews Materials* **5,** 482–500 (2020).

Magneto-thermal microscopy of complex topological spin textures

Gregory D. Fuchs, Cornell University Applied and Engineering Physics, Ithaca, NY

Keywords: Near-field, scanning-probe, magneto-thermal, magnetic microscopy

Research Scope

This research project aims to develop magneto-thermal microscopy for the study of unconventional magnetic materials and heterostructures with picosecond time resolution and nanometer spatial resolution. Our table-top approach is based time-resolve anomalous Nernst effect (ANE) microscopy[1,2] and time-resolved spin Seebeck effect microscopy[3] that has ~10 ps temporal resolution for magnetic order and applied currents. Magneto-thermal microscopy has proven to be a flexible probe of magnetism in both metal and insulator samples, and for both ferromagnetic[1-4] and antiferromagnetic[5] samples.

We have three principle aims in this project. First, we seek to extend and develop magneto-thermal microscopy as a table-top probe of magnetism and current that combines picosecond temporal with nanosecond spatial resolution, limited only by the sharpness of a scanning metal tip. Second, we seek to apply this capability to the study of magnetization dynamics in topological magnetic materials including magnetic skyrmions. Third, we seek to further develop our understanding of magneto-thermal microscopy.

Recent Progress

Recently we have implemented near-field scanning probe microscopy based on scanning a sharp gold tip and using near-field interactions to enhance local sample heating. The advantage of this approach relative to the conventional focused-light magneto-thermal microscopy is that the near-field confinement provided by a sharp metal tip confines local heating to an area with dimensions comparable to the tip radius.

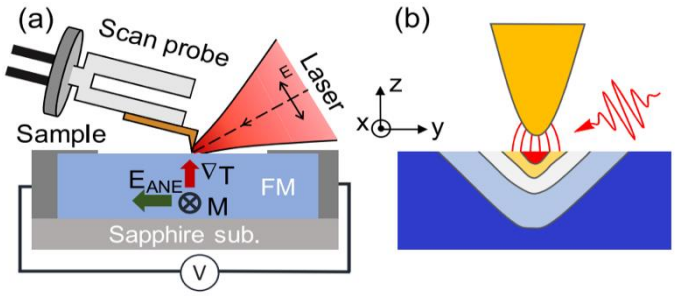

Figure 3. (a) Geometry of scanning probe magneto-thermal microscopy. (b) The electric field enhancement in the near-field between sample and tip leads to enhanced local sample heating over an area comparable to the tip radius.

To create a scanning-probe magneto-thermal microscope, we adapt a tuning fork atomic force microscope (AFM) by integrating it with a o.28 NA microscope objective focused on the tip (Figure 3). For the tip, we use Au-coated Si cantilevers that we purchase and glue to a standard tuning fork. The laser light is focused from the output of a Ti:sapphire laser at 785 nm with a 76 MHz repetition rate, a 3 ps pulse duration, and a fluence of 1 mJ/cm^2. We then use a time-domain homodyne detection scheme to recover the ANE (or current density-based) voltage signal, which requires synchronization of an electrical pulse reference with the laser pulse repetition rate. We lock-in to the signal voltage at the first harmonic (e.g. 2 times the chopper frequency) which recovers the near-field signal selectively for a spurious signal that comes from light heating that

sample that is not enhanced by a near-field interaction. We have verified that we can also lock-in to higher harmonics, which is an important test of near-field behavior.

First we investigate the near-field nature of the tip-sample interaction. For the sample, we use a lithographically patterned 12x5 μm^2 CoFeB film. We test both magnetic contrast via the ANE voltage and current density contrast via voltage generated by local resistivity changes due to heating. Figure 4(a) shows how the ANE (and current density) signal changes as a function of tip-sample distance. We are operating the tip in "tapping" mode, e.g. it modulates the tip-sampled distance. When the tip is nominally 100 nm from the sample, each of the voltages increase. This increase is accompanied by an increase in the probe frequency and a decrease in the probe amplitude, indicating that for tip-sample distances below 100 nm the tip is interacting with the sample. This indicates that our measurement only recovers a signal when the scanning probe is in the near field of the sample.

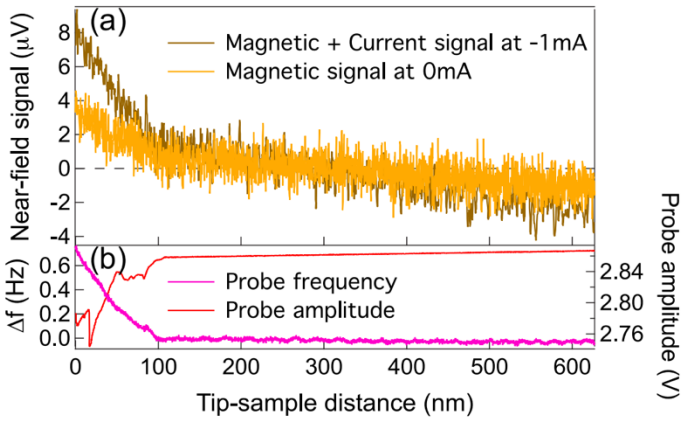

Figure 4. Near-field characteristics. (a) The magnetic and current signals as a function of tip-sample distance. (b) Corresponding changes in the probe frequency and amplitude showing that range over which the tip is interacting with the sample.

Next we explore imaging with scanning probe magneto-thermal microscopy. First we magnetize CoFeB sample into a uniform domain and take line cuts, with and with-out applied current (Figure 5(a)-(b)). We find high spatial resolution responses to both magnetization and current density. We notice that although the signal drops at the sample edge, it doesn't quite drop to zero, indicating we may be still recovering a small artifact signal at the sample edges.

We then de-magnetize the sample to put it into a multi-domain state. We image that state using both conventional focused light (far field) magneto-thermal microscopy and

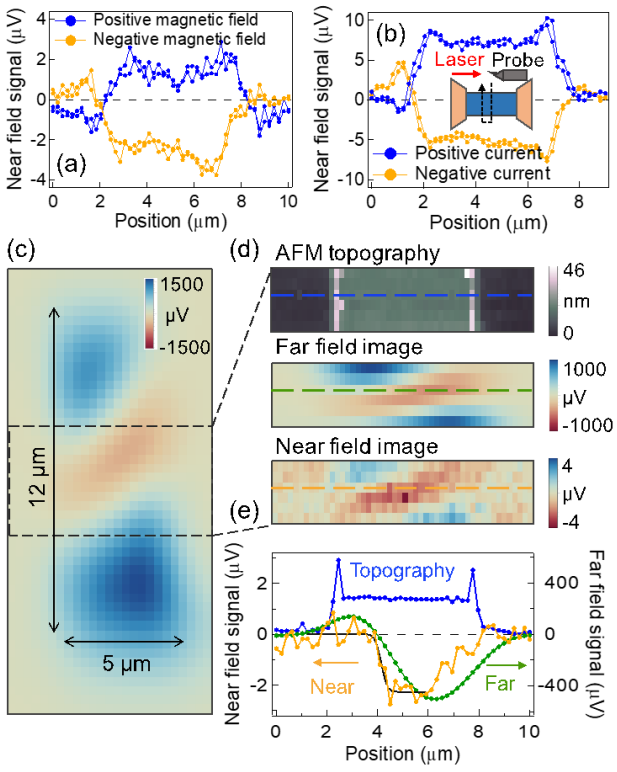

Figure 5. The near field signal varies with direction of (a) magnetization and (b) current. (c) – (d) show far-field, topography, and nearfield magnetization near a domain wall. (e) Line cuts through the domain wall.

scanning-probe (near-field) magneto-thermal microscopy (Figure 5(c)-(e)). We immediately see the trade-off between the two techniques: while the scanning-probe microscopy has much higher spatial resolution than the focused-light version, it has a smaller signal. Further analysis of the sensitivity of magneto-thermal microscopy reveals a sensitivity to in-plane magnetic angle of $4.9^{o}/\sqrt{Hz}$ as compared to a typical value of ~$0.1^{o}/\sqrt{Hz}$ for the focused light version with the same sample geometry. This is because the signal size scales as the r^2/w, where r is the radius of the thermal excitation and w is the width of the electrical channel. For the same value of w, the scanning probe version is exciting a dramatically smaller area.

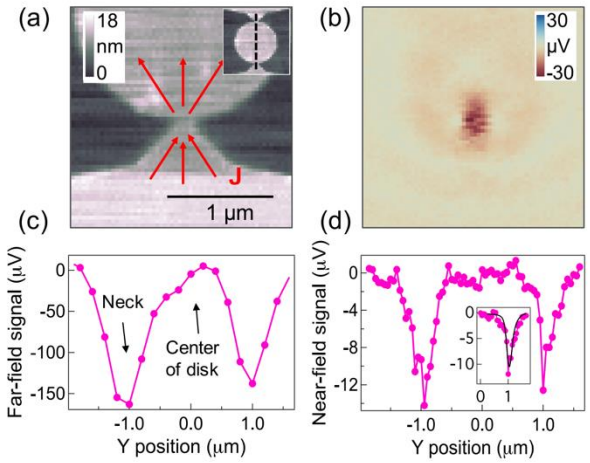

Figure 6. Current imaging and spatial resolution. (a) AFM topography of a current construction. (b) current image acquired using the near-field tip. (c) and (d) are current imaging line-cuts taken using high-NA focused light imaging and the scanning probe, respectively.

To put limits on the spatial resolution of this technique we fit the domain wall width in Figure 5(e). We find that the magnetic reversal happens over 445 nm even at the shallow 37º angle of the line cut with respect to the domain wall direction. Given that CoFeB is a soft ferromagnetic material, this is likely to be the actual domain wall width, and not yet a test of the microscope resolution. However, it is far smaller than the diffraction-limited value of resolution, 1.4 μm.

Given the materials challenges of engineering and stabilizing a particular domain wall width, we benchmarked the instrument resolution in current imaging mode. To accomplish this we fabricated a sample with a narrow construction for current (Figure 6(a)). When passing a current we then image the sample using the scanning probe and find a narrow response. When we analyze line-cuts acquired by focused light (0.9 NA) and the scanning probe (Figure 6(c)-(d)) we can directly analyze the instrument resolution. For the focused light microscopy, we find a spatial resolution of ~0.7 μm, which is consistent with the wavelength and NA. For the scanning probe microscope, we the resolution is given by a Gaussian width of 74 nm (FWHM of 165 nm), which again is far below the optical diffraction limit. This value is consistent with the radius of the probe tip as imaged in the SEM after the experiment.

We also wish to demonstrate that scanning probe magneto-thermal microscopy does not sacrifice the temporal resolution of focused-light magneto-thermal microscopy. Figure 7 shows a direct measurement of duration of the voltage pulses generated at the sample due to the current-density imaging and magnetic imaging. In these measurements combine the voltage pulse created from the transient sample voltage on an electrical mixer along

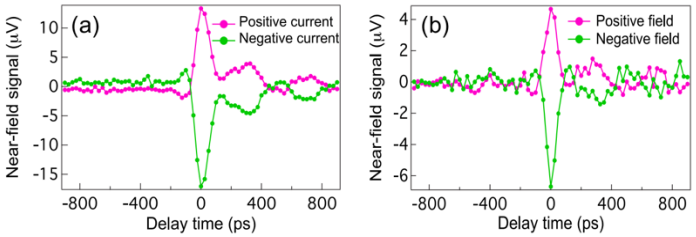

Figure 7. A measurement of the (a) current-density signal voltage and the (b) ANE signal voltage duration based on homodyne mixing with a 100 ps electrical reference pulse.

with a 100 ps electrical reference pulse. We then delay the reference pulse and stroboscopically measure the result, which can be interpreted as the convolution of the two pulses. In both cases, we see responses of ~100 ps, which implies that the interactions in the sample are taking place with a timescale far below that of the 100 ps reference pulse. This is an exciting result because it demonstrates we combine high spatial resolution (~100 nm) with high temporal resolution (<100 ps), enabling study of a range of interesting nanoscale spin textures, their dynamics, and their interactions with microwave-frequency current density.

The work discussed above is magneto-thermal microscopy based on near-field excitation and electrical detection. We have also recently been developing multi-modal scanning probe microscopy in which we simultaneously detect the scattered infred light from the near-field probe – an imaging mode more commonly known as apertureless SNOM (scanning near-field optial microscopy). This is beneficial for our research in magnetic materials for two reasons: the SNOM signal turns out to be easier to acquire and with excellent signal-to-noise ratios. This helps by enabling us to always monitor that we have a 'good' tip, improve our alignment (which can be a laborious procedure using purely electrical readout) and provide a second modality of imaging. The magnetic metal samples that we've been investigating thus far do not have "interesting" magnetic contrast from a SNOM point-of-view, however, as discussed below, we've also been investing 2D magnetic materials that are more interesting for SNOM.

To investigate a 2D magnetic material using magneto-thermal microscopy, we must first select a material with some in-plane magnetic texture, since the geometry of magneto-thermal microscopy is most sensitive to the component of magnetization perpendicular to the electrical channel. We choose Fe_5GeTe_2 (F5GT), which has in-plane magnetic anisotropy. This material system is known to host interesting magnetic texture and undergo magnetic phase transitions that has been suggested to be related to a competition between spin and charge order.

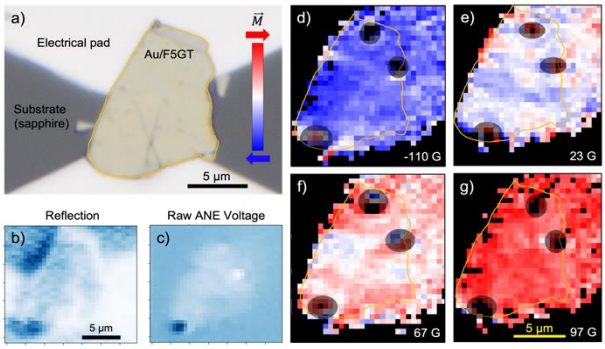

Figure 8. (a) Optical micrograph of a Au/F5GT flake between two leads. (b) and (c) are scanning reflection and raw ANE voltage, respectively. (d) – (f) are images at different magnetic field showing domain nucleation and reversal.

To make a sample suitable for magneto-thermal microscopy, we exfoliate a flake (in collaboration with the Ramesh group at Berkeley) and evaporate ~5 nm of Au. The resulting Au-coated flake is then transferred to bridge two electrical contacts (Figure 8). The Au helps to protect the air-sensitive F5GT from oxidation and serves as a thermal transducer. One key challenge associated with magneto-thermal microscopy of 2D magnets is being sure that the electrical contacts to the flake are good. In fact, the contacts are generally not ideal, and as a result we detect a complicated raw ANE voltage in scanning (Figure 8(c)). Nonetheless, by measuring the sample under positive and negative magnetic saturation, we can extract the purely magnetic signal as function of voltage (Figure 8(d)-(g)), were we observe the magnetic nucleation of reversal domains followed by saturation in the opposite direction. This promising preliminary work suggests that this material system is a good fit for magneto-thermal microscopy, however, we still have work to prepare the samples and eliminate artifacts.

Future Plans

We plan to continue in two areas. First, we will continue to refine and extend our understanding of scanning probe magneto-thermal microscopy. Key goals include improving the signal-to-noise ratio. We recently boosted our ANE voltage by a factor of 5-10 by choosing different scanning tips. We will also continue to investigate applications of our microscope for dynamic imaging studies. Additionally, we plan to continue to explore van der Waals magnetic materials via magneto-thermal microscopy.

References

1. J. M. Bartell, D. H. Ngai, Z. Leng, and G. D. Fuchs, "Towards a table-top microscope for nanoscale magnetic imaging using picosecond thermal gradients," Nature Communications 6, 8460 (2015).

2. J. M. Bartell, C. L. Jermain, S. V. Aradhya, J. T. Brangham, F. Yang, D. C. Ralph, and G. D. Fuchs, "Imaging Magnetization Structure and Dynamics in Ultrathin Y3Fe5O12/Pt Bilayers with High Sensitivity Using the Time-Resolved Longitudinal Spin Seebeck Effect," Physical Review Applied 7, 044004 (2017).

3. I. Gray, T. Moriyama, N. Sivadas, G. M. Stiehl, J. T. Heron, R. Need, B. J. Kirby, D. H. Low, K. C. Nowack, D. G. Schlom, D. C. Ralph, T. Ono, and G. D. Fuchs, "Spin Seebeck Imaging of Spin-Torque Switching in Antiferromagnetic Pt/NiO Heterostructures," Physical Review X 9, 041016 (2019).

4. H. Zhang, R. Chen, K. Zhai, X. Chen, L. Caretta, X. Huang, R. V. Chopdekar, J. Cao, J. Sun, J. Yao, R. Birgeneau, and R. Ramesh, "Itinerant ferromagnetism in van der Waals Fe5-xGeTe2 crystals above room temperature," Physical Review B 102, 064417 (2020).

5. X. Wu, L. Lei, Q. Yin, N.-N. Zhao, M. Li, Z. Wang, Q. Liu, W. Song, H. Ma, P. Ding, Z. Cheng, K. Liu, H. Lei, and S. Wang, "Direct observation of competition between charge order and itinerant ferromagnetism in the van der Waals crystal Fe5-xGeTe2," Physical Review B 104, 165101 (2021).

Publications

1. C. Zhang, J. M. Bartell, J. C. Karsch, I. Gray, and G. D. Fuchs, "Nanoscale Magnetization and Current Imaging Using Time-Resolved Scanning-Probe Magnetothermal Microscopy," Nano Letters **21**, 4966 (2021).

Probing Fast Local Photodynamics in Halide Perovskite Semiconductors: A Robust Regression Neural Network for Extracting Dynamics

PI: David S. Ginger, University of Washington, Department of Chemistry

Keywords: scanning probe microscopy, halide perovskites, optoelectronics, quantum, solar

Research Scope

This project seeks to develop and apply new microscopy methods that merge high-data-bandwidth scanning probe techniques with machine learning to probe the local optoelectronic response of halide perovskite semiconductors that are currently of interest for future technologies ranging from photovoltaics and light-emitting diodes (LEDs) to sources of quantum light. Along the way, the project aims to demonstrate an economical path to provide wavelength-agile, high-intensity, and high-temporal-bandwidth *in situ* excitation of a sample allowing high temporal and spatial resolution detection of local charge carrier motion. The project is pursuing this goal by (1) integrating and synchronizing a broadband light source with an oscillating atomic force microscope (AFM) tip; (2) exploiting the improved time and spectral resolution in this optical excitation to enable significant improvements in two specialized time-domain atomic force microscopy methods: intensity-modulated scanning Kelvin probe microscopy (IM-SKPM) to locally measure the carrier recombination and time-resolved electrostatic force microscopy (trEFM) to directly probe carrier dynamics; and (3) to apply data science methods to enable faster, more accurate extraction of experimentally meaningful signals from our microscopy data.

Recent Progress

We have made significant progress since this project began in July 2021. A significant portion of the first half of the project has been devoted to the simulation, design, acquisition, and installation of key components, including the white-light laser source, along with modifying our existing atomic force microscope (AFM) instrumentation and code. We purchased several components required for these experiments: a high-speed digitizer card for the AFM, two fast modulable electrically-driven fixed wavelength laser sources for prototyping (405 nm and 705 nm), a 2 MHz high voltage amplifier to modulate an electrooptic modulator, and a NKT Photonics white-light laser source. The NKT laser was received and installed in April 2022; however, it exhibited a number of faults over the summer and is currently with the vendor for repair. In the meantime, our group has been productive in making progress on the science goals of studying wide bandgap halide perovskites with AFM by (i) developing neural networks to extract dynamics from both simulated and real-world time-resolved electrostatic force microscopy data, (ii) using the fast modulable diode laser sources to study intensity modulated scanning Kelvin probe (IM-SKPM) dynamics on halide perovskites, which is now close to realizing our long-held goal of probing the same carrier dynamics underpinning photoluminescence decay in a semiconductor but with scanning probe resolution using mechanical detection.

A Robust Regression Neural Network for Extracting Dynamics from Time-Resolved Electrostatic Force Microscopy Data

Advances in scanning probe microscopy (SPM) methods such as time-resolved electrostatic force microscopy (trEFM) now permit the mapping of fast local dynamic processes with high resolution in both space and time, but these methods are often time consuming to analyze and can be difficult to calibrate. In this period, we designed and trained a regression neural network (NN) that accelerates and simplifies the extraction of local dynamics from SPM data directly in a cantilever-independent manner, allowing the network to process data taken with different cantilevers. We validated the NN's ability to recover local dynamics with a fidelity equal to or surpassing traditional, more time-consuming, experimental calibrations using both simulated and real microscopy data. We applied this method to extract accurate photoinduced carrier dynamics on n=1 butylammonium lead iodide, a halide perovskite semiconductor film that is of interest for applications in both solar photovoltaics and quantum light sources. Finally, we used SHapley Additive exPlanations (SHAP) to evaluate the robustness of the trained model, and confirmed its cantilever-independence, and we explored which parts of the trEFM signal are important to the network and to extracting dynamics. This work has now been published[1] and the code is freely available online.[2]

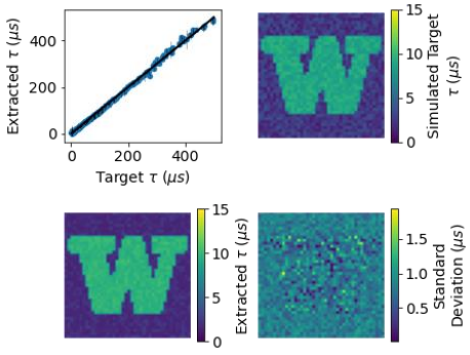

Fig. 1 Performance of the neural network on simulated dynamic SPM data. (a) Parity plot of 500 randomly sampled network-extracted τ vs. target τ values from 3,000 simulated test instantaneous frequency traces where the black line represents perfect agreement with an R2 score of 0.89, demonstrating the network's excellent performance on simulated data; we calculated a mean absolute error of 2.14 μs on average with a mean standard deviation of 3.82 μs; error bars indicate the standard deviation obtained via a quasi-ensembling technique discussed in the full paper (b) separately simulated target τ values used as the basis for the simulation of a trEFM image datacube; (c) the trained network-extracted τ values from data simulated according to (b), showing excellent qualitative agreement with the simulated target values; and (d) standard deviations for the extraction for (c) given quasi-ensembling of 100 network outputs as discussed in the text. Reproduced from Ref 1.

Intensity Modulated-Scanning Kelvin Probe Microscopy Resolves both Ionic and Electronic Carrier Dynamics in Halide Perovskite Semiconductors

We have been using fast modulable diode lasers to probe carrier dynamics in wide bandgap perovskites at the nanoscale by combining a modulating excitation source and scanning Kelvin probe microscopy (SKPM) to perform intensity-modulated scanning Kelvin probe microscopy (IM-SKPM) as outlined in our project proposal. SKPM measures the contact potential difference (CPD) between the atomic force microscope (AFM) tip and the sample. When a sample is illuminated, this CPD value will change in response, with a characteristic time defined by the optoelectronic properties of the sample such as carrier lifetime. Here, we use perovskites to probe samples at the nanoscale using an intensity-modulated SKPM (IM-SKPM) method, wherein the CPD is measured while an illumination source is modulated at varying frequencies. By comparing the actual frequency response with simulations of multi-timescale relaxation, we can use IM-SKPM to extract local carrier lifetimes across many orders of magnitude in time. In previous work

using IM-SKPM, we were severely limited in what time constants were accessible to ~50 µs, which is much longer than the lifetime in a typical perovskite solar cell. Using newly purchased laser sources, we can now modulate the excitation at frequencies over 100 MHz, which is enabling us to measure local carrier lifetimes on the order of 10s of nanoseconds. Using new long-lifetime perovskite samples, prepared with surface passivation, we see good correlation between the extracted changes in ionic and both electronic and ionic (Fig. 2 top) carrier motion, and can even perform imaging (Fig. 2 bottom). In our work so far, we have compared lifetimes of different perovskite formulations measured via bulk photoluminescence lifetime with the IM-SKPM lifetime, and we have observed excellent correlation, thus validating our approach.

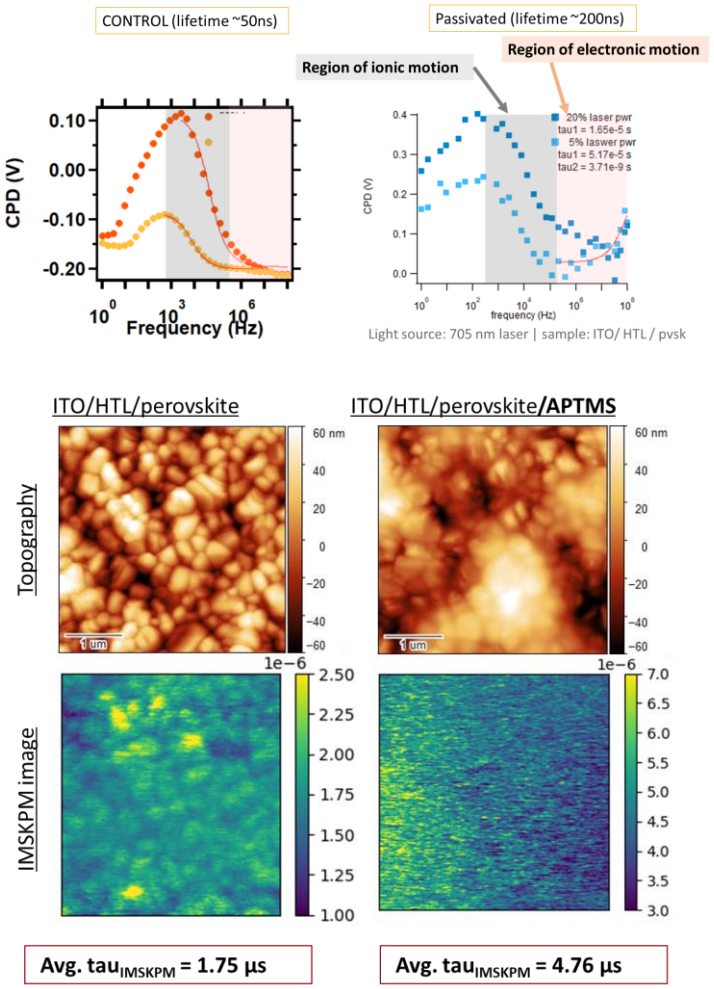

Fig. 2 (Top) IM-SKPM data taken on (left) unpassivated, and (right) silane passivated $FA_{0.83}Cs_{0.17}(I_{0.85}Br_{0.15})_3$ perovskite films on ITO with a phosphonic acid hole transport layer. The unpassivated samples show a peak at ~1-10 kHz associated with slow ionic motion (likely halide vacancies) whereas the passivated samples show a new peak with a time of ~10-100 ns emerging, consistent with the PL lifetime of those films. In addition, the passivated samples show a weaker and slower (lower defect density) ionic peak. (Middle) 2 images (brown) topography of unpassivated and passivated perovskite films, and (Bottom) 2 images, IM-SKPM images of the same 2 samples. The passivated film shows longer carrier lifetimes and less morphology-dependent structure, as expected, providing confidence in the analysis procedure.

Future Plans

Over the remainder of the project we plan to finish the IM-SKPM work by demonstrating imaging of perovskites with heterogeneous surface passivation chemistry. We plan to expand our neural network analysis package to faciliate analysis of non-single-exponential decays in trEFM, and, using IM-SKPM to benchmark the trEFM analysis, demonstrate that trEFM can extract spatially-resolved dynamic information about electronic carrier motion on fast time scales in halide perovskite samples, and correlate these maps with maps of local crystallinity in halide perovskites to better undrestand the origin and distribtuion of defects that currently limit the perofmrance of these materials as both ligh absorbers in solar energy applications as well as light emitters in conventional and

quantum optoelectronics. Because of challenges in accessing electron backscatter differaction (EBSD) detectors with sufficient sensitivity to make routine EBSD measurements, we also plan to use DOE synchrotron facilites to conduct nano-XRD and other spatially-resolved structure maps to correlate with the IM-SKPM and trEFM imaging.

References

(1) Breshears, M. D.; Giridharagopal, R.; Pothoof, J.; Ginger, D. S. "A Robust Neural Network for Extracting Dynamics from Electrostatic Force Microscopy Data." *J. Chem. Inf. Model.* **2022**, *62*, 4342–4350. DOI: 10.1021/acs.jcim.2c00738.

(2) M. D. Breshears, R. Giridharagopal, J. Pothoof, D. S. Ginger. A Robust Neural Network for Extracting Dynamics from Time-Resolved Electrostatic Force Microscopy Data: Accompanying code and example Jupyter notebook. (2022). https://github.com/mdbresh/NN_trEFM

Publications citing BES

1. M. D. Breshears, R. Giridharagopal, J. Pothoof, D. S. Ginger. “A Robust Neural Network for Extracting Dynamics from Electrostatic Force Microscopy Data.” *J. Chem. Inf. Model.* 62, 4342–4350 (2022). DOI: 10.1021/acs.jcim.2c00738

2. M. D. Breshears, R. Giridharagopal, J. Pothoof, D. S. Ginger. A Robust Neural Network for Extracting Dynamics from Time-Resolved Electrostatic Force Microscopy Data: Accompanying code and example Jupyter notebook. (2022). https://github.com/mdbresh/NN_trEFM

3. S. Sidhik, Y. Wang, M. De Siena, R. Asadpour, A. J. Torma, T. Terlier, K. Ho, W. Li, A. B. Puthirath, X. Shuai, A. Agrawal, B. Traore, M. Jones, R. Giridharagopal, P. M. Ajayan, J. Strzalka, D. S. Ginger, C. Katan, M. A. Alam, J. Even, M. G. Kanatzidis, A. D. Mohite. “Deterministic fabrication of 3D/2D perovskite bilayer stacks for durable and efficient solar cells.” *Science*, 377, 1425-1430. (2022).
4. Y. Shi, E. Rojas-Gatjens, J. Wang, J. Pothoof, R. Giridharagopal, K. Ho, F. Jiang, M. Taddei, Z. Yang, C. Silva-Acuña, D. S. Ginger. “(3-Aminopropyl) trimethoxysilane Surface Passivation Improves Perovskite Solar Cell Performance by Reducing Surface Recombination Velocity”. *arXiv preprint arXiv:2209.15105*. (2022).
5. J. Chen, J. Wang, X. Xu, J. Li, J. Song, S. Lan, S. Liu, B. Cai, B. Han, J. T. Precht, D. S. Ginger. “Efficient and bright white light-emitting diodes based on single-layer heterophase halide perovskites”. *Nature Photonics*, 15, 238-244 (2021).
6. F. Jiang, J. Pothoof, F. Muckel, R. Giridharagopal, J. Wang, D. S. Ginger. “Scanning Kelvin probe microscocpy reveals that ion motion varies with dimensionality in 2D halide perovskites”. *ACS Energy Letters.* 6, 100-108. (2021).

Cryogenic Electron Microscopy and Spectroscopy for Topological Spin Textures in Two-Dimensional van der Waals Magnetic Materials

Kai He, Department of Materials Science and Engineering, University of California, Irvine, CA 92697

Keywords: cryogenic electron microscopy, vibrational EELS, 2D materials, topological spin textures

Research Scope

Two-dimensional (2D) van der Waals (vdW) materials are considered as one of the most promising candidates to revolutionize the information- and energy-related technologies not only because of their exotic properties enabled by the unique atomically thin crystal structures under the reduced dimensionality and quantum confinement, but also due to the feasibility to integrate such enormous properties into the silicon technology for foreseeable device functionalization. The 2D vdW materials provide an ideal platform to allow the competition between the spin, charge, orbital, and lattice degrees of freedom, which leads to various novel magnetic phenomena, including the recently discovered intrinsic magnetism and frustrated magnetism at the 2D atomic limit, opening up a new horizon for quantum spintronics. However, the knowledge regarding the topological spin textures in 2D magnetic systems remains missing. Specifically, the knowledge gap still remains in the fundamental understanding of the physical origin of topological spin textures at the ground and excited states and how they can be controlled by the crystal lattice, reduced dimensionality, and externally tunable (i.e., magnetic, electrical, thermal) probes. Additional studies are required to develop a specific, mechanistic understanding of interplays between spin and the other competing orbit, lattice, and charge orders that may lead to the enhanced control of 2D magnetic ordering and correlated spin-charge transport.

The goal of this Early Career project is to identify, understand, and manipulate the topological spin textures in 2D vdW magnetic materials and elucidate the underlying spin-orbit, spin-lattice, and spin-charge interactions using cryogenic transmission electron microscopy (cryo-TEM) and vibrational spectroscopy approaches. This project will generate experimental results to determine the topological charge and spin configuration of the topologically protected quasiparticles in 2D magnetic materials and further uncover the correlated spin-lattice and spin-phonon coupling mechanisms. The findings will help to elucidate the fundamental physics underpinning the spin-orbit, spin-lattice, and spin-charge interactions, which may be leveraged to facilitate desirable manipulation of topological spin excitation and dynamics via external control of magnetic and electrical probes, providing practical implications to future spintronics and quantum information technologies.

Future Plans

To achieve the goal within the five-year period, we will develop microscopy techniques and use them as enabling tools to solve fundamental science questions. In the next two years, we will develop advanced TEM methodology and instrumentation that allow unprecedented spatial

and energy resolutions at extremely low temperatures through commercial and homemade solutions for the state-of-the-art electron microscopy facilities at the PI's institution. Specifically, we expect to combine cryogenic capabilities with phase-retrieval imaging techniques, such as electron holography and 4D-STEM, to enable direct visualization of topological spin textures in 2D magnetic materials at low temperatures. Using the developed methods and tools, we will first investigate air-insensitive materials, such as metallic and chalcogenide magnets, and later push the limit of reducing air sensitivity by further incorporating air-free transfer to allow studies on notoriously sensitive metal halides.

Deep learning studies for massive, atom-by-atom studies of atomic structure and rearrangements in two-dimensional materials

Pinshane Y. Huang (Materials Science and Engineering, University of Illinois at Urbana-Champaign), Bryan Clark (Physics, University of Illinois at Urbana-Champaign)

Keywords: Two-dimensional materials, Scanning Transmission Electron Microscopy, Machine Learning, In-situ electron microscopy

Research Scope

Cutting-edge electron microscopy methods such as aberration correction and electron ptychography have unlocked the ability to study materials at the level of individual atoms. It remains challenging to connect high-precision atomic-scale information with device-scale properties as well as to understand structural or electronic transformations that involve the collective behavior of large numbers of atoms. To bridge this gap, a key bottleneck is the processing time needed to fully utilize massive, atomic resolution datasets. In our work, we develop and apply experimental and machine learning (ML) methods to generate and exploit large, atomic resolution datasets of two-dimensional (2D) materials acquired using scanning transmission electron microscopy (STEM). Key aspects of this work in the last two years include: the development of an automated acquisition and data processing workflow to collect and process data on the million-atom scale, the use of cycle-generative adversarial networks to generate labeled training data for deep learning that are nearly indistinguishable from real experimental data, and the development and application of an in-situ platform to study phase transformations and interfacial reconstruction of 2D materials.

Recent Progress

Progress has proceeded in three main areas:

a. Automated Acquisition and Deep Learning of 2D Materials on the Million-Atom Scale

Here, we develop a series of techniques including automated acquisitions of STEM images, realistic training data enhanced by generative adversarial network (GAN), defect identification with deep learning, and class averaging for high signal-to-noise ratio (SNR) images for massive all-atom analysis of 2D materials. First, we build a scripting framework using *pywinauto* to integrate different functionalities to control electromagnetic lens settings, stage motion, aberration correction, and acquisition parameters. This allows us to automatically acquire atomic-resolution datasets on the million-atom scale, or ~μm^2 size within a day.

Next, we construct a CycleGAN-enhanced workflow to generate realistic training data from both simulated and experimental images. The CycleGAN extracts subtle features from the

experimental images and applies those features onto the simulated images while preserving the defect labeling from the simulation that is required for ML training. Our CycleGAN works on a relatively small subset of images, ensuring that even microscopy parameters which drift over time, such as aberrations, can be correctly transferred. This results in high-quality, experiment-like simulated data with the benefits of being automatically labeled. We developed a novel discriminator which is sensitive to features in the Fourier transform of the image data, which we found was key to generating realistic ML image outputs. We have also produced an efficient workflow including a series of hyperparameters and image preprocessing steps which is robust over multiple different materials; our CycleGAN and workflow is incorporated into a series of open-source codes[1]. The resulting CycleGAN images appear experimentally realistic both to domain experts as well as with respect to various metrics including success in training for defect identification (**Figure 1**).

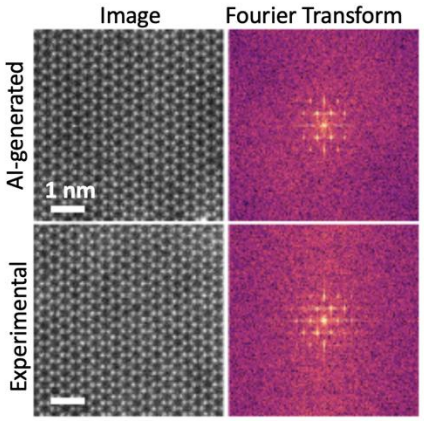

Figure 1. Real and Fourier space images of WSe_2 both experimentally and AI generated via CycleGAN. The CycleGAN enables the creation of labeled ML training data that matches experimental conditions.

The resulting high-quality training data enables accurate defect identification using a fully convolutional network (FCN). The performance is comparable to or even exceeding human labeling with much less human intervention. We examine hundreds of atomic resolution images with FCN and identify thousands of point defects, including vacancies, substitution, and antisite defects from 2D materials. The defect distribution and statistics are used to correlate with its photoluminescence yield, showing an inversely proportional relation across the μm scale. We further perform class averaging to generate high SNR images from nominally identical defects, which allows us to circumvent the fundamental limitations set by electron beam damage and achieve 0.3 pm precision of the 2D coordinates of these defects. These techniques may pave the way towards self-driving microscopy, unsupervised feature identification, and high-precision analysis of beam sensitive samples.

b. In-situ Imaging of Twisted Bilayer Transition Metal Dichalcogenides

Moiré superlattices in twisted two-dimensional materials host a variety of emergent quantum phenomena, including unconventional superconductivity, quantum anomalous Hall effect and ferroelectricity[2,3]. These phenomena are highly sensitive to twist angle, a degree of freedom unique to 2D interfaces that can be used to modulate the periodic potential of the resulting moiré. After fabrication, post-annealing and spontaneous rotations of twisted crystals can occur, adding further complexity to precise control of twist angle. Understanding the interfacial reconstruction mechanism of the moiré superlattice is crucial to understanding and controlling the properties of these quantum systems. In our work, we discover a new atomistic mechanism of local reconstruction from moiré patterns to parallel (3R) and/or antiparallel (2H) domains in twisted bilayer 2D transition metal dichalcogenides (TMDCs). Unlike previous reports, where the twist angle is altered by the rotation of a whole flake, we observe the nucleation and growth of commensurate domains through the formation and migration of grain boundaries.

Here, we study the thermally activated, local reconstruction of twisted bilayer TMDCs using *in situ* aberration-corrected STEM and dark-field transmission electron microscopy (DFTEM). We fabricate graphene encapsulated twisted WSe_2 homo-bilayers and $MoSe_2$-WSe_2 hetero-bilayers on MEMS-based chips for *in situ* pulsed heating. We show that heat-pulses induce *local* reconstruction to parallel/antiparallel structures (referred to as aligned structures) ranging from a few nanometers to micrometers in size with short (<1 s) temperature pulses between 200-1000°C. Such reconstruction is observed in all samples exhibiting five different twist angles. *In situ* aberration-corrected ADF STEM imaging reveals that the aligned structure is formed by the nucleation of a new grain within one layer, surrounded by grain boundaries formed by 5|7 ring defects. We capture the dynamic process of nucleation and growth of the aligned structure through a series of atomic resolution STEM images combined with atom-tracking analysis. These data show a surprising mechanism, in which the twisted moiré structures transform into rotationally aligned bilayers through the local, collective rotation of atoms in each moiré unit cell, facilitated by the formation and migration of 5|7 ring defects (**Figure 2**). These results provide new insights into the mechanisms of interlayer rotation at the atomic scale and potential method into engineering the structure of moiré superlattices.

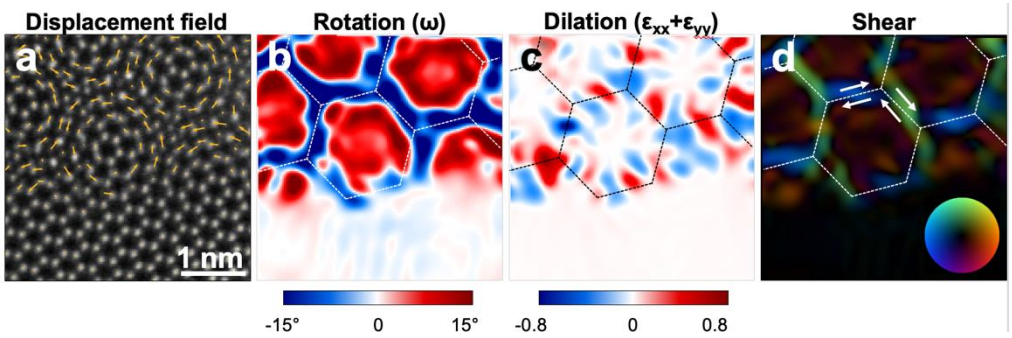

Figure 2. Atom tracking at a twisted bilayer WSe_2 interface reveals a new mechanism for interlayer alignment. **a**, ADF-STEM image of moiré interface overlayed with displacement vector fields showing atomic rearrangements after a 700°C heat pulse. Rotational displacements occur in one of the layers, with the largest displacements at the edges of each moiré unit cell. Vectors are at 1:1 scale. **b-d**, Changes in local strain due to the atomic rearrangements indicate that each moiré cell rotates independently, facilitated by the formation and migration of grain boundary defects. Color in **d** represents shear direction.

c. In-situ Imaging of Anisotropic Layer-by-layer Phase Transition in Few-layer $MoTe_2$

Understanding the mechanisms and kinetics of phase transitions in two-dimensional (2D) materials is key to precisely tailoring their properties at the nanoscale. In particular, $MoTe_2$ exhibits multiple structural and electronic phases at room temperature (2H, 1T', and T_d) that can be easily manipulated with different stimuli[4], making it a promising candidate for phase-change memories, high-performance transistors, and broadband photodetectors. We use graphene (Gr) encapsulation to create an enclosed, in-situ reaction cell for TEM studies of few-layer $MoTe_2$ on a MEMS-based heating holder. The graphene encapsulation protects $MoTe_2$ from sublimation while being highly electron transparent, allowing atomic resolution studies of $MoTe_2$ down to a single unit cell thick. The encapsulated $MoTe_2$ was then laser-irradiated to locally convert the 2H phase into the metastable T_d phase. In order to capture the dynamics of T_d-to-2H phase transition at both micro and atomic scales, we apply heat pulses as short as 0.5s using a MEMS-based heating holder to "freeze" the growth front of the 2H phase at different temperatures. Next, we combine dark-field TEM and aberration-corrected STEM to image the phase transitions of few-layer $MoTe_2$

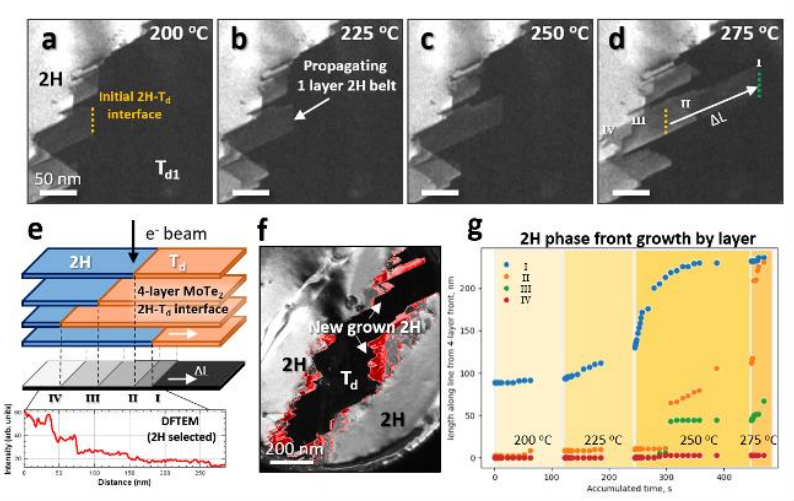

Figure 3. Anisotropic layer-by-layer, T_d-to-2H phase transition. (a-d) DFTEM images show the 2H phase front propagating after each pulse. (e) Schematic of the intensity differences of 4-layer $MoTe_2$ phase boundaries in DFTEM. (f) DFTEM image with newly formed 2H regions marked in red. (g) 2H phase front positions of different layers as a function of accumulated heating time.

in situ from the micro- to atomic scales (**Figure 3**). We find that T_d-to-2H phase transitions initiate at the phase boundary at temperatures as low as 200-225 C, much lower than previously thought. We individually measure the phase front of each layer and find that the linear growth rate of the 2H phase at 275ºC varies from 5 to 14 nm/sec between different layers, which suggests that factors such as strain and local defect densities affect the energy barrier of the phase transition. In addition, the 2H-T_d interfaces propagate primarily along the b-axis of the T_d grain, producing an anisotropic, layer-by-layer phase transformation. These results should lead to new methods to manipulate the quantum and electronic properties within individual atomic layers.

Future Plans

In the next year, a main focus will be using a newly installed EMPAD pixel array detector to conduct 4D STEM measurements and electron ptychography of two-dimensional materials. We will expand our machine learning methods to improve reconstruction quality and speed, search for optimal collection parameters, and to analyze super-resolution images from electron ptychography. We will use these studies to investigate correlations between the atomic structure and properties of twisted 2D multilayers.

References

1. D. L. Abid Khan, Chia-Hao Lee, Pinshane Y. Huang, Bryan Clark. *STEM-learning*, <https://github.com/ClarkResearchGroup/stem-learning> (2020).
2. Y. Cao, V. Fatemi, S. Fang, K. Watanabe, T. Taniguchi, E. Kaxiras & P. Jarillo-Herrero. *Unconventional superconductivity in magic-angle graphene superlattices*. Nature **556**, 43-50 (2018).
3. M. Serlin, C. L. Tschirhart, H. Polshyn, Y. Zhang, J. Zhu, K. Watanabe, T. Taniguchi, L. Balents & A. F. Young. *Intrinsic quantized anomalous Hall effect in a moire; heterostructure*. Science **367**, 900-903 (2020).
4. D. H. Keum, S. Cho, J. H. Kim, D.-H. Choe, H.-J. Sung, M. Kan, H. Kang, J.-Y. Hwang, S. W. Kim, H. Yang, K. J. Chang & Y. H. Lee. *Bandgap opening in few-layered monoclinic MoTe2*. Nature Physics **11**, 482-486 (2015).

Publications

1. C.-H. Lee, A. Khan, D. Luo, T. P. Santos, C. Shi, B. E. Janicek, S. Kang, W. Zhu, N. A. Sobh, A. Schleife, B. K. Clark & P. Y. Huang. *Deep Learning Enabled Strain Mapping of Single-Atom Defects in Two-Dimensional Transition Metal Dichalcogenides with Sub-Picometer Precision*. Nano Letters **20**, 3369-3377 (2020).
2. D. Chen, Y. Zheng, C.-H. Lee, S. Kang, W. Zhu, H. Zhuang, P. Y. Huang & Y. Jiao. *Nearly hyperuniform, nonhyperuniform, and antihyperuniform density fluctuations in two-dimensional transition metal dichalcogenides with defects*. Physical Review B **103**, 224102 (2021).
3. C.-H. Lee, A. Khan, Y. Zhang, M. Abir Hossain, A. van der Zande, B. Clark & P. Huang. *Automated Acquisition and Deep Learning of 2D Materials on the Million-Atom Scale*. Microscopy and Microanalysis **28**, 3062-3063 (2022).
4. Y. Zhang, C.-H. Lee, G. Nolan, J.-H. Baek, G.-H. Lee & P. Y. Huang. *In-situ Imaging of Thermally Activated Atomic Reconstruction of Twisted Bilayer Transition Metal Dichalcogenides*. Microscopy and Microanalysis **28**, 1732-1734 (2022).
5. C.-H. Lee, Y. Zhang, M. Abir Hossain, Y. Zhang, A. M. van der Zande & P. Y. Huang. *Tuning the Optical Properties of 2D Materials with Defects and Strain*. Microscopy and Microanalysis **28**, 2014-2014 (2022).

Ultrafast dynamics of correlated insulators

Anshul Kogar, University of California – Los Angeles

Keywords: Ultrafast, photo-induced, phase transitions

Research Scope

Discovering new states of matter with unique properties and controlling these properties for various functionalities are fundamental goals of condensed matter physics and materials science [1]. Our group aims to realize these targets using intense femtosecond light pulses to drive material systems far from thermodynamic equilibrium. Under the influence of light pulses, macroscopic properties of matter can be altered over extremely short timescales. But under certain circumstances, those altered properties are retained even once the light pulses are removed. These stable manipulations can realize new states of matter that are inaccessible under equilibrium conditions but are nonetheless long-lasting under ambient conditions. One of the most promising material platforms for such metastable manipulations are correlated insulators. By studying the electronic and structural response of these materials to pulsed photo-excitation, we seek to achieve the following goals: (i) understand the microscopic interactions that give rise to the energy barriers that prevent metastable states from decay, (ii) elucidate the role of structural and electronic inhomogeneity in photo-induced phase transitions and (iii) discover new metastable transitions that can be stabilized with light pulses. To accomplish these goals, our group is using ultrafast electron scattering and time-resolved second harmonic generation to understand the dynamics of correlated insulators on ultrafast timescales. Taken as a whole, our research seeks to further our knowledge of out-of-equilibrium physics, push the boundaries of current ultrafast technology and yield schemes for stable optical engineering of material properties.

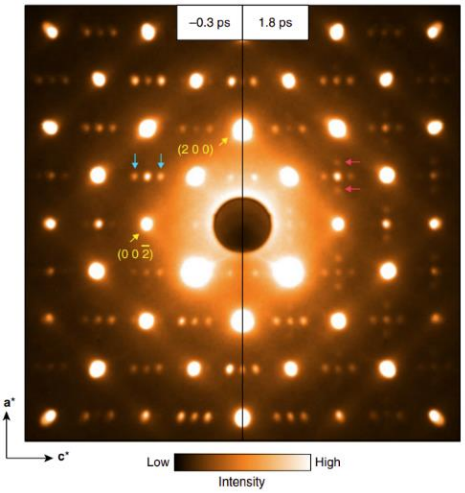

Figure 1: Diffraction pattern before and after excitation with a femtosecond light pulse. On the left, the system shows diffraction peaks only along the c-axis. On the right, after photo-excitation, the system exhibits superlattice peaks along the a-axis also.

Recent Progress

We have so far found that photo-thermal manipulation of thin films of 1*T*-TaS_2 can yield an entirely new crystal phase as shown by our ultrafast electron scattering measurements. After photo-thermally heating samples of ~50nm thickness for ~five seconds, the film transforms into a self-doped 2H-TaS_2. These intercalants can then order in various ways, and transport

measurements indicate that these films undergo two successive phase transitions at 271 K and 231 K. We strongly suspect that the lower transition is magnetic in origin due to previous studies on self-doped TaS_2. Our studies on this compound so far indicate that laser illumination can completely change the properties of TaS_2 and give rise to a novel form of intercalant manipulation.

In addition, we have started investigating the role of inhomogeneity through the photo-induced insulator-metal phase transition in $Ca_3Ru_2O_7$. Our time-resolved second harmonic generation measurements indicate that structural and electronic inhomogeneity play pronounced roles in the transition kinetics as the system proceeds from insulator to metal upon photo-excitation. Our measurements of the characteristic transition time exhibit a dramatic slowing down effect which peaks near a "percolation threshold". We have come up with a simple statistical model to explain our results, which on a qualitative level, agrees with experiments surprisingly well.

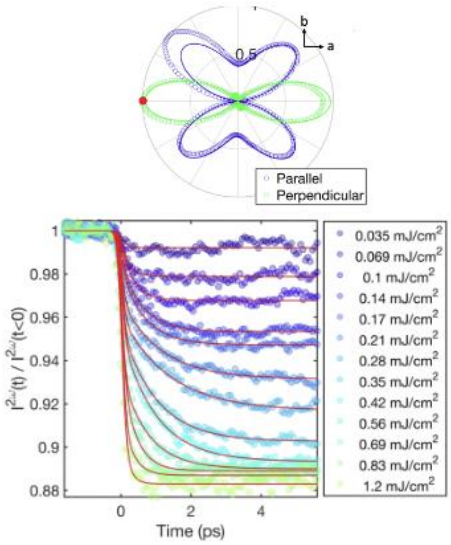

Figure 2 Time-resolved second harmonic generation measurements on $Ca_3Ru_2O_7$. (Top) Rotational anisotropy second harmonic generation with parallel and perpendicular polarization configurations. (Bottom) Time evolution of the second harmonic intensity with varying photo-excitation fluences. The time traces show a noticeable non-monotonic transition rate from insulator to metal.

Future Plans

As this program is new, we are in a phase where instrumentation development and materials studies are occurring side-by-side. On the instrumentation front, one of our big efforts is the development and usage of a radio-frequency cavity for electron compression in performing lab-scale ultrafast electron scattering experiments. Without the RF cavity, the pulse width in these experiments is typically in the range of 2-3 ps. However, with the aid of the RF compressor, our target temporal resolution is in the range of 100 fs. In the far future, we hope that this technology will also branch out into performing electron energy loss spectroscopy with two radio frequency cavities. On the materials front, we are in the process just beginning to study several material platforms under that are particularly promising from the vantage point of photo-manipulation. Our preliminary studies have been conducted on 1*T*-TaS_2, $Ca_3Ru_2O_7$ and Mn-substituted Ca_2RuO_4.

Our major plans for the future is to be able to use our preliminary results as a springboard towards the metastable manipulation of these materials, which can yield stable and switchable properties. So far, our studies of TaS_2 illustrate a change that is remarkable, but cannot be reverted. On the other hand, our studies of $Ca_3Ru_2O_7$ show that while a metastable state exists for a hundred or so picoseconds, the state is not indefinitely metastable. We seek in the future, in collaboration with our partners in crystal growth, to substitute and dope various atoms in both platforms to yield materials that hold the promise of switchable properties at room temperature.

References

1. D.N Basov, R.D. Averitt, D. Hsieh, *Towards properties on demand in quantum materials*, Nature Materials **16**, 1077 (2017).

Publications

N/A

Multi-stimuli Nanoscale Conductivity Imaging of Strongly Correlated Materials

PI: Keji Lai (kejilai@physics.utexas.edu)

Department of Physics, University of Texas at Austin, Austin, TX 78712

Keywords: Electron correlation, microwave microscopy, phase coexistence, complex oxides

Research Scope

The goal of this DOE program is to investigate the response of strongly correlated electron systems to multiple external stimuli with nanoscale spatial resolution. Due to the suppression of electron kinetic energy, other energy scales associated with the Coulomb repulsion, exchange interaction, orbital effect, and lattice strain become crucial and usually lead to a plethora of mesoscopic coexisting phases. Combining a novel microwave impedance microscope (MIM)[1,2] with variable temperature, electric field, magnetic field, illumination, and mechanical stress, the proposed work will reveal key information of correlated systems in the nanoscale, which is of great interest to energy-related science and technology.

Recent Progress

In the past two years, we have studied coexisting phases in $BiFeO_3/TbScO_3$ superlattices and stripe phases in Mn-doped $Ca_3Ru_2O_7$ single crystals. Our dilution-refrigerator-based MIM is now fully up and running, with preliminary data obtained on quantum anomalous Hall states. Details of the accomplishments are as follows.

Coexistence of insulating and semiconducting $BiFeO_3$ phases

In condensed-matter systems, competition between ground states at phase boundaries can lead to significant changes in material properties.[3] A key scientific and technological challenge is to stabilize and control coexistence of symmetry-distinct phases with external stimuli. A major effort of this DOE program is to investigate the nature of these coexisting phases with nanoscale spatial resolution.

In this work, we studied the electrical properties of the coexisting centrosymmetric (antipolar) and non-centrosymmetric (polar) phases in $BiFeO_3/TbScO_3$ (BFO/TSO) superlattices. As shown in the cross-sectional scanning transmission electron microscopy (STEM) image in Fig. 1a, the BFO layers confined between TSO layers exhibit two distinct phases with bright and dark contrast. The second-harmonic generation (SHG) image in Fig. 1b indicates that the two phases correspond to the non-centrosymmetric *Pc* phase and centrosymmetric *Pnma* phase, respectively, with substantially different nonlinear optical response. In order to understand the electrical response of the two phases, we performed piezo-force microscopy (PFM) and MIM studies on the same sample. Fig. 1c shows the experimental setup of our measurement, as well as the scanning electron microscopy (SEM) image of the MIM tip apex. The lateral PFM phase image in Fig. 1d stripe-like regions of high piezoelectric response (white and black regions) and zero piezoelectric response (noisy brown regions). By comparing with the SHG data, we conclude that the background is the antipolar phase, whereas the stripe-like regions correspond to the polar phase

with two in-plane-polarized subdomains. The imaginary (MIM-Im) and real (MIM-Re) parts of the 2.513 GHz impedance images acquired on the same area are displayed in Figs. 1e and 1f, respectively. The one-to-one correlation between the PFM and MIM images is apparent, with the polar phase showing a significantly enhanced signal compared to the antipolar phase. Note that the microwave signal is uniform throughout the polar non-centrosymmetric regions of the sample, regardless of the orientation of the net polarization.

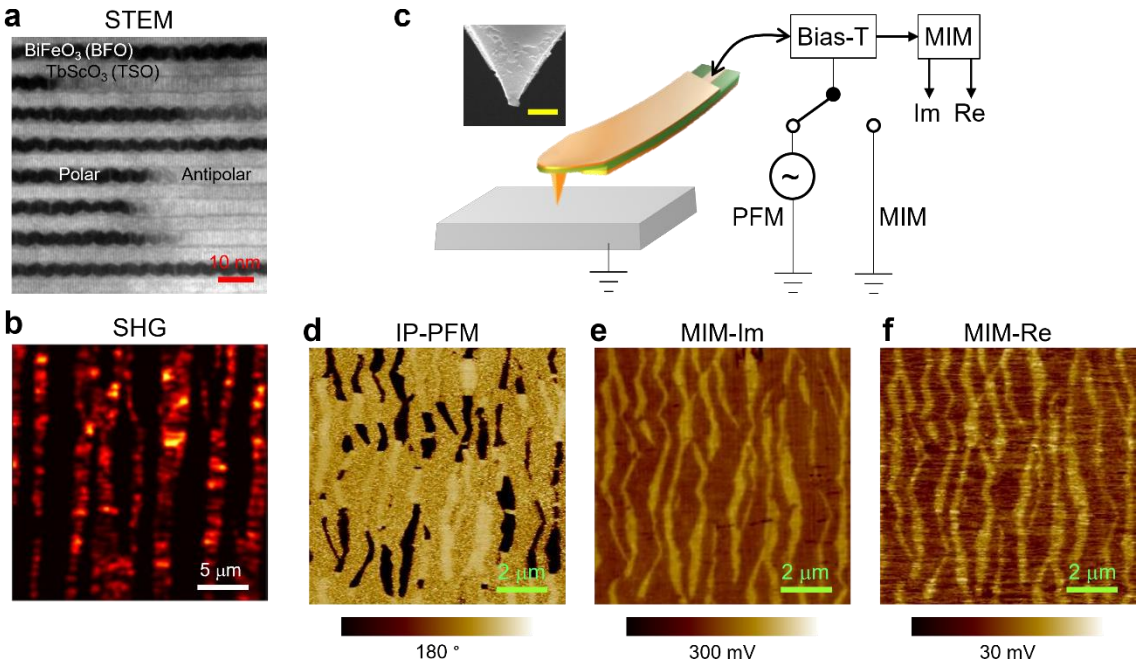

Figure 1. (a) Cross-sectional STEM image of the BFO/TSO superlattice sample, showing the polar and antipolar phases in the BFO layer. (b) SHG map on the same sample. Areas showing high and low SHG intensity contain polar and antipolar BFO, respectively. (c) Schematic of the PFM/MIM setup. The inset shows the SEM image of the tip. (d) In-plane PFM phase image of the BFO/TSO sample, where the contrast is sensitive to polarization along the $[100]_{pc}$ direction. (e) MIM-Im and (f) MIM-Re images taken in the same area as (d).

For quantitative understanding on the MIM results, we used finite-element analysis to model the near-field tip-sample interaction.[1] As shown in Fig. 2a, the measured MIM-Im contrast between the two phases is mostly due to the difference in dielectric constants, as independently verified by DC measurements on in-plane capacitors (not shown). More importantly, the weak but discernible contrast in the MIM-Re channel is indicative of a finite GHz conductivity (σ) in the non-centrosymmetric phase. As shown in Fig. 2b, a direct comparison between the measured signals and the simulated σ-dependent MIM contrast suggests that the polar phase has a conductivity of ~ 1 S/m (i.e. resistivity of ~100 Ω·cm). The fact that this resistivity is approximately 5 orders of magnitude lower than that of bulk BFO indicates that the polar phase displays semiconducting behavior. As a control experiment, the application of an in-plane electric field by lateral electrodes, which removes or introduces the centrosymmetry, can induce a change up to 5 orders of magnitude in the DC resistivity, as seen in Fig. 5c. This work establishes a materials platform for novel cross-functional devices which take advantage of changes in optical, electrical, and ferroic responses.

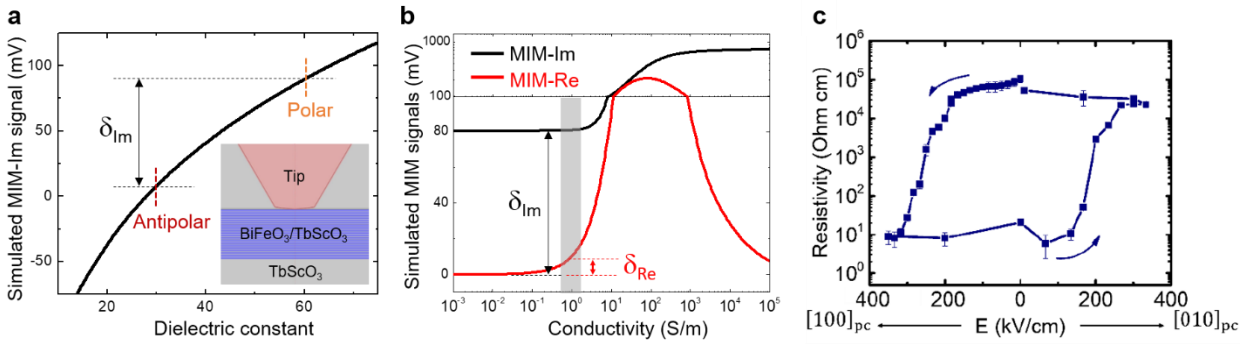

Figure 2. (a) FEA simulated MIM-Im signal as a function of the dielectric constant of the BFO layer. The inset shows the tip-sample configuration for the FEA modeling. (b) Simulated MIM signals as a function of the conductivity of the polar phase. The measured contrasts between the two phases in both channels are denoted in the plot. The shaded region indicates the range of conductivity within the measurement errors. (c) Hysteresis of DC resistivity with electric field across two sets of electrodes along perpendicular directions.

Competing stripe phases in doped $Ca_3Ru_2O_7$

As a prototypical strongly correlated electron system, the bilayer $Ca_3Ru_2O_7$ is an ideal testbed to explore the correlation physics in complex oxides.[4] A major effort of this DOE program is to investigate the nature of mesoscopic phase separation, which is widely observed in 3*d* correlated materials such as manganites but less studied in 4*d* electrons such as ruthenates.

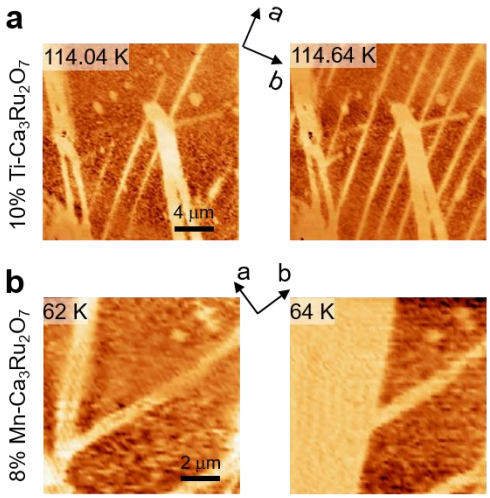

c

Characteristics	10% Ti-doped	8% Mn-doped
Stripe orientation	Parallel to a-axis	45° between a-axis and b-axis
Evolution of coexisting phases	Increasing number of metallic stripes	Widening of metallic stripes
Electronic phase of stripes	A new metallic phase different from high-T phase	Same as high-T metallic phase
Width of transition temperature	3 – 5 K	< 1 K

Figure 3. (a) MIM images of 10% Ti-doped $Ca_3Ru_2O_7$ during the metal-insulator transition, showing the increasing number of metallic stripes. (b) MIM images of 8% Mn-doped $Ca_3Ru_2O_7$ during the transition, showing the widening of metallic stripes. (c) Comparison of stripe phases in the two samples in terms of their orientation, evolution, electronic nature, and temperature range of appearance.

In a previous study,[5] we showed that for $Ca_3(Ru_{0.9}Ti_{0.1})_2O_7$ single crystals, a new stripe-like phase different from the high-T metallic state emerges within a narrow range of the metal-insulator transition, as shown in Fig. 3a. In contrast, our recent data on a $Ca_3(Ru_{0.92}Mn_{0.08})_2O_7$ crystal (Fig. 3b) show that the stripe-like phase in this sample is the same as the high-T metallic

state, which widens in a broad temperature range during the transition. The table in Fig. 3c provides a summary of characteristics of the stripe phases in these two samples, including the orientation, evolution, electronic nature, and temperature range of the occurrence. The striking difference between Ti-doped and Mn-doped materials suggests that the underlying correlation physics could be very different due to the magnetic orders. We are currently working on the theoretical understanding of such distinct behaviors.

Finally, an important ingredient of this DOE program is to establish the MIM capability in a dilution-refrigerator platform. In the past year, we have obtained preliminary results on the quantum anomalous Hall and Axion insulator states in Cr- and V-doped $(Bi,Sb)_2Te_3$ samples at 120 mK. More experiments are underway to further investigate the nanoscale electrical properties of these topological states.

Future Plans

In addition to completing the ruthenate and $(Bi,Sb)_2Te_3$ projects discussed above, we will extend the MIM experiments to several areas. First, our pulsed-laser MIM setup is in the final stage of testing. With this new experimental apparatus, we plan to carry out spatial mapping of light-induced phase transitions in V_2O_3 and Sm-doped $NdNiO_3$ thin films. The samples are already in place and have been characterized by conventional transport experiments. Secondly, we will perform low-T/high-B MIM studies on the correlated states realized in moire superlattices of transition metal dichalcogenides. The accessible temperature and field range in our apparatus is crucial for the realization of certain correlated quantum states. Finally, we have started the low-T MIM imaging of quasi-1D materials such as Ta_2Se_8I in order to resolve the conductive hinge states. We expect to continue with exciting discoveries through the unique MIM measurements.

References

1. Z. Chu, L. Zheng, and K. Lai, "*Microwave Microscopy and Its Applications*", Annual Review of Materials Research **50**, 105 (2020).
2. M. E. Barber, E. Y. Ma and Z.-X. Shen, "*Microwave impedance microscopy and its application to quantum materials*", Nature Reviews Physics **4**, 61 (2022).
3. E. Dagotto, *Nanoscale Phase Separation and Colossal Magnetoresistance*, Springer Berlin Heidelberg, 2003.
4. G. Cao, X. N. Lin, L. Balicas, S. Chikara, J. E. Crow, and P. Schlottmann, "*Orbitally driven behaviour: Mott transition, quantum oscillations and colossal magnetoresistance in bilayered $Ca_3Ru_2O_7$*", New Journal of Physics **6**, 159 (2004).
5. A. Gangshettiwar, Y. Zhu, Z. Jiang, J. Peng, Y. Wang, J. He, J. Zhou, Z. Mao, and K. Lai, "*Emergence of a competing stripe phase near the Mott transition in Ti-doped bilayer calcium ruthenates*", Physical Review B **101**, 201106(R) (2020).

Publications

1. Y. Cho, S. M. Anderson, B. S. Mendoza, S. Okano, N. Arzate, A. I. Shkrebtii, D. Wu, K. Lai, R. Carriles, D. Zahn, and M. C. Downer, "*Second-harmonic and linear spectroscopy of α-In_2Se_3*", Physical Review Materials **6**, 034006 (2022).

2. L. Caretta, Y.-T. Shao, J. Yu, A. B. Mei, B. F. Grosso, C. Dai, P. Behera, D. Lee, M. McCarter, E. Parsonnet, K.P. Harikrishnan, F. Xue, X. Guo, E. Barnard, S. Ganschow, Z. Hong, A. Raja, L. W. Martin, L.-Q. Chen, M. Fiebig, K. Lai, N. A. Spaldin, D. A. Muller, D. G. Schlom, and R. Ramesh, "*Nonvolatile Electric-Field Control of Inversion Symmetry*", arXiv:2201.00289, accepted in Nature Materials 2022.

Tuning quantum paramagnetism and d-wave superconductivity in single layer Fe-chalcogenides by chemical pressure

Lian Li

Department of Physics and Astronomy, West Virginia University, Morgantown, WV

Keywords: Fe-chalcogenides, quantum paramagnetism, MBE, chemical pressure, d-wave superconductivity

Research Scope

The goal of this project is to explore pathways to synthesize high temperature superconductors by better understanding the interplay of magnetism and superconductivity in epitaxial iron chalcogenide FeX (X=Se, Te, S) thin films. By the isovalent substitution of chalcogens, chemical pressure is applied to tune 1) spin-orbit coupling (SOC) and 2) magnetic coupling to facilitate superconducting Cooper pairing and topological transition in these films.

Recent Progress

1. *Tomonaga–Luttinger liquid in the topological edge channel of multilayer FeSe*

The helical edge states, a hallmark of Quantum Spin Hall Insulators, are topologically protected by time-reversal symmetry (TRS) from single-particle backscattering, providing disspassionless transport with quantized conductance of $2e^2/h$. When TRS protection breaks down due to strong electron-electron interactions, the density of states can be suppressed at the Fermi level, leading to a Tomonaga–Luttinger liquid (TLL). The breaking of TRS can also occur when magnetic ordering or fluctuations are present at the edges, thus correlating magnetism with topology, two intriguing subjects but challenging to verify due to the lack of appropriate material systems. To this end,

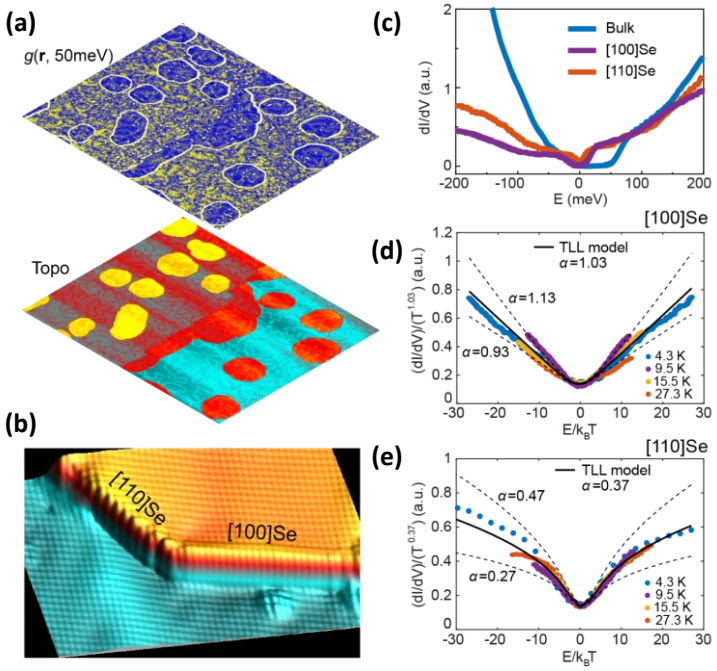

Fig. 1 Interacting topological edge channel in epitaxial FeSe/STO films. (a) STM image of FeSe/STO film. (Set point V=200 mV, I = 0.1 nA), and dI/dV map g(r, 50 meV) taken simultaneously showing robust edge states along all edges. (b) 3D STM image of an FeSe island with the [100]Se and the [$\bar{1}$10]Se step edges. Setpoint: V = 100 mV, I = 1.0 nA. (c) Typical dI/dV spectra taken at edges and the bulk. (d)-(e) Universal scaling behavior of the dI/dV spectra as a function of temperature for both edges.

tetragonal FeSe exhibits nontrivial topology and checkerboard antiferromagnetic (CB-AFM) spin fluctuations as the ground state, where the [100]Se and [110]Se step edges are ferromagnetically (FM) and antiferromagnetically (AFM) arranged, respectively, providing an ideal platform to probe edge-dependent correlation between magnetism and topology.

In this work, we report the 1st edge-dependent TLL behavior in multilayer FeSe films epitaxially grown on $SrTiO_3$ (001) substrates by molecular beam epitaxy (MBE). Using scanning tunneling microscopy/spectroscopy (STM/S), we observe robust edge states at both [100]Se and [110]Se step edges, and further identify that the suppression of density of states near the Fermi level follows a universal scaling with both energy and temperature, providing solid evidences for the TLL behavior. The corresponding Luttinger parameter K is found to be 0.26 and 0.43 for the [100]Se and [110]Se step edges, respectively. The smaller K for the [100]Se edge also indicates strong correlations, attributed to the ferromagnetic ordering of the edge due to the checkerboard AFM fluctuations in the FeSe system. These observations indicate edge-dependent TLL in the 1D helical channels of FeSe films, providing a model system for future studies to realize novel topological excitations such as Z_4 parafermions at the interface arising from coupling of superconductivity and interacting helical edge states. These results have been published in Nano Lett. **21**, 6253 (2021), https://doi.org/10.1021/acs.nanolett.1c02069.

2. Tuning quantum paramagnetism in single layer iron chalcogenides by chemical pressure

In most Fe-based superconductors, symmetry-breaking quantum fluctuations are commonly believed to drive Cooper pairing. In this part of the research, we test this theory in the Fe-chalcogenide FeSe that is likely a quantum paramagnet driven by simultaneous CB and collinear (CL) AFM fluctuations. By the isovalent substitution of S into single layer FeSe epitaxially grown on $SrTiO_3$(001) substrates by MBE, chemical pressure is applied to determine the role of AFM fluctuations on superconductivity.

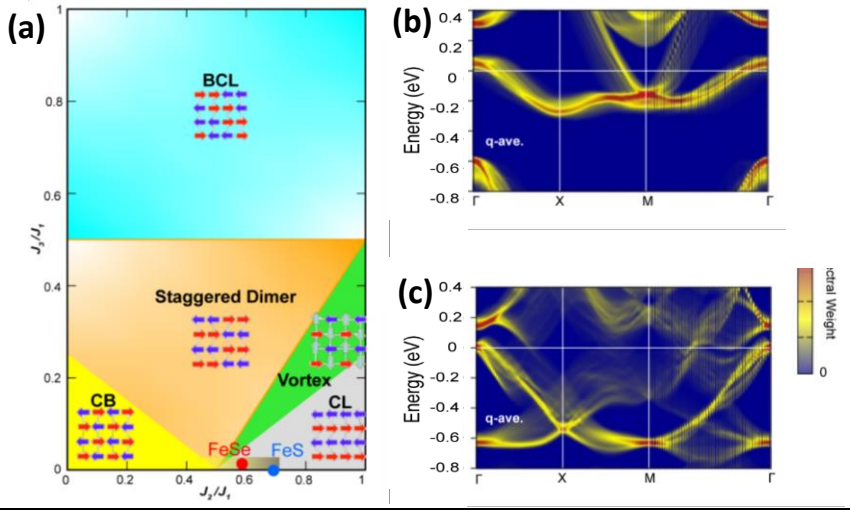

Fig. 2 (a) Mean-field phase diagram for the 2D square collinear Heisenberg (Ising plus the vortex phase) model. The yellow shaded region for $J_2/J_1 > ½$ indicates where quantum fluctuations for S=1 push the boundary for the CB phase, resulting in a disorder paramagnetic phase. The values of J_2/J_1 and J_3/J_1 obtained from fits to the spin-spiral calculations for the unsupported FeS and FeSe monolayers indicated. The q-averaged spectral weight calculated around the (b) CB and (c) CL phases. The Fermi level is set to zero.

First, we have modeled the paramagnetic state of single layer FeSe/S as an incoherent superposition of spin-spiral states calculated within density functional theory (DFT). Fits of the spin-spiral dispersions to spin models yield Heisenberg

parameters J_2/J_1 of 0.55 for FeSe and 0.72 for FeS, placing both in the region of the phase diagram where CB quantum fluctuations lead to a disordered paramagnetic state.

Next, we compare the angle-resolved photoemission spectroscopy (ARPES) results to that modeling the single layer FeSe(S) as an incoherent superposition of spin-spiral states calculated within DFT. Figures 2b and c are electronic spectral weights $A_q(k, \varepsilon)$ of FeS in the ideal CB-AFM, **q** = 0 and CL-AFM, **q** = M configurations, respectively. As is the case for FeSe, the **q** = 0 CB-AFM configurations (Fig. 2b) are in good agreement with the ARPES results (cf. Fig. 3), rather than those around the lowest energy CL-AFM configuration (Fig. 2c). The CB-AFM electronic bands for monolayer FeS, however, depend critically on the height of the S above the Fe plane with the best agreement with the ARPES data for a value around 1.319 Å used in the spin-spiral calculations. For values around the relaxed value of 1.143 Å, there is a large pocket around Γ and two pockets around M, both of which are inconsistent with experiment.

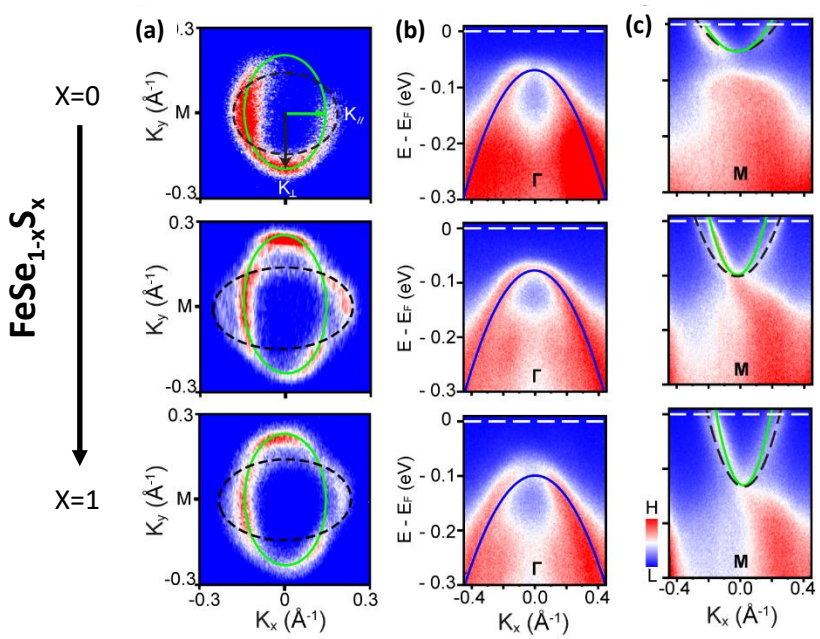

Fig. 3 Evolution of APRES intensity at M and Γ as the function of S concentration. (a) Fermi surface at M point, and (b,c) energy dispersion near Γ and M. The white dashed line marks the Fermi level. The bands in (black and green)/(blue dash) curves are obtained from the peaks extracted from (four)/(two) Lorentzian peaks of the energy dependent momentum distribution curves.

Experimentally, ARPES measurements show that the Fermi surface of $FeSe_{1-x}S_x$ consists of two elliptical electron pockets around M points and no pocket near Γ, in excellent agreement with the calculations. As S is incorporated into films, the two elliptical electron pockets become more anisotropic at the M point, as measured by the magnitude of two perpendicular wave vectors $k_\perp$ and $k_\parallel$, and their ratio. The $k_\perp/k_\parallel$ ratio increases as S increases, reaching a maximum at 80% S, and then decreases to 1.63 in FeS.

The intricate connection between the magnetic configuration and the electronic band structure suggests that magnetic fluctuations inherent in $FeSe_{1-x}S_x$ systems will likely also influence the superconducting properties.

3. *Transition from nodal to nodeless d-wave superconductivity in single layer iron chalcogenides driven by chemical pressure*

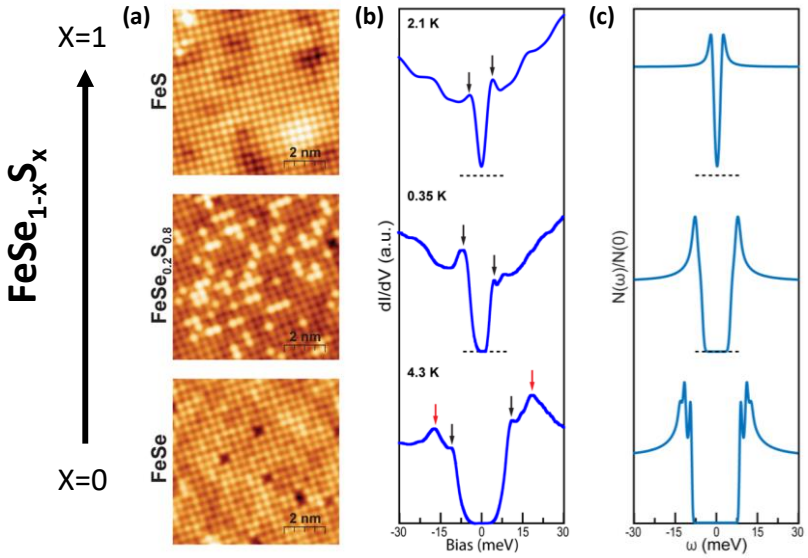

Fig. 4 Evolution of superconducting gap structure as a function of S concentration. (a) STM images of single layer $FeSe_{1-x}S_x$ taken at 4.3 K. (b), dI/dV spectra for the single layer $FeSe_{1-x}S_x$ taken at the temperature indicated. (c), Density of states calculated using the fitting parameters from ARPES and DFT calculations.

To examine this hypothesis, we carry out dI/dV tunneling spectroscopy measurements in single-layer $FeSe_{1-x}S_x$ films. The results reveal a gap structure evolution from U-shaped with two coherence peaks for FeSe to V-shaped with only one coherence peak for FeS and with decreasing gap size (Fig. 3b), which is explained by a d-wave superconducting state for which nodes emerge once the gap size is smaller than the effective SOC. Such a state naturally arises when considering a single four-fold electronic representation at the M-point and coupling these electrons to CB AFM fluctuations. The key physics can be understood as an interplay between the superconducting gap and $v_{so}k_F$ (here k_F is the average Femi wavevector). When $\Delta_0 \gg v_{so}k_F$, the dI/dV spectrum is U-shaped. Once $\Delta_0 \ll v_{so}k_F$, the spectrum becomes V-shaped. Since the SOC is predominantly due to Fe d-electrons, it is not strongly changed by S doping. However, the weakening of the gap with increasing S concentration leads to the evolution from a fully gapped to a nodal spectrum. A manuscript has been submitted for publication.

Future Plans

We will continue the systematic studies already underway to investigate the topological states near topological defects, including edge and screw dislocations, and TLL behavior in edge channels of Fe(S/Te) multilayers. By the isovalent substitution of Te, we will explore utilizing chemical pressure to further drive the magnetic fluctuation spectrum to allow other magnetic correlations, and probe their impact on d-wave superconductivity.

Publications supported by the DOE grant over the previous two years (2021 - 2022)

1. "Tomonaga–Luttinger liquid in the topological edge channel of multilayer FeSe", H. Zhang, Q. Zou, and L. Li, Nano Lett. **21**, 6253 (2021), https://doi.org/10.1021/acs.nanolett.1c02069.

2. “Topological band and superconductivity in UTe_2”, T. Shishidou, H. G. Suh, P. M. R. Brydon, M. Weinert, and D. F. Agterberg, Phys. Rev. B **103**, 104504 (2021), https://doi.org/10.1103/PhysRevB.103.104504.
3. “Nonsymmorphic symmetry and field-driven odd-parity pairing in $CeRh_2As_2$”, D. C. Cavanagh, T. Shishidou, M. Weinert, P. M. R. Brydon, and Daniel F. Agterberg, Phys. Rev. B **105**, L020505 (2022). (Editors' Suggestion) https://doi.org/10.1103/PhysRevB.105.L020505.
4. “Tuning quantum paramagnetism and d-wave superconductivity in single layer iron chalcogenides by chemical pressure”, Q. Zou, B. D. Oli, H. Zhang, T. Shishidou, D. F. Agterberg, M. Weinert, and L. Li, Nat. Phys. (submitted).
5. “Discovery of room-temperature ferromagnetism in one-unit-cell $FeSb/SrTiO_3(001)$ films with a Kagome lattice”, Huimin Zhang, Qinxi Liu, Liangzi Deng, Yanjun Ma, Samira Daneshmandi, Cheng Cen, Chenyu Zhang, Paul M. Voyles, Xue Jiang, Jijun Zhao, Ching-Wu Chu, and Lian Li, Sci. Adv. (submitted).

Cryo-EM imaging battery liquid-solid interfaces

Yuzhang Li (University of California, Los Angeles)

Keywords: Batteries, lithium anode, cryo-EM, liquid-solid interface

Research Scope: Liquid-solid interfaces are foundational in broad areas of science, from surfactant self-assembly for oil recovery to electrochemical processes governing fuel cells and batteries. However, liquids are unstable in the vacuum environments typically needed for high-resolution techniques. Therefore characterizing the local features of this delicate interface is inherently difficult and remains a grand challenge in energy research. This program will develop innovative cryogenic-electron microscopy (cryo-EM) techniques to reveal and understand the liquid-solid interfaces in lithium (Li) metal batteries, which have the highest possible energy density of all battery chemistries. Specifically, we aim to investigate how (1) swelling, (2) reactions, and (3) wetting proceed at the liquid-solid interface and correlate their nanoscale features with overall battery performance. New insights from our program will fill a major unmet need for identifying quantitative descriptors to engineer high-performing Li metal batteries. Together, these findings will enable our future efforts to design new high performance electrolytes that optimize the liquid-solid interfacial structure and chemistry, which would represent a significant breakthrough towards safer and longer-lasting batteries. To achieve these goals, we will develop a facile and simple thin-film vitrification protocol that can preserve the sensitive liquid-solid interface in one step. This will allow us to study and quantify critical properties of the liquid-solid interface that were previously inaccessible to characterization, three of which we highlight in this proposal (see figure below).

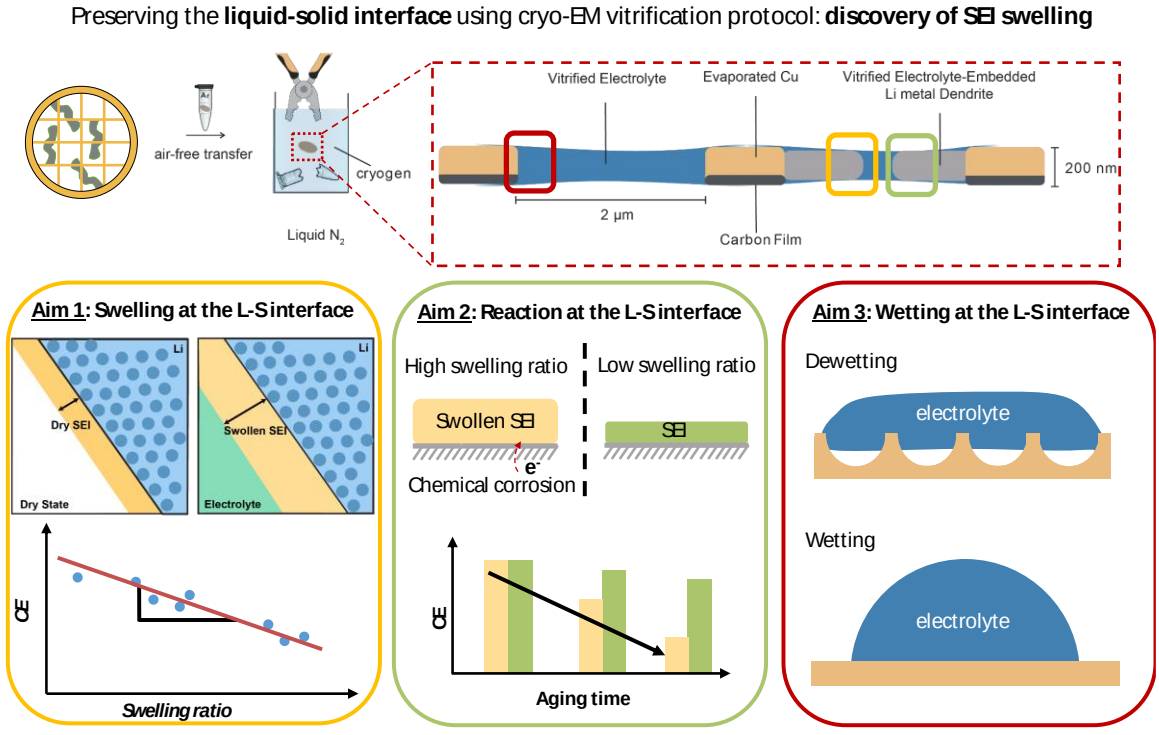

Optically-Stimulated Electron Energy Gain/Loss Nanospectroscopy With Transverse Phase-Structured Electron Beams

PI: David J. Masiello, University of Washington, Department of Chemistry

Keywords: electron energy gain spectroscopy, phase-shaped beams, vortex beams, local chirality, scanning transmission electron microscopy

Research Scope

Alongside the recent proliferation of quantum materials comes the companion need to develop new measurement techniques to characterize these materials on their natural energy, length, and momentum scales. While optical methods offer unparalleled momentum and energy resolution, diffraction limits the achievable spatial resolution to hundreds of nanometers in the visible spectrum. Modern monochromated and aberration-corrected scanning transmission electron microscopes (STEMs), on the other hand, offer nanometer spatial resolution and 5 − 10 meV energy resolution with a broadband spectrum spanning from vibrational to core excitations. *The broad objective of this DOE ESPM project is the theoretical development of a new class of STEM observables that combine the best aspects of optical and electron probes to map the full local density of electromagnetic states of an important class of polaritonic quantum materials formed in photonic crystal lattices with high energy, momentum, space, polarization, and time resolution.*

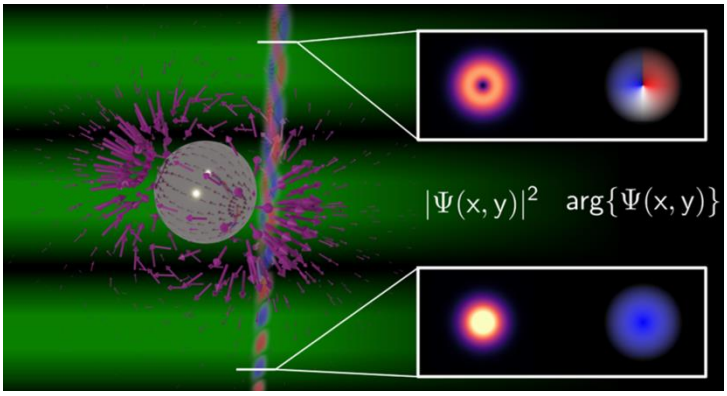

Figure 1. A phase-shaped electron energy gain process in which an incoming free electron with a vortex transverse phase profile transitions to an outgoing Gaussian profile during its interaction with a laser-stimulated plasmonic nanoparticle.

Recent Progress:

Polarization-Resolved Electron Energy Gain Nanospectroscopy With Phase-Structured Electron Beams (Publication 1)

Free-electron-based measurements in scanning transmission electron microscopes (STEMs) reveal valuable information on the broadband spectral responses of nanoscale systems with deeply subdiffraction-limited spatial resolution. By leveraging transitions between phase-structured free electron transverse states combined with continuous-wave laser excitation we have developed a version of electron energy gain (EEG) nanospectroscopy capable of probing the 3D polarization-resolved response field of an excited target with nanoscale spatial resolution (**Fig. 1**).

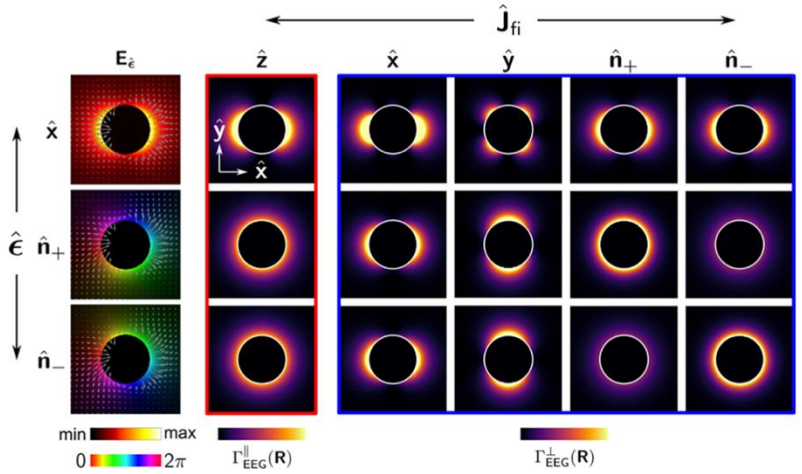

Figure 2. Conventional and transverse EEG spectrum images for a 90 nm diameter Ag sphere in the dipolar limit. Each row considers optical excitation polarization described by unit vector $\hat{\boldsymbol{\epsilon}}$. Column 1 presents the optical response field of the excited target, column 2 (red) contains spectrum images resulting from conventional EEG measurements, and columns 3−6 (blue) present transverse gain spectrum images for four different initial states on the Bloch sphere.

Specifically, we have derived a general expression for the EEG probability spectrum for transitions between arbitrary incoming and outgoing transverse electron states that is valid in the fully retarded regime. By monitoring selected transition channels between incoming and outgoing Hermite-Gauss and Laguerre-Gauss transverse states, specific vector components of the laser-stimulated response field can be selectively probed. Example calculations for several prototypical nanophotonic systems were investigated to highlight the utility of phase-shaped EEG nanospectroscopy for determining mode symmetries, which is currently challenging using other experimental techniques. **Fig. 2** compares conventional (non phase-shaped) EEG spectrum images to those obtained for four specified phase-resolved electron beam transitions.

We also demonstrated that phase-shaped EEG measurements allow the local helicity of the target's laser-stimulated response field to be probed directly at the nanoscale in contrast to the global chirality probed by optical circular dichroism; see **Fig. 3**. This work will enable a flexible form of 3D field tomography where the identity of the source generating the response field produced by the excited target is fully decoupled from the probing electron in EEG processes. Taken together, phase-shaped EEG nanospectroscopy builds on recently developed STEM technology, such as vortex beam generation and state-sorters, and will constitute a powerful addition to the rapidly developing nanoscale field imaging toolset in the near-future.

Future Plans

As this is a new ESPM award (beginning 7/1/22), there is far more work ahead of us than behind. We are currently pursuing the following two theoretical projects in parallel:

- Generalized theory of cw EEL and EEG signals including transverse phase-structuring of the electron probe and, in the case of EEG, transverse phase-structuring of light, both in the fully-retarded limit. In the case of phase-structured EEL, we are currently working on understanding the mathematical connection of this signal to momentum-resolved EELS

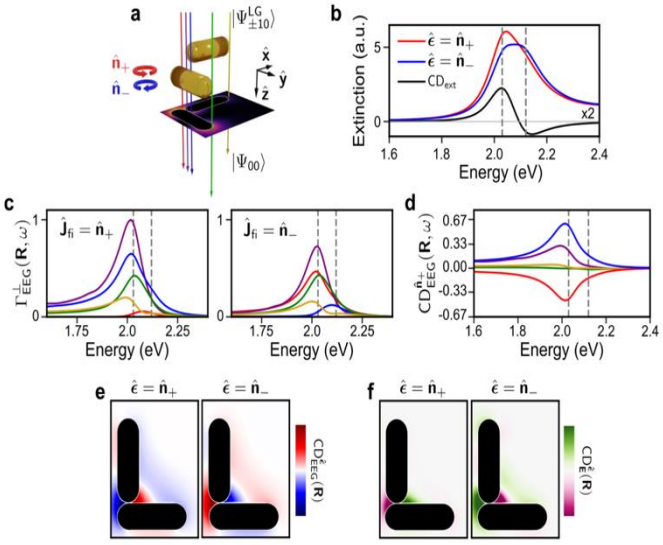

Figure 3. EEG characterization of a chiral plasmonic rod system. (a) Scheme of the Au rod system with colored arrows indicating locations of various electron trajectories. The conventional EEG spectrum image at 2.03 eV is included below the structure for $\boldsymbol{\epsilon} = \mathbf{n}_+$. (b) Optical extinction spectra for incident wave vectors along $\hat{z}$ and $\boldsymbol{\epsilon} = \mathbf{n}_+$ (blue) and $\mathbf{n}_-$ (red). The optical CD spectrum, scaled by a factor of 2 for improved visibility, is shown in black. (c) EEG spectra for $\boldsymbol{\epsilon} = \mathbf{n}_+$ and $\mathbf{J}_{fi} = \mathbf{n}_+$ (left) and $\mathbf{n}_-$ (right). Trace colors correspond to the electron trajectories marked in panel (a). (d) EEG CD spectra for each of the electron trajectories in panel (a). (e) Spatial maps of the EEG CD at 2.03 eV. (f) Spatial variation of the local response field CD at z = 0 nm and 2.03 eV.

and determining their common ability to perform 3D field tomography without need for tilting the sample under the electron beam.

- Extension of cw phase-structured EEL/EEG signals to the time domain to develop generalized pump-probe phase-structured photon-induced near-field electron microscopy (PINEM) signals capable of resolving transient material optical responses with particular emphasis placed on probing the time-dynamics of exciton polaritons formed in photonic crystal lattices with high energy, momentum, space, polarization, and *time* resolution. **Fig. 4** shows unpublished results from our first numerical calculation of the PINEM signal in the absence of phase-structured pump and probe pulses. Next we will add the polarization degree of freedom to the electron probe and use it to map the structure and dynamics of transition metal dichalcogenide exciton polaritons formed in moire and kagome photonic crystal lattices which we have already found to exhibit local chiral behavior.

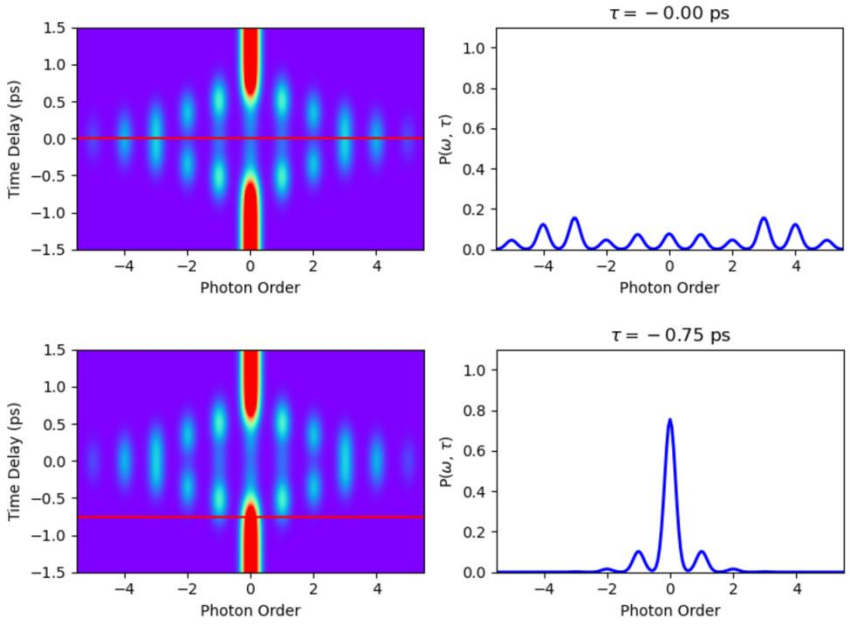

Figure 4. Numerical PINEM spectra as a function of time delay between optical pump and electron probe calculated within our generalized PINEM code, capable of treating target specimens of arbitrary shape, material composition, and cluster patterning. The spectra on the right exhibit the probability for the electron probe to gain/lose multiple quanta of laser photons via interaction with a plasmonic gold nanorod at two different pump/probe delay times.

References

(1) Marc R. Bourgeois, Austin G. Nixon, Matthieu Chalifour, Elliot K. Beutler, and David J. Masiello, *Nano Letters* 22, 7158−7165 (2022)

Probing solid-solid interfaces and phase changes with cryogenic and in situ analytical electron microscopy

PI: Dr. Y. Shirley Meng

University of California San Diego (The University of Chicago)

Keywords: Solid-Solid Interface, Cryogenic Electron Microscopy, In situ observation, Electrochemical Devices, Dynamic Phase Change

Research Scope

The goal of this project is to leverage the advancement of our unique *in-situ* and cryogenic analytical electron microscopy (AEM) techniques and the development of additional high-end capabilities to unequivocally investigate buried solid-solid interfaces and quantitatively elucidate the mechanisms of resistive state changes in solid-state electrochemical materials for neuromorphic applications. The objectives of the proposed research involve (1) characterizing a buried, beam-sensitive solid interface between $LiNi_{0.5}Mn_{1.5}O_4$ (LNMO) and lithium phosphorus oxynitride (LiPON) and elucidating the origin of its electrochemical stability via cryogenic AEM; (2) innovation of LiPON synthesis method to achieve a freestanding form, and its impact on fundamental research and applications of LiPON and LiPON-associated interfaces; (3) elucidating the mechanisms by which electronic state changes occur in amorphous lithium lanthanum titanate (a-LLTO) to build guiding principles for electrochemically activated smart materials via in situ AEM.

Recent Progress

1. <u>Characterization of buried solid-solid interface between high-voltage cathode and thin film solid electrolyte via cryo-AEM:</u>

To meet the requirement of electrification for completing a sustainable energy landscape, high voltage cathode material such as spinel-type $LiNi_{0.5}Mn_{1.5}O_4$ (LNMO) come to play. Outstanding the solid-state battery chemistry, lithium phosphorus oxynitride (LiPON) is one of the promising candidates for coupling with high voltage cathode due to its wide electrochemical stability window up to 5.5 V[1], which have enabled LiPON's exemplary cycling stability against LNMO cathodes and lithium metal anodes.[2,3] Although tremendous research efforts have been invested in the study of the electrode/electrolyte interfaces in LNMO/LiPON/Li system, the cathode electrolyte interface (CEI) was yet poorly understood, partial due to the air- and beam-sensitivity of LiPON that limits the choices of suitable characterization tools. In this work, we leveraged our strength in previously developed cryogenic AEM to investigate the nature of interface stability between LNMO and LiPON after electrochemical cycling. Cryo-TEM images at the LNMO/LiPON interface before and after cycling are summarized in Figure 1. Figure 1A shows the high-resolution TEM (HRTEM) image of pristine LNMO/LiPON interface. No voids or cracks are formed when LiPON is deposited on LNMO. Detailed nanostructure was also inspected and shown in Figure 1B and C. Lattice fringes observed in these images match well with

(111) lattice plane of LNMO[4] and indicates that LNMO maintains its crystal structure after the full cell preparation. The cycled LNMO/LiPON interface shown in Figure 1D displays surprisingly intimate contact between the LNMO and LiPON layers and an absence of voids or cracks after 500 cycles. Figure 1E and F demonstrate that the crystal structure of LNMO is maintained in both the bulk and interface regions. In Figures 1D, a clear contrast difference between crystalline region and amorphous region is highlighted by the yellow curve along the cycled LNMO/LiPON interface. Little CEI is observed in this region. Above observations provide evidence for the long-term structural stability of the LNMO/LiPON interface.

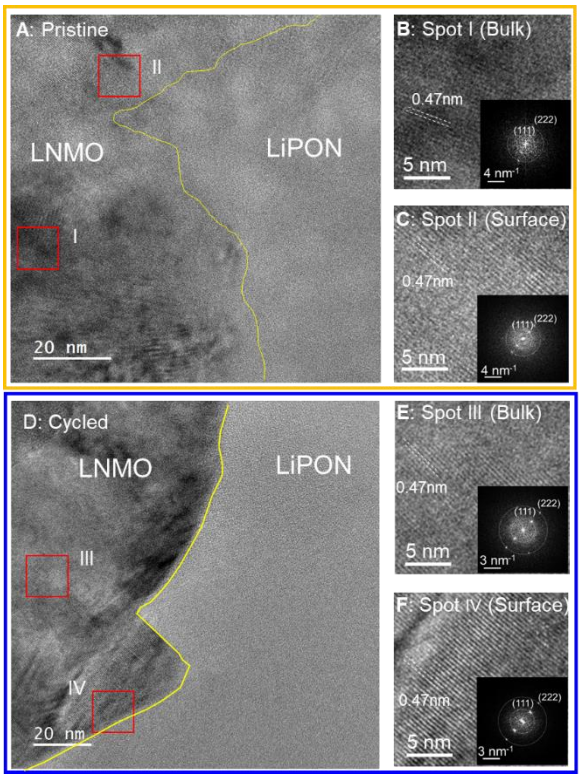

Figure 1. Interfacial nanostructure and morphology at the LNMO/LiPON interface. (A) Bright-field cryo-TEM image of pristine LNMO/LiPON interface and (B) zoomed LNMO images of bulk (inset; FFT image) and (C) surface (inset; FFT image). (D) Bright-field cryo-TEM image of cycled LNMO/LiPON interface and (E) zoomed LNMO images of bulk (inset; FFT image) and (F) surface (inset; FFT image).

Examinations of an LNMO/LiPON interface using cryo-EM coupled with other experimental and computational analysis yields intriguing results that are closely related to the stability of the materials' interface. An ideal cathode electrolyte interface requires the electrolyte to remain either chemically or electrochemically stable against the cathode and mechanically robust. An as-formed CEI ought to be uniform and conformal, consisting of species that are electronical insulating and ionically conductive to prevent further decomposition of electrolyte. Above findings provide guidelines for interface engineering to enable high voltage cathode with more electrolyte systems.

2. *Developing freestanding LiPON film for fundamental research and enabling uniformly dense Li metal deposition:*

Despite the promises to enable Li metal anode and various cathode materials, the presence of rigid substrate and its unique amorphous, air-sensitive characteristics set limitations to comprehensively understand LiPON's intrinsic properties for next-stage advancement and applications. Herein we introduce photoresist to LiPON synthesis procedure and demonstrates a new methodology to synthesize LiPON in a freestanding form that removes the substrate and shows remarkable flexibility (Figure 2A). Subsequent characterizations were carried out to validate that the structure, chemical bonding environments and electrical properties of freestanding LiPON (FS-LiPON) are not affected during the above synthesis procedure. Figure 2B illustrates the electrochemical impedance spectroscopy (EIS) of a typical FS-LiPON, which yields an ionic conductivity of 2.5×10^{-6} S/cm, in line with normal substrate-based LiPON thin film.[1] As an model

example to demonstrate the advantages of applying FS-LiPON for fundamental research aspects, Figure 2C depicts the result of differential scanning calorimetry (DSC) on FS-LiPON for thermal analysis, where a glass transition temperature is identified around 207 °C and crystallization and melting behaviors are captured. Such processes lead to a further understanding of LiPON's intrinsic chemical and thermal properties. FS-LiPON further manifests the ability to electrochemically shuttle lithium ions. Flexible Li-Cu cells were fabricated using the configuration in Figure 2D and shown in Figure 2E and F, where the cell retains the electrochemical activity regardless of mechanical bending. With the presence interfacial stress and an introduction of gold seeding layer in Li-Cu cell, a uniformly dense Li metal deposition with zero external pressure was realized. Figure 2G demonstrates a cross-section morphology of Li-Cu cell after Li plating between Cu and FS-LiPON, where a uniform but full dense metal layer is present. Such practice combining interfacial stress and seeding layer provide valuable insights for ideal Li metal deposition and new perspectives for interface engineering in all-solid-state batteries.

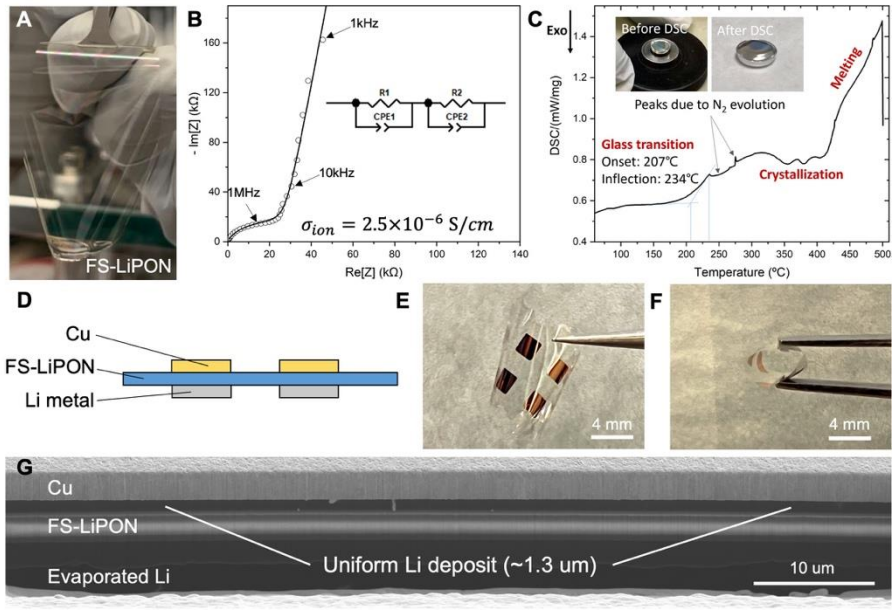

Figure 2. (A) Photo of FS-LiPON film. (B) EIS spectrum and (C) DSC results of FS-LiPON. (D) Li-Cu cell configuration schematic. (E,F) Photos of Li-Cu FS-LiPON cell showing the flexibility. (G) Cross-section image of plated Li-Cu cell with gold seeding layer.

3. *Switching Mechanism Exploration of Amorphous LLTO (a-LLTO) for neuromorphic applications:*

Neuromorphic device aims to mimic human brain and facilitate a revolutionary computing system, which has attracted interests in the field.[5,6] The underlying mechanisms for the resistance change of associated material under an external electric field are proposed to be the formation of conductive filaments inside insulator, resulting in reduced resistance of the whole device.[7] However, a more comprehensive understanding of the resistive switching mechanisms is lacking for emerging smart materials such as amorphous lithium lanthanum titanate (a-LLTO), which calls for novel characterization methods to identify the growth of such nanoscale conductive pathway at various metastable states. In this part of work, we have investigated the resistive switching behaviors of bulk a-LLTO device by both experimental and computational approaches. In order to proceed with nanoscale characterization employing our in situ AEM capabilities, a-LLTO nanodevices were fabricated as shown in Figure 3A and tested in focused ion beam/scanning

electron microscope (FIB/SEM) with low current potentiostat. Figure 3B shows SEM images of the device configuration under biasing test in FIB/SEM. Figure 3C displays relaxed voltage as a function of each current setting, which indicates obvious change in voltage response at around 1 V. the voltage profile of the nanodevice demonstrates remarkably consistent trend with that of the bulk device (Figure 3C inset). Figure 3D depicts a dV/dI plot as a function of voltage, where dV/dI value strikingly drops at around 0.1-1 V and serves as a sign of resistive switching. From the voltage feature and morphology observation, LLTO nanodevice has been successfully fabricated and will be examined under TEM using our in situ AEM setup.

Future Plans

As the current progress has demonstrated the resistive switching on nanodevice, the next step will proceed to utilizing our unique in situ AEM capability to observe oxygen vacancy distribution and visualize the potential filament growth inside LLTO material. By combining scanning transmission electron microscopy/energy dispersive spectroscopy (STEM/EDS) and electron energy loss spectroscopy (EELS), we aim to elucidate the resistive switching mechanisms in overall LLTO systems and obtain guidelines for designing neuromorphic materials with improved switching efficiency and designing associated smart devices for neuromorphic applications.

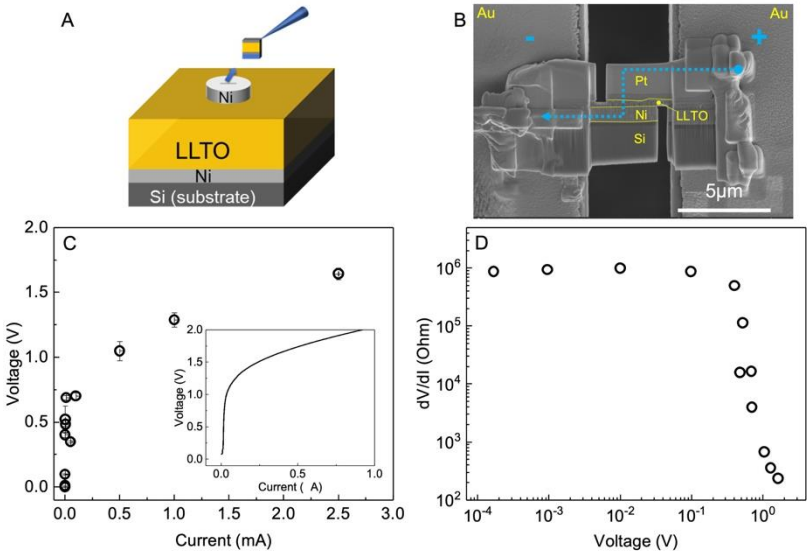

Figure 3. Biasing test of a-LLTO nanodevice in FIB/SEM. (A) Schematic image of lamella lift out from LLTO bulk device. (B) SEM images of LLTO nanodevice as prepared on chip. (C) V vs. I plot of nanodevice obtained from constant current test of the nanodevice and (inset) V vs. I plot obtained from voltage sweep test at 0.04 V/sec of bulk LLTO device. (D) dV/dI vs. V plot, where dV/dI is equivalent to differential resistance of the device.

References

1. Yu, X., Bates, J. B., Jellison, G. E. & Hart, F. X. A Stable Thin-Film Lithium Electrolyte: Lithium Phosphorus Oxynitride. J. Electrochem. Soc. 144, 524 (1997).
2. Li, J., Ma, C., Chi, M., Liang, C. & Dudney, N. J. Solid electrolyte: The key for high-voltage lithium batteries. Adv. Energy Mater. 5, 1–6 (2015).
3. Sawa, A. Resistive switching in transition metal oxides. Mater. Today 11, 28–36 (2008).
4. Li, Y., Wang, Z., Midya, R., Xia, Q. & Joshua Yang, J. Review of memristor devices in neuromorphic computing: Materials sciences and device challenges. J. Phys. D. Appl. Phys. 51, (2018).
5. Dearnaley, G., Morgan, D. V. & Stoneham, A. M. A model for filament growth and switching in amorphous oxide films. *J. Non. Cryst. Solids* **4**, 593–612 (1970).

Publications

1. Shimizu, R., Cheng, D., Weaver, J. L., Zhang, M., Lu, B., Wynn, T. A., Burger, R., Kim, M.-c., Zhu, G., Meng, Y. S., *Unraveling the Stable Cathode Electrolyte Interface in all Solid-State Thin-Film Battery Operating at 5 V*. Adv. Energy Mater. **12**, 2201119 (2022)
2. D. Cheng, B. Lu, G. Raghavendran, M. Zhang and Y. S. Meng, *Leveraging cryogenic electron microscopy for advancing battery design*, Matter, **5**, 26–42 (2022)
3. M. Kim, N. Ahn, D. Cheng, M. Xu, S. Ham, X. Pan, S. J. Kim, Y. Luo, D. P. Fenning, D. H. S. Tan, M. Zhang, G. Zhu, K. Jeong, M. Choi and Y. S. Meng, *Imaging Real-Time Amorphization of Hybrid Perovskite Solar Cells under Electrical Biasing*, ACS Energy Lett. **6**, 3530−3537 (2021)
4. W. Bao, C. Fang, D. Cheng, Y. Zhang, B. Lu, D. H. S. Tan, R. Shimizu, B. Sreenarayanan, S. Bai, W. Li, M. Zhang and Y. S. Meng, *Quantifying lithium loss in amorphous silicon thin-film anodes via titration-gas chromatography*, Cell Reports Physical Science, **2**,100597 (2021)
5. M. Kim, S. Ham, D. Cheng, T. A. Wynn, H. S. Jung and Y. S. Meng, *Advanced Characterization Techniques for Overcoming Challenges of Perovskite Solar Cell Materials*, *Adv. Energy Mater*. 2001753 (2020)
6. D. Cheng, T. A. Wynn, X. Wang, S. Wang, M. Zhang, R. Shimizu, S. Bai, H. Nguyen, C. Fang, M. Kim, W. Li, B. Lu, S. J. Kim and Y. S. Meng, *Unveiling the Stable Nature of the Solid Electrolyte Interphase between Lithium Metal and LiPON via Cryogenic Electron Microscopy*, Joule, **4**, 11, 2484-2500 (2020)
7. M. A. T. Marple, T. A. Wynn, D. Cheng, R. Shimizu, H. E. Mason, and Y. S. Meng, *Local structure of glassy lithium phosphorus oxynitride thin films: a combined experimental and ab initio approach*, Angew. Chem. Int. Ed. **59**, 2–11 (2020)
8. D. Cheng, T. Wynn, B. Lu, B. Han, R. Shimizu, B. Sreenarayanan, M. Marple, Y. Yang, Han. Nguyen, W. Li, G. Zhu, M. Zhang and Y. S. Meng, *Freestanding LiPON: Fundamental Study and Enabling Uniform, Fully Dense Li Metal Deposition Under Zero External Pressure*, Nature Nanotechnology, **Under review** (2022)

Three-Dimensional Structure Determination of Non-Crystalline Materials at the Single-Atom Level

Jianwei (John) Miao

Department of Physics & Astronomy and California NanoSystems Institute, University of California, Los Angeles, CA 90095-1547

Keywords: atomic electron tomography, ptychography, amorphous materials, energy materials, and quantum materials

Research Scope

Over the last century, crystallography has been fundamental to the development of many scientific fields by determining the 3D atomic structure of crystalline samples. However, perfect crystals are rare in nature. Real materials often contain crystal defects and structural disorders. These crystal defects and disorders strongly influence material properties and functionality, but their 3D atomic structures are not accessible to crystallography. Although cryo-electron microscopy has revolutionized the 3D structural determination of macromolecules with identical or similar conformations at atomic resolution, physical science samples usually do not have identical copies and cannot be averaged to achieve atomic resolution. These difficulties have made the objective of solving the 3D atomic structure of crystal defects and non-crystalline systems a major challenge for structural characterization in the physical sciences.

To address this challenge, Miao and collaborators have pioneered atomic electron tomography (AET) to determine the 3D structure of crystal defects and non-crystalline materials at atomic resolution[1-3]. Over the last two years, we have made several major research achievements using AET. We determined the 3D atomic coordinates of amorphous materials and discovered a new type of medium-range order, named the pentagonal bipyramid network. We captured the 3D local atomic positions at the interface of a MoS_2-WSe_2 heterojunction with picometer precision and correlated 3D atomic defects with localized vibrational properties at the epitaxial interface. We also resolved the 3D atomic structure, surface morphology, and chemical composition of Pt-alloy nanocatalysts, and used machine learning to identify the active catalytic sites toward the oxygen reduction reaction from the experimental 3D atomic coordinates. Building on these successes, we will develop ptychographic AET (pAET) as a low-dose method for the determination of the 3D atomic positions and defects in quantum and energy materials. We will use pAET to correlate the 3D atomic structure of the defect centers in ZnO nanomaterials with their optical and quantum spin measurements. We will also apply pAET to determine the 3D atomic structure and defects in $CsPbBr_3$ perovskite nanocrystals. Because atomic-scale phenomena give rise to the uniqueness of these materials, structural characterization at the single-atom level is essential for understanding the fundamental nature of quantum and energy materials.

Recent Progress

Observation of a new type of medium-range order in amorphous materials. For the past 60 years, icosahedral order has been widely considered as the prevalent atomic motif in monatomic liquids and amorphous materials[4]. we have recently advanced atomic AET to determine, for the first time, the 3D atomic structure of monatomic amorphous materials, including a Ta thin film and two Pd nanoparticles[5]. Despite the different synthesis methods, we found that pentagonal bipyramids are the most abundant atomic motifs in these amorphous materials. Instead of forming icosahedral order, the pentagonal bipyramids are closely connected with each other to form networks that extend to medium-range order (Fig. 1). Using molecular dynamics simulations, we found that pentagonal bipyramid networks (PBNs) are also prevalent in the monatomic liquid. During the quench from a liquid to metallic glass state, the PBNs quickly grow in size and form a small fraction of icosahedral order, indicating an important role of the PBNs during the glass transition. This work offers two surprising important insights into monatomic liquids and amorphous materials. First, contrary to the traditional understanding, we observed that PBNs instead of icosahedral order are the main atomic motifs in monatomic liquids and amorphous materials. Second, we found that the 3D atomic structure of the monatomic liquid is similar to that of the experimental amorphous material. This result poses a deep question on why these monatomic amorphous materials and liquids, as two different states of matter, have the similar 3D atomic structure.

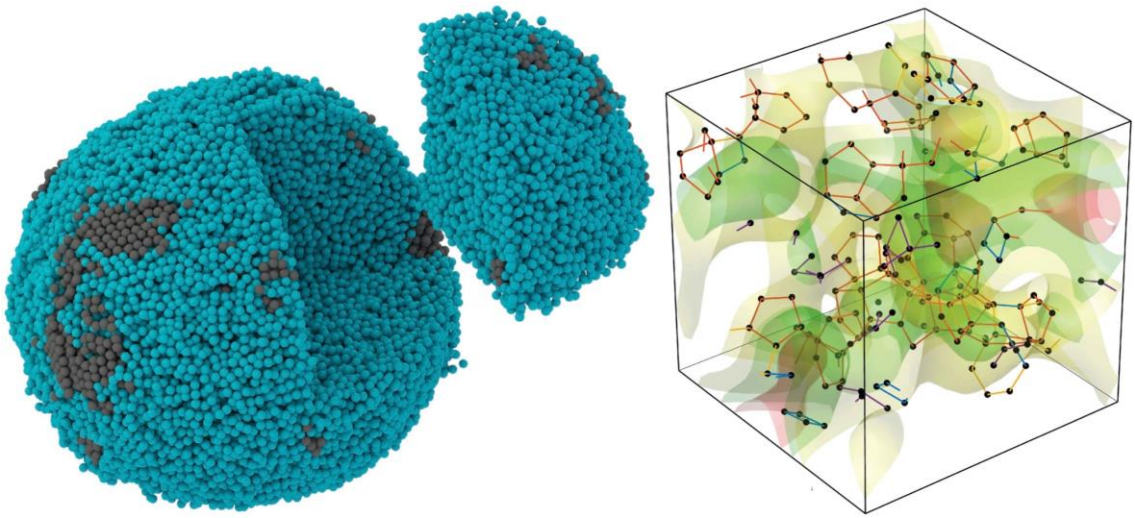

Fig. 1. Experimental 3D atomic image of an amorphous Pd nanoparticle (left), in which pentagonal bipyramids (orange lines) are the most prevalent motif for how atoms pack together (right). The pentagonal bipyramids are closely connected with each other to form a new type of medium-range order.

Atomic-scale identification of the active sites of nanocatalysts. Heterogeneous catalysts play a key role in the chemical and energy industries[6]. To date, most industrial-scale heterogeneous catalytic reactions have relied on nanocatalysts[7,8]. However, despite significant progress from theoretical, experimental and computational studies, identifying the active sites of alloy nanocatalysts remains a major challenge. This limitation is mainly due to an incomplete understanding of the three-dimensional (3D) atomic and chemical arrangement of different constituents and structural reconstructions driven by catalytic reactions. We have recently applied

atomic electron tomography to determine the 3D local atomic structure, surface morphology and chemical composition of 11 Pt alloy nanocatalysts for the electrochemical oxygen reduction reaction (ORR)[9]. We reveal the facet, surface concaveness, structural and chemical order/disorder, coordination number, and bond length with unprecedented 3D detail. The experimental 3D atomic coordinates are used by first-principles trained machine learning to identify the active sites of the nanocatalysts, which are corroborated by electrochemical measurements. A striking feature is the difference of the ORR activity of the surface Pt sites on the nanocatalysts by several orders of magnitude. Furthermore, by analyzing the structure-activity relationship, we formulate an equation named the local environment descriptor to balance the strain and ligand effects and gain quantitative insights into the ORR active sites of the Pt alloy nanocatalysts. The ability to determine the 3D atomic structure and chemical composition of realistic nanoparticles coupled with machine learning could transform our fundamental understanding of the catalytic active sites and provide a guidance for the rational design of optimal nanocatalysts.

Capturing 3D atomic defects and phonon localization at the 2D heterostructure interface. 2D lateral and vertical heterostructures have been actively studied for fundamental interest and practical applications. Although aberration-corrected electron microscopy and scanning probe microscopy have been used to characterize various 2D heterostructures, the 3D local atomic structure and crystal defects at the heterostructure interface have thus far defied any direct experimental determination. We have recently applied scanning AET (sAET) to determine the 3D atomic positions and crystal defects in a MoS_2-WSe_2 heterojunction with picometer precision and capture the localized vibrational properties at the epitaxial interface[10]. We observed various crystal defects, including vacancies, substitutional defects, bond distortion and atomic-scale ripples, and quantitatively characterize the 3D atomic displacements and full strain tensor across the heterointerface. The experimentally measured 3D atomic coordinates, representing a metastable state of the structure, were used as direct input to first principles calculations to reveal new phonon modes localized at the heterointerface, which were corroborated by spatially resolved electron energy-loss spectroscopy. In contrast, the phonon dispersion derived from the minimum energy state of the heterojunction is absent of the local interface phonon modes, indicating the importance of using experimental 3D atomic coordinates as direct input to better predict the properties of heterointerfaces. Although in this study we revealed 3D atomic defects and local interface phonon modes in a MoS_2-WSe_2 heterojunction, the correlative method could be used to probe the physical, material, chemical and electronic properties of a wide range of heterointerfaces at the single-atom level.

Future Plans

Development of ptychographic AET (pAET) for 3D atomic structure determination of low-Z and dose-sensitive materials. Building upon our extensive expertise in AET and coherent diffractive imaging methods such as ptychography, we will develop pAET to determine the 3D atomic positions and crystal defects in dose-sensitive materials. Compared with ADF-based AET, pAET measures all the electrons by a pixelated detector and then uses phase retrieval algorithms to reconstruct both the magnitude and phase of the exit wave of a sample. Our numerical simulations have demonstrated that pAET can significantly reduce the electron dose required to resolve 3D atom positions in materials, especially for light elements[11]. pAET can also incorporate multi-slice phase retrieval algorithms into the ptychographic reconstruction to alleviate the dynamic scattering effect, which will enable us to probe the 3D atomic structure of thick samples.

Furthermore, the spatial resolution of ptychography is not limited by the electron lens, but by the spatial frequency of the diffraction signal. This will allow us to choose accelerating voltages far below the threshold displacement energy to dramatically reduce the knock-on damage in the pAET experiment, which will be crucial for the 3D imaging of surface-sensitive materials. In this project, we will develop robust computational algorithms for pAET by combining multi-slice phase retrieval algorithms with powerful tomographic methods such as REal Space Iterative REconstruction (RESIRE)[12]. We will also take advantage of a state-of-the-art pixel array detector, the 4D camera at the Molecular Foundry, which operates at 87 kHz to produce a data rate of 400 Gigabits/s.

3D atomic structure determination of beam-sensitive quantum and energy materials. We will experimentally demonstrate low-dose pAET for 3D atomic structure determination of radiation-sensitive quantum and energy materials. We will then apply pAET to decipher the 3D structure of defect centers in ZnO nanomaterials. The structural and chemical properties of vacancies and impurities in the lattice will be experimentally determined and correlated with the optical and quantum spin measurements of the ZnO nanomaterials. For energy materials, we will characterize heterogeneous single-atom catalysts (SACs) in 4D (3D space + 1D stimuli). We will use pAET to capture the real structure of SACs under applied bias and/or at elevated temperatures through a combination of state-of-the-art electron microscopes and powerful reconstruction algorithms. We will also apply pAET to determine the 3D atomic structure and crystal defects of $CsPbBr_3$ perovskite nanocrystals, which will be correlated to photoluminescence measurements to provide a fundamental understanding of their structure-property relationships. Finally, we have committed to post all the methods and algorithms developed in this project on a public website and make them freely accessible to a broad user community.

References

1. J. Miao, P. Ercius & S. J. L. Billinge. *Science* **353**, aaf2157 (2016).
2. F. C. Frank, *Proc. R. Soc. Lond*. A **215**, 43–46 (1952).
3. Y. Yuan et al., *Nature Mater*. **21**, 95–102 (2022).
4. Y. Yang et al., arxiv.org/abs/2202.09460 (2022).
5. X. Tian et al., *Sci. Adv*. **7**, eabi6699 (2021).

Publications supported by the DOE BES MSE grant over the last two years

Primarily supported by DOE

1. Y. Yang, J. Zhou, Z. Zhao, G. Sun, C. Ophus, S. Moniri, Y. Yang, Z. Wei, Y., C. Zhu, H. Heinz, J. Ciston, P. Sautet, P. Ercius, Y. Huang, J. Miao, "Atomic-scale identification of the active sites of nanocatalysts", submitted, arxiv.org/abs/2202.09460 (2022).
2. D. J. Chang, C. M. O'Leary, C. Su, D. Jacobs, S. Kahn, A. Zettl, J. Ciston, P. Ercius, J. Miao, "Deep learning coherent diffractive imaging", *Phys. Rev. Lett.*, in revision.
3. Y. Yuan, D.S. Kim, J. Zhou, D.J. Chang, F. Zhu, Y. Nagaoka, Y. Yang, M. Pham, S. J. Osher, O. Chen, P. Ercius, A. K. Schmid, J. Miao, "Three-dimensional atomic packing in amorphous solids with liquid-like structure", *Nature Mater*. **21**, 95–102 (2022).
4. X. Tian, X. Yan, G. Varnavides, Y. Yuan, D. S. Kim, C. J. Ciccarino, P. Anikeeva, M.-Y. Li, L.-J. Li, P. Narang, X. Pan, J. Miao, "Capturing 3D atomic defects and phonon localization at the 2D heterostructure interface", *Sci. Adv*. **7**, eabi6699 (2021).
5. X. Tian, D. S. Kim, S. Yang, C. J. Ciccarino, Y. Gong, Yo. Yang, Ya. Yang, B. Duschatko, Y. Yuan, P. M. Ajayan, J. C. Idrobo, P. Narang, J. Miao, "Correlating the three-dimensional atomic defects and electronic properties of two-dimensional transition metal dichalcogenides", *Nature Mater.* 19, 867-873 (2020).

6. D. J. Chang, D. S. Kim, X. Tian, J. Zhou, P. Ercius, J. Miao, “Ptychographic Atomic Electron Tomography: Towards 3D Imaging of Individual Light Atoms in Materials”, *Phys. Rev. B* **102**, 174101 (2020).

Partially supported by DOE

7. Y. Yao, Q. Dong, A. Brozena, J. Luo, J. Miao, M. Chi, C. Wang, I. G. Kevrekidis, Z. J. Ren, J. Greeley, G. Wang, A. Anapolsky, L. Hu, “High entropy nanoparticles: Synthesis-structure-property relationships and data-driven accelerated discovery”, *Science* **376**, eabn3103 (2022).
8. Y. Yang, J. Zhou, F. Zhu, Y. Yuan, D. Chang, D. S. Kim, M. Pham, A. Rana, X. Tian, Y. Yao, S. Osher, A. K. Schmid, L. Hu, P. Ercius, J. Miao, "Determining the three-dimensional atomic structure of an amorphous solid", *Nature* **592**, 60–64 (2021).
9. P. Ci, X. Tian, J. Kang, A. Salazar, K. Eriguchi, S. Warkander, K. Tang, J. Liu, Y. Chen, S. Tongay, W. Walukiewicz, J. Miao, O. Dubon, J. Wu, "Chemical trends of deep levels in van der Waals semiconductors", *Nat. Commun*. **11**, 5373 (2020).
10. J. Zhou, Y. Yang, P. Ercius, J. Miao, "Atomic electron tomography in three and four dimensions", *MRS Bulletin* **45**, 290 (2020).

Nano-polaritonics of graphene-based twisted heterostructures

PI: Guangxin Ni (guangxin.ni@magnet.fsu.edu), Assistant Professor

Department of Physics, Florida State University, Tallahassee, FL 32306

Keywords: Plasmons, Nano-Optics, 2D Materials, Twistronics, Moiré Potential

Research Scope

The goal of this project is to explore the nanoscale polaritonics and electronics of the new generation of graphene-based twisted heterostructures, which have demonstrated rich physical phenomena, including correlated insulating states, superconductivity and ferromagnetism, to name a few. In particular, we utilize the scanning near-field optical microscopy (SNOM), a novel local optical probe capable of resolving nanoscale collective excitations and optical responses of the buried 2D interfaces. The direct visualization of quasiparticle excitations in low-dimensional quantum materials is scientifically important for the understanding of its complex electronic structures and optical effects at the finite frequencies.

Recent Progress

i. Instrumentations

An essential component of this project is to design, construct and establish advanced SNOM platforms for nano-optical imaging at the nanometer length scales, and at the selected infrared (IR) & terahertz (THz) long-wavelength frequencies. Thanks to the DOE's support, we have two SNOM systems either in the running mode or in the construction stage: this includes 1) an operating SNOM platform that produces nano-optical imaging with 20 nm spatial resolution across a wide range of frequencies in the middle-IR regime. The SNOM platform (Fig. 1b) working at elevated temperatures (260 K – 340 K) is based on an atomic force microscopy (AFM) coupled with external tunable laser sources (Fig. 1a). 2) In the meantime, the low-temperature/high-magnetic field (low-T/high-B) SNOM system which is purely home-designed is currently in the constructing stage (Fig. 1c). Due to COVID and the global supply chain issue, some of the customer designed parts, i.e., components of the ultra-high vacuum (UHV) chambers and the large-bore superconducting magnet have been substantially delayed. While we are still waiting for the remaining delivery, the microscopy housing has been implemented with tested AFM topography images shown in Fig. 1d. In the meantime, we have been continuously working on the further testing, improving and optimizations of the constructed microscopy and its coupling to external optics.

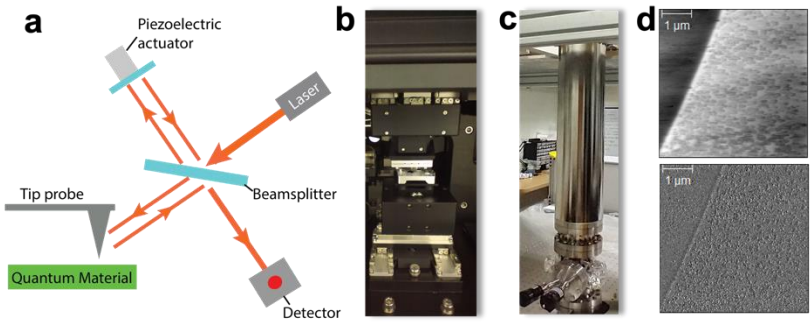

Figure 1. a) Sketch of the optical path for SNOM, which contains an optical interferometer with a reflection path which couples to the tip probe and detectors. b) SNOM system operating at elevated temperatures and c) Home-build SNOM UHV chambers that is in the construction stage. d) Topography and phase images obtained from the home-build SNOM in the PI's laboratory.

ii. Scientific Progress

Moiré superlattices from twisted bilayer graphene (TBG) have emerged as a great platform to study correlated effects with high tunability. By further align TBG with underlying hexagonal (hBN) dielectric, a super moiré pattern forms where the two set of moiré patterns, namely TBG and G/hBN, are nearly commensurate. Such a super moiré system is expected to have important effects and distinguish itself from the magic angle TBG where no ferromagnetism and anomalous Hall effect was found. Currently, the investigation of TBG/hBN super moiré system is mainly carried out through the d.c. charge transport studies with exotic discoveries. On the other hand, explore the collective excitations that originate from the coupling between incident photons and mobile electrons in TBG has remained challenging, mostly because of the mismatch of the crystal lateral dimension with respect to the diffraction-limited phonon beam size.

The PI has carried out nano-IR imaging of super moiré plasmons in the PI's lab by means of the SNOM apparatus (Fig. 2b). Briefly, in this instrument a metallic tip of an AFM was illuminated by IR light, generating a strong enhancement of the local electric field underneath the tip. This antenna-based nano-IR setup circumvents the momentum mismatch between IR light and surface plasmons in TBG, allowing us to launch and detect plasmonic signal and waves at the nanoscale. The PI has been able to show, by direct nano-IR imaging, that these surface plasmon polaritons can be effectively visualized and modulated in a TBG/hBN super moiré heterostructures by varying their relative twist angles. The obtained nano-IR imaging clearly resolved distinct nano-plasmonic contrast within 20 nm spatial resolution at the selected infrared frequencies. The physics behind this tunability originates from the local optical conductivity which is highly sensitive to the twist angles and photon frequencies. Our nano-infrared imaging thus offers a unique way to not only explore the collective excitations in twistronic heterostructures, but also shed light on the local optical responses of the super moiré lattices under study.

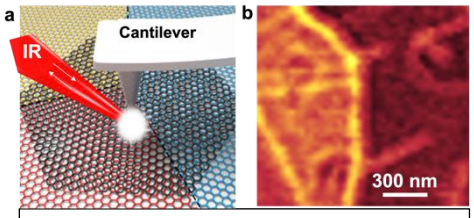

Figure 2. a) Schematic diagram illustrating the nano-IR configuration of the TBG samples under study. b) SNOM nano-imaging of TBG/hBN where different domains of the stacking are associated with the nano-plasmonic responses that obtained in the PI's laboratory.

Future Plans

In the next steps, the PI will continue work on the construction, testing, and optimization of the SNOM microscopy housing, with the goal to achieve improved AFM and SNOM signal-to noise ratio. This includes enhancing the microscope housing's rigidity and stability through optimized microscopy architecture designs and improved machining. The PI will construct and complete the UHV chambers, linear translation stages, and cryostat in consequences. The superconducting magnet will be finally implemented for the testing of low-T/high-B SNOM operations.

In the meantime, the PI will conduct the proposed projects and SNOM measurements in the PI's lab. The PI will work on the existing accomplished results in terms of data analysis and manuscript writing. The super moiré heterostructures will also be studied in the low-T/high-B SNOM, which is expected to be crucial for the study of collective excitations close to the transition temperatures. In the meantime, the PI plans to perform nano-optical studies of similar types of super moiré systems, the dual-gated bilayer graphene etc. Moreover, the PI also plans to conduct optical spectroscopy studies of the proposed layered quantum materials at the cryogenic temperatures and high magnetic fields conditions.

Combining microscopy and quantum calculations to unveil nanostructure properties

Sokrates T. Pantelides

Department of Physics and Astronomy, Vanderbilt University, Nashville, TN 37235

Keywords: STEM/phonon EELS, STM, PFM, DFT calculations, superlattices

Research Scope

Research under this project focuses on highlighting the power of combining microscopy or proximal probes with quantum calculations based on density functional theory (DFT) to unveil the structural, electronic, magnetic, electromechanical, and optical properties of complex materials and nanostructures. Theoretical research is conducted collaboratively with experimentalists. Representative examples are described based on piezoresponse force microscopy (PFM) – layered ferroelectrics – and novel capabilities of scanning transmission electron microscopy (STEM/ EELS) – electrides, vibrational EELS of complex-oxide superlattices and h-BN.

Recent Progress

Ionic control over ferroelectricity in 2D layered van der Waals capacitors

Collaboration with ORNL proximal-probe microscopists Nina Balke, Petro Maksymovych, Sabine Neumayer and other contributors.[1]

$CuInP_2S_6$ (CIPS) is a layered van der Waals (vdW) material that exhibits both ferrolectricity (FE) and ionic conductivity mediated by the same ionic species, namely Cu. An initial theoretical discovery[2] anchored subsequent experimental and theoretical work. Using DFT calculations, we found that spontaneous Cu displacements from the mid-layer centrosymmetry planes lead to a quadruple potential well with two "low-polarization" (LP) and two "high-polarization" (HP) states. In the latter state, the Cu atoms lie in planes just outside the layers. The prediction was validated by PFM, measuring piezoelectric-coefficient (*d*) hysteresis loops (*d*-loops) that were transcribed to polarization loops using DFT results.

In the most recent work, ionic conductivity was activated in a controllable way at room temperature and its impact on FE switching of CIPS microcapacitors was studied. After activation, the measured ionic and polarization-switching currents were distinguished and ionically controlled FE behavior was demonstrated by applying selected DC voltage pulses and then probing FE

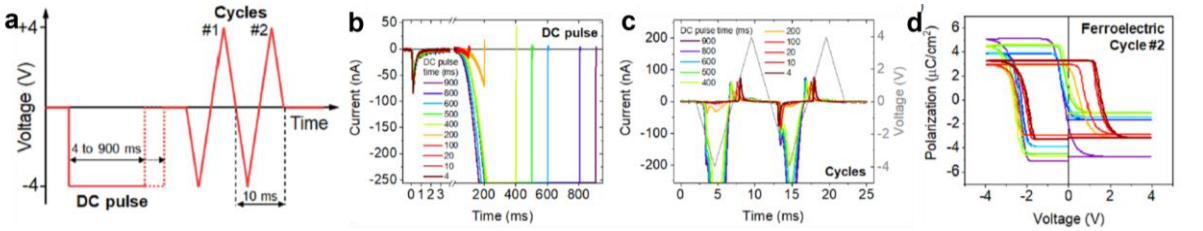

Fig. 1 a. Applied voltage sequence preceding two triangular voltage cycles. **b**. Currents measured during DC pulses of varying duration. The square voltage pulses were turned on at 0 s. **c**. Currents measured during triangular cycles. **d**. Polarization hysteresis loops.

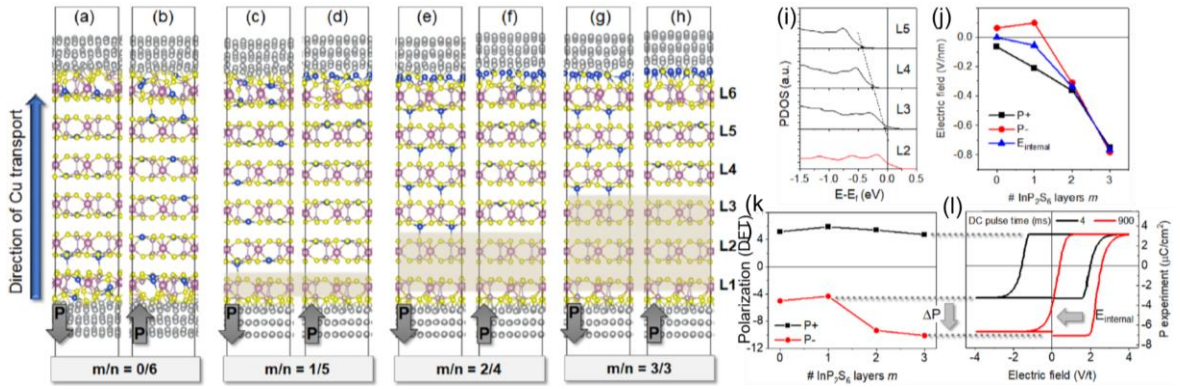

Fig. 2 a-h. Stack of six CIPS layers with Ni-layer top and bottom electrodes at various stages of the upward Cu motion. **i**. The internal electric field is determined from layer-projected densities of states (DOS) in the insulating layers. k. DFT-calculated average up and down polarization in the stacks of panels **a-h**. **d**. Comparison between theory and experimental loops.

switching during fast triangular voltage sweeps (Fig. 1**a**). Specifically, increasing DC pulse duration results in higher ionic currents that alter the timing and intensity of switching peaks (Fig. 1**b**, **c**), which then leads to evolving polarization loops (Fig. 1**d**). DFT calculations of a stack of six CIPS layers attached to Ni electrodes (Fig. 2**a**-**h**) in which Cu atoms are gradually moved upward, as if driven by an applied voltage, depleting one layer at a time from the bottom up and piling up Cu atoms at the top CIPS-Ni interface. The net result is the build-up of an internal electric field (Fig. 2**i**,**j**), caused by the upward movement of Cu ions, which provides an elegant explanation for the observed evolution of polarization loops. The bottom CIPS layers that are depleted of Cu become metallic, maintaining the circuit integrity. Moreover, the internal field favors the HP state over the LP state in the direction of the electric field, which explains an observed 50% increase in polarization. Finally, at much higher voltages, ionic conduction fully suppresses FE hysteretic switching, a process that is reversible, allowing the FE characteristics to be turned on and off.

Direct imaging of anionic electrons in an electride unveils a puzzle resolved by theory

Collaboration with ORNL STEM microscopists Miaofang Chi, Jordan Hachtel, and Juan Carlos Idrobo, using samples grown by Brian Sales' group at ORNL.[3]

Electrides are a relatively new class of compound materials in which the cation and anion sublattices have a net positive effective charge that is compensated by loosely bonded "anionic electrons" that are localized at interstitial sites, forming an effective anion sublattice. Anionic electrons in electrides have been demonstrated to exhibit catalytic activity, high mobility, unconventional magnetism, superconductivity, and nontrivial topological behavior. Electrides have also been demonstrated to be good for storing hydrogen. All these features nurture expectations for real applications.

Differential phase contrast (DPC) in STEM was used for the first time to map electric fields and charge densities with sub-Å spatial resolution in an electride, Y_5Si_3, in which the anionic electrons are localized in interstitial columns, ~4 Å in diameter, surrounded by hexagonal rings of six Y atoms. DPC images of charge densities are shown in Fig. 1(**a**) **A**-**E**, which reveal inhomogeneities. Only a few columns show uniform densities in accord with DFT-calculated

charge densities in pristine Y_5Si_3 [Fig. 1(**a**) **F-G**], while others reveal substantial deviations [1(**a**) **H-I]**, even small positive values in some cases. Experimental artifacts were ruled out as the cause of these inhomogeneities. Such inhomogeneities could not have been detected by the usual macroscopic techniques that are used to characterize anionic electrons, as they are insensitive to such local variations.

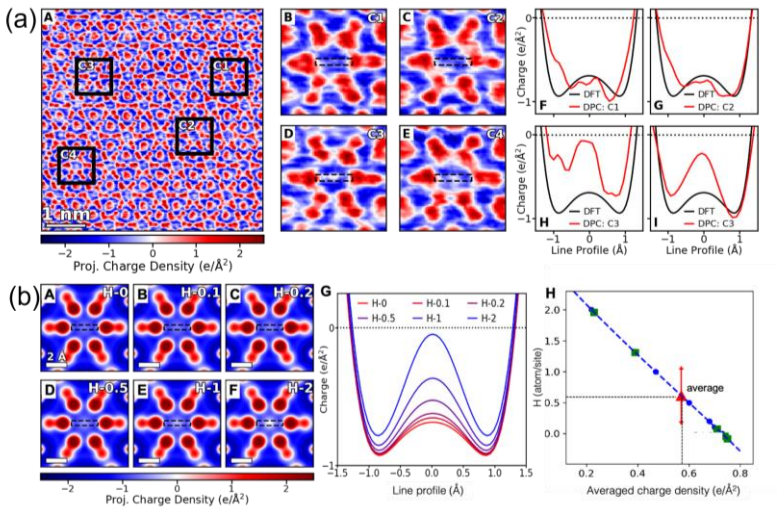

Fig. 1 (**a**) DPC images of anionic-charge columns (**A**) reveal inhomogeneities highlighted in in **B-E.** Red curves in **F-I** are horizontal line scans from **B-E**. The line scans in **F**, **G** are in accord with DFT curves in pristine Y_5Si_3 while **H**, **I** exhibit inhomogeneities. (**b**) **A-F** DFT images for indicated H concentrations. **G** Corresponding line profiles. **H** H concentration vs. average charge density from theory (blue dots) and DPC images.

Extensive prior experience of the PI with H in materials led to the suggestion that the inhomogeneities are caused by traces of H in the interstitial columns. DFT calculations documented this explanation by showing that the calculated charge profile in pristine Y_5Si_3 is in accord with the measured profile of only the few columns featuring roughly identical charge profiles [Fig. 1(**a**)**F**,**G**]. Calculated charge-density profiles in columns with various concentrations of H atoms [Figs. 1(**b**) **A-G**] revealed a linear dependence of the H concentration on the average charge density that coincides with experimental average charge densities [Fig. 1(**b**) **G**]. Supporting evidence for H traces in the samples was subsequently provided by neutron scattering data. The significance of the joint experimental/theoretical discovery is that generally unavoidable H traces may play a role in the measured properties of electrides and should be considered in interpreting data.

Emergent vibrational properties in oxide superlattices (SLs) of different layer thicknesses

Collaboration with Jordan Hachtel (ORNL), Eric Hoglund, Patrick Hopkins, James Howe (University of VA), Joshua Caldwell (Vanderbilt University), Ramamoorty Ramesh (UC Berkeley), and others.[4]

The collaboration carried out the first exploration of emergent vibrational properties in complex-oxide SLs [$(SrTiO_3)_n/(CaTiO_3)_n$, n=2, 4, 6, 27] using monochromated, STEM/EELs with high spatial and energy resolution, observing energy loss to phonons with atomic-scale spatial resolution. Annular dark-field (ADF) and integrated DPC imaging were used to quantify the octahedral tilting. DFT calculations of structures, octahedral tilting, and projected phonon DOS (PPhDOS) provided mutual validation, revealed the vibrational displacement patterns of emergent vibrational modes, and provided insights into the origins of the differing vibrational states in the

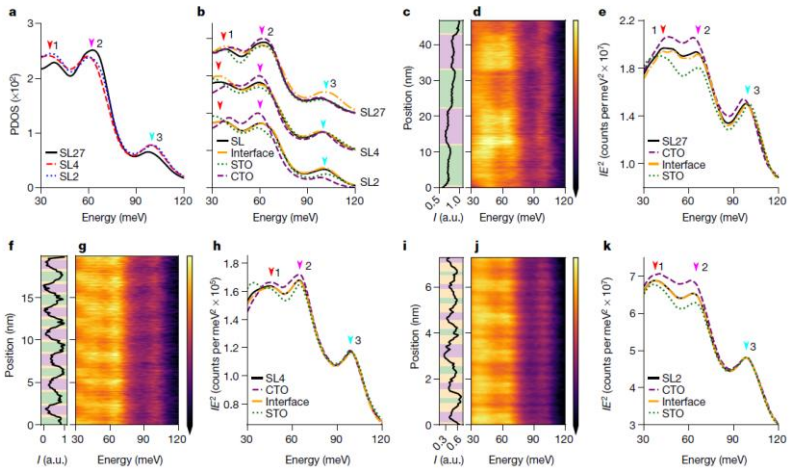

Fig. 3. Localized vibrational response of superlattices indicates the emergent role of the interfacial symmetry. **a**. DFT-calculated PDOS projected on the octahedron O and Ti atoms of the SL27, SL4 and SL2 models. The arrows indicate the dominant phonon peaks. **b**. Cascade of DFT-calculated PDOS projected on STO (green), CTO (purple) and interface (orange) layers and the total DOS (black) for each superlattice model. **c**–**k**, Monochromated STEM-EELS line profile analyses of the three SL structures SL27 (**c**–**e**), SL4 (**f**–**h**) and SL2 (**i**–**k**) with the ADF intensity (I) profile (**c**, **f**, **i**), EELS profile (**d**, **g**, **j**) and integrated spectra from each layer (**e**, **h**, **k**) (as indicated by colored regions in the ADF profile). Energy-loss spectra are normalized by multiplying intensity by the energy squared (IE2). The color bars in **d**, **g**, **j** share the same labels and scales as **e**, **h**, **k**.

superlattice progression (EELS and DFT vibrational response of several superlattices are shown in Fig. 3). Additional experimental data (infrared, second-harmonic generation, etc. provided complementary information.[4]

Key conclusions are: As the period thickness decreases, the system converges toward a single, emergent structure, a "supercrystal of interfaces"; as the layer thickness increases, there are features in the interface spectra that cannot be reproduced by a mixture of the bulk-like neighboring phases in the superlattices. Thermal measurements, reported earlier,[3] found a crossover from incoherent to coherent phonon transport as the SL periodicity decreases. Overall, the results described here demonstrate that experimental and theoretical tools are available to quantify emergent SL vibrational properties, with mutual validation, and ultimately enable the design of structures with custom thermal properties.

Phonon dispersions in h-BN from 300 to 1300 K by monochromated EELS and theory

Collaboration with Tracy Loveyjoy, Niklas Dellby, and Benjamin Plotkin-Swing (Nion Co.) and Juan Carlos Idrobo (U of Wash).[5]

This project, based on momentum-resolved monochromated STEM/EELS carves new ground by measuring vibrational response and phonon dispersions across three Brillouin zones (BZs) at temperatures from 300 to 1300 K in layered h-BN. A narrow zero-loss peak allows observation of all in-plane phonon modes. Temperature-induced anharmonic phonon softening is observable (Fig. 4**a**,**b**). DFT calculations of phonon frequency shifts, including both thermal expansion and many-body phonon-phonon effects, provide mutual validation of both the direction and magnitudes of the observed frequency shifts (Fig. 4**c**,**d**) and the underlying mechanisms are identified.

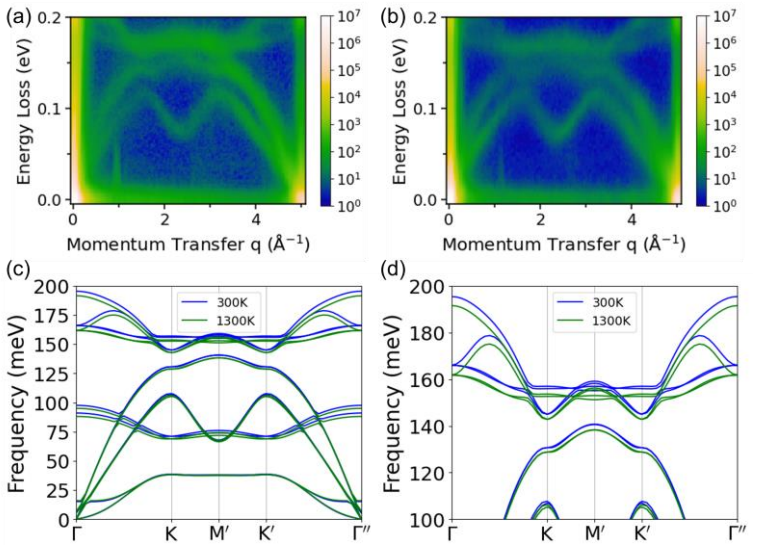

Fig. 4(a),(b) Measured dispersions along the GKM′K′G′ line in reciprocal space at 300 K and 1300 K. (c) DFT-calculated dispersions along the same axis. (d) Zoom-in of (c) in the 100-200 meV frequency range.

As expected, frequency shifts at equivalent momenta within and outside the first BZ are identical, The corresponding EELS intensities differ significantly, however, and also undergo significant evolution with increasing temperature. The currently available theory based on the Stokes cross-section reproduces EEL spectra well only at first-BZ momentum transfers at low temperatures. The major deficiencies of the theory are identified. Umklapp scattering, not included in the theory, is the most likely major contributor to the evolution of the observed intensities deficiency in the case of large momentum transfers.

References

1. S. M. Neumayer et al., "Ionic Control over Ferroelectricity in 2D Layered van der Waals Capacitors" *ACS Appl. Mater. Interf.* **14**, 3018 (2022).
2. J. A. Brehm et al., "Tunable quadruple-well ferroelectricity in a van-der-Waals crystal", *Nature Mater.* **19**, 43 (2020).
3. Q. Zheng et al., "Direct visualization of anionic electrons in an electride reveals inhomogeneities", *Science Adv.* **7**, eabe6819 (2021).
4. E. R. Hoglund et al., "Emergent interface vibrational structure of oxide superlattices", *Nature* 601. 556 (2022).
5. A. O'Hara et al., "High-temperature Phonon Dispersions at the Nanometer Scale by Electron Energy-Loss Spectroscopy", to be published.

Publication list

1. T. Feng, Y. Wang, A. Herklotz, M. F. Chisholm, T. Z. Ward, P. C. Snijders, S. T. Pantelides, "Determination of the rutile transition-metal-oxide surface structures by a universal scanning-tunneling-microscopy contrast reversal", *Physical Review B* **103**, 035409, 11 January 2021.
2. Q. Zheng, T. Feng, J. A. Hachtel, R. Ishikawa, Y.-Q. Cheng, L. Daemen, J. Xing, J.-C. Idrobo, J.-Q. Yan, N. Shibata, Y. Ikuhara, B. C. Sales, S. T. Pantelides, M. Chi, "Direct visualization of anionic electrons in an electride reveals inhomogeneities", *Science Advances* **7**, eabe6819, April 7, 2021.
3. S. Kouser, S. T. Pantelides, "Quantum physical reality of polar-nonpolar oxide heterostructures", *Physical Review B* **104**, 075411, August 6, 2021.
4. S. M. Neumayer, M.-W. Si, J.-K. Li, P.-Y. Liao. L. Tao, A. O'Hara, S. T. Pantelides, P. D. Ye, P. Maksymovych, N. Balke, "Ionic Control over Ferroelectricity in 2D Layered van der Waals Capacitors", *ACS Applied Materials and Interfaces* **14**, 3018-3026, January 19, 2022.
5. E. R. Hoglund, D.-L. Bao, A. O'Hara, S. Makarem, Z. T. Piontkowski, J. R. Matson, A. K. Yadav, R. C. Haislmaier, R. Engel-Herbert, J. F. Ihlefeld, J. Ravichandran, R. Ramesh, J. D. Caldwell, T. E. Beechem, J. A. Tomlo, J. A. Hachtel, S.T. Pantelides, P. E. Hopkins, J. M. Howe, "Emergent interface vibrational structure of oxide superlattices", *Nature* **601**, 556, January 27, 2022.

6. Z. Ali, Z. Wang, A. O'Hara, M. Saghayezhian, D. H. Shin, Y. Zhu, S. T. Pantelides, J.-D. Zhang, "Origin of insulating and nonferromagnetic $SrRuO_3$ monolayers", *Physical Review B* **105**, 054429, February 25, 2022.
7. A. O'Hara, N. Balke, S. T. Pantelides, "Unique features of polarization in ferroelectric ionic conductors", *Advanced Electronic Materials* **8**, 2100810, March 2022.
8. S. M. Neumayer, Z. Zhao, A. O'Hara, M. A. McGuire, M. A. Susner, S. T. Pantelides, P. Maksymovych, N. Balke, "Nanoscale control of polar surface phases in layered van der Waals $CuInP_2S_6$", *ACS Nano* **16**, 2452 (2022).
9. A. O'Hara, L. Tao S. M. Neumayer, P. Maksymovych, N. Balke, and S. T. Pantelides, "Effects of thin metal contacts on few-layer van der Waals ferrielectric $CuInP_2S_6$" *Journal of Applied Physics* **132**, 114102, September 16 2022 (by invitation, published as part of the special topic on 2D Piezoelectrics, Pyroelectrics, and Ferroelectrics; the paper was selected as "Featured article").
10. Z. Ali, M. Saghayezhian, Z. Wang, A. O'Hara, D. H. Shin, W.-B. Ge, Y.-T. Chan, Y. Zhu, W. Wu, S. T. Pantelides, J.-D. Zhang, "Emergent quantum Griffiths-phase-like ferromagnetic ordering and insulator-metal transition in δ-doped ultrathin ruthenates", under review by *NJP Quantum Materials*.

Probing Exotic Vibrational States and Emergent Phonon Phenomena at Interfaces by Vibrational Electron Microscopy

PI: Xiaoqing Pan, Department of Materials Science & Engineering and Department of Physics & Astronomy, University of California, Irvine, CA 92697

Keywords: Electron energy-loss spectroscopy, scanning transmission electron microscopy, phonons, interfaces, ferroelectrics

Research Scope

As the minimization of microelectronic devices continues, nanoscale thermal interface conductance becomes increasingly imperative to dissipate the heat flux generated in the integrated circuit and prolong their lifetime. Phonon transport can be greatly modulated by nanostructures, interfaces, and defects. Interfaces between two differing materials can scatter phonons efficiently. In addition, the conventional phonon theory fails to describe the thermal properties at interfaces. Thus, uncovering nanoscale phonon transport mechanisms at interfaces is crucial in determining thermal conductivity in materials. Recently, local interfacial phonon modes, which are absent in the phonon structure of bulk counterparts, have been theoretically predicted to play a significant role in promoting heat transport across semiconductor interfaces. However, it is challenging to detect such emerging modes due to the lack of effective tools to investigate local vibrational spectra. Recent developments in scanning transmission electron microscopy (STEM) and monochromated electron energy-loss spectroscopy (EELS) have enabled the acquisition of vibrational spectra with few-meV energy resolution and sub-ångström spatial resolution. In this project, we develop novel space- and angle-resolved vibrational EELS methods to probe vibrational modes and map phonon dynamics at nanoscale interfaces. These methods have been used to reveal vibrational states localized at crystalline defects such as stacking faults and semiconductor interfaces, and phonon dynamics in SiGe quantum dots (QDs).

Recent Progress

1. *Direct observation of the local vibrational modes at single planar crystalline defect by space- and angle-resolved vibrational EELS.*

Since the first demonstration of sub-10 meV energy resolution of monochromated electron energy-loss spectroscopy (EELS) in 2014, we have witnessed a rapid growth of this emerging tool for detecting vibrational spectra of diverse materials with unparalleled spatial resolution in STEM. However, applying such a technique to study the phonon behavior at individual defects in a material that has important practical applications is still a “missing piece”. One major issue is the insufficient momentum resolution under traditional experimental settings, which cannot distinguish individual phonon branches in reciprocal space. In this project, we developed a new strategy of space- and angle-resolved vibrational spectroscopy in TEM to overcome this issue by combining both wide and narrow convergence semi-angle conditions.[1] We demonstrated this new approach in SiC and revealed a red-shifted defect phonon mode confined to within a few nanometers of a commonly occurred stacking fault.

To isolate individual phonon branches, we then chose the beam convergent semi-angle α = 3 mrad (0.5 $Å^{-1}$ momentum resolution) and collected vibrational signals at the X point on the edge of Brillouin zone. With a spatial resolution of ~2.6 nm in this condition, the location of the same stacking fault can be identified (Fig. 1a). The line-scan angle-resolved vibrational spectra (Fig. 1b) shows three discernable peaks corresponding to transverse, longitudinal acoustic (TA, LA) phonons and a mixture of longitudinal/transverse optical (LO/TO) phonons, respectively. At the stacking fault, the acoustic phonons undergo an energy red shift of 3.8 meV (Fig. 1c). First-principles calculations were performed to simulate the angle-resolved and site-specific vibrational spectra with consideration of the scattering probability of fast electrons, as shown in Fig. 1d. The peak position of TA mode in the simulated spectrum shows an energy red shift of 3.8 meV from defect-free SiC (46.4 meV) to stacking fault (42.6 meV) regions, which is consistent with the experimental measurement. Meanwhile, the simulation results also reproduced the intensity modulation of both TA and LA modes. We further confirm that these striking features arise from the symmetry breaking and variation of interatomic force constants and are assigned to the local defect phonon modes. Moreover, the propagation width of the local phonon resonance is revealed by the variation of the vibrational signal. The peak width of line profile in Fig. 1c is 7.8 nm and considerably larger than either the structural size of stacking fault (0.25 nm) or the beam broadening (2.6 nm). The increased width can be explained by the penetration of the defect phonon modes into the surrounding SiC region following Schrödinger equation.

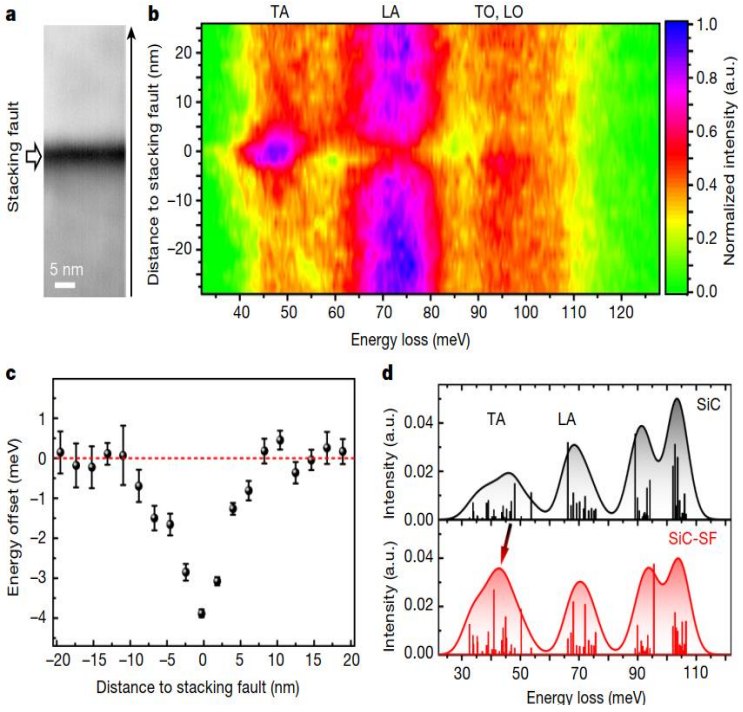

Fig. 1. a, STEM image with α = 3 mrad. **b,** EELS line profile at the X point of the FBZ across the stacking fault in the direction denoted by the black arrow in **a**. **c**, Energy offset of the 40−50 meV peak. **d**, Simulated angle-resolved vibrational spectra of defect-free SiC (top, black) and of SiC with a stacking fault (bottom, red). Bars represent the mode-resolved calculated intensities, which were then broadened with a Gaussian peak with 8 meV FWHM.

2. Local vibrational modes at semiconductor interfaces probed by vibrational EELS.

The Si-Ge interface is a model system for studying thermal boundary conductance (TBC) due to its relatively low lattice mismatch and its wide range of applications in microelectronic devices. Fig. 2a displays an atomic resolution STEM image of a high-quality interface at an epitaxially grown Si–Ge heterojunction. We first employed a space-resolved condition with a large convergence semi-angle (33 mrad) to probe the local vibrational spectra as shown in Fig. 2b. The spectra in Si and Ge regions exhibit prominent longitudinal/transverse optical (LO/TO) phonon peaks at about 60 meV and 34 meV respectively, as well as low-energy acoustic phonon modes (10-30 meV), which all match with the calculated phonon density of states (PDOS) of the

corresponding materials. Interestingly, there are additional signals at 50 meV (12 THz) at the interface, which cannot be ascribed to the bulk phonon modes of either Si or Ge or be fitted by their linear combination (Fig. 2c). The line-scan results reveal that the 50-meV mode is confined to within a few nanometers of the interface. In the simulated eigen-displacement of the interface mode at 51.3 meV in Fig. 2d, only the atoms near the interface undergo obvious atomic motions, which is consistent with the experimentally observed localization of such interfacial phonon mode. Considering the phonon dispersion relation, angle-resolved vibrational spectra with a small convergence semi-angle (3 mrad) also validate the occurrence of the interfacial vibrational modes. First-principles calculations shows that this exotic mode could contribute to 5% of total TBC [2]. This study demonstrates that the solid interfaces exhibit exotic interfacial vibrational states, which are spatially localized near interfaces and boost local heat transport across interfaces.

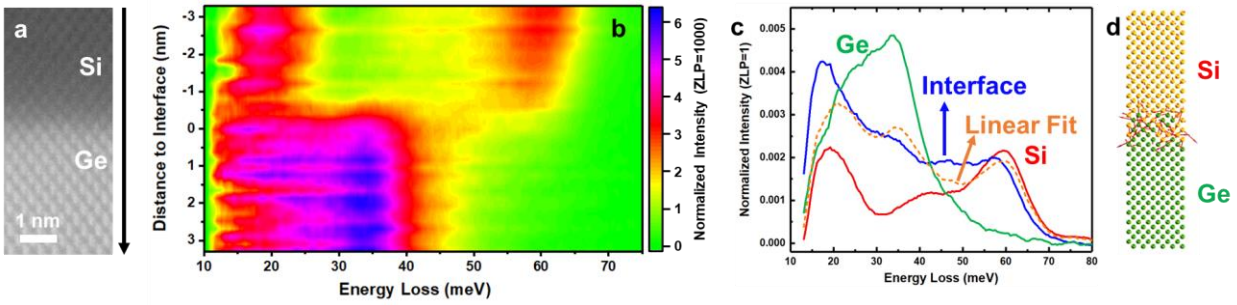

Fig. 2. Vibrational EELS spectra across a Si-Ge interface. **a**, STEM image at the interface. **b**, Line profile of spatially resolved vibrational spectra along the direction denoted by the black arrow in a. Color scale shows the intensity normalized by the zero-loss peak height. **c**, Representative vibrational spectra of Si (red), Ge (green), and interface (blue) regions. The orange dashed curve is a linear regression fitting of interface spectrum from a linear combination of Si and Ge spectra. d, Simulated eigen-displacements of an interfacial mode at 51.3 meV.

3. Nanoscale imaging of phonon dynamics in SiGe quantum dots.

We also studied the phonons in a single SiGe quantum dot (QD) using monochromated EELS in STEM. The growth mechanism of SiGe QDs produces two types of interfaces that form the boundary of the QDs: a gradual interface at the top and an abrupt one at the bottom (Fig. 2A). By tracking the variation of the Si optical mode in and around the QD, we observed the nanoscale modification of the composition-induced red shift, revealing non-equilibrium phonons that only exist near the interface.[3] In order to see the effect of various interfaces on phonon transport, we employ a 3 mrad convergence semi-angle probe to probe phonon modes at specific points in momentum space within the first Brillouin zone (FBZ). As shown in Fig. 3B, the points Δ_+ and Δ_- in the momentum space (Fig. 2B) correspond to backward and forward propagating phonon modes, respectively. By taking the difference of forward and backward propagating modes, net momentum information i.e., direction of propagation, is obtained. Fig. 3C shows the differential

momentum mapping which reveals that there is indeed a strong reflection from the abrupt interface while the gradual interface provides a weaker directionality. The differential mapping of phonon momenta provide direct evidence that the interplay between diffuse and specular reflection largely depends on the detailed atomistic structure and composition. Our work unveils the non-equilibrium phonon dynamics at nanoscale interfaces and can be used to study actual nanodevices and aid in the understanding of heat dissipation near nanoscale hotspots, which is crucial for future high-performance nanoelectronics.

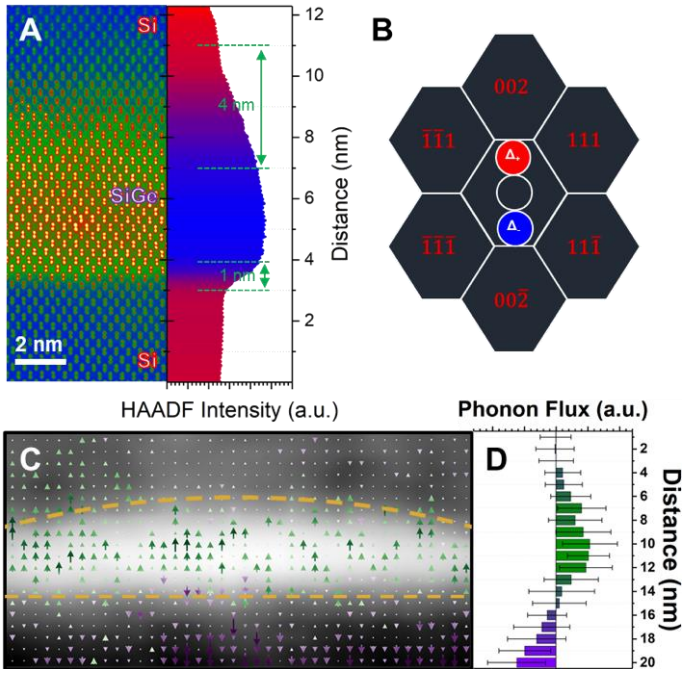

Figure 3: A. HAADF image of a SiGe QD. Line profile to the right shows a gradual, 4-nm-wide interface and an abrupt, 1-nm-wide one, respectively. **B.** Reciprocal space schematic of Si. White borders denote individual Brillion zones. Red and blue regions in the FBZ correspond to the areas where momentum resolved differential data was obtained. The regions indicated by circles are 3 mrad in diameter. **C.** Phonon flux vector map. **D.** Horizontally average line profile of **C**.

Future Plans

Our work described above paves an avenue to studying emerging vibrational modes at various interfaces and provides guidance to manipulating thermal interface transport for microelectronic devices.The methodology developed is generally applicable to diverse ferroelectric oxides systems for investigating the exotic phonon resonance generated at domain walls, antiphase boundaries, and interfaces between ferroelectric materials and oxide supports and could gain more insight into the thermal properties and the electron-phonon coupling in functional oxides devices. Our future work will further develop the method for differentially mapping the phonon momenta and use it, in combination with 4D STEM techniques, to study the properties and phonon dynamics emerged from ferroelectric interfaces, domain walls, and novel polarization states in nanoscale heterostructures.

References

1. X.X. Yan, C.Y. Liu, C. A. Gadre, et al. *Single-defect phonons imaged by electron microscopy*. Nature **589**, 65 (2021).
2. Z. Cheng, R.Y. Li, X.X. Yan, et al. *Experimental observation of localized interfacial phonon modes*. Nature Communications **12**, 6901 (2021).
3. C. A. Gadre, X. X. Yan, Q. C. Song, et al. *Nanoscale imaging of phonon dynamics by electron microscopy*. Nature **606,** 292 (2022).

Publications

1. C. A. Gadre, X. X. Yan, Q. C. Song, et al. *Nanoscale imaging of phonon dynamics by electron microscopy*. Nature **606,** 292 (2022).
2. L. Han, C. Addiego, S. Prokhorenko, et al. *High-density switchable skyrmion-like polar nanodomains integrated on silicon.* Nature **603,** 63 (2022).
3. L. Su, H. X. Huyan, A. Sarkar, et al. *Direct observation of elemental fluctuation and oxygen octahedral distortion-dependent charge distribution in high entropy oxides*. Nature Communications **13,** 2358 (2022).
4. Y. Zhang, E. Parsonnet, A. Fernandez, et al. *Ferroelectricity in a semiconducting all-inorganic halide perovskite*. Science Advances **8**, eabj5881 (2022).
5. X. X. Yan, C. A. Gadre, T. Aoki, and X. Q. Pan. *Probing molecular vibrations by monochromated electron microscopy*. Trends in Chemistry **4**, 76 (2022).
6. X.X. Yan, C.Y. Liu, C. A. Gadre, et al. *Single-defect phonons imaged by electron microscopy*. Nature **589**, 65 (2021).
7. Z. Cheng, R.Y. Li, X.X. Yan, et al. *Experimental observation of localized interfacial phonon modes*. Nature Communications **12**, 6901 (2021).
8. X.Z. Tian, X.X. Yan, G. Varnavides, et al. *Capturing 3D atomic defects and phonon localization at the 2D heterostructure interface*. Science Advances **7**, eabi6699 (2021).
9. H.X. Huyan, C. Addiego, X.X. Yan, et al. *Direct observation of polarization-induced two-dimensional electron/hole gases at ferroelectric-insulator interface*. npj Quantum Materials **6**, 88 (2021).
10. J. W. Lee, K. Eom, T. R. Paudel, et al. In-plane quasi-single-domain BaTiO3 via interfacial symmetry engineering. Nature Communications **12**, 6784 (2021).

Nano-optical imaging, spectroscopy, and control of quantum materials

Markus B. Raschke, Department of Physics, and JILA, University of Colorado, Boulder

Keywords: Optical nano-imaging, ultrafast spectroscopy, quantum dynamics, 2D materials

Research Scope: Optical nano-probe imaging of 2D quantum materials. The combination of scanning probe microscopy with optical spectroscopy provides deep sub-diffraction limited optical nanometer spatial resolution imaging. Over the past decade, these techniques have become increasingly well established and found ever more widespread applications for the study from molecular to quantum materials. Unique to our approach has been the generalization of the nano-localized light-matter interaction, with the implementation of new optical modalities in tip-enhancing and tip-scattering scanning near-field microscopy (*s*-SNOM) with broadband and precision nano-spectroscopy, enhanced nonlinear light-matter interaction, symmetry selectivity, and ultrafast and coherent femtosecond temporal resolution.

The goal of this project is to extend optical nano-imaging into a new regime of imaging competing quantum dynamic processes in 2D layered materials through *nano-optical control of the light matter interaction*. As a new approach, we in part break with the traditional paradigm of minimally invasive nano-optical tip-sample interaction. Instead, through active perturbation via tip nano-cavity Purcell enhancement, ultrashort pulse and strong field excitation, and nano-localized strain modulation, we separate and resolve competing relaxation pathway. Through the combination of enhanced spatio, spectral, and temporally resolved nano-imaging, we study selected problems in 2D materials science in graphene and transition metal dichalcogenides (TMDs) and their heterostructures.

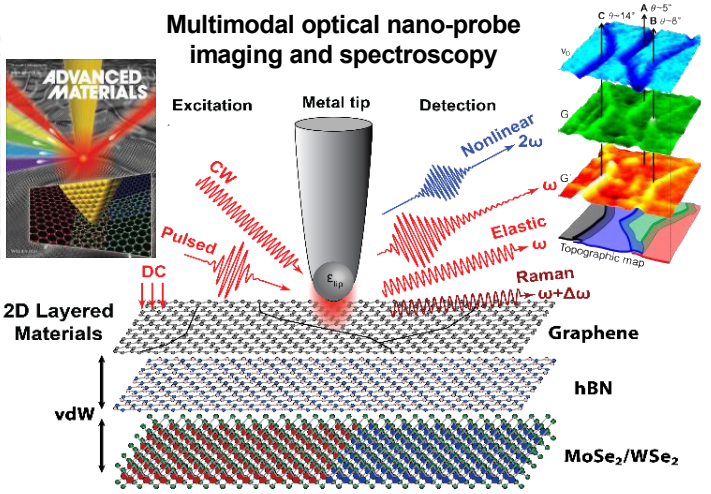

Fig. 1 Multimodal optical nano-probe imaging and spectroscopy: Combining tip-sample distance control with sub-nm precision for Purcell-enhanced tip nano-cavity interaction with different continuous wave and ultrafast nano-spectroscopies, we probe in spatio-spectral and spatio-temporal imaging the coupled coherent, incoherent, and nonlinear quantum dynamics of plasmon and phonon polaritons, excitons, and other intra- and inter-band excitations in 2D layered materials and their heterostructures.

Recent Progress: In different optical modalities we used optical nano-imaging to study dark excitons in TMDs under controlled strain [1], interlayer exciton excitons [8], and investigated the heterogeneity of their ultrafast coherent electron dynamics [2]. Understanding of graphene and its heterostructures has been advanced [3,4,7], electric field control of chirality achieved [6], and ultrafast pump-probe nano-imaging with far from equilibrium excitation established [5].

A) Tip-enhanced dark exciton nano-imaging and local strain control in WSe_2 [1] Dark excitons in transition metal dichalcogenides, with their expected long lifetimes and strong binding

energies provide potential platforms from photonic and optoelectronic applications to quantum information science and Bose-Einstein condensation even at room temperature. These excitons are dipole forbidden and optically dark and to date have primarily been activated through coupling with magnetic fields and plasmonic nanostructures.

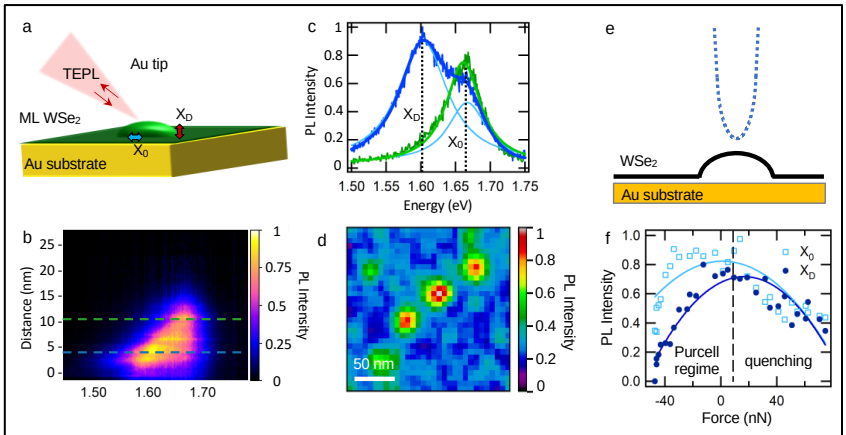

Fig. 2 Nano-opto-mechanical TEPL with cantilever gold tips for calibrated force control (a). Approach curve with few-nm spatial confinement of pico-cavity Purcell enhanced dark exciton emission (b) with corresponding X_0 bright and X_D dark exciton spectra (c). Dark exciton image with heterogeneity associated with nano-bubbles (d). Schematic for correlated exciton pico-cavity force spectroscopy (e). Interplay of Purcell enhancement and quenching quantitatively controlled by bubble deformation (f) [1].

However, their spatial heterogeneity and sensitivity to strain is not yet understood. In this project, we combine tip-enhanced photo-luminescence spectroscopy with atomic force induced strain control to nano-image dark excitons in WSe_2 and their response to local strain. Dark exciton emission is facilitated by out-of-plane pico-cavity Purcell enhancement giving rise to spatially highly localized emission providing for higher spatial resolution compared to bright exciton nano-imaging (**Fig. 2**). Further, tip-antenna induced dark exciton emission is enhanced in areas of higher strain associated with bubbles. In addition, active force control shows dark exciton emission to be more sensitive to strain with both compressive and tensile lattice deformation facilitating emission. This interplay between intrinsic and extrinsic strain in competition with Purcell enhancement provides novel pathways for nano-mechanical exciton emission control for active optoelectronic and nanophotonic devices [1].

B) Ultrafast nano-imaging of electronic coherence of monolayer WSe_2 [2]

Transition metal dichalcogenides (TMDs) have demonstrated a wide range of novel photonic, optoelectronic, and correlated electron phenomena for more than one decade. However, their exciton coherence dynamics with possibly long dephasing times yet sensitive to spatial heterogeneities, have been poorly understood. Here we implement our unique correlative adiabatic plasmonic nanofocused four-wave mixing (FWM) to image the coherent electron dynamics in monolayer WSe_2 (**Fig. 3**). We

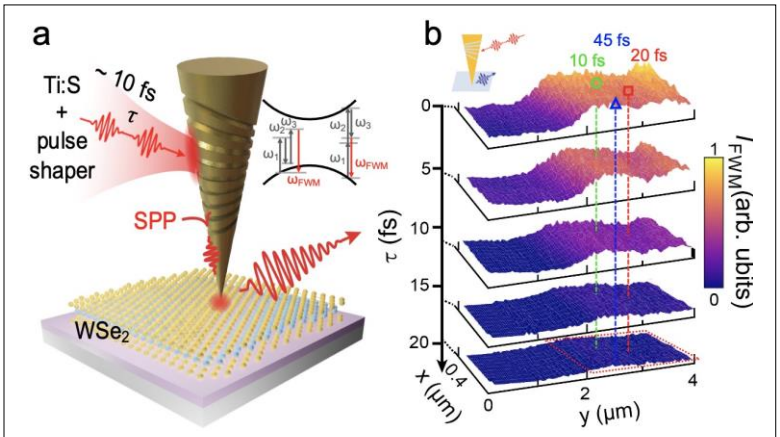

Fig. 3 WSe_2 four-wave mixing (FWM) nano-imaging. (a) Schematic of grating-coupling and femtosecond adiabatic nanofocusing combined with pulse shaping for nano-localized FWM excitation. (b) spatio-temporal FWM images as a function of inter-pulse delay (τ). 3D rendered FWM images with selected spots with decoherence times of 10, 20, and 45 fs. [2].

resolve nanoscale heterogeneity on time scales ranging from less than 10 to greater than 45 fs at room temperature. A counterintuitive spatial anti-correlation between FWM and dephasing time is observed which we interpret as the result of an interplay between the spatial coherence of the nonlinear FWM polarization and scattering on disorder. Our results highlight not only the fundamental challenge associated with a wide range of heterogeneity in TMDs, which limits their photophysical properties, but also new phenomena of coherence and non-locality in nonlinear nano-optics.

C) Anomalous graphene electron-phonon interactions [3,4] In collaboration with Ado Jorio from the Federal University of Minas Gerais (Brazil), we produced a novel graphene device to decouple the optoelectronics properties of 2D materials from their surroundings and eliminate photodoping effects (**Fig. 4(a)**). The device revealed, for the first time, an explicit behavior of the graphene G Raman peak's frequency vs. Fermi energy due to the breakdown of the adiabatic approximation at room temperature [3]; see **Fig. 4(b)**.

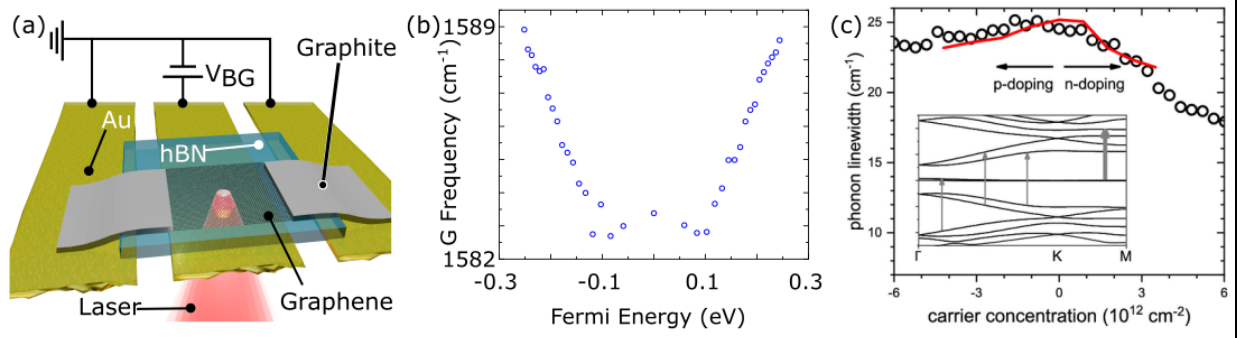

Fig. 4 Gate-dependent Raman experiments. (a) schematic of the optoelectronic device [3]. (b) G frequency as a function of the Fermi energy [3]. (c) phonon linewidth as a function of the carrier concentration for MATBG (inset: band structure) [4]. (b) device used similar to panel (a), while in (c) an ion gate as used.

Using an ionic gate, we probed the electron-phonon properties of magic-angle twisted bilayer graphene (MATBG). **Fig. 4(c)** shows the G phonon linewidth, which depends on the electron-phonon coupling, as a function of the carrier concentration for the MATBG device. Furthermore, it exhibits an unconventionally strong electron-phonon coupling compared to graphitic-related materials and an asymmetry between p and n doping regimes [4]. These results are due to the particular MATBG electronic structure, see the inset in Fig. 4(c), in which matrix elements and available electronic states mediate the coupling between phonons and electrons [4].

D) Ultrafast pump-probe nano-imaging [5] Ultrafast infrared nano-imaging has demonstrated access to ultrafast carrier dynamics on the nanoscale in semiconductor, correlated-electron, or polaritonic materials. However, mostly limited to short-lived transient states, the contrast obtained has remained insufficient to probe long-lived excitations, which arise from many-body interactions induced by strong perturbation among carriers, lattice phonons, or molecular vibrations. Here , we demonstrate ultrafast infrared nano-imaging based on excitation modulation and sideband detection to characterize electron and vibration dynamics with nano- to m icro-second lifetimes. As an exemplary application to quantum materials, in phase-resolved ultrafast nanoimaging of the photoinduced insulator-to-metal transition in vanadium dioxide, a distinct transient nano-domain behavior compared to the thermally induced phase transition has been quantified [5].

Future Plans: In *twisted bilayer graphene and transition metal dichalcogenide (TMD) homo-bilayers*, we will image electron-phonon coupling, interlayer coupling, and exciton localization by variable temperature. With the newly developed approach of *pico-cavity clock nano-imaging*, we will resolve competing intra-, localized, and inter-layer exciton radiative and nonradiative dynamics, including the demonstration of near-field momentum induced indirect band-gap excitations and emission, extending the range of nano-photonic applications of TMDs. In *ultrafast coherent nano-imaging*, we resolve in four-wave mixing the homogeneous electron dynamics in graphene and TMDs, including their nano-localized and nonlinear control. Further, with the first realization of fully *spatio-temporal-spectral pump-probe nano-imaging*, we will image the coupled electron and lattice dynamics, including interfacial thermalization dynamics from the fs to ns scale.

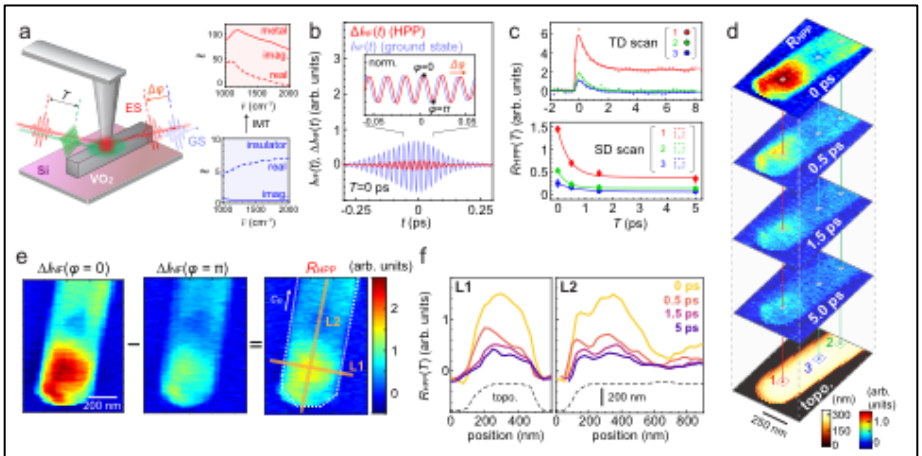

Fig. 4 Phase-controlled ultrafast nanoimaging of insulator-to-metal transition in a VO_2 nanobeam. a) Schematic of NIR pump (1.2 eV, ~2 mJ/cm2) infrared-probe (0.2 eV) ultrafast nanoimaging of VO_2 (left) probing the complex dielectric functions of the insulator and metallic states (right). d) Ultrafast HPP nanoimaging of the VO_2 nanobeam with the AFM topography.

Publications (supported by BES, past 2 years)

[1] K. Hasz, Z. Hu, K.-D. Park, and M.B.Raschke, *Tip-enhanced dark exciton nano-imaging and local strain control of WSe_2* (submitted).

[2] W. Luo, B.G. Whetten, V. Kravtsov, A. Singh, Y. Yang, D. Huang, X. Cheng, T. Jiang, A. Belyanin, M.B. Raschke, *Ultrafast nano-imaging of spatial heterogeneity in electronic coherence in monolayer WSe_2* (submitted).

[3] A. C. Gadelha, R. Nadas, T. C. Barbosa, K. Watanabe, T. Taniguchi, L. C. Campos, M. B Raschke and A. Jorio; *Observation of well-defined Kohn-anomaly in high-quality graphene devices at room temperature*, 2D Mater. **9**, 045028 (2022)

[4] A. C. Gadelha, V. Nguyen, E. G. S. Neto, F. Santana, M. B. Raschke, M. Lamparski, V. Meunier, J. C. Charlier, and A. Jorio, *Electron-phonon coupling in magic-angle twisted-bilayer graphene devices from gate-dependent Raman spectroscopy and atomistic modeling*, Nano Lett. **22**, 6069 (2022).

[5] J. Nishida, S.C. Johnson, P.T.S. Chang, D.M. Wharton, S.A. Dönges, O. Khatib, and M.B. Raschke, *Ultrafast infrared nano-imaging of cooperative carrier and vibrational dynamics*, Nature Commun. **13**, 1083 (2022).

[6] P. Behera, M.A. May, … (18 additional co-authors) … M.B. Raschke, and R. Ramesh, *Electric-field control of chirality*, Science Advances **8**, eabj8030 (2022).

[7] F. Menges, H. Yang, S. Berweger, A. Roy, T. Jiang, and M. B. Raschke, *Substrate-enhanced photothermal nano-imaging of surface polaritons in monolayer graphene*, APL Photonics **6**, 041301 (2021).

[8] M. A. May, T. Jiang, C. Du, K.-D. Park, X. Xu, A. Belyanin, and M. B. Raschke, *Nanocavity clock spectroscopy: resolving competing exciton dynamics in $WSe_2/MoSe_2$ heterobilayers*, Nano Lett. **21**, 522 (2020).

Exploring Energy Conversion and Non-Equilibrium Carrier Distributions at the Nanoscale via Novel Scanning Probe Approaches

Pramod Reddy, Departments of Mechanical Engineering and Materials Science and Engineering, Univ. of Michigan, MI, USA

Edgar Meyhofer, Department of Mechanical Engineering, Univ. of Michigan, MI, USA

Keywords: Scanning Thermal Microscopy, Band Edge Thermometry, Carrier Distributions, Thermoelectrics, Single Molecule Junctions

Research Scope

This project aims to develop novel scanning probe microscopy and thermometry tools and employ them to answer a number of crucial questions. Specifically, we have recently made important advances in scanning thermal microscopy and have demonstrated how temperature fields can be probed quantitatively with nanometer spatial resolution and millikelvin temperature resolution. Recently we have also developed a novel, photonic approach to measure temperature changes with nanokelvin resolution at room temperature and are currently working towards integrating this approach into scanning thermal probes to dramatically enhance their temperature resolution. Using novel scanning thermal probes we have recently probed thermal radiation in nanoscale gaps between metallic surfaces between and demonstrated how heat transfer rates exceeding the blackbody limit can be achieved. Further, we have also explored the temperature-dependence of nanoscale thermal radiation and established that the temperature-dependence deviates significantly from that expected from the far-field Stefan-Boltzmann law. Moreover, we have also explored heat dissipation in tunnel diodes and established how carefully engineered devices can feature internal cooling. Finally, we have explored how charge transport in molecular junctions can be controlled via quantum interference effects and how molecular junctions can be employed to obtain information regarding non-equilibrium charge carrier distributions.

Recent Progress

Quantitative Measurement of Temperature Fields with Nanometer Spatial Resolution and Millikelvin Temperature Resolution (A. Reihani et al., ACS Nano (2021):

The ability to probe temperature fields with nanoscale resolution is critical to understand not only the novel thermal transport phenomena that arise at the nanoscale, but also energy dissipation in nanoscale electronic and photonic devices. In recent years, significant progress has been made by us and others to quantitatively map temperature fields at the nanoscale. In fact, our past work (K. Kim *et al.*, ACS Nano (2012)) has shown how quantitative measurements can be made on smooth surfaces and spatially homogenous materials with nanometer resolution. However, practical devices usually feature topographical variations and spatially varying material composition, which results in spatially varying tip-sample thermal contacts that make it extremely challenging to obtain artifact-free quantitative thermal images. In this work, we developed an

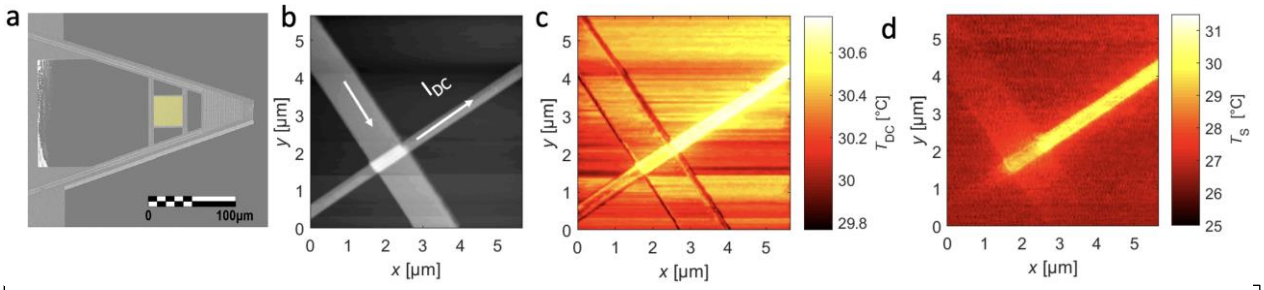

Fig. 1: Quantitative scanning thermal microscopy a) Scanning thermal probe (SThM) with embedded heaters and thermometers, b) Topographical image obtained using SThM probe, c) Scanning thermal image without correction for variations in topography and thermal contact resistance and d) Artifact free image after corrections. Adapted from A. Reihani *et al*., ACS Nano (2021).

approach that overcame the challenge of probing the temperature fields of unmodulated devices to achieve quantitative thermal imaging of surfaces with topographical variations with excellent thermal (~50 mK) and spatial (~7 nm) resolutions. We accomplished this advance by developing and custom-nanofabricating novel scanning probes with integrated heaters and temperature sensors that enable accurate quantification of the tip-sample contact resistance and correction of the directly recorded temperature fields. Finally, to demonstrate the potential of our approach, we directly imaged the thermal fields associated with nanofabricated self-heated metallic lines with nanoscale resolution.

Room Temperature Nanokelvin-Resolution Thermometry with a Photonic Microscale Sensor (*A. Reihani et al., Nature Photonics (2022)*):

High resolution thermometry is critical for a range of applications in scanning thermal microscopy, bio-calorimetry, bolometry, thermal imaging, and the development of ultrastable laser sources. Recent work has aimed to accomplish ultra-high resolution (i.e. nanokelvin resolution) thermometry using whispering gallery mode resonators (e.g. W. Weng *et al*., Phys. Rev. Lett. 112, 160801 (2014)) and other optical resonators with a large mode-volume. However, since such devices feature dimensions that are on the several millimeters to meter scale, they are ill-suited for microscale applications, especially for integration into scanning thermal probes. In this work we overcame the challenging goal of creating a microscale (~200 micrometer diameter) nanokelvin-resolution, non-contact photonic thermometer by creating a Fabry-Pérot resonator from GaAs, which enables extremely high resolution (60 nK/√Hz) thermometry due to the sharp resonance at the Urbach edge of GaAs and a temperature dependent bandgap. This thermometer outperforms currently available room temperature thermometers in the critical size or resolution range by a factor of 10.

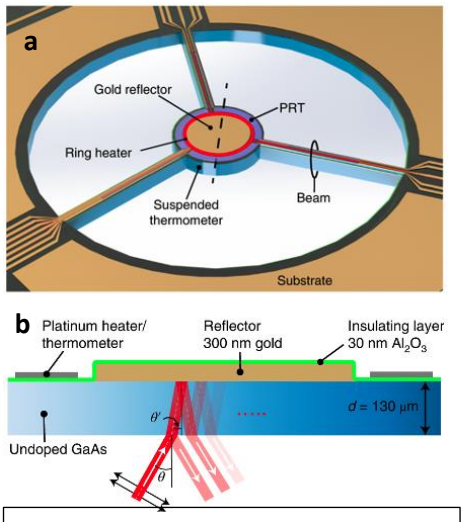

Fig. 2: Schematic of band thermometer a) GaAs based band edge thermometer with embedded heaters. b) Cross sectional view of the band edge thermometer. Adapted from A. Reihani *et al*., Nature Photonics (2022).

Probing Energy Transport via Photons in Nanoscale Gaps (*L. R. Garcia et al., Phys. Rev. Lett. (2022):*

R. Mittapally et al., In Review; S. Yan et al., To be Submitted): Groundbreaking theoretical work pertinent to radiative heat transfer in nanoscale gaps (i.e., in the near-field) was first reported by Polder and Van Hove (Polder and Van Hove, Phys. Rev. B (1971)), when they quantitatively predicted, using the theory of fluctuational electrodynamics (FED), the heat transfer rates between planar metallic surfaces. From this work two seminal conclusions were drawn that suggested (1) that, upon decreasing the gap-size from microns to ~100 nm, heat transfer rates would increase exponentially with reduced gap size by several orders of magnitude — even exceeding the far-field Blackbody limit — due to contributions from evanescent modes and (2) that for gap-sizes below 100 nm the heat flux increases rather slowly with decreasing gaps (i.e. saturates) due to the presence of a characteristic cut-off wave vector. Despite the central importance of these theoretical predictions for the overall understanding of near-field radiative heat transfer, no consistent, replicated experimental evidence has been established, rather a number of contradictory measurements have been reported, some going as far as seriously challenging the validity of the theory of fluctuational electrodynamics. In this work, using novel scanning thermal probes, we performed first measurements of nanoscale heat transfer down to gap sizes of 25 nm between planar metallic surfaces and conclusively show that heat transfer rates increase rapidly with decreasing gap-sizes as well as feature saturation of heat fluxes below gaps of 100 nm. Further, we show that our results are in excellent quantitative agreement with the theory of fluctuational electrodynamics employed by Polder and Van Hove.

In another related work, which is currently in review, we explored the following questions regarding nanoscale radiative heat transfer (RHT): 1) What are the theoretical limits to nanoscale radiative heat transfer rates, and 2) Can the theoretically predicted limits be experimentally confirmed and how close, in magnitude, can real devices match the predictions for a given class of materials? Specifically, we first established a theoretical framework that allows us to explore the limits to near-field RHT for phonon polaritonic materials. By optimizing for maximum RHT over the space of practical polaritonic materials, we showed that properly chosen materials can increase the RHT approximately 5-fold compared to SiO_2 (the material which up to now had the highest reported RHT rate) at a given gap size. Next, we experimentally probed near-field RHT in three carefully selected material systems—doped Si, Al_2O_3 and MgF_2 that closely approximate the theoretically predicted optimal properties—using specifically designed and meticulously micro-fabricated devices. Our experiments reveal that the polariton resonance in MgF_2 matches quite well with the predicted, optimal material response and thus results in a record, 2.5-fold enhanced RHT as compared to SiO_2. Taken together, the results presented in this work disprove the generally accepted idea that materials with resonances corresponding to the frequencies near the peak spectral power density of the classical "Wien's Displacement Law" maximize RHT. Instead, we obtained strong support for the proposed concept of a "Near-field Wien's Law", where the near-field RHT rate is maximized in materials that support strong polaritonic resonances that are red-shifted from the classical Wien's frequency as per the predictions of our Near-Field Wien's Law.

Finally, in a recent unpublished work we explored the temperature-dependence of nanoscale radiative heat transfer (NRHT). Past studies, at room temperature, have shown that NRHT rates between polar dielectric materials can exceed the blackbody limit by several orders of magnitude. However, the temperature-dependence of such NRHT between polar dielectrics

remains unknown. In this work, we explored NFRHT from 300 K to 77 K in nanoscale gaps between polar dielectric surfaces and found that surface phonon polaritons of polar dielectrics strongly influence NRHT, even at low temperatures. More importantly, we find that the temperature-dependence of NRHT is dramatically different from that of far-field thermal radiation.

Probing Hot Carriers in Plasmonic Thin Films (*H. Reddy et al., Science (2020)*:

Plasmonic nanostructures are of great current interest due to their potential for controlling and tailoring light-matter interactions at unprecedented length scales. More recently they have drawn significant attention due to their potential for generating hot carriers that can be exploited for use in a number of important applications, including novel energy conversion approaches, catalysis, photo-detection and photo-thermal therapy. However, experimental elucidation of steady-state hot carrier energy distributions, which is key for systematically advancing and evaluating competing theoretical frameworks as well as for rationally engineering the aforementioned technologies, has not been possible to date. In recent work, we developed a novel scanning probe-based method that overcame this challenge and showed first direct measurements of hot carrier distributions under steady-state conditions.

In our approach, we combined single molecule charge transport measurements with nanoplasmonics making possible quantitative measurement of hot carrier distributions generated from the excited surface plasmon polaritons. The central idea of this technique is to create single molecular junctions (SMJs) by trapping single molecules between the gold surfaces of the tip of a scanning probe and an excited plasmonic nanostructure. With appropriately selected molecules, the SMJs feature sharp resonances in their transmission characteristics and serve as tunable, voltage-controlled and energy-dependent filters—which in turn are used to directly quantify the hot carrier distributions from charge transport measurements through the junctions. From our measurements we provide the first direct experimental evidence that hot carrier generation is significantly enhanced in nanostructures due to “Landau damping” that arises from surface scattering in tightly confined nanostructures.

Probing the Effect of Quantum Interference Effects on Thermoelectric Properties (*S. Yan et al., To be Submitted*):

Recently, we reported first experimental evidence that quantum interferences can be used to enhance the thermoelectric properties of molecular junctions. Specifically, we performed both single-molecule and ensemble measurements of the electrical conductance and thermopower on molecular junctions using novel scanning probe tools. Our experiments showed that *meta*-OPE3 junctions, which are expected to exhibit destructive interference effects, yield a higher thermopower (a factor of two larger) compared to *para*-OPE3 junctions, which do not feature quantum interferences. These results show that quantum interference effects can indeed be employed to enhance the thermoelectric properties of molecular junctions at room temperature.

Building upon this work, we systematically explored the role of substituents on thermoelectric properties of molecular junctions. Specifically, we synthesized and studied charge transport and thermoelectricity in *meta*-OPE3 derivatives with an electron-withdrawing substituent, and an electron-donating substituent at two different positions of central phenylene ring. Our studies revealed how such substitution can lead to the control of the electrical conductance and thermopower, indicating that the substituents can be used to tune the effect of quantum interferences on the charge and energy transport properties of MJs.

Future Plans

In the future we plan to dramatically advance scanning thermal microscopy techniques to enable measurements of quantum systems to understand energy flow and dissipation. Using these tools we will explore the roles of individual scatterers on energy dissipation in quantum materials as well as quantum oscillations in temperature fields. Further, we will explore the influence of phonon quantum interferences on thermal transport in molecular systems and the control of heat dissipation in functional electronic devices. Finally, we will take develop new approaches to systematically quantify quantum friction—a topic that is of intense theoretical debate but with very little experimental data to date.

Publications

1. S. Yan, et al., "Effect of Destructive Quantum Interference on the Electrical Conductance and Thermopower of Molecular Junctions Containing Centrally Substituted meta-OPE3 Derivatives" (to be submitted)
2. S. Yan, Y. Luan, S. H. Fan, P. Reddy, E. Meyhofer, "Surface phonon polariton-mediated near field radiative heat transfer at cryogenic temperatures" (to be submitted)
3. A. Majumder, D. Thompson, P. Reddy, and E. Meyhofer, "Quantifying the Spatial Distribution of Radiative Heat Transfer in Sub-Wavelength Planar Nanostructures" (Submitted to *ACS Photonics*)
4. R. Mittapally, J. W. Lim, L. Zhang, O. D. Miller, P. Reddy, and E. Meyhofer, "Identifying the Limits to Near-Field Heat Transfer Enhancements in Polaritonic Materials" (In Review *Science Advances*)
5. L. R. García, D. Thompson, R. Mittapally, N. Agraït, E. Meyhofer, and P. Reddy, "Enhancement and saturation of near-field radiative heat transfer in nanogaps between metallic surfaces" Physical Review Letters **129**, 145901 (2022)
6. A. Reihani, E. Meyhofer and P. Reddy, "Nanokelvin-resolution thermometry with a photonic microscale sensor at room temperature" Nature Photonics **16**, 422 (2022)
7. A. Reihani, Y. Luan, S. Yan, J. W. Lim, E. Meyhofer and P. Reddy, "Quantitative mapping of unmodulated temperature fields with nanometer resolution" ACS Nano **16**, 939 (2021)
8. A. Reihani, S. Yan, Y. Luan, R. Mittapally, E. Meyhofer and P. Reddy, "Quantifying the temperature of heated microdevices using scanning thermal probes" Applied Physics Letters **118**, 163102 (2021)
9. H. Reddy, K. Wang, Z. Kudyshev, L. Zhu, S. Yan, A. Vezzoli, S. J Higgins, V. Gavini, A. Boltasseva, P. Reddy, V. M. Shalaev and E. Meyhofer, *Determining plasmonic hot-carrier energy distributions via single-molecule transport measurements*, Science **369**, 423-426 (2020)
10. D. Thompson, L. Zhu, E. Meyhofer and P. Reddy, *Nanoscale radiative thermal switching via multi-body effects*, Nature Nanotechnology **15 (2)**, 99-104 (2020)

Nonthermal control of excited quantum materials

Chong-Yu Ruan, Michigan State University

Keywords: ultrafast electron diffraction, ultrafast electron microscopy, hidden states, quantum materials, coherent controls

Research Scope

This project involves fundamental sciences centered on strongly correlations developed in one or two-dimensional potential, leading to novel phases that have fueled many technical interests. The research methods are time, spatial and momentum resolved ultrafast electron probes designed to elucidate the transient states and associated processes during the phase transformation. The project will leverage on the high-brightness electron beam technology for high-throughput to critically address two research areas. The first one is on the still largely unresolved processes leading to hidden broken-symmetry states in many charge-density waves (CDW) and strongly correlated electron systems. This research will detail the subtle collective lattice fluctuations, the short-range ordering, and emergent states through momentum and time-resolved diffusive scattering and coherent diffraction. The second will address the universal nature of the nonequilibrium steady state, which represent a new class of metastable state involving universal scaling in their dynamics manifested in space and time. It is in this regime the highly controllable material properties may emerge. The research will focus on elucidating the particular dynamics near the nonthermal transition point. The knowledge developed from this research program will have significant ramifications in understanding the control mechanism responsible for insulator-metal switching and other emergent properties associated with these strongly correlated and cooperative systems.

Recent Progress

New table-top RF-enabled femtosecond coherent diffraction and imaging capabilities were employed to capture the transient evolution of long-range-ordered quantum systems driven far from equilibrium. One prototypical example is the discovery of the hidden state driven by the laser quench in the rare-earth tritelluride (RTe_3) system. The RTe_3 compound is one of the most systematically studied CDW systems to undergo continuous phase transition. This system consists of square Te planes, alternating with weakly coupled RTe slabs. Despite the fundamental C4 symmetry in the 2D Te sheet to host CDW formation along two symmetric axes (a and c), bearing on a weak coupling between the two nonequivalent square Te nets, the dominant ground state is the singular stripe c-phase (ordering along the c-axis). This broken C4 symmetry state is a prototypical example of common spontaneous symmetry breaking (SSB) under an equilibrium process, which dictates that, upon ordering along the c-axis which removes a significant amount of the potential a-CDW spectral weight, subsequent formation of a-CDW will be suppressed.

Recent discoveries of light-induced formation of a new checkerboard order in RTe_3, encompassing both c- and a-phase clearly break this paradigm. In particular, the two light rare-earth RTe_3 family members of $LaTe_3$[1] and $CeTe_3$ (our work)[2] exhibiting the novel bi-directional

phase in fact do not have the corresponding checkerboard phase anywhere in the equilibrium phase diagram. The discoveries of light-induced checkerboard states are thus surprising and have spurred extensive discussions on understanding SSB phenomena in the nonequilibrium regime. Given that the a-CDW does not exist in the system prior to applying a fs near-infrared pulse, this is a rare scenario where the suppressed field of a new broken-symmetry phase can be created from scratch over a relatively short timescale, leading ways to nonthermal control of collective behavior in quantum materials.

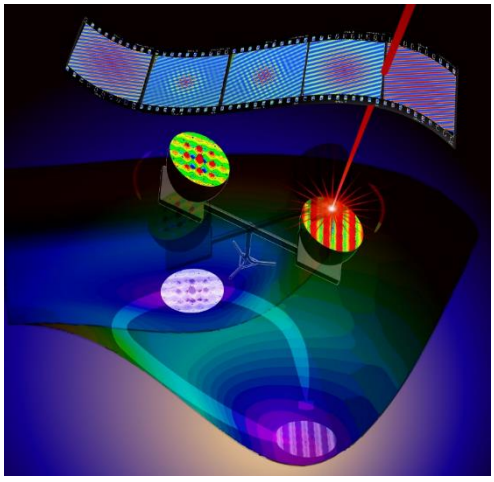

A short laser pulse spontaneously modifies the patterns of the charge ordering in a quantum material to engineer new properties. The process is captured by the coherent femtosecond electron scattering technique.

To understand the surprising experimental findings, our recent effort focused on establishing an effective theoretical framework based on extending the time-dependent Landau Ginzburg (TD-LG) theory into the nonequilibrium regime driven by ultrafast laser interaction quench. In this theory, the local order parameters are defined based on the competing broken-symmetry fields to capture the nonequilibrium system evolution into novel symmetry-breaking phases. Central to this is the integration of the scattering theory for the long-range-ordered state and the associated fluctuation waves into the field theory, leading to simple sum rules to understand the interconversion between the long-range states and field fluctuations central for depicting the critical phenomena in the nonequilibrium stage. Important to the joint theory-experiment investigations are the high-fidelity measurements of total structure factor detailing the dynamics of the static and the diffuse elements, made possible by the coherent electron scattering invigorated with the RF-optics – which is employed to effectively tailor the high-density probe pulse into suitable phase-space structures for high momentum and high temporal resolution operations. We demonstrate that the dynamical mean-field model can in fact successfully predict the emergences of nonthermal critical points and surprising hidden phases identified in our experimental systems with minimal tuning of the model[3].

A key feature of the new development of an RF-enabled ultrafast electron microscope (UEM) is unleashing the multi-modality afforded by the elaborate electron optical system in the traditional static TEM into the femtosecond domain (≈100 fs) while maintaining a high throughput [4]. The ultrafast multi-messenger approach thus offers new opportunities for studying the nonequilibrium physics via modality control over tight and controlled information context; here one selectively retrieves information from both coherently and incoherently (and inelastically) scattered electrons through a combination of traditional and new RF-optics in the TEM column. With the new tools, we tackle a different type of light-induced hidden phase involving competitions but not in the same vein as the RTe_3 system. The systems (TaS_2, $TaSe_2$) belong to a broad class of layered transition metal dichalcogenide (TMDC) compounds. Like RTe_3, these TMDC compounds have isolated 2D metallic layers. However, the in-layer atomic structure is triangular rather than square lattices within which the triply degenerate CDWs emerge. Of particular interest here is 1T-TaS_2, which hosts nontrivial charge-density wave orders driven by several factors: the instabilities at the Fermi surface, the large lattice distortion possible, and the

localized orbital that leads to a Mott–Hubbard gap at the low temperature. The hidden CDW state formation in 1T-TaS_2 was among the first that was demonstrated in TMDC and since cross-examined by various ultrafast techniques (optical, scan tunneling microscopy (STM), X-ray and electron scattering).

The new focus here however is the elusive inverted phase of the CDW on the tantalum triangular lattice. The existence of such a novel excited order parameter, or so-called inverted order parameter state, has been suggested in qasi-1D or 2D (square lattice) CDW systems recently based on careful analyses of the dynamical response functions through time-resolved optical and X-ray diffraction techniques. Nonetheless, in these systems the new inverted phase and the initial CDW order represent two extrema phases governed by the same free-energy landscape, thus topologically (and diffraction-wise) indistinguishable. Meanwhile, the two extrema phases in a triangular lattice is expect to highly differ in their ordering and possibly even in topology and so the inverted phase may represent a genuinely new ordered phase with untapped potential for nonthermal control in a distinctly different way.

Inspired by the success of TD-LG modeling for the order parameter evolution in the scenarios offered by the RTe_3 system, we explored the landscape control for creating the inverted phase in TaS_2 as guided by the TD-LG predictions. In this central aspect, the dynamics of the excited many-body systems is governed by an effective transient free-energy landscape, which one can investigate in a controlled fashion via tuning the profile of the exciting laser pulses. This in turn yields the nonthermal control of excited system evolution, in particular, upon increasing laser fluence where the shifting landscape gives new access to different vestigial broken-symmetry orders even on the ultrafast timescale, i.e. a mechanism for coherent control[5].

Following the spatiotemporal patterns developed during the strongly driven phase transitions is key to unveiling the subtle nonequilibrium control of free-energy surfaces, and hence the routes for novel nonthermal switching and property controls. We achieved that by fully utilizing the multi-messenger feature of the UEM system. The dynamical events were characterized with different modalities: the coherently scattered electrons are tapped to report on the long-range ordering, the bright-field imaging for the sample morphology and stress state, and incoherent and inelastically scattered electrons for the nonequilibrium electronic responses. The high intensities of the photo-electron pulses afforded in the new UEM setting gave the possibility of surveying a large body of exfoliated TaS_2 samples; in each case, we utilized the film-thickness-dependent optical interferometry (Fabry-Perot effect) to tune excited profile for the landscape control to understand the novel phase-change behaviors. We investigated the behavior of coherent responses of the order parameter to the increasing laser quench near and at criticality, exploring the relation between specimen thickness selection, laser fluence control and ultimately witnessed the emergence of new inverted CDW phase with a fluence well beyond the criticality.

Here, we unveiled a nonthermal pathway to the novel inverted CDW by pumping the system transiently into the normal state landscape to coherently reverse the CDW lattice distortion in 1T-TaS_2 and back. We tracked the signatures of this novel CDW state based on coherent diffraction and the time-dependent Landau-Ginzburg theory to validate that it does exhibit a unique lattice and charge arrangement never before materialized. The in-situ obtained ultrafast nonequilibrium electronic signatures further reveal its novel properties that are characterized by an increased metallicity and damping times.

Future Plans

We have demonstrated the nonthermal control of the excited quantum materials; more specifically, engineering novel hidden phases and metastability via tuning the laser excitations and specimen configurations in two different regimes. In the study of TaS_2, the control aspect focused on the early-stage evolution. Nonetheless, our other studies (not shown here) also demonstrated a regime of nonequilibrium criticality beyond the initial landscape that can be utilized to further direct the dynamical phase-ordering events on a much longer timescale. The abundance of information reveals the wide and varied possibilities for controlling the collective behaviors and their functional properties in quantum material systems not available in the conventional semiconductors or metals. The future works will build on these knowledges and further develop a more precise predicative model based on TD-LG approach – to achieve this, we will combine optical spectroscopy measurements and the ultrafast electrons scattering experiments in the same setup to establish a direct correlation in the electronic and structural phase transitions in the same systems.

References

1. A. Kogar, A. Zong, P.E. Dolgirev, X. Shen, J. Straquadine, Y.-Q. Bie, X. Wang, T. Rohwer, I.C. Tung, Y. Yang, R. Li, J. Yang, S. Weathersby, S. Park, M.E. Kozina, E.J. Sie, H. Wen, P. Jarillo-Herrero, I.R. Fisher, X. Wang, N. Gedik, *Light-induced charge density wave in $LaTe_3$.* Nature Physics **16,** 159-163 (2020).
2. F. Zhou, J. Williams, S. Sun, C.D. Malliakas, M.G. Kanatzidis, A. Kemper, C.-Y. Ruan, *Nonequilibrium dynamics of spontaneous symmetry breaking into a hidden state of charge-density wave*. Nature Communications **12,** 566 (2021).
3. X. Sun, S. Sun, C.-Y. Ruan, *Toward nonthermal control of excited quantum materials: framework and investigations by ultrafast electron scattering and imaging*. Comptes Rendus. Physique **22** (S2), 15-73 (2021).
4. S. Sun, X. Sun, D. Bartles, E. Wozniak, J. Williams, P. Zhang, C.-Y. Ruan, *Direct imaging of plasma waves using ultrafast electron microscopy.* Structural Dynamics **7,** 064301 (2020).
5. C.-Y. Ruan, *Hidden in plain light*. Nature Physics **17**, 884-885 (2021).

Publications

1. S. Sun, X. Sun, D. Bartles, E. Wozniak, J. Williams, P. Zhang, C.-Y. Ruan, *Direct imaging of plasma waves using ultrafast electron microscopy.* Structural Dynamics **7,** 064301 (2020).
2. S. Sun, X. Sun, J. Williams, C.-Y. Ruan, *Development of RF-compressed high-throughput femtosecond electron microscope.* Microscopy and Microanalysis **26**, 1-4 (2020).
3. C.-Y. Ruan, Electron spectroscopy system. 10607807, 2020.
4. F. Zhou, J. Williams, S. Sun, C.D. Malliakas, M.G. Kanatzidis, A. Kemper, C.-Y. Ruan, *Nonequilibrium dynamics of spontaneous symmetry breaking into a hidden state of charge-density wave.* Nature Communications **12,** 566 (2021).
5. X. Sun, S. Sun, C.-Y. Ruan, *Toward nonthermal control of excited quantum materials: framework and investigations by ultrafast electron scattering and imaging*. Comptes Rendus. Physique **22** (S2), 15-73 (2021).

Probing Local Symmetry Breaking in Quantum Matter

Susanne Stemmer, Materials Department, University of California, Santa Barbara

Keywords: Scanning transmission electron microscopy, oxides, superconductivity, ferroelectricity

Research Scope

The overarching goal of the current project is to elucidate the role that local breaking of spatial symmetries plays in controlling emergent phenomena in quantum materials, such as superconductivity, ferroelectricity, and unusual transport phenomena in magnetic materials. The project is motivated by recent discoveries of nanoscale polar regions in several classes of unconventional superconductors that do not exhibit any macroscopic changes in their symmetry. The role that such locally symmetry broken regions play in the properties of quantum materials remains poorly understood. Using a combination of quantitative scanning transmission electron microscopy (STEM) techniques, systematic tuning of thin film materials, and macroscopic measurements, the proposed project aims at determining the nature of locally symmetry-broken regions as a function of materials parameters and temperature. The project will develop advanced STEM techniques that can probe key microscopic interactions, such as between nanoscale polar domains, electronic carriers, and disorder. The project also aims at contributing to the development of STEM techniques that can reveal the three-dimensional configuration of atomic displacements.

Recent Progress

Although the ferroelectric transition of strained, undoped $SrTiO_3$ is usually described as a classic displacive transition, a major discovery in this project was that it has pronounced order-disorder characteristics. In this project, we showed that static, polar crystal distortions already exist in the *paraelectric* phase of epitaxially strained, undoped $SrTiO_3$ films, consistent with an order-disorder transition. Next, we studied the evolution of polar distortions and nanodomains in the paraelectric phase of epitaxially strained $SrTiO_3$ films as a function of doping density. We investigated films with carrier densities in a regime where both ferroelectric and superconducting transitions are observed. Increasing the carrier concentration causes the polar nanodomains to break up into smaller clusters. No ferroelectric transition is observed in the highest doped film with only random distortions and no nanodomains. The results show that a high configurational entropy makes the ferroelectric phase transition energetically unfavorable. Moreover, we found a second, distinct type of Ti-column displacements, which are uncorrelated and are directly associated with the Sm dopant atoms. The locations of the large displacements due to the dopants coincide with the disordered regions that break up the nanodomains. Our results elucidate the microscopic mechanisms by which doping suppresses the ferroelectric transition. It is this second factor that contributes to the complete destruction of the nanodomains at high doping, e.g., by frustrating the dipole interactions leading to the polar displacements, thereby completely suppressing the ferroelectric transition.

Based on the insights describe above, we focused on additional studies aimed at understanding the interaction between polar and superconducting order parameters that may hold the key to several classes of superconductors that remain poorly understood, including $SrTiO_3$. We showed that doped, strained $SrTiO_3$ films can exhibit both global or local polar order, respectively, depending on the amount of epitaxial mismatch strain, thereby providing a platform to understand how inversion symmetry breaking affects superconductivity. We found that the superconducting critical temperature correlates with the length scale of polar order [2]. In particular, the transition temperature is enhanced when polar nanodomains are sufficiently large or, in the extreme limit, films are globally ferroelectric. In these cases, the Cooper pairs reside in a non-centrosymmetric environment. Conversely, low transition temperatures are found when the nanodomains are small. The findings point to the length scale of polar nanodomains and spin-orbit coupling as important parameters controlling the superconductivity of $SrTiO_3$. The ability to control the size of the polar domains opens up new opportunities to design and control the nature of superconductivity in a wide range of materials. In another study (ref. [3]), we showed that large concentrations (up to a few percent) of rare earth ions with unpaired *f*-electrons, such as Sm and Eu, do not reduce the superconducting critical temperature and critical fields.

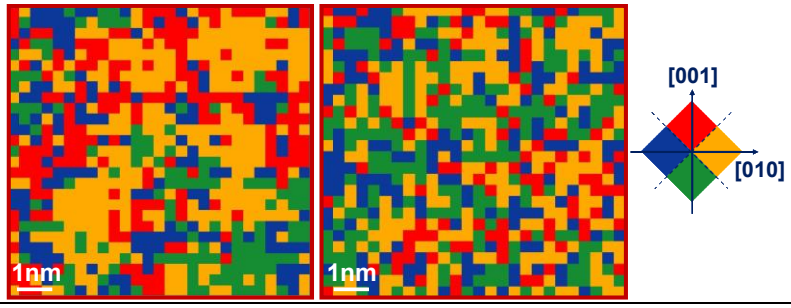

Fig. 1: Polar nanodomains in (left) unstrained, doped $SrTiO_3$ films and absence of these domains in (right) overdoped, strained $SrTiO_3$ films. Each unit cell is color-coded according to which [100] direction the Ti-O column displacements are closest to. All images are taken at room temperature. The value of T_c for the unstrained film is 227 mK while it is 160 mK for the overdoped, strained film. In both films, T_c is **not** enhanced, consistent with a small nanodomain size (left) or absence of nanodomains (right). From ref. [2].

Another recent focus was advanced STEM characterization of thin films of a topological semimetal, cadmium arsenide. For example, in ref. [7], we elucidated the role of threading dislocations in the transport properties of bulk and topological surface states. One important finding was that they have little influence on bulk transport, possibly because of the topological protection. Another focus was on determining the point group symmetry of both unstrained and strained cadmium arsenide. The bulk point group had been controversial. Using CBED, we were able to show that it is centrosymmetric, which classifies cadmium arsenide as a Dirac (not Weyl) semimetal. A very surprising result was our recent discovery that tensile (but not compressive) coherency strains cause loss of inversion symmetry, turning cadmium arsenide into a Weyl semimetal (Fig. 2) [4]. The result is surprising, because epitaxial strains do not usually cause loss of inversion symmetry, unless there is already a proximal phase that lacks it (prominent examples are $SrTiO_3$ or $EuTiO_3$). It indicates that bulk cadmium arsenide must already be close to a structural instability, which was subsequently confirmed by DFT calculations reported by our collaborator in the same publication. Like the discovery of the nanodomains, the study is another example of the many unexpected discoveries about quantum materials that are revealed by S/TEM investigations.

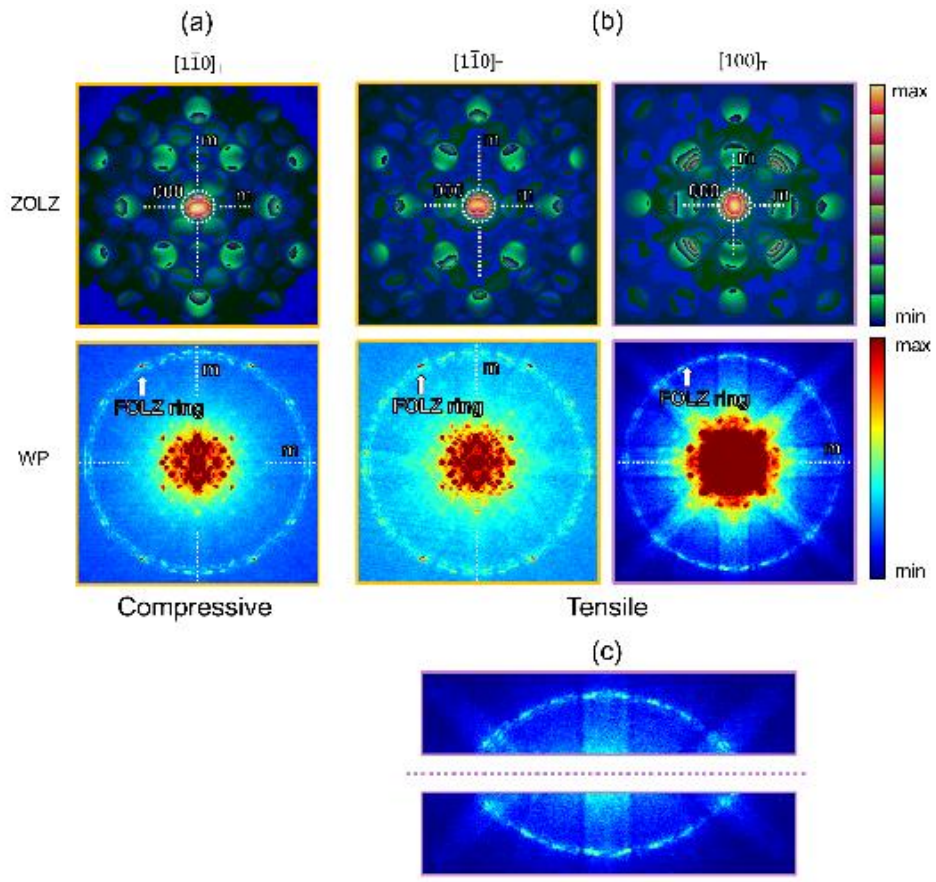

Fig. 2: CBED patterns of strained (001) Cd_3As_2 films. (a) Experimental CBED pattern along $[1\bar{1}0]_T$ for a compressively strained (001) Cd_3As_2 film, showing the ZOLZ pattern (top) and whole patter (WP) (bottom), which includes the HOLZ ring. (b) Experimental CBED patterns along $[1\bar{1}0]_T$ and $[100]_T$ for a tensile strained (001) Cd_3As_2 film, showing the ZOLZ pattern (top) and WP (bottom), which includes the HOLZ ring. (c) Magnified view of the *m* in the HOLZ ring in the $[100]_T$ pattern of tensile (001) Cd_3As_2. The loss of the second mirror in the WP is one key difference that distinguishes it from the compressive and unstrained films and indicates a transition to a lower symmetry. The lack of inversion symmetry in 4*mm* implies the loss of the mirror plane, which results in a single mirror in the projection. From ref. [4].

Future Plans

We plan to focus on the role of local symmetry breaking in topological films and we also plan to continue our investigations into the role of local symmetry breaking in correlated oxide films. In the former, we are particularly interested in surfaces and interfaces, because they host topological surface states that dominate the interesting electrical transport in these materials. In the latter, we will use the new capabilities of the newly installed aberration corrected STEM to better understand the nature of the local displacements.

Publications (2020 – 2022)

1. H. Jeong, R. Russell, N. G. Combs, T. N. Pardue, J. W. Harter, and S. Stemmer, *Similarity in the critical thicknesses for superconductivity and ferroelectricity in strained $SrTiO_3$ films*, Appl. Phys. Lett. 121, 012601 (2022).
2. S. Salmani-Rezaie, H. Jeong, R. Russell, J. W. Harter, and S. Stemmer, *Role of locally polar regions in the superconductivity of $SrTiO_3$*, Phys. Rev. Mater. 5, 104801 (2021).
3. S. Salmani-Rezaie, L. Galletti, T. Schumann, R. Russell, H. Jeong, Y. Li, J. W. Harter, and S. Stemmer, *Superconductivity in Magnetically Doped $SrTiO_3$*, Appl. Phys. Lett. **118**, 202602 (2021) (Editor's pick).
4. T. N. Pardue, M. Goyal, B. Guo, S. Salmani-Rezaie, H. Kim, O. Heinonen, M. D. Johannes, and S. Stemmer, *Controlling the symmetry of cadmium arsenide films by epitaxial strain*, APL Mater. 9, 051111 (2021).
5. S. Salmani-Rezaie, K. Ahadi, and S. Stemmer, *Polar nanodomains in a ferroelectric superconductor*, Nano Lett. **20**, 6542–6547 (2020).
6. S. Salmani-Rezaie, K. Ahadi, W. M. Strickland and S. Stemmer, *Order-Disorder Ferroelectric Transition of Strained $SrTiO_3$*, Phys. Rev. Lett. **125**, 087601 (2020).
7. M. Goyal, S. Salmani-Rezaie, T. N. Pardue, B. Guo, D. A. Kealhofer, and S. Stemmer, *Carrier mobilities of (001) cadmium arsenide films*, APL Mater. **8**, 051106 (2020).

Tunable Few-Layer van der Waals Crystals and Heterostructures as Emerging Energy and Quantum Materials

PIs: Peter Sutter, Dept. of Electrical & Computer Engineering, University of Nebraska-Lincoln, Lincoln, NE 68588 (psutter@unl.edu); Eli Sutter, Dept. of Mechanical & Materials Engineering, University of Nebraska-Lincoln, Lincoln, NE 68588 (esutter@unl.edu)

Keywords: Van der Waals semiconductors, heterostructures, electron microscopy, cathodoluminescence, electron energy loss spectroscopy

Research Scope

2D and layered (van der Waals, vdW) semiconductors offer extraordinary opportunities for manipulating optically excited charge carriers, many-body excitations, and non-charge based quantum numbers. To date, research has focused on a limited group of materials, mostly transition metal dichalcogenides in the monolayer limit. Other classes of vdW semiconductors, in particular few-layer to multilayer crystals and their heterostructures, carry large potential for discovery of phenomena of interest for future energy and information technologies; but they remain largely unexplored, often due to a lack of high-quality materials and of approaches for measuring their properties at the relevant scales. We are developing an EPSCoR-State/National Laboratory Partnership that addresses the challenges of preparing high-quality vdW semiconductors and of probing their structure, composition, and especially their optoelectronic and photonic properties, using advanced electron microscopy techniques.

The partnership involves the PIs at the University of Nebraska-Lincoln and leading scientists specializing in electron microscopy (EM) and theory/computation at the Center for Nanophase Materials Sciences (CNMS) at Oak Ridge National Laboratory, including R.R. Unocic (EM), J.A. Hachtel (EM), and P. Ganesh (theory). Advanced electron microscopy and electron stimulated spectroscopy methods, available at the partner institutions and being developed within this program, are applied to address geometries of increasing complexity and fill knowledge gaps to realize the promise of van der Waals semiconductors (Figure 1):

(i) *Large-scale crystals:* Identify the atomistic mechanisms that support the scalable synthesis of van der Waals crystals with control over their unique structural features, such as number of atomic layers and stacking order; use precisely tuned, high-quality crystals to study optoelectronics and photonics in the few-layer and multilayer regime.

(ii) *Heterostructures:* Gain control over structure, composition, and the placement of interfaces between and within 2D sheets in layered heterostructures; establish the role of interfaces in managing optical excitation and recombination processes.

(iii) *Hierarchical architectures:* Assemble van der Waals semiconductors into hierarchical systems capable of complex modes of energy and information transfer; probe the transduction of energy and information *via* propagating light-matter hybrid modes.

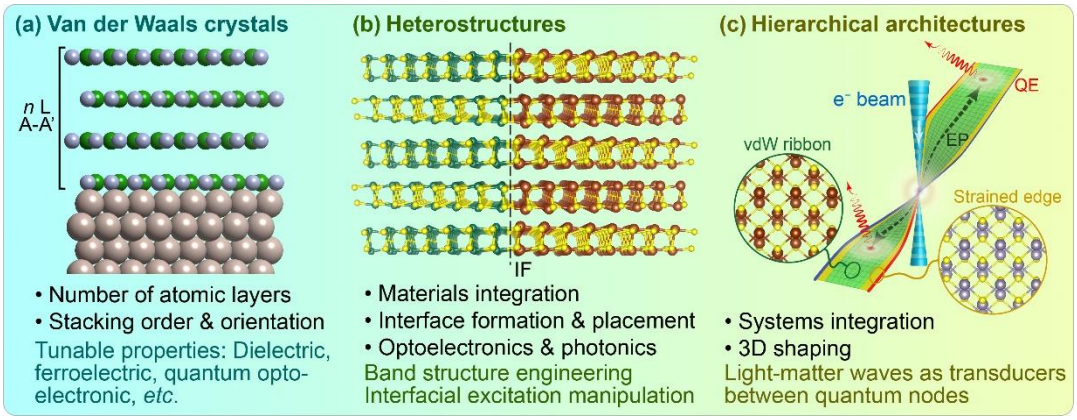

Figure 1. Van der Waals semiconductors for future energy and information technologies. (a) Atomically controlled layered crystals: Wafer-scale h-BN with defined layer number and stacking order. (b) Materials integration in heterostructures: Lateral junctions for intralayer exciton manipulation and carrier separation. (c) Hierarchical energy/information transduction systems: 3D-shaped van der Waals ribbons hosting quantum emitters communicating *via* exciton-polariton waves.

Recent Progress

Work under prior BES support has established a base of materials platforms that will be developed and investigated here using atomic-scale structural and chemical analysis in (scanning) transmission electron microscopy ((S)TEM) and advanced electron-stimulated spectroscopy methods, including STEM-cathodoluminescence (STEM-CL) to measure light emission and monochromated low-loss electron energy loss spectroscopy (EELS) to locally probe optical absorption and phonons. We have also developed unique capabilities, *e.g.*, for real-time microscopy of the synthesis of few-layer vdW semiconductors and the characterization of single-photon quantum emitters in STEM-CL, which support the research under this project.

Future Plans

Large-scale vdW crystals – h-BN: Few-layer sp^2-bonded hexagonal boron nitride (h-BN) is a crucial component for condensed-matter research and emerging materials and information technologies. To date, a majority of scientific studies have relied on bulk-exfoliated h-BN flakes as building blocks. But further advances in the complexity of engineered vdW structures require access to large (wafer-scale) h-BN films with uniform layer number, atomically smooth surfaces, and crystal quality approaching that of bulk single crystals. While it is comparatively easy to grow a h-BN monolayer, *e.g.*, using chemical vapor deposition of a suitable precursor that is catalytically dissociated on a metal,[1] adding further h-BN layers in a controlled way to build a layered single-crystalline film is challenging due to the low reactivity of the BN surface.[2] We will use real-time low-energy electron microscopy to identify approaches for assembling h-BN with thickness beyond the range of electron tunneling, *i.e.*, from ~10 nm to >50 nm. Once available, uniform, thickness-controlled h-BN will be shared to assess its use in building complex vdW heterostructures at unprecedented scale. In addition, controlled atomistic modifications will be developed for layer-specific doping and the deterministic generation of quantum emitters, which can be further localized in the plane by local strain. Addressed by our distinctive electron

microscopy and spectroscopy capabilities, such tunable vdW materials will provide unprecedented insight into the physics of quantum emitters in boron nitride.

Heterostructures – Lateral integration of vdW crystals: Lateral heterostructures with covalently stitched line interfaces between different 2D crystals have enabled studies of interfacial electronic structure and excitation manipulation. We recently pioneered a new form of lateral heterostructures, in which line interfaces are embedded within each of up to several hundred individual layers in a van der Waals stack.[3] The controlled placement of lateral interfaces across many layers promises distinct advantages in light-harvesting applications by combining a large optical thickness with facile carrier separation within the vdW layers. We will extend this concept to the integration of semiconductors with different interfacial band alignments, apply momentum-resolved monochromated EELS to establish the dispersive properties of phonons and excitons near interfaces, and develop STEM-CL capabilities for quantifying interfacial exciton flows and radiative recombination processes.

Hierarchical architectures: An emerging frontier that is uniquely enabled by vdW crystals involves a shift from materials exhibiting a single functionality towards multifunctional integrated systems. Here, we pursue this vision by exploring 3D-shaped vdW waveguides with integrated active elements, such as single photon sources. The work builds on two recent discoveries: The identification of synthesis methods that use edge-stress to drive the controlled axial twisting (and hence 3D shaping) of vdW ribbons; and the development of approaches for the local excitation of propagating exciton-polariton waves in such ribbons.[4] We will develop EELS and STEM-CL measurements to understand the coherent excitation of propagating waves and the strong coupling between excitons and the Fabry-Perot cavity modes in 3D-shaped waveguides. And we will build complex systems for studying photonic information transfer between quantum nodes by integrating quantum emitters into vdW polariton waveguides.

References

1. P. Sutter, J. Lahiri, P. Albrecht, and E. Sutter, *Chemical Vapor Deposition and Etching of High-Quality Monolayer Hexagonal Boron Nitride Films*, ACS Nano **5**, 7303 (2011).

2. P. Sutter, J. Lahiri, P. Zahl, B. Wang, and E. Sutter, *Scalable Synthesis of Uniform Few-Layer Hexagonal Boron Nitride Dielectric Films*, Nano Letters **13**, 276 (2013).

3. E. Sutter, J. Wang, and P. Sutter, *Lateral Heterostructures of Multilayer GeS and SnS van der Waals Crystals*, ACS Nano **14**, 12248 (2020); E. Sutter, R.R. Unocic, J.-C. Idrobo, and P. Sutter, *Multilayer Lateral Heterostructures of Van Der Waals Crystals with Sharp, Carrier–Transparent Interfaces*, Advanced Science **9**, 2103830 (2022).

4. P. Sutter, L. Khosravi-Khorashad, C. Argyropoulos, and E. Sutter, *Cathodoluminescence of Ultrathin Twisted $Ge_{1-x}Sn_xS$ van der Waals Nanoribbon Waveguides*, Advanced Materials **33**, 2006649 (2021).

Visualizing emergent phenomena in topological and quantum materials

Weida Wu

Department of Physics and Astronomy, Rutgers University, Piscataway, NJ, 08854

Keywords: MFM, topological insulators, domain walls, antiferromagnets, chiral edge states

Research Scope

The objective of this proposal is to visualize emergent topological quantum phenomena such as chiral spin texture, antiferromagnetic domains and domain walls and chiral edge states to understand the fundamental mechanisms. Combining magnetic imaging and other complementary techniques such as *in-situ* transport, the PI will investigate magnetic domains, domain walls and chiral edge states in magnetic topological insulators, surface magnetism and possible surface spin-flop/flip transitions, and chiral spin texture such as skyrmions and chiral domain walls.

Recent Progress

Direct Visualization of Surface Spin-Flip Transition in $MnBi_4Te_7$

Our previous magnetic force microscopy (MFM) studies confirmed that the A-type antiferromagnetic order persists to the surface layer of $MnBi_2Te_4$ [1]. The robust A-type antiferromagnetic order is further corroborated by the observation of the long-sought surface spin-flop transition. In spite of mounting evidence of the robust A-type AFM order, it is possible that surface relaxation is limited to the very top layer and strictly follows morphology of surface steps. If this is the case, a further reduction of interlayer coupling by increasing the interlayer separation would favor a stronger surface relaxation effect. The natural superlattice compounds $MnBi_2Te_4$–$(Bi_2Te_3)_n$ provide perfect systems to test such a hypothesis. In these systems, *n* layers of Bi_2Te_3 are inserted between $MnBi_2Te_4$ layers, dramatically reducing the interlayer coupling without much impact on the uniaxial anisotropy [2–7]. We carried out MFM studies on cleaved surface of $MnBi_4Te_7$.[i] Our results confirm that the A-type AFM order persists to the surface of with $MnBi_2Te_4$ termination, excluding the

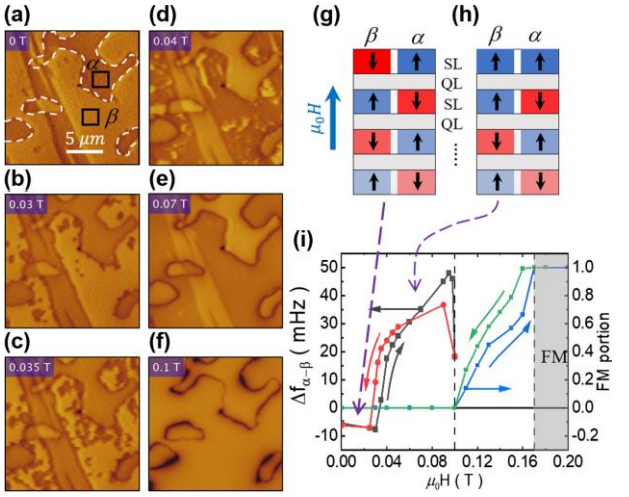

Fig. 1 | (a)–(f) Selected MFM images taken at 5.5 K with increasing magnetic fields, which are labeled on the corner of each image. The color scales from (a) to (f) are 0.06, 0.11, 0.12, 0.12, 0.26 and 3 Hz, respectively. The AFM domain walls are traced out with dashed lines in (a). The boxed areas α and β in (a) corresponds to parallel and antiparallel surfaces, respectively. (g),(h) Magnetic structures of areas α and β before and after the surface spin-flip transition, respectively. (i) *H* dependence of MFM contrast between areas α and β and that of forced ferromagnetic (FM) domain population during the BSF transition (between 0.1 and 0.17 T). The colored arrows indicate the field sweeping direction. Above 0.17 T, the system is in the FM state.

previous proposed surface relaxation of the A-type AFM order [2,5,7]. More interestingly, we discover a first-order spin-flip transition on the $MnBi_2Te_4$ surface termination of $MnBi_7Te_7$ that precedes the bulk spin-flip transition, as shown in Fig. 1. Our analysis further reveals no reduction of the magnetization of surface layer despite the reduced number of neighbors, indicating that the Ising-like ferromagnetism could persist in single-layer $MnBi_2Te_4$ [8]. Therefore, $MnBi_4Te_7$ is a promising material platform for achieving high-temperature quantized transport in few-layer thin films [4].

Direct evidence of ferromagnetism in $MnSb_2Te_4$

$MnSb_2Te_4$ is isostructural to $MnBi_2Te_4$, the first antiferromagnetic TI [9]. In stoichiometric compound, it is also A-type antiferromagnet [9]. However, a recent study revealed that the magnetism in $MnSb_2Te_4$ can be tuned from antiferromagnetic to ferromagnetic by changing the Mn/Sb site mixing [10]. Neutron diffraction, transport, and magnetization studies have been reported on ferromagnetic $MnSb_2Te_4$, yet the direct visualization of the ferromagnetic state in $MnSb_2Te_4$ is still lacking. Using cryogenic MFM, we visualized the domain behavior of ferromagnetic $MnSb_2Te_4$ single crystals from two different sources.[ii] Micron size ferromagnetic domains are found on both samples after zero-field cooling (ZFC) below $T_C \approx 33$ K. We observed typical uniaxial ferromagnetic domain behavior with very weak domain wall pinning. The magnetic field dependence of domain population shows little hysteresis, in good agreement with that of bulk magnetization. The temperature dependence of domain contrast follows mean field behavior, in good agreement with that of the saturation magnetization.

Magnetic Skyrmions in room temperature polar ferromagnet $(Fe,Co)_5GeTe_2$

Novel magnetic ground states have been stabilized in two-dimensional (2D) magnets such as skyrmions, with the potential next-generation information technology. In the collaboration with colleagues at UC Berkeley, we observed a Néel-type skyrmion lattice at room temperature in a single-phase, layered 2D magnet, specifically a 50% Co–doped Fe_5GeTe_2 (FCGT) system.[iii] The thickness-dependent magnetic domain size follows Kittel's law. The static spin textures and spin dynamics in FCGT nanoflakes were studied by Lorentz electron microscopy, MFM, micromagnetic simulations, and magnetotransport measurements. This discovery of a skyrmion lattice at room temperature in a noncentrosymmetric material opens the way for layered device applications and provides an ideal platform for studies of topological and quantum effects in 2D.

Chiral-Bubble-Induced THE in Ferromagnetic Topological Insulator Heterostructures

Previously we report the discovery of spin-chirality fluctuation induced topological Hall effect (THE) above Curie temperature in 2D ferromagnets [11]. Following this work, we report compelling evidence of THE emerged from chiral bubbles in a 2D uniaxial ferromagnet, specifically V-doped Sb_2Te_3 heterostructure.[iv] The sign of THE signal is determined by that of the net curvature of domain walls in different domain configurations, and the strength of THE signal is correlated with the density of nucleation or pinned bubble domains, as shown in Fig. 2. The experimental results are in excellent agreement with the integrated linear transport and Monte Carlo simulations, corroborating the emergent gauge field at chiral magnetic bubbles. Our findings

not only reveal a general mechanism of THE in two-dimensional ferromagnets but also pave the way for the creation and manipulation of topological spin textures for spintronic applications.

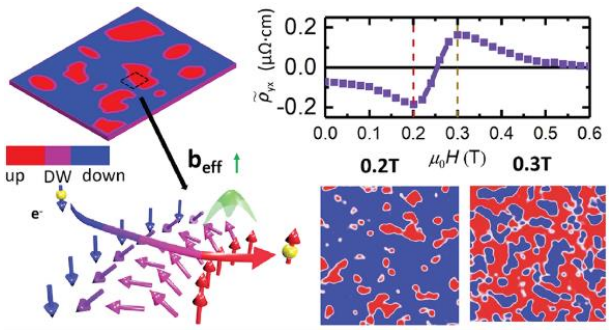

Fig. 2 | Left: Cartoon of noncoplanar spin texture on the curved chiral domain walls carrying Berry curvature which behaves as an effective magnetic field that deflects electrons as they pass through, resulting in extra Hall effect. Right: *H*-dependence of THE signal with sign changes at coercive field and corresponding MFM images of domain structure.

Magnetic domain engineering in $SrRuO_3$ thin films

In this work,[v] we report the control of magnetic domain formation in $SrRuO_3/SrTiO_3$ heterostructures via structural domain engineering, specifically by controlling the miscut direction of substrate. The combination of *x*-ray diffraction analysis of structural twin domains and magnetic imaging of reversal process demonstrates a one-to-one correspondence between structural domains and magnetic domains, which results in multi-step magnetization switching and anomalous Hall effect in films with twin domains.

In addition to above highlighted works, the PI's group also contribute to the understanding of correlated Wely semimetal physics in $Eu_2Ir_2O_7$ films[vi], and the review article on the challenges in identifying chiral spin textures via the topological Hall effect.[vii]

Future Plans

Magnetic imaging of antiferromagnetic domain walls and surface magnetism

The PI and his students will continue explore the magnetic imaging of antiferromagnetic domain walls in other topological antiferromagnets using the susceptibility contrast mechanism established by the PI's group. The PI and his students will also explore the surface spin-flop/flip transitions in other A-type antiferromagnets, which would have substantial impact on spintronic devices using antiferromagnetic thin films.

Magnetic imaging of QAH systems and chiral edge states

The PI and his students will investigate ferromagnetic domain behaviors in magnetic TIs, using VT-MFM with *in situ* high magnetic/electric field capabilities. The ultimate goal is to visualize one-way conduction of chiral edge states in these fascinating systems. Another direction is to investigate Axion insulators in magnetic TI heterostructure to explore the Axion physics.

Design and development of an ultra-low temperature MFM

The PI's group will continue the effort of developing a He3 temperature MFM with 14 T magnet. With the current BES support, the PI and his student finished designing the scanner head. Most parts have been ordered and machined. The PI's student is assembling the MFM head which will be integrated with the He3 refrigerator soon. The delivery of cryostat and magnet was delayed

several months by the impact of COVID-19 pandemic. The PI and his student expect to perform preliminary cryogenic tests of He3 MFM with 14 T magnet in the next few months.

References

[1] P. M. Sass, J. Kim, D. Vanderbilt, J. Yan, and W. Wu, Phys. Rev. Lett. **125**, 037201 (2020).

[2] H. Sun, B. Xia, Z. Chen, Y. Zhang, P. Liu, Q. Yao, H. Tang, Y. Zhao, H. Xu, and Q. Liu, Phys. Rev. Lett. **123**, 096401 (2019).

[3] Y. Liu, L. Wang, Q. Zheng, Z. Huang, X. Wang, M. Chi, Y. Wu, B. C. Chakoumakos, M. A. Mcguire, B. C. Sales, W. Wu, and J. Yan, Phys. Rev. X **11**, 021033 (2021).

[4] W. Wang, M. W. Daniels, Z. Liao, Y. Zhao, J. Wang, G. Koster, G. Rijnders, C.-Z. Chang, D. Xiao, and W. Wu, Nat. Mater. **18**, 1054 (2019).

Publications (supported by BES in recent 2-year)

[i] Wenbo Ge, Jinwoong Kim, Ying-Ting Chan, David Vanderbilt, Jiaqiang Yan, and **Weida Wu**, "Direct visualization of surface spin-flip transition in $MnBi_4Te_7$", ***Phys. Rev. Lett.***, **129**, 037201, (2022).

[ii] Hongrui Zhang, David Raftrey, Ying-Ting Chan, Yu-Tsun Shao, Rui Chen, Xiang Chen, Xiaoxi Huang, Jonathan T. Reichanadter, Kaichen Dong, Sandhya Susarla, Lucas Caretta, Zhen Chen, Jie Yao, Peter Fischer, Jeffrey B. Neaton, **Weida Wu**, David A. Muller, Robert J. Birgeneau, Ramamoorthy Ramesh, "Room-temperature skyrmion lattice in a layered magnet $(Fe_{0.5}Co_{0.5})_5GeTe_2$", ***Science Advance***, **8**, eabm7103 (2022).

[iii] Wenbo Ge, Paul M. Sass, Jiaqiang Yan, Seng Huat Lee, Zhiqiang Mao, and **Weida Wu**, **"**Direct evidence of ferromagnetism in $MnSb_2Te_4$", ***Phys. Rev. B***, **103**, 134403, (2021).

[iv] Wenbo Wang, Yi-Fan Zhao, Fei Wang, Matthew W. Daniels, Cui-Zu Chang, Jiadong Zang, Di Xiao, and **Weida Wu**, "Chiral-Bubble-Induced Topological Hall Effect in Ferromagnetic Topological Insulator Heterostructures", ***Nano Lett.***, **21,** 1108 (2021).

[v] Wenbo Wang, Lin Li, Junhua Liu, Binbin Chen, Yaoyao Ji, Jun Wang, Guanglei Cheng, Yalin Lu, Guus Rijnders, Gertjan Koster, **Weida Wu**, Zhaoliang Liao, "Magnetic domain engineering in $SrRuO_3$ thin films", ***npj Quantum Materials***, **5**, 73 (2020).

[vi] Xiaoran Liu, Shiang Fang, Yixing Fu, Wenbo Ge, Mikhail Kareev, Jong-Woo Kim, Yongseong Choi, Evguenia Karapetrova, Qinghua Zhang, Lin Gu, Eun-Sang Choi, FangdiWen, Justin H.Wilson, Gilberto Fabbris3 Philip J. Ryan, John Freeland, Daniel Haskel, **Weida Wu**, J. H. Pixley, Jak Chakhalian, "Observation of a magnetic Weyl semimetal in thin films of $Eu_2Ir_2O_7$", ***Phys. Rev. Lett.***, **127**, 277204 (2021).

[vii] Graham Kimbell, Changyoung Kim, **Weida Wu**, Mario Cuoco and Jason W. A. Robinson, "Challenges in identifying chiral spin textures via the topological Hall effect", ***Communications Materials***, **3**, 19 (2022).

Machine Learning-Enabled Advanced Electron Microscopy for Resolving Chemical Inhomogeneity and Materials Dynamics

Huolin Xin, Department of Physics and Astronomy, University of California, Irvine, CA

Keywords: machine learning, artificial intelligence, electron tomography, fast and statistical imaging, cryoEM.

Research Scope

The development of lithium-ion batteries (LIB) is one of the key innovations in the past several decades that have revolutionized many aspects of our lives and changed how we interact with machines and the environment. However, building safe, high-energy, long cycle-life and low-cost batteries is still a grand challenge for the research community. Many of the long-standing issues in the field are due in part, if not entirely, to the lack of characterization tools to resolve the electrode materials' failure modes and degradation mechanisms. The central goal of this project is to develop machine learning-aided electron microscopy as well as three-dimensional imaging techniques for the study of lithium battery electrodes.

This project aims to use the machine learning aided imaging technology to reveal novel phenomena related to the evolution of the surfaces and interfaces in compositionally complex oxide electrodes as well as alkaline metal anodes. Fundamental descriptions of interfaces' energy, structure, chemistry, and mechanical/functional behavior are sought to help uncover characteristics that improve the electrodes' performance in order to devise ways to optimize their performance and design rules for future development.

Recent Progress

(1) TEMImageNet training library and AtomSegNet deep-learning models for high-precision atom segmentation, localization, denoising, and deblurring of atomic-resolution images

We have developed an important forward model that incorporates realistic scan and Poisson noises in simulated images. This enables us to synthesize a large number of experimental-like atomic-scale ADF-STEM images from any crystal structures with known atomic structures. Using this method, we have developed an ADF-STEM image library, also termed as the TEMImageNet, which includes atomic-scale ADF-STEM images of eight materials projected along multiple different orientations, i.e. zone axes. Randomized linear and nonlinear low-frequency background patterns and interferences are added to the ADF-STEM images to improve the robustness of our deep-learning models during training. To reduce the false-positive rate, we have also included images of clusters and nanoparticles with tapered edge and sharp facets. We have provided a total of ten types of ground truth labels to train different types of models for tasks like atom

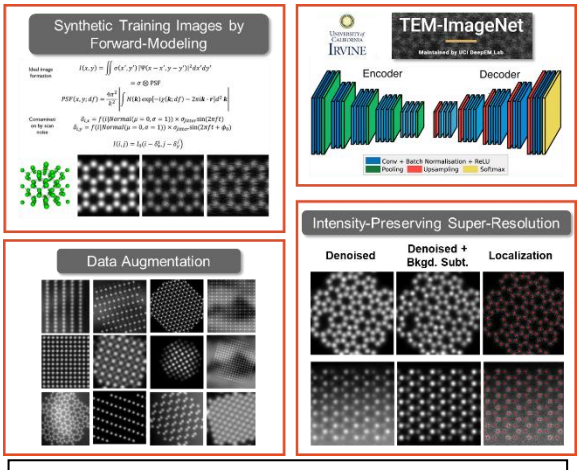

The TEMImageNet project.

segmentation and detection, noise reduction, background removal, and super-resolution processing. Based on our well labeled TEMImageNet library, we show that our encoder–decoder-type deep learning models achieve superior performance in atomic column localization, segmentation, noise reduction and deblur/super-resolution processing of experimental ADF-STEM images of crystal structures that were not included in the training library. For the atomic column segmentation, super-resolution/deblur processing, we deployed an encoder–decoder type, U-net architectured CNN network. The precision of our atomic-column localization model can even outperform the state-of-the-art two-dimensional (2d) Gaussian fit method—the gold standard in the TEM field. In the meantime, all deep learning models described in this article are released and incorporated in the open-source application, AtomSegNet, that is available for download from Github. AtomSegNet is intended to become a preprocessing module of a complete TEM image processing workflow that include extensions of materials and zone axis recognition, crystal phase mapping, dislocation and defect detection, atomic counting, strain mapping, etc. The training data sets and labels are available for download, searching and browsing at the project website.

Shortly after its release, AtomSegNet has already been successfully applied to the fundamental studies of lithium-ion battery materials by my group (Nano Lett. 2021, 21, 8, 3657–3663, Matter 4, 2013–2026, Nano Lett. 2022, 22, 3818−3824, and Nano Lett. 2021, 21, 9797−9804) and 2D materials by the ASU/UIUC groups (Phys. Rev. B 103, 224102).

(2) Super-compression of large electron microscopy time series by deep compressive sensing learning

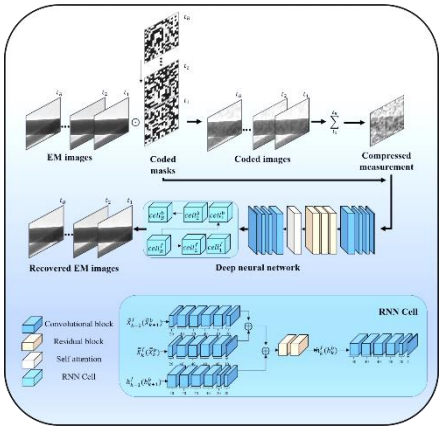

The TCS-DL4 framework.

Driven by the recent advances in computer science and electron microscopes, EM techniques, especially in-situ transmission electron microscopy (TEM), electron tomography and four-dimensional scanning transmission electron microscopy (4D-STEM), become more and more dependent on big data storage. In particular, due to the deployment of the state-of-the-art direct electron detectors, sequential images could be generated with extraordinary frame rates up to thousands of frames per second (fps). This, on the one hand, empowers researchers the capability to acquire more data with ultrahigh temporal resolution to discover new phenomena in nature. On the other hand, it poses grand challenges of processing, storing and transmitting the large-scale high-resolution EM videos or images. Compressive sensing (CS) as an efficient signal processing technique, has been widely used in EM for data acquisition and reconstruction. It has been wildly used in capturing high-dimensional data, such as videos and hyperspectral images. As long as the data or signal is compressible or sparse in a certain transform domain, a measurement matrix that is not related to the transform base can be used to project the high-dimensional data obtained by the transformation onto a low-dimensional space, and by solving an optimization problem, the original data can be reconstructed with high probability from few projections. Extensive attempts have been made to apply CS to meet the growing demand for efficient EM data acquisition and processing, however, challenges still remain due to the following drawbacks. On one hand, the iteration-based nature makes the conventional reconstruction algorithms time consuming. On the other hand, some tasks have higher requirement

for hardware, even that, the performance could still be unsatisfactory when the compression ratio is higher.

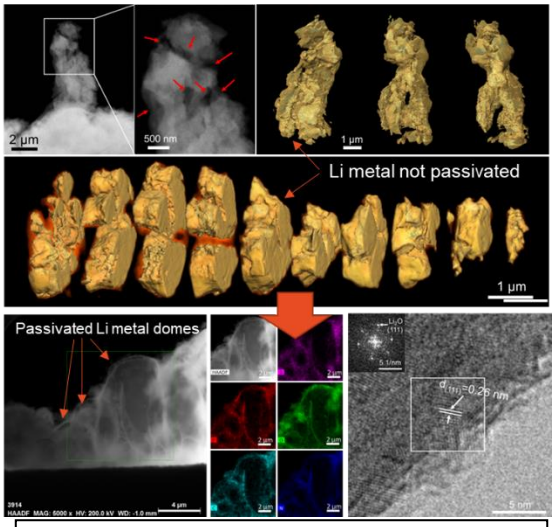

CryoEM/ET imaging of the Li0/SPE

In the past review period, by combining compressive sensing and deep learning, we propose a novel encoding-decoding strategy--TCS-DL4 to tackle the challenge facing big data EM. [Patterns 2, 100292 (2021)] Specifically, CS will be used as an encoder to compress multiple frames into a single frame measurement with significantly reduced (on the order of 10x) bandwidth and memory requirements for data transmission and storage. An end-to-end deep learning (DL) network is then constructed to reconstruct the original image series from the single-frame measurement with extremely high speed. Peak-signal-to-noise-ratio (PSNR) and Structural similarity (SSIM) evaluations show that the TCS-DL framework exhibits superior performance over the conventional JPEG compression method.

The performance of TCS-DL is tested on sequential EM images of different samples under varied imaging conditions (beam dose, magnification, etc). For instance, the test on sequential atomic-resolution images of Au nanocrystals shows that distinct from the conventional JPEG which introduces information loss during compression, the TCS-DL framework is capable to recover the lost high frequency information in the raw data. In addition, the built-in denoising capability of TCSDL could further improve the quality of raw images with enhanced surface atomic details. Moreover, the average PSNR for JPEG compression and TCS-DL is 23.98 dB and 25.91 dB, respectively. The test result shows that due to the relatively simple morphology of the carbon fibers compared with Au nanocrystals, the PSNR of both JPEG compression and TCS-DL framework are evidently higher than that of the atomic-resolution images of the Au nanocrystals. Yet, the TCS-DL framework still outperforms JPEG compression with a considerable PSNR improvement of approximately 3dB, from 32.38 dB (JPEG compression) to 35.41 dB (TCS-DL). [Patterns 2, 100292 (2021)]

(3) Development of cryoSTEM and cryoET techniques for imaging the lithium filaments, interphases at the interface of Li metal anode and the solid polymer electrolyte

In 2017, the cryoEM work published in Science by Yi Cui's group marks the beginning of atomic-resolution observation of the native interphases between Li metal (Li0) and organic battery electrolytes. Since then, more than a handful of impactful studies have devoted to resolving the solid-electrolyte interphase (SEI) on Li0 deposited in liquid-electrolyte batteries. While these studies have pushed the development of liquid-electrolyte Li0-anode batteries, what remains unresolved is the mysterious interfaces between Li0 and the solid ionic conductors in solid-state batteries. Li0-anode solid-state batteries are considered the next-generation alternative to existing liquid-electrolyte Li-ion batteries because they are safer and offer higher energy density. In this

work, we take the first step to use cryoSTEM and cryo-electron tomography (cryoET) to resolve the low Coulombic efficiency conundrum in of Li0||solid polymer electrolytes (SPEs) batteries.

Solid polymer electrolytes (SPEs) are a highly promising candidate because of its tunable mechanics and easy manufacturability. They are compatible with roll-to-roll processing in high-volume production; however, their electrochemical/chemical instability against the lithium metal (Li0), mediocre conductivity and poorly understood Li0-SPE interphases prevented the extensive application in real batteries. In particular, the origin of the low Coulombic efficiency associated with SPEs remains elusive as the debate continues whether it is originated from the unfavored interfacial reaction or lithium dendritic growth and dead lithium formation. In this work, cryoET imaging and cryoSTEM spectroscopic techniques were developed for solid state batteries and they were applied on the complex structure and chemistry of the interface between Li0 and a SPE based on polyacrylate. Contradicting to the conventional knowledge, we found that no protective interphase can be formed due to the sustained reactions between the deposited Li dendrites and the polyacrylic backbones as well as the succinonitrile plasticizer. Due to the reaction induced volume change, large amounts of cracks were formed inside the Li dendrites with a stress corrosion cracking behavior indicating that Li0 cannot be passivated in this SPE system.

Based on this observation, we introduced additives to the SPE and use cryoSTEM to demonstrated that the Li0 surface can be effectively protected against corrosion leading to densely packed Li0 domes with conformal and stable SEIs films—this has practical impact on improving the cycle life of the solid state batteries. This work is now published in Nature Nanotechnology 17, 768–776 (2022) and the article is available at the following doi: https://doi.org/10.1038/s41565-022-01148-7

Future Plans

To address the spectroscopic and high dimensional data challenge, we are exerting effort on the following machine learning models for TEM images and spectroscopic data.

1. To date, detection and localization of core loss edges on raw electron energy loss spectrum (EELS) has been a manual and tedious task for human researchers primarly due to the low jump ratio and low signal-to-nose. In this task, we would like to show that it is possible to synthesize a ground truth labelled EELS dataset by forward modeling and use it train machine learning models. [https://arxiv.org/abs/2209.13026]

2. In the field of electron tomography, there is no lack of algorithms for reconstructing the tomograms. Then, the big question becomes: can we integrate the advantages of all the existing algorithms and remove their disadvantages? The simple idea behind this question sounds intriguing but it is extremely difficult to tackle until recently when GPUs in PCs are powerful enough to train deep and generative convolutional neural networks. In this task, we would like to demonstrate for the first time that it is possible to ‘intelligently’ integrate multiple reconstruction algorithms together in a high

dimensional manifold so the deep fused result show remarkable information recovery and artifact removal capabilities.

Publications

1. R. Lin, Y. He, C. Wang, P. Zou, E. Hu, X.-Q. Yang, K. Xu & H. L. Xin, *Characterization of the structure and chemistry of the solid–electrolyte interface by cryo-EM leads to high-performance solid-state Li-metal batteries*, Nature Nanotechnology, **17**, 768–776 (2022)
2. R. Lin, R. Zhang, C. Wang, X.-Q. Yang, H. L. Xin, *TEMImageNet training library and AtomSegNet deep-learning models for high-precision atom segmentation, localization, denoising, and deblurring of atomic resolution images*, Scientific Reports, **11**, 5386 (2021)
3. S Zheng, CY Wang, X Yuan, HL Xin, *Super-compression of large electron microscopy time series by deep compressive sensing learning*, Patterns, **2**,100292 (2021)
4. R. Zhang, C. Wang, M. Ge, and H. L. Xin, *Accelerated Degradation in a Quasi-Single-Crystalline Layered Oxide Cathode for Lithium-Ion Batteries Caused by Residual Grain Boundaries*, Nano Letters, **22**, 3818–3824 (2022)
5. C. Wang, R. Zhang, C. Siu, M. Ge, K.Kisslinger, Y. Shin, and H. L. Xin, *Chemomechanically stable ultrahigh-Ni single-crystalline cathodes with improved oxygen retention and delayed phase degradations*, Nano Letters, **21**, 9797–9804 (2021)
6. C. Wang, R. Zhang, K. Kisslinger, and H. L. Xin, *Atomic-scale observation of O1 faulted phase-induced deactivation of LiNiO2 at high voltage*, Nano Letters, **21**, 3657-3663 (2021)
7. C Wang, L Han, R Zhang, H Cheng, L Mu, K Kisslinger, P Zou, Y Ren, P Cao, F Lin, HL Xin, *Resolving atomic-scale phase transformation and oxygen loss mechanism in ultrahigh-nickel layered cathodes for cobalt-free lithium-ion batteries*, Matter, **4**, 2013-2026 (2021)

Transport and Imaging of Mesoscopic Phenomena in Novel Low-Dimensional Materials

Yacoby, Amir - Harvard University, yacoby@physics.harvard.edu

Jarillo-Herrero, Pablo – MIT, pjarillo@mit.edu

Keywords: Magnons, Chern Insulators, Chemical Potential, Graphene, Topological

Research Scope

Moiré materials open an entirely new platform for exploring the interplay between band structure, interactions, symmetry and topology. Strong effects of interaction can result from antiferromagnetic correlations as is commonly found in high temperature superconductors. Alternatively, the effects of interactions can be strengthened by reducing the role of kinetic energy as is commonly done in quantum Hall systems. Interestingly, moiré materials are a new class of materials where both types of effects can be present simultaneously, even at zero magnetic field, leading to a plethora of new correlated topological phases. Here we harness the expertise of our groups in synthesis, fabrication, and novel measurement techniques to unravel and elucidate some of the mysteries of moiré materials.

Recent Progress

During the past two years we have investigated the following topics.

Thermodynamics of free and bound magnons in graphene

Symmetry-broken electronic phases support neutral collective excitations. For example, monolayer graphene in the quantum Hall regime hosts a nearly ideal ferromagnetic phase at filling factor $\nu=1$ that spontaneously breaks spin rotation symmetry. This ferromagnet has been shown to support spin-wave excitations known as magnons which can be generated and detected electrically. While long-distance magnon propagation has been demonstrated via transport measurements, important thermodynamic properties of such magnon populations—including the magnon chemical potential and density—have thus far proven out of reach of experiments. Here, we present local measurements of the electron compressibility under the influence of magnons, which reveal a reduction of the $\nu=1$ gap by up to 20%. Combining these measurements with estimates of the temperature, our analysis reveals that the injected magnons bind to electrons and holes to form skyrmions, and it enables extraction of the free magnon density, magnon chemical potential, and average skyrmion spin. Our methods furnish a novel means of probing the thermodynamic properties of charge-neutral excitations that is applicable to other symmetry-broken electronic phases.

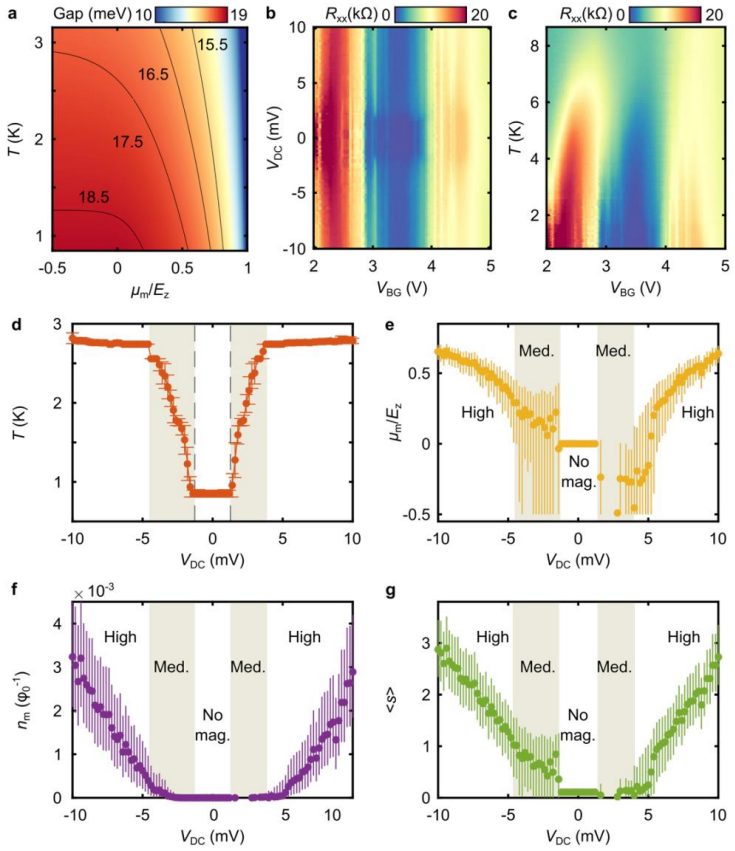

Fig. 1- Thermodynamics of free and bound magnons. a, Filling 1 gap as a function of magnon chemical potential. b, Longitudinal resistance as a function of bias near filling 1. c, Longitudinal resistance as a function of temperature. d, Electron temperature as a function of DC bias. e, Magnon chemical potential vs DC bias. f, Number of free magnons vs DC bias. g, Average spin of bound skyrmions.

Integer and fractional Chern insulators in twisted graphene

The interplay between strong electron-electron interactions and band topology can lead to novel electronic states that spontaneously break symmetries. The discovery of flat bands in magic-angle twisted bilayer graphene (MATBG) with nontrivial topology has provided a unique platform in which to search for new symmetry-broken phases. Recent scanning tunneling microscopy and transport experiments have revealed a sequence of topological insulating phases in MATBG with Chern numbers $C=\pm3,\pm2,\pm1$ near moiré band filling factors $\nu=\pm1,\pm2,\pm3$, corresponding to a simple pattern of flavor-symmetry-breaking Chern insulators. Here, we report high-resolution local compressibility measurements of MATBG with a scanning single electron transistor that reveal a new sequence of incompressible states with unexpected Chern numbers observed down to zero magnetic field. We find that the Chern numbers for eight of the observed incompressible states are incompatible with the simple picture in which the $C=\pm1$ bands are sequentially filled. We show that the emergence of these unusual incompressible phases can be understood as a consequence of broken translation symmetry that doubles the moiré unit cell and splits each $C=\pm1$ band into a $C=\pm1$ band and a $C=0$ band. Our findings significantly expand the known phase diagram of MATBG, and shed light onto the origin of the close competition between different correlated phases in the system. Additionally, we observe Chern states with fractional Chern numbers down to 5T. These states are lattice analogues of fractional quantum Hall states that carry fractional charge.

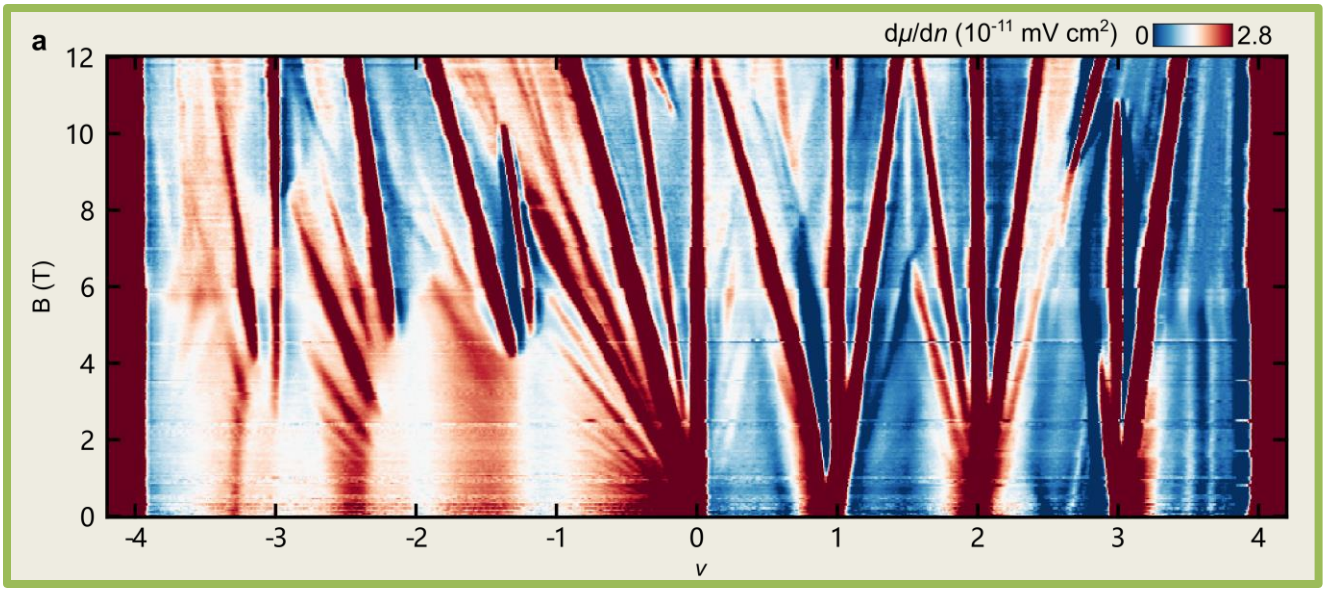

Fig. 2- Inverse compressibility measurements of twisted bilayer graphene measured as a function of filling and magnetic field. Sloped features correspond to Chern states.

Thermodynamic measurements on twisted bilayer graphene

Interaction-driven spontaneous symmetry breaking lies at the heart of many quantum phases of matter. In moiré systems, broken spin/valley 'flavour' symmetry in flat bands underlies the parent state from which correlated and topological ground states ultimately emerge. However, the microscopic mechanism of such flavour symmetry breaking and its connection to the low-temperature phases are not yet understood. In this work we investigate the broken-symmetry many-body ground state of magic-angle twisted bilayer graphene (MATBG) and its nontrivial topology using simultaneous thermodynamic and transport measurements. We directly observe flavour symmetry breaking as pinning of the chemical potential at all integer fillings of the moiré superlattice, demonstrating the importance of flavour Hund's coupling in the many-body ground state. The topological nature of the underlying flat bands is manifested upon breaking time-reversal symmetry, where we measure for the first time the energy gaps corresponding to Chern insulator states with Chern numbers 3, 2, 1 at filling factors 1, 2, 3, respectively, consistent with flavour symmetry breaking in the Hofstadter butterfly spectrum of MATBG. Concurrent measurements of resistivity and chemical potential provide the temperature-dependent charge diffusivity of MATBG in the strange-metal regime —a quantity previously explored only in ultracold atoms. Moreover, we extract the entropy of the system, which reveal that there is a Pomeranchuk effect in MATBG, analogous to the ^{3}He system. Our results reveal a unified framework for understanding interactions in the topological bands of MATBG.

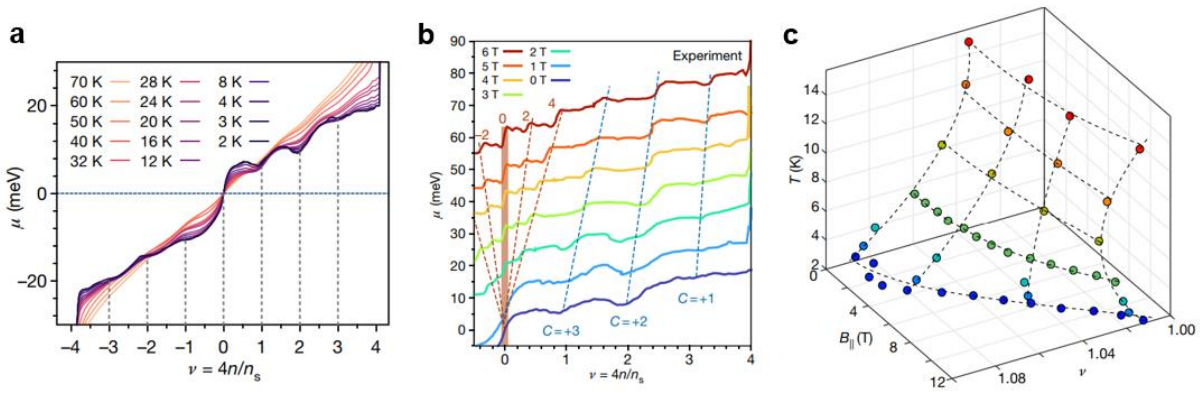

Fig. 3- Chemical potential measurements reveal Flavour Hund's coupling and cascade of phase transitions (a), correlated Chern insulators (b), and Pomeranchuk effect (c).

Strongly coupled superconductivity and Pauli limit violation in twisted trilayer graphene

We discover a new moiré superconductor in magic-angle twisted trilayer graphene (MATTG), which has better tunability of its electronic structure and superconducting properties than magic-angle twisted bilayer graphene. Measurements of the Hall effect and quantum oscillations as a function of density and electric field enable us to determine the tunable phase boundaries of the system in the normal metallic state. Zero-magnetic-field resistivity measurements reveal that the superconductivity is very closely related to the broken-symmetry phase that emerges from two carriers per moiré unit cell. We also find that the superconducting phase is suppressed and bounded at the Van Hove singularities that partially surround the broken-symmetry phase, which is difficult to reconcile with weak-coupling Bardeen–Cooper–Schrieffer theory. Moreover, we can tune the system to the ultrastrong-coupling regime, characterized by a Ginzburg–Landau coherence length that reaches the average inter-particle distance, and very large T_{BKT}/T_F values, in excess of 0.1 (where T_{BKT} and T_F are the Berezinskii–Kosterlitz–Thouless transition and Fermi temperatures, respectively). Furthermore, when external magnetic fields are applied in parallel direction to the two-dimensional plane, the superconducting states persisted up to high fields that are 2~3 times larger than the nominal Pauli limit. Under certain displacement and magnetic fields, new superconducting phase emerges. Our results establish reveal that the superconductivity in MATTG, and possibly MATBG, can be of highly unusual character.

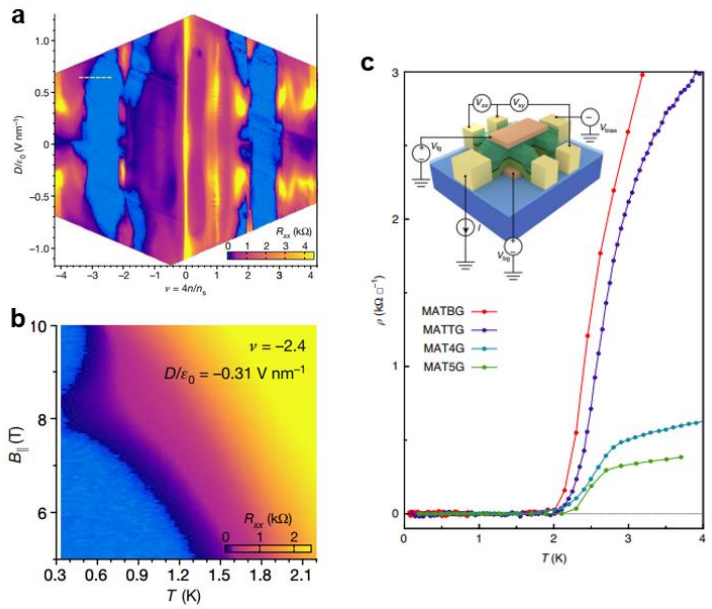

Fig. 4- Magic-angle multilayer graphene family. (a) Phase diagram of MATTG versus electric displacement and carrier density. (b) Pauli limit violation and reentrant superconductivity in MATTG. (c) All members of the newly established magic-angle twisted graphene family show robust superconductivity.

Establishing a magic-angle twisted graphene family

MATBG and MATTG, which have been the only robust moiré superconductors, are part of a hierarchy of magic-angle graphene systems, which exhibit a series of twist angles for different number of twisting layers. These structures, despite having different overall electronic band structures, share the same kind of flat band. We experimentally realize magic-angle twisted 4-layer and 5-layer graphene structures, and show that they also exhibit robust superconductivity. With the application of electric displacement and magnetic fields, it is revealed that there is a noticeable difference between MATBG and multilayer family members, mainly arising from the fact that MATBG has large orbital coupling in comparison. This effect enables the observation of nematicity of MATBG in the superconducting transition upon application of in-plane magnetic fields, which is a spontaneous rotational symmetry breaking. Our results establish the alternating-twist magic-angle multilayer graphene as a family of moiré superconductors, which shows the importance of flat bands in forming moiré superconductivity and provides insights into the design of a new class of unconventional superconductors.

Publications

1. J. M. Park* Y. Cao*, L. Xia, S. Sun, K. Watanabe, T. Taniguchi, P. Jarillo-Herrero. “Robust superconducti vity in magic-angle multilayer graphene family.” *Nature Materials 21*, 877-883 (2022).
2. A. T. Pierce*, Y. Xie*, S. H. Lee, P. R. Forrester, D. S. Wei, K. Watanabe, T. Taniguchi, B. I. Halperin, A. Yacoby "Thermodynamics of free and bound magnons in graphene" Nature Physics **18**, 37 (2022).
3. Y. Xie*, A. T. Pierce*, J. M. Park*, D. E. Parker, E. Khalaf, P. Ledwith, Y. Cao, S. H. Lee, S. Chen, P. R. Forrester, K. Watanabe, T. Taniguchi, A. Vishwanath, P. Jarillo-Herrero, A. Yacoby "Fractional Chern insulators in magic-angle twisted bilayer graphene" Nature **600**, 439 (2021).
4. Y. Cao*, J. M. Park*, K. Watanabe, T. Taniguchi, P. Jarillo-Herrero, “Pauli-limit violation and re-entrant s uperconductivity in moiré graphene.” *Nature 595*, 526–531 (2021).
5. J. M. Park*, Y. Cao*, K. Watanabe, T. Taniguchi, P. Jarillo-Herrero, “Flavour Hund’s coupling, Chern gap s and charge diffusivity in moiré graphene.” *Nature 592*, 43–48 (2021).

6. J. M. Park*, Y. Cao*, K. Watanabe, T. Taniguchi, P. Jarillo-Herrero, “Tunable strongly coupled supercond uctivity in magic-angle twisted trilayer graphene.” *Nature 590,* 249–255 (2021).
7. A. Rozen*, J. M. Park*, U. Zondiner*, Y. Cao*, D. Rodan-Legrain, T. Taniguchi, K. Watanabe, Y. Oreg, A . Stern, E. Berg, P. Jarillo-Herrero, S. Ilani, “Entropic evidence for a Pomeranchuk effect in magic angle gra phene.” *Nature 592*, 214–219 (2021).
8. A. T. Pierce*, Y. Xie*, J. M. Park*, E. Khalaf, S. H. Lee, Y. Cao, D. E. Parker, P. R. Forrester, S. Chen, K. Watanabe, T. Taniguchi, A. Vishwanath, P. Jarillo-Herrero, and A. Yacoby "Unconventional sequence of correlated Chern insulators in magic-angle twisted bilayer graphene" Nature Physics **17**, 1210 (2021).
9. T. X. Zhou, J. J. Carmiggelt, L. M. Gächter, I. Esterlis, D. Sels, R. J. Stöhr, C. Du, D. Fernandez, J. F. Rodriguez-Nieva, F. Büttner, E. Demler, and A. Yacoby "A Magnon Scattering Platform" PNAS **118**, 25 (2021).
10. M. Ku*, T. X. Zhou*, Q. Li, Y. J. Shin, J. K. Shi, C. Burch, L. E. Anderson, A. T. Pierce, Y. Xie, A. Hamo, U. Vool, H. Zhang, F. Casola, T. Taniguchi, K. Watanabe, P. Kim, A. Yacoby, R. L. Walsworth "Imaging Viscous Flow of the Dirac Fluid in Graphene." Nature **583**, 537 (2020).

Atomic-scale characterization of strain-tunable moiré quantum materials

Matthew Yankowitz, Department of Physics and Materials Science & Engineering, University of Washington, Seattle, WA 98195

Keywords: scanning tunneling microscopy, moiré quantum materials, transition metal dichalcogenides, uniaxial strain

Research Scope

Understanding and controlling the properties of strongly correlated states of matter is a long-standing goal in condensed matter physics. A wide array of interesting phases can arise in systems of strongly interacting electrons, including high-temperature superconductivity, magnetism, electron crystals, and more. However, achieving a complete understanding of the physics of these strongly correlated states has been extremely challenging, as it is nearly impossible to exactly calculate the ground state of a large number of interacting electrons. As an alternative approach, these states can be 'simulated' within a simpler model system that nevertheless captures the salient features of the full many-body quantum problem. Recent work has shown that the Hubbard model can be simulated in moiré systems constructed from monolayer transition metal dichalcogenide (TMD) building blocks [1]. However, the scope of the Hamiltonians that can be achieved is currently limited by restrictions in the shapes of moiré lattices that can be created. The goal of this project is to develop a new technique to directly modify the moiré geometry using various forms of in-plane strain, including uniaxial, biaxial, and shear strain. Our approach will enable the simulation of a more general class of extended Hubbard model Hamiltonians with continuous tuning capabilities. We are integrating the strain platform into a scanning tunneling microscope (Fig. 1), enabling atomic- and moiré-scale characterization of the emergent many-body physics in these systems as a function of controlled mechanical deformation of the samples.

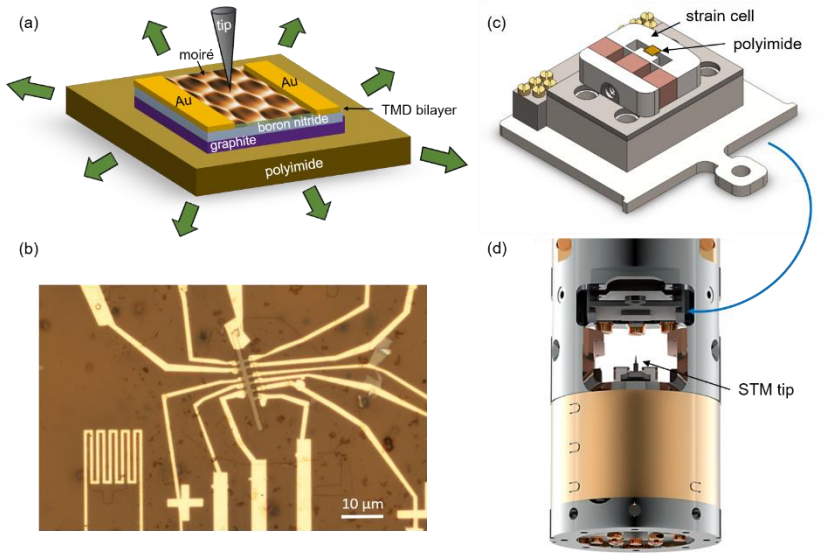

Figure 1. (a) Cartoon schematic of strain applied to a moiré heterostructure device. The surface of the sample is probed by an STM tip. (b) Optical micrograph of a vdW heterostructure device fabricated directly onto a thin polyimide substrate. (c) Custom uniaxial strain cell designed to fit onto a flag-style STM plate with 10 electrical contacts (gold screws). A polyimide film (orange) is epoxied across a gap in the sample holder, and can be stretched by the piezos. (d) The sample holder slides into the STM chamber as indicated by the blue arrow, and is cooled to 4.5 K. A 5 T magnet (not shown) surrounds the microscope.

Recent Progress

Our recent progress is limited since this program was established just two months ago. Nevertheless, the project is strongly supported by our foundational preliminary work in developing continuous cryogenic strain-tuning capabilities for van der Waals devices. Although strain has been widely used to tune the properties of bulk crystals, it has so far been extremely challenging to apply continuous uniaxial strain to atomically-thin vdW heterostructure devices with numerous electrical contacts and gate electrodes. Our group has led an effort (in collaboration with Prof. Jiun-Haw Chu at the University of Washington) to develop a novel experimental technique in which purely uniaxial tensile or compressive strain is applied to arbitrary vdW heterostructure devices. Figure 2 shows a picture of the experimental strain setup used for cryogenic transport measurements.

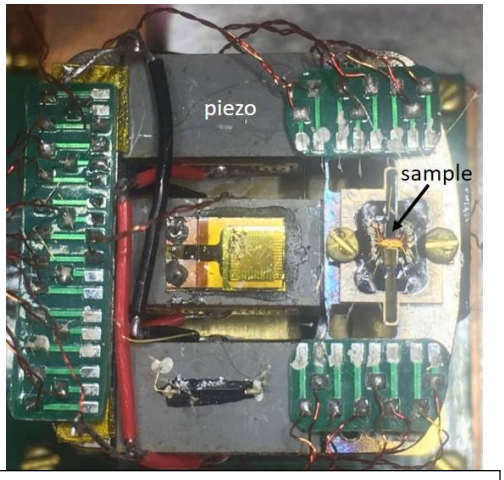

Figure 2. Home-built strain cell, assembled from three piezoelectric stacks and custom titanium end-plates. The sample is affixed

As a proof of principle, we have measured magnetotransport in magic-angle twisted bilayer graphene (tBLG) with dynamic uniaxial strain down to millikelvin temperatures. Figure 3a shows the basic transport characterization of a device with θ = 1.19° at the two extreme accessible values of the piezo bias, V_p, determining the amount of uniaxial strain applied to the sample. Although the basic transport features of the device are similar for both tensile and compressive strain, we see clear changes in the measured resistance over certain portions of the flat band. The temperature dependence of the elastoresistance reveals important insights into the role of strain on the tBLG transport. Fig. 3b shows resistance measurements near ν = -2 at various values of V_p and temperature. At this band filling, we find that the resistance grows as the sample is stretched (i.e., towards more positive V_p) at all temperatures up to at least 40 K. We quantify the sample's response to strain by calculating the gauge factor, $GF = (\Delta R/R)/\varepsilon$, where ε is the magnitude of the applied uniaxial strain, and ΔR is the change in device resistance with strain. Fig. 3c shows the temperature dependence

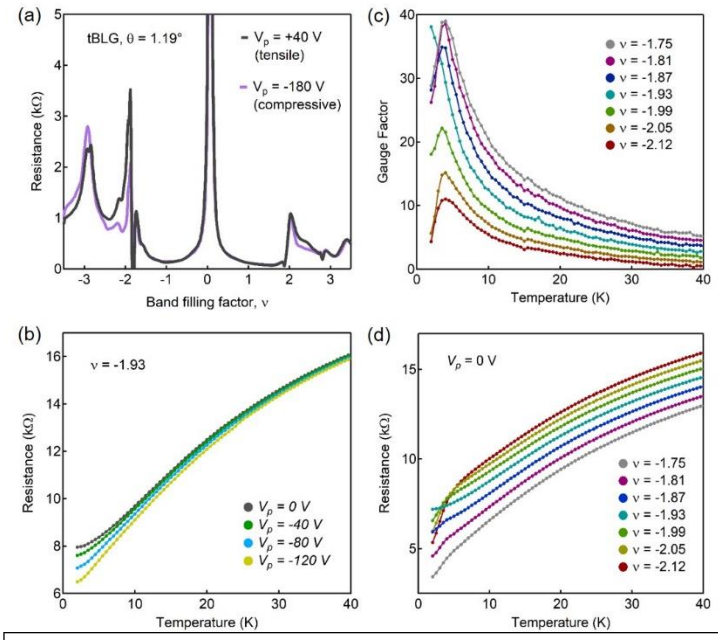

Figure 3. (a) Resistance of a tBLG device with θ = 1.19° at different values of the piezo bias. (b) Temperature dependence of the resistance at various V_p at ν = -1.93. (c) Temperature dependence of the gauge factor and (d) resistance at various filling factors near ν = -2.

of the gauge factor at various ν surrounding half-filling. We find that GF grows as the temperature decreases, but eventually reaches a maximum and then decreases. The gauge factor is an order of magnitude larger than in typical metals, indicating a non-trivial origin. Additionally, the turnover temperature depends sensitively on ν. Very near $\nu = 2$, we find that GF is well described by a Curie-Weiss law dependence, in which it scales as $1/T$ down to the lowest measured temperature. Interestingly, this behavior arises around the same $\nu = -1.9$ in which the temperature dependence of the resistance is the most linear down to the base temperature (Fig. 3d), indicating a possible connection between the strain response and quantum critical scattering in tBLG.

We also find that strain can control the magnetic order in this sample, substantially modifying the anomalous Hall amplitude at fixed band filling (Fig. 4a). We are able to deterministically switch the orbital magnetic state by cycling the strain at zero external field (Fig. 4b). Overall, our results indicate that strain can couple sensitively to the electronic properties of moiré materials. Although tBLG is not the focus of the work in this program, these preliminary results demonstrate the feasibility of using strain to dynamically modify the properties of a moiré vdW heterostructure.

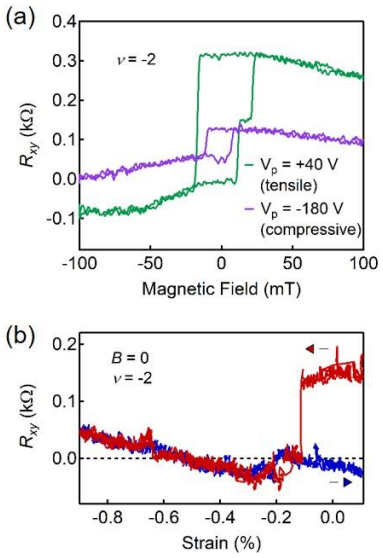

Figure 4. (a) R_{xy} measured as B is swept back and forth at $\nu = -2$ with different values of applied strain. (b) The magnetic state can be switched from positive to negative while at $B = 0$ by cycling the strain. The temperature is 50 mK.

Future Plans

Using our newly developed strain techniques, we plan to investigate an array of strongly correlated states realized in a number of different TMD moiré platforms, including aligned WSe_2/WS_2, and twisted bilayers of WSe_2 and WTe_2. Our work in the coming years will address three intertwined objectives in which we use strain to study and control the properties of (i) the moiré structure and extended Hubbard model parameters, (ii) generalized Wigner crystals, and (iii) arrays of Luttinger liquids.

To address our first objective, we plan to benchmark our technique by imaging the atomic and moiré lattices as we continuously tune the applied strain. We will compare these measurements across different types of applied in-plane strain (e.g., uniaxial, biaxial, shear) in order to build a basic understanding of the atomic- and moiré-scale strain response of these materials with different forms of deformation. We will then make use of a correlated discharge effect of electrons tunneling into the moiré trapping sites [2] in order to extract the extended Hubbard model parameters as the sample is deformed, breaking the intrinsic rotational symmetry of the moiré.

To address our second objective, we will study the generalized Wigner crystal states that arise at rational fractional filling of the moiré bands of twisted WSe_2 and aligned WSe_2/WS_2 [3]. Monte Carlo simulations raise the possibility of competing charge-ordered states at a given fractional band filling, distinguished by either broken or preserved rotational symmetry. We will attempt to tune between these two states with applied strain.

To address our third objective, we will create twisted bilayers of WTe_2. Recently, evidence for two-dimensional arrays of Luttinger liquids has been reported from transport measurements in

such samples [4]. We will investigate these structures with STM while tuning the coupling strength between the 1D Luttinger liquids with strain.

Our work will be supported by the development of novel experimental techniques for applying continuous strain combined with in situ STM characterization. This will involve building strain cells small enough to mount directly onto the STM sample plate, following the design scheme used in the preliminary transport experiments. We will additionally explore the development of new strain cell geometries that may enable the application of biaxial and shear strain.

References

1. Y. Tang, L. Li, T. Li, Y. Xu, S. Liu, K. Barmak, K. Watanabe, T. Taniguchi, A. H. MacDonald, J. Shan and K. F. Mak, *Simulation of Hubbard model physics in WSe_2/WS_2 moiré superlattices*, Nature **579**, 353 (2020).

2. H. Li, S. Li, M. H. Naik, J. Xie, X. Li, E. Regan, D. Wang, W. Zhao, K. Yumigeta, M. Blei, T. Taniguchi, K. Watanabe, S. Tongay, A. Zettl, S. G. Louie, M. F. Crommie and F. Wang, *Imaging local discharge cascades for correlated electrons in WS_2/WSe_2 moiré superlattices*, Nature Physics **17**, 1114 (2021).

3. Y. Xu, S. Liu, D. A. Rhodes, K. Watanabe, T. Taniguchi, J. Hone, V. Elser, K. F. Mak, and J. Shan, *Correlated insulated states at fractional fillings of moiré superlattices*, Nature **587**, 214 (2020).

4. P. Wang, G. Yu, Y. H. Kwan, Y. Jia, S. Lei, S. Klemenz, F. A. Cevallos, R. Singha, T. Devakul, K. Watanabe, T. Taniguchi, S. L. Sondhi, R. J. Cava, L. M. Schoop, S. A. Parameswaran, and S. Wu, *One-dimensional Luttinger liquids in a two-dimensional moiré lattice*, Nature **605**, 57 (2022).

Probing Correlated Superconductors and Their Phase Transitions on the Nanometer Scale

Ali Yazdani

Department of Physics

Princeton University, Princeton, NJ 08544

Research scope:

Studies of correlated and topological quantum states of matter are at the forefront of research in condensed matter physics. With the advent and rapid advance of utilizing two-dimensional (2D) materials as a platform to create novel nanostructures, the study of 2D materials has entered an exciting new chapter. The ability to engineer electronic correlations and topology using crystalline monolayer materials and their stacks has become a powerful approach to creating new quantum phases in materials. The discovery of superconductivity and plethora of correlated and topological phases in bilayers of graphene that are stacked and twisted at a magic-angle has catalyzed this emerging area of research in condensed matter physics. The possibility that these chemically pristine materials can elucidate long-standing puzzles, such as understanding high temperature superconductivity in correlated electron systems, is tantalizing. At the same time, the opportunity to create fundamentally new phenomena, such as strongly correlated topological phases without a magnetic field that host exotic quasiparticles, is motivating intense exploration of 2D materials and their stacks.

Over the last few years, our program made a fundamental shift to develop the capabilities to apply high-resolution techniques with the scanning tunneling microscope (STM) to study crystalline devices made of 2D materials and their stacks. Over the last two decades, we have continuously advanced the application of these techniques to a wide range of complex materials, from high-temperature superconductors and heavy fermion systems to topological insulators and semimetals. This shift allowed us to explore some of the deep questions linked to complex bulk materials by utilizing new methodologies afforded by advances in 2D crystalline materials and devices. This current program broadly expands this exploration by focusing on understanding superconducting, correlated, and topological phases in two classes of 2D crystalline materials and their stacks. We have explored the rich physics of magic-angle twisted bilayer graphene (MATBG) and monolayer WTe_2 and their stacks with our high-resolution techniques.

The program builds on the last cycle's fundamental breakthroughs that have uncovered signatures of strong correlations in MATBG, discovered new correlation-driven topological phases, and established strong evidence for unconventional superconductivity in this system. We are focused on fundamental questions as to the nature of superconducting, correlated, and topological phases in MATBG, and monolayer WTe2 and their stacks. The program will also expand on the application of new microscopy and spectroscopy techniques — from novel methods of analysis that we successfully utilized with our recent direct observation of topological defects in correlated quantum phases of monolayer graphene at high magnetic fields (16 Tesla) — to the development and deployment of new experimental tools. We are establishing capabilities for millikelvin atomic force microscopy (AFM), developing charge sensing microscopy and

spectroscopy techniques using monolayer graphene as a sensor, and implementing scanning noise spectroscopy to explore the novel quantum phenomena in our crystalline devices.

Highlights of breakthroughs under the DOE grant in last two years:

- Discovery of a cascade of transitions between the correlated electronic states of magic-angle twisted bilayer graphene (Nature 2020a) (this was discussed in 2020 abstract) [1]
- Discovery of correlation-driven Chern insulators in MATBG (Nature 2020b) [2]
- Evidence for nodal and unconventional nature of superconductivity in magic angle twisted bilayer graphene. (Nature 2021) [3]
- Visualizing broken symmetry and topological excitations in quantum Hall ferromagnets (Science 2021) [4]

Recent Progress:

A. Discovery of correlation-driven Chern insulators in MATBG (Nature 2020b) [2]

Early studies recognized the possible emergence of topological electronic states in the MATBG of this system and that potentially, an underlying alignment of the MATBG with the hexagonal BN underneath can gap the single-particle Dirac nodes of this system and give rise to a Chern insulating phase. Experimental studies uncovered a Chern insulating phase (with a C = +1 phase) near integer filling of the moiré flat band of n = +3 relative to the charge neutral point. Although interactions play a role in the emergence of this phase, the primary driving element behind this transition is breaking of the sub-lattice symmetry due to alignment with the h-BN. In a 2020 *Nature* paper, we reported that Chern insulating phases can be driven by interactions alone, without alignment with BN, but stabilized with the application of weak magnetic field. Typically, Chern insulating phases are probed using transport measurements of the quantized Hall conductance ($\sigma_{xy} = Ce^2/h$) , however, we developed a new powerful spectroscopic technique to probe such phases. Our technique probes the development of a Chern state by detecting its gap with spectroscopy. We recognized that measurements of the magnetic field dependence of such gaps with density- tuned STM spectroscopy (DT-STS) can identify their topological nature and measure their Chern number (**Figure 1**). The charge density of a Chern insulating phase changes with magnetic field at a rate equal to its quantized Hall conductance, $dn/dB = \sigma_{xy}/e = C/\Phi_0$. Therefore, tuning both the density and the magnetic field measurements allowed us to

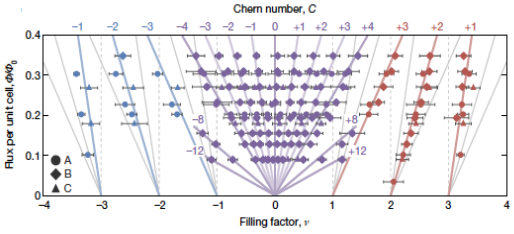

Figure 1. Mapping the field and density dependency of gaps is used to quantify the Chern number associated with insulating states detected with DT-STS in MATBG. The sequence of Chern numbers seen here has also been detected in transport studies. From ref. 14.

identify topological gaps and their associated Chern numbers in DT-STS measurements. With this technique, we uncovered a sequence of topological insulators in MATBG with Chern numbers C = ±1, ±2, ±3, which form near ν = ±3, ±2, ±1 electrons per moiré unit cell, respectively, and are stabilized by modest magnetic fields.

In addition to detecting such phases, STM spectroscopy provided the means to demonstrate that the formation of these phases is fundamentally due to interactions. We show that the Chern gap opens only at the chemical potential, distinguishing them from such phases that might form due to single-particle effects. In addition, we could rule out alignment with h-BN substrate from the STM images as a cause of such a transition. Broadly speaking, the techniques deployed in this methodology will have application to the study of topological phases of any material system using the DT-STS technique.

C. Evidence for unconventional superconductivity in MATBG (Nature 2021) [4]

The emergence of superconductivity at remarkably low carrier densities with doping from correlated insulators in MATBG has raised the intriguing possibility that this system hosts a pairing mechanism that is distinct from that of conventional superconductors, as described by the Bardeen-Cooper-Schrieffer (BCS) theory. While there is strong evidence for electronic correlation in MATBG, recent studies have claimed that unlike correlated insulators, superconductivity persists even when these interactions are partially screened. This suggests that the pairing in MATBG might be conventional in nature, a consequence of the large density of states of its nearly flat bands. Prior to our experiments, there had been no experimental, detailed study to address this significant question, and any conclusive evidence for any mechanism beyond the BCS paradigm has been lacking. In a 2021 *Nature* paper, we used density-tuned scanning tunneling and point-contact spectroscopy (DT-STS, DT-PCS) techniques to show that the superconducting phase of MATBG, specifically when hole-doping its flat valence band, shares a remarkable number of features with unconventional cuprate superconductors (**Figure 2**). Our experiments show a V-shaped gap at low temperatures and the emergence of an unusual pseudogap state as a precursor phase at higher temperatures and higher magnetic fields, from which phase-coherent superconductivity emerges. The low-energy region of the V-shaped gap supports an anisotropic pairing mechanism and the presence of nodes in the superconducting gap function, as anticipated by some theoretical studies; whereas the pseudogap state may signify either pairing without phase coherence or a secondary phase forming above T_c and B_c. We observe a large discrepancy between the tunneling energy gap Δ_T, which far exceeds the mean-field BCS ratio (with $2\Delta_T/k_BT_c \sim 25$) and the energy gap Δ_{AR} extracted from Andreev

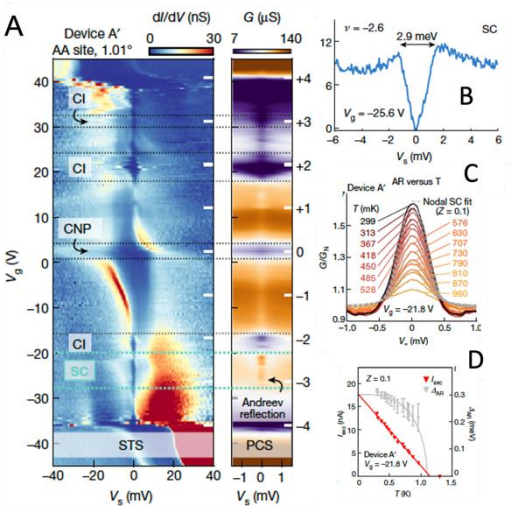

Figure 2. Evidence for unconventional superconductivity in MATBG. (A) DT-STS and DT-PCS measurements showing insulating and superconducting gaps. (B) Nodal tunneling gap of the superconductor, which persists above T_c. (C) Andreev reflection from the superconductor in PCS that vanishes at T_c. (D) Temperature dependence of excess current in PCS. From ref. 15.

reflection spectroscopy ($2\Delta_{AR}/k_BT_c \sim 6$)**.** The dichotomy between PCS Andreev reflection, both in the size of its gap and its disappearance at T_c with the results of STS measurements is remarkably reminiscent of similar behavior in the high-Tc cuprates. Finally, we find that both the pseudogap and superconducting phases are microscopically absent when MATBG is commensurately aligned with the hBN substrate, suggesting that the structural characteristics and/or the C_2T-symmetry of unaligned MATBG are required for the stability of these ground states. Although we cannot rule out a phonon-based pairing mechanism, our results provide key experimental constraints for developing an accurate theory of superconductivity in MATBG.

D. Visualizing broken symmetry and topological excitation in quantum Hall ferromagnets (Science 2021) [3]

Mapping electronic wavefunctions with the STS has the power to distinguish the nature of electronic states in ways that are not possible from other measurements. Although such measurements have been carried out on graphene-based systems for more than a decade, many of the key problems that can benefit from such characterization have been hampered by the fact that the STM tip may act as a local gate and modify the nature of electronic states when the carrier concentration is low. With our efforts to use STM/STS to probe MATBG, we developed several methodologies, such as a better work function match between the STM tip and graphene or cleaning procedures, and very sharp tips that do not locally gate the samples. With these improvements, we explored the unresolved problem of the nature of electronic states for 0^{th} Landau level of monolayer graphene in a magnetic field. Graphene's SU(4) isospin space consisting of spin and valley gives rise to a rich array of quantum Hall ferromagnetism (QHFM) phases, which have been studied using transport and thermodynamic measurements. Particularly intriguing is the electric insulating phase at charge neutrality point at high magnetic fields, because when two out of four isospin flavors are occupied, spin and valley cannot be simultaneously polarized due to Pauli exclusion. Theoretical efforts had predicted a rich phase diagram of four possible broken symmetry QHFM states at charge neutrality. 1) A charge density wave phase and a sublattice that is valley polarized with an un-polarized spin; 2) the spin ferromagnet that is a quantum spin Hall insulator; 3) the canted anti-ferromagnet in which spins on different sublattices point in the near-opposite directions; and 4) intervalley coherent (IVC) states with a Kekulé reconstruction, which is spin unpolarized. While transport studies have constrained aspects of the phase diagram, in the absence of microscopic measurements that probe the order parameter, the nature of the ground state of graphene at charge neutrality was unresolved prior to our experiments.

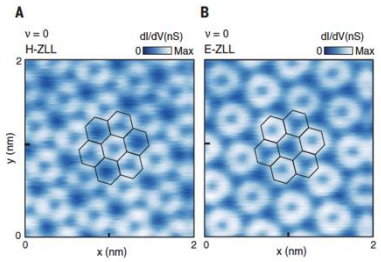

Figure 3. Spectroscopic map of the 0^{th} Landau level's filled and empty states show signature of Kekulé reconstruction of the electronic state and direct visualization of the intervalley coherent state with a bond-like feature of the state's atomic scale wavefunction. From ref. 16.

Visualizing atomic scale electronic wavefunctions with STS, we resolve microscopic signatures of valley ordering in QHFM and fractional quantum Hall phases of graphene. Because of direct mapping of valley degree of freedom to the graphene sublattice, STS provides a powerful tool to examine the nature of valley-polarized/coherent states and the defects in such valley-textured states. At charge neutrality, we observed a field-tuned continuous quantum phase transition from a valley-polarized state at low field to an intervalley coherent state, with a Kekulé distortion of its electronic density, at high fields (**Figure 3**). The Kekulé phase had long been anticipated theoretically. While mapping the valley texture extracted from STS measurements of the Kekulé phase, we visualized valley skyrmion excitations localized near charge defects (**Figure 4**). Skyrmions of such quantum crystals are remarkable topological objects that had been anticipated theoretically; however, they had never been imaged. As we describe here, these techniques can be applied to examine valley-ordered phases and their topological excitations in other systems, such as those in MATBG.

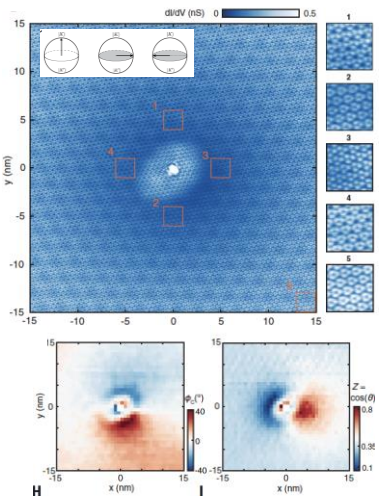

Figure 4. Analysis of the Kekulé pattern around a charge defect shown in the top panels is used to extract valley coherence texture and associated phase angles in the bottom panels. The patterns of the phases are consistent with valley skyrmions (meron-anti-meron pair). From ref. 16.

Other notable research efforts supported by DOE:

Evidence for exitonic insulator in WTe2 (Nature Physics 2021) [4] In our first STM studies of gated monolayer WTe2, we fabricated structures in which a single monolayer of BN protects the WTe_2, thereby preventing oxidation of this air-sensitive material. With the success of this encapsulation process, we were able to perform DT-STS studies of this system to demonstrate that the insulating gap in this system is caused by electronic correlation. These measurements, along with transport measurements carried out by our collaborator on WTe2, showed improved insulating behavior in cleaner samples, providing us with evidence that this system is an exitonic insulator. This is a remarkable situation in that the correlated phase of this material also hosts a topological edge state. These experiments set the stage for the proposed studies on various gated structures of WTe_2.

Spectroscopy of twisted double-bilayer graphene: A tunable moiré system with a correlated and topological flat band (Nature Communication 2021) [5] The twisted, double bilayer graphene (TDBG), where two Bernal bilayers of graphene are stacked with a twist angle, is a moiré system with tunable flat bands. We used DT-STS to directly demonstrate the tunability of the band structure of TDBG with an electric field and to show spectroscopic signatures of electronic correlations and topology for its flat band. We found that our spectroscopic experiments agree with a continuum model of TDBG band structure and revealed signatures of a correlated insulator gap at partial filling of its isolated flat band. In this study we also probed the topological properties of this flat band with the application of a magnetic field, which leads to valley polarization and the splitting of Chern bands with a large, effective g-factor.

DOE-supported publications: A total of 12 publications resulted from work performed during the 2020-22 grant period, including three papers in *Nature*, one paper in *Science*, and one paper in *Nature Physics*. The papers are listed below.

Future plans:

Our plans moving forward will focus on the following key ideas:

1. Our work on MATBG will focus on wavefunction imaging of the correlated insulators and superconducting phase to uncover the nature of these states. Our theoretical work with collaborators show how such measurements can distinguish between different ground states. [6] The work that is described above on broken symmetry states on graphene shows that such measurements are possible.

2. Our AFM module has been completed and awaiting commissioning on our instrument after our latest experiments on MATBG is concluded.

3. The use of graphene as a sensor layer has started and initial experiments using graphene as a sensor for quantum Hall states of another graphene layer are being used to full develop the technique and its spatial resolution for charge sensing. This technique is also being used for measurements of electronic compressibility, which will be invaluable if it can be performed on sub-nanometer length scales.

Publications supported by the DOE-BES (2020-2022):

In addition to publications directly related to DOE-BES projects, the DOE funding supports the instrumentation in our lab that has also assisted other projects. The publications from these projects benefiting from DOE support are also included in the list below (marked as partially supported by DOE).

1. D. Wong, K. P. Nuckolls, M. Oh, B. Lian, Y. Xie, S. Jeon, K. Watanabe, T. Taniguchi, B. A. Bernevig and A. Yazdani, "Cascade of transitions between the correlated electronic states of magic-angle twisted bilayer graphene," Nature **582**, 198-202 (2020). https://doi.org/10.1038/s41586-020-2339-0.

2. K. P. Nuckolls, M. Oh, D. Wong, B. Lian, K. Watanabe, T. Taniguchi, and B. A. Bernevig, Ali Yazdani, "Strongly Correlated Chern Insulators in Magic-Angle Twisted Bilayer Graphene," Nature **588**, 610-615 (2020). https://doi.org/10.1038/s41586-020-3028-8.

3. M. Oh, K. P. Nuckolls, D. Wong, R. L. Lee, X. Liu, K. Watanabe, T. Taniguchi and A. Yazdani, "Evidence for unconventional superconductivity in twisted bilayer graphene," Nature **600**, 240-245 (2021). https://doi.org/10.1038/s41586-021-04121-x.

4. Y. Jia, P. Wang, C.-L. Chiu, Z. Song, G. Yu, B. Jäck, S. Lei, S. Klemenz, F. A. Cevallos, M. Onyszczak, N. Fishchenko, X. Liu, G. Farahi, F. Xie, Y. Xu, K. Watanabe, T. Taniguchi, B. A. Bernevig, R. J. Cava, L. M. Schoop, A. Yazdani and S. Wu, "Evidence for a monolayer excitonic insulator," Nat. Phys. **18**, 87-93 (2022). DOI: 10.1038/s41567-021-01422-w

5. X. Liu, C.-L. Chiu, J. Y. Lee, G. Farahi, K. Watanabe, T. Taniguchi, A. Vishwanath, and A. Yazdani, “Spectroscopy of a tunable moiré system with a correlated and topological flat band,” Nature Communications **12**, 2732 (2021) DOI: 10.1038/s41467-021-23031-0.

6. D. Călugăru, N. Regnault, M. Oh, K. P. Nuckolls, D. Wong, R. L. Lee, A. Yazdani, O. Vafek, B. A. Bernevig, “Spectroscopy of twisted bilayer graphene correlated insulators,” Phys. Rev. Lett. **129**, 117602 (September 2022)

7. B. Lian, Z.-D. Song, N. Regnault, D. K. Efetov, A. Yazdani, and B. A. Bernevig, "Twisted bilayer graphene. IV. Exact insulator ground states and phase diagram," Phys. Rev. B **103**, 205414 (2021). DOI: 10.1103/PhysRevB.103.205414. (Partial support by DOE.)

8. D. Wong, S. Jeon, K. P. Nuckolls, M. Oh, S. C. J. Kingsley and A. Yazdani, “A modular ultra-high vacuum millikelvin scanning tunneling microscope,” Review of Scientific Instruments **91**, 023703 (2020). https://doi.org/10.1063/1.5132872.

9. E. Y. Andrei, D. K. Efetov, P Jarillo-Herrero, A. H. MacDonald, K. F. Mak, T. Senthil, E. Tutuc, A. Yazdani and A. F. Young, “The marvels of moiré materials,” Nat Rev Mater **6**, 201-206 (Viewpoint) (2021). https://doi.org/10.1038/s41578-021-00284-1 (Partial support by DOE.)

10. S. Lei, J. Lin, Y. Jia, M. Gray, A. Topp, G. Farahi, S. Klemenz, T. Gao, F. Rodolakis, J. L. McChesney, C. R. Ast, A. Yazdani, K. S. Burch, S. Wu, N. P. Ong and L. M. Schoop, “High mobility in a van der Waals layered antiferromagnetic metal,” Science Advances **07**, 6, (2020). https://doi.org/10.1126/sciadv.aay6407.

Visualizing the magnetic structure and domain formation using spin-polarized scanning tunneling microscopy and spectroscopy

Ilija Zeljkovic, Boston College

Keywords: spin-polarized scanning tunneling microscopy (SP-STM), antiferromagnetic ordering, magnetic transition, iridates, Fe-based quantum materials.

Research Scope

A complicating factor in unraveling the interplay between magnetism, electronic correlations and chemical doping in many quantum materials lies in the inhomogeneous nature of these systems. The overarching goal of this project is to use spectroscopic-imaging spin-polarized scanning tunneling microscopy (SP-STM) to simultaneously visualize atomic-scale magnetic and electronic structure in novel quantum materials. The project has been largely focused on doped Iridium-based oxides (iridates) Sr_2IrO_4 and $Sr_3Ir_2O_7$. Recently, we have used SP-STM to also image magnetic structure of kagome magnet FeSn and the end-member of Fe(Te,Se) family of superconductors, FeTe.

While it is well-established that the undoped parent state of many iridates hosts an antiferromagnetically (AF) ordered spin-orbit Mott phase, the evolution of the AF order with doping and temperature remains difficult to extract. Specific objectives of our project include visualizing the evolution and collapse of the AF order as a function of charge carrier doping and temperature in iridates, and elucidating the relationship between the inhomogeneous electronic structure and the AF order at the nanoscale. We imaged how temperature fluctuations induce atomic-scale changes to the AF domain distribution in electron-doped $Sr_3Ir_2O_7$ and AF metal FeTe. Cluster analysis theory of the distribution and the size of AF domains in $Sr_3Ir_2O_7$ near the AF transition reveals scale-invariant fractal geometry, suggestive of a continuous transition near criticality. We also for the first time applied SP-STM to a kagome magnet, and revealed robust AF ordering at the surface of a kagome antiferromagnet FeSn. The comprehensive experimental approach we aim to establish here will provide a foundation for the SP-STM studies of other families of quantum materials in which spin, charge and orbital degrees of freedom intertwine to create new states of matter.

Recent Progress

1. Imaging temperature-driven fluctuations of antiferromagnetic domains

One of the intriguing questions in inhomogeneous magnetic systems remains what sets the emergence and distribution of magnetic domains. To that extent, we investigated antiferromagnetic (AF) domain structure and its robustness upon sequential sample cool-downs through the magnetic transition in two different classes of materials: doped Mott insulator iridate $(Sr_{1-x}La_x)_3Ir_2O_7$ (La-doped Sr-327) and FeTe, the end-member of the Fe(Te,Se) superconductor family.

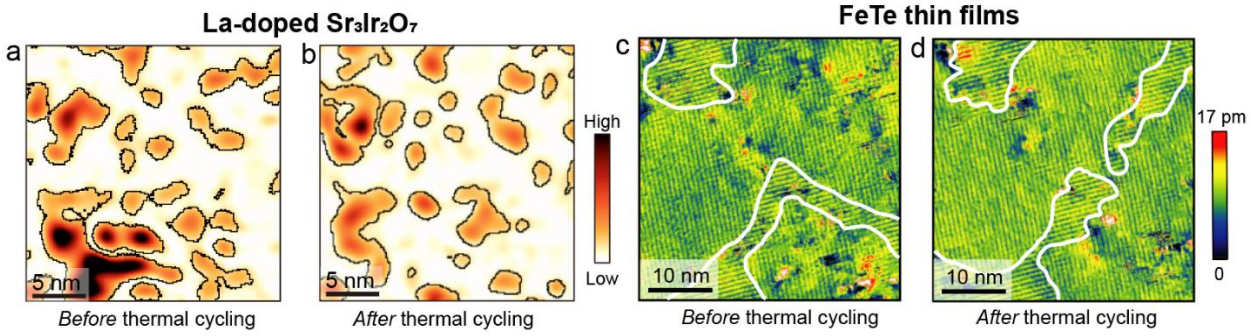

Figure 1. **Temperature-driven AF domain re-configuration.** Local strength of antiferromagnetic order over the same area of the x~0.03 La-doped $Sr_3Ir_2O_7$ extracted from SP-STM images (a) before and (b) after the erasure of AF domains by increasing temperature and cooling the sample back down. White regions indicate the absence of local AF order. (c,d) SP-STM images of an identical region of FeTe (c) before and (d) after thermal cycling showing the change in the direction of AF ordering in different regions. All data was taken at ~4.5 K.

To extract the AF signal, we subtract SP-STM topographs acquired over an identical region of the sample at different magnetic fields (magnetic field serves to "flip" the spin polarization of the tip without significantly affecting the sample) [1]. In La-doped Sr-327 at ~5 K we observe nanoscale AF puddles within a non-magnetic matrix (Fig. 1a). We track an identical area of the sample as a function of temperature, warm up the sample to erase the domains, and cool it back down to ~5 K. The comparison of AF amplitude maps before and after thermal cycling shows a pronounced difference (Fig. 1a,b) [2]. Interestingly, we find that the spectral gapmap over the same region of the sample shows almost no change, thus demonstrating that the spectral gap near Fermi level is not due to short-range AF ordering [2].

We repeat the same experiment on FeTe thin films (Fig. 1c,d), which harbors bi-collinear "stripe"-like AF ordering. We reveal that warming up the sample to only 10-20 K and cooling it back down to ~5 K already significantly re-arranges the domain structure. These experiments show that defect and strain pinning plays only a minor role in the formation of the domains, which are easily perturbed by small thermal fluctuations.

2. *Fractal analysis of AF domains obtained from SP-STM images*

Having imaged the spatial distribution of AF puddles in Sr-327, we studied their size, shape and spatial distribution in more detail [2]. We apply 2D cluster analysis theory, a statistical analysis tool that can be used to probe the strength of electronic correlations and near-critical behavior from the geometric metrics of the clusters [3]. We binarize the AF amplitude map in Fig. 1a based on an intensity cutoff (Fig. 2a). Then using logarithmic binning we plot the relationship between several geometrical descriptors of the clusters, for example area A, perimeter P and several others shown in Fig. 2b-d. Remarkably, we find that the domain area distribution histogram $D(A)$ vs. A shows a linear dependence on a logarithmic scale spanning over 2.5 decades. By examining the dependence of various parameters, one can extract the so-called "critical" exponents [3–6]. For example, by fitting $D(A) = A^{-\tau}$, we determine the critical exponent $\tau = 0.76 \pm 0.18$ (Fig. 2b). The coefficients extracted

from our data suggest that the formation of AF patterns near insulator-to-metal transition in this family of iridates may be influenced by electronic correlations in the presence of disorder.

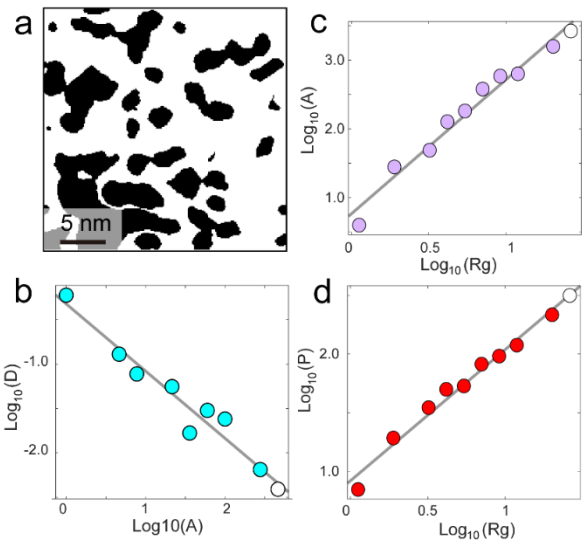

***Figure 2.* Scale-invariant magnetic texture of La-doped $Sr_3Ir_2O_7$ at ~5 K.** (**a**) Binarized AF domains obtained from Fig. 1a. (**b**) Logarithmically binned domain area distribution $D(A)$, following a scale-free power-law distribution ($D(A) \sim A^{-\tau}$) with the critical exponent $\tau = 0.76 \pm 0.18$. (**c,d**) Area (A) and perimeter (P) vs. gyration radius (R_g) plotted using logarithmic binning. Solid lines are power-law fits of $P \sim R_g^{dh^*}$ and $A \sim R_g^{dv^*}$, with critical exponents $dh^* = 1.12 \pm 0.04$ and $dv^* = 1.95 \pm 0.18$. Values of P and R_g are in units of pixels and A is in units of area occupied by a single pixel. The single pixel size in the raw STM topograph used to obtain image in (a) is 1.2 Å by 1.2 Å. Adapted from Ref. [2].

3. *Imaging the surface magnetic structure of a kagome antiferromagnet FeSn using in-situ fabricated spin-polarized tips*

Another goal of the project includes establishing new pathways for spin-resolved tip preparation, and applying SP-STM to new quantum materials of interest. We performed SP-STM measurements of kagome magnet FeSn by using conventional spin-averaged W tips prepared *in-situ* by scanning on top of FeSn (Figure 3). FeSn is a layered antiferromagnet composed of alternating Fe_3Sn layers and Sn layers: Fe spins within each layer align ferromagnetically, but couple antiferromagnetically between adjacent layers. Despite the well-known magnetic structure in the bulk, magnetic ordering at the surface and its tunability with external perturbations was yet

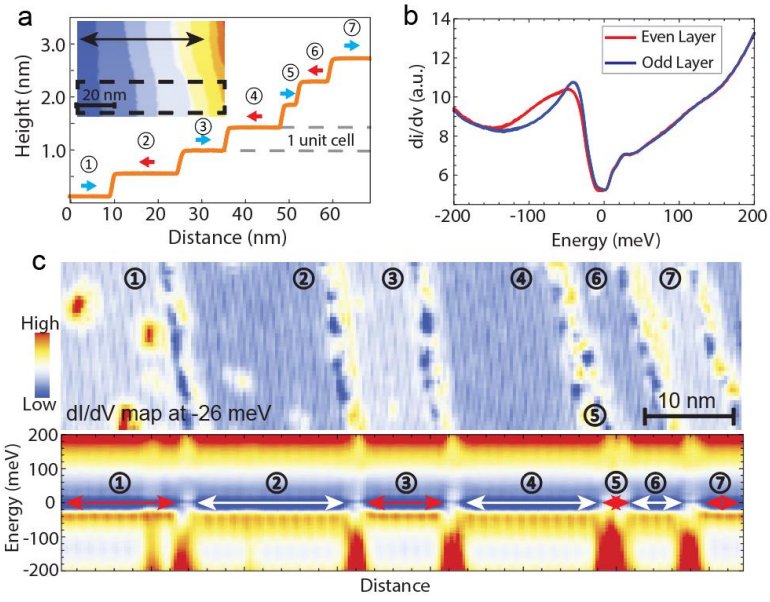

***Figure 3.* SP-STM imaging of the layered AF structure of FeSn. (a)** A topographic line profile along the black line in the inset. The red and blue arrows denote the sample spins. Inset shows an STM topograph of a region containing 7 unit cell step heights (Sn termination) using a spin-polarized tip. **(b)** Average dI/dV spectra taken over even (red curve) and odd (blue curves) steps in (a). Note that 1st, 3rd, 7th layer have exactly overlapping spectra (the blue one); 2nd, 4th, 6th layers also share same spectrum (red one). **(c)** Upper panel is a dI/dV map across the 7 steps (same region as the dashed rectangle in panel (a)); the lower panel is a dI/dV linecut taken across the same region.

to be fully investigated. Experimentally establishing this has been essential for several reasons. First, given the broken crystal symmetry at the surface, the magnetic structure may be different than that in the bulk. Dichotomy between surface and bulk magnetism has indeed been hypothesized to occur in other magnetic topological systems [8]. Second, surface magnetization can lead to the transition from massless to massive Dirac fermions [9], the latter of which in principle carrying a non-trivial Chern number.

To create a spin-polarized tip from a non-magnetic W tip, we intentionally inject the tip into the sample by one to a few nanometers, which likely leads to the tip picking up a cluster of magnetic atoms from the sample; the tip in turn becomes spin-polarized. This is demonstrated by performing spectroscopic measurements across a series of Sn-layer terminated steps (Fig. 3a). In particular, we observe a difference between dI/dV spectra acquired on consecutive terraces (supposed to be nominally identical except for the direction of Fe spin) and the staggered modulation of dI/dV conductance (Fig. 3b,c). Our experiments provide the first visualization of magnetic ordering at the surface of a kagome magnet and demonstrate that the surface AF structure in this material is consistent with that in the bulk.

Future Plans

We will continue to study the effects of substituting Ir for Ru in this family of iridates, which in contrast to the expected electron doping by La at the Sr site, effectively hole-dope the system. We will utilize the newly installed vector magnet with rotating in-plane magnetic field to precisely tune the tip's magnetization direction in different in-plane directions (as opposed to using out-of-plane magnetic field only that we have used in all our SP-STM experiments thus far). We will also begin to explore other oxides beyond Ruddlesden-Popper iridates, in which the interplay of magnetism and electron correlation gives rise to novel phenomena.

References

1. Zhao, H. *et al.* Atomic-scale fragmentation and collapse of antiferromagnetic order in a doped Mott insulator. *Nat. Phys.* **15**, 1267–1272 (2019).
2. Zhao, H. *et al.* Imaging antiferromagnetic domain fluctuations and the effect of atomic scale disorder in a doped spin-orbit Mott insulator. *Sci. Adv.* **7**, abi6468 (2021).
3. Phillabaum, B., Carlson, E. W. & Dahmen, K. A. Spatial complexity due to bulk electronic nematicity in a superconducting underdoped cuprate. *Nat. Commun.* **3**, 915 (2012).

Publications

He Zhao, Zach Porter, Xiang Chen, Stephen D. Wilson, Ziqiang Wang and Ilija Zeljkovic, "Imaging antiferromagnetic domain fluctuations and the effect of atomic-scale disorder in a doped spin-orbit Mott insulator", ***Science Advances*** **7**, abi6468 (2021)

Hong Li, He Zhao, Qiangwei Yin, Qi Wang, Zheng Ren, Shrinkhala Sharma, Hechang Lei, Ziqiang Wang and Ilija Zeljkovic, "Spin-polarized imaging of the antiferromagnetic structure and field-tunable bound states in kagome magnet FeSn", ***Scientific Reports*** **12**, 14525 (2022)

Shrinkhala Sharma, Hong Li, Zheng Ren, He Zhao and Ilija Zeljkovic, "Evolution of antiferromagnetic domains with thermal cycling in FeTe thin films", *in preparation*

Author
Index